Autochthonous Mouse Models as Tools to Study Diffuse Large B-Cell Lymphoma

Inaugural-Dissertation

zur

Erlangung des Doktorgrades

der Mathematisch-Naturwissenschaftlichen Fakultät

der Universität zu Köln

vorgelegt von

Julia Hansen

aus Konstanz

Berichterstatter:	Prof. Dr. Hamid Kashkar
	Prof. Dr. Niels Gehring
Tag der mündlichen Prüfung:	02.09.2024

0 Table of contents

1 Abstract

Diffuse Large B-cell Lymphoma (DLBCL) is the most commonly diagnosed lymphoma. The DLBCL subtype C5/MCD recurrently features concurrent mutations of *MYD88* and *CD79B*, overexpression of *BCL2*, and a plasma cell differentiation block. C5/MCD patients respond particularly poorly to standard first-line chemo-immunotherapy or experience early relapse. This highlights an urgent need for novel therapeutic strategies. In this thesis, an optimized autochthonous mouse model of C5/MCD DLBCL, the PPMBC mouse model, was established. PPMBC mice developed (oligo-)clonal DLBCLs with additional genetic alterations often found in the C5/MCD subtype. These lesions expressed cell surface markers typical for DLBCL and metastasized to extranodal regions. This model enabled the evaluation of treatment strategies, disentangling the effects of a common pro-oncogenic mutation, and exploring metabolic properties. Specifically, we identified a *Cd79b* ITAM mutation recurrent in C5/MCD DLBCL to confer a targetable tumor reliance on B-cell receptor (BCR) signaling. This *CD79B*^{Y196X} mutation may identify a patient subgroup benefitting of treatment with ibrutinib, an inhibitor for the BCR signaling adaptor BTK, either as a single agent or in combination with other treatments. Furthermore, we determined metabolic alterations accompanying the *Cd79b* ITAM mutation and ibrutinib treatment in our mouse models. Combining ibrutinib with IACS-010759, an inhibitor of oxidative phosphorylation, demonstrated synergistic viability reduction of murine DLBCL cell lines. Taken together, this work highlights the PPMBC model as a powerful preclinical tool for investigation of targetable C5/MCD DLBCL vulnerabilities and for testing of novel therapy options.

2 List of abbreviations

Abbreviation	Term
79-MBC	*Cd**79**b*$^{cond.p.Y195H}$*; **M**yd88*$^{cond.p.L252P/wt}$*; Rosa26*$^{LSL.\mathbf{B}CL2.IRES.GFP/wt}$*; **C**d19*$^{Cre/wt}$
79-PPMBC	*Cd**79**b*$^{cond.p.Y195H}$*; **P**rdm1*$^{fl/fl}$*; **M**yd88*$^{cond.p.L252P/wt}$*; Rosa26*$^{LSL.\mathbf{B}CL2.IRES.GFP/wt}$*; **C**d19*$^{Cre/wt}$
ABC-DLBCL	Activated B-cell-like diffuse large B-cell lymphoma
AcCa	Acylcarnitine
AID	Activation-induced cytidine deaminase
ATP	Adenosine triphosphate
AZ	Aktenzeichen (for animal experiment permissions)
BAX	Bcl-2-associated X protein
BCL2	B-cell lymphoma 2
BCL6	B-cell lymphoma 6
BCL10	B-cell lymphoma 10
BCR	B-cell receptor
bp	Base pair
BRCA2	Breast cancer 2
BTK	Bruton's tyrosine kinase
C3/EZB	Cluster 3/EZB subtype
C5/MCD	Cluster 5/MCD subtype
C57BL/6J	C57 black 6, Jackson Laboratory
CAGGS	Cytomegalovirus early enhancer/chicken β actin
CAR-T	Chimeric antigen receptor T
CARD11	Ccaspase recruitment domain 11 protein
CBM complex	CARD11-BCL10-MALT1 complex
CD19	Cluster of differentiation 19
CD3e	Cluster of differentiation 3 epsilon subunit
CD40	Cluster of differentiation 40
CD79A	Cluster of differentiation 79A
CD79B	Cluster of differentiation 79B
CD138	Cluster of differentiation 138
cDNA	Copy DNA
Cer	Ceramide
CI	Combination index

CoA	Coenzyme A
COO	Cell-of-origin
Cre	Cre recombinase
CREBBP	CREB-binding protein
dCTP	Deoxycytidine triphosphate
DG	Diglyceride
DICOM	Digital Imaging and Communications in Medicine
DLBCL	Diffuse large B-cell lymphoma
DMEM	Dulbecco's modified Eagle's medium
DMSO	Dimethylsulfoxide
DNA	Desoxyribonucleic acid
dTTP	Deoxythymidine triphosphate
DZ	Dark zone
ECAR	Extracellular acidification rate
ELISA	Enzyme-linked immunosorbent assay
EZH2	Enhancer of zeste homolog 2
Fab	Fragment antigen-binding region
FACS	Fluorescence-activated cell sorting
FCS	Fetal Calf Serum
FFPE	Formalin-fixed and paraffin-embedded
FDG-PET	^{18}F-fluorodeoxyglucose-positron emission tomography
FoB	Follicular B cell
FRT	Flippase recognition target
g	Gravitational force equivalent
GC	Germinal center
GCB	Germinal center B cell
GCB DLBCL	Germinal center B-cell-like diffuse large B-cell lymphoma
GFP	Green fluorescent protein
GSEA	Gene set enrichment analysis
H&E	Hematoxylin and eosine
Hex3Cer	Hexyl-3-ceramide
HL	Hodgkin's lymphoma
ICOS	Inducible T-cell costimulator
Ig	Immunoglobulin

IL-2	Interleukin-2
IL-4	Interleukin 4
IL-21	Interleukin 21
ITAM	Immunoreceptor tyrosine-based activation motif
ITIM	immunoreceptor tyrosine-based inhibitory motifs
IRAK1/4	Interleukin-1 receptor-associated kinase 1/4
IRES	Internal ribosome entry site
KBC	Kmt2d, Bcl2, Cre
Ki67	Marker of proliferation Kiel 67
KMT2D	Histone-lysine N-methyltransferase 2D
LDH	Lactate dehydrogenase
LPC	lysophosphocholine
loxP	Locus of x-over
LSL	LoxP-Stop-LoxP
LZ	Light zone
MALT1	Mucosa-associated lymphoid tissue lymphoma
MB	Memory B cell
Mb1	MB-1 membrane glycoprotein
MBC	***M****yd88*$^{cond.p.L252P/wt}$***;*** *Rosa26*$^{LSL.\mathbf{B}CL2.IRES.GFP/wt}$***;*** ***C****d19*$^{Cre/wt}$
MMLV	Moloney murine leukemia virus
MRI	Magnetic Resonance Imaging
MS	Mass spectrometry
MYD88	Myeloid differentiation primary response 88
My-T-BCR	MYD88-TLR9-BCR
MZB	Marginal Zone B cell
NF-κB	Nuclear factor kappa-light-chain-enhancer of activated B cells
NHL	Non-Hodgkin's lymphoma
OCR	Oxygen consumption rate
OxPhos	Oxidative phosphorylation
PB	Plasmablast
PBS	Phosphate buffered saline
PC	Plasma cell
PCR	Polymerase chain reaction
PD-1	Programmed cell death protein 1

PD-L1	Programmed death-ligand 1
PE	phosphoethanolamine
PI3K	Phosphatidylinositol 3-kinase
PKCβ	Protein kinase Cβ
PLA	Proximity ligation assay
PLCγ2	phospholipase Cγ2
PNA	Peanut agglutinin
PCh	Phosphocholine
PPMBC	***P****rdm1*$^{fl/fl}$*;* ***M****yd88*$^{cond.p.L252P/wt}$*; Rosa26*$^{LSL.\mathbf{B}CL2.IRES.GFP/wt}$*;* ***C****d19*$^{Cre/wt}$
PRDM1	PR domain zinc finger protein 1
R-CHOP	Rituximab, cyclophosphamide, hydroxydaunorubicin, oncovin, prednisone
RNA	Ribonucleic acid
RNAi	RNA interference
rpm	Revolutions per minute
SD	Standard deviation
SDS	Sodium dodecylsulfate
SHMT2	Serine hydroxymethyltransferase 2
SMBC	***M****yd88*$^{cond.p.L252P/wt}$*; Rosa26*$^{LSL.\mathbf{B}CL2.IRES.GFP/LSL.\mathbf{S}pib.IRES.GFP}$*;* ***C****d19*$^{Cre/wt}$
SYK	Spleen tyrosine kinase
TBL1XR1	F-box-like/WD repeat-containing protein
TE	Time to echo
Tfh	T follicular helper cell
TG	Triglyceride
TLR	Toll-like receptor
TME	Tumor microenvironment
TNF	Tumor necrosis factor
TR	Repetition time
TRAF6	TNF receptor associated factor 6
TSE	Turbo spin echo
UMI	Unique Molecular Identifier
VDJ	Variable–diversity–joining
VEP	Varian Effect Predictor
WES	Whole-exome sequencing
wt	Wildtype

3 Introduction

3.1 The human immune system constitutes several protection levels

The human immune system is the body's primary protection against infection (Murphy et al. 2012; Janeway 1992). Different levels of immunity protect against pathogens: The first line of defense are anatomic barriers like the skin or the mucosa, prohibiting pathogen entry (Leceta et al. 2022; Hornef et al. 2002). If this fails, innate immune features, such as the complement system (Gros, Milder, and Janssen 2008) or other antimicrobial proteins (De Smet and Contreras 2005), combat the pathogen, often helped by innate immune cells like macrophages, natural killer cells or innate lymphoid cells (Zhang et al. 2021). Under pathogen persistence, adaptive immunity is activated, mainly driven by B cells secreting antibodies and T cells killing infected cells or providing B cell help (Murphy et al. 2012).

The typical course of an acute infection requiring clearance by the adaptive immune response begins with the entry of the pathogen into the body (Murphy et al. 2012). Initially, the innate immune response keeps the pathogen in check, slowing its advance (Murphy et al. 2012). When a minimal pathogen level is reached, the adaptive immune response is elicited (Freedman and Gatica 1977), initiating B and T cell activation and subsequent reactions like the germinal center (GC) reaction (see 3.2) (De Silva and Klein 2015). After maturation of the adaptive response, effector cells and antibodies start to clear the infection (Murphy et al. 2012). Reaching antibody clearance, the immune response ceases, but residual effector cells convey immune memory (Fig. I1) (Inoue and Kurosaki 2024; Farber, Yudanin, and Restifo 2014).

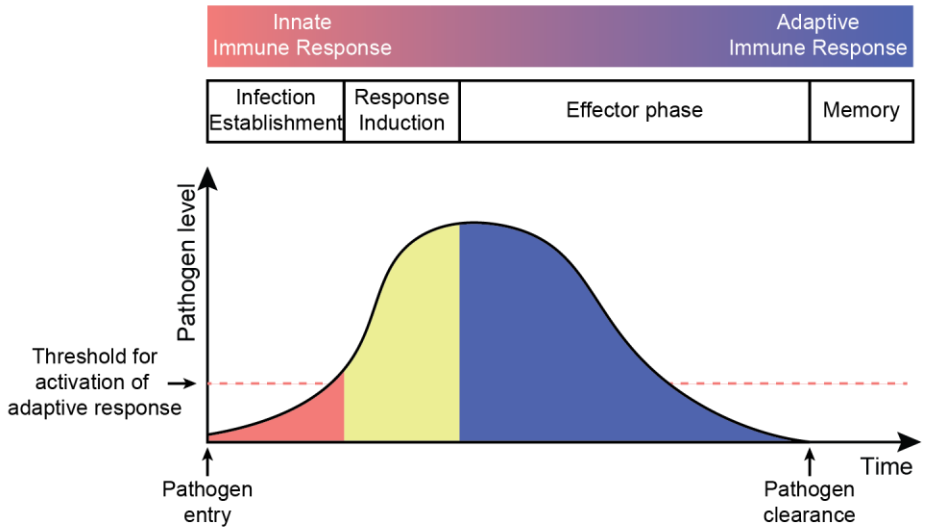

***Figure I1 The course of an infection resolved by the adaptive immune response**. After pathogen entry, a pathogen's growth rate is impeded by the innate immune response. Upon reaching a certain pathogen level threshold, the adaptive immune response is activated. Response induction leads to preparation of immunity to move to the effector phase, where the pathogen is defeated. Following pathogen clearance, the immune system retains memory cells to be prepared to launch a rapid immune response upon encountering the same pathogen.*

In all immune responses, balance is key for the human immune system: While an insufficient response provoked by immune dysfunction fails to clear infections, an overactive response may lead to autoimmunity or even carcinogenesis (Murphy et al. 2012).

3.2 B cells evolve upon antigen exposure

Hematopoietic stem cells in the bone marrow are the precursors of all blood cells (Murphy et al. 2012). Some differentiate into common lymphoid progenitor cells, which in turn are the origin of B cells, T cells, and natural killer cells (Carsetti 2000). Within the bone marrow, VDJ recombination generates a diverse B-cell receptor (BCR) repertoire (Nagasawa 2006; Hughes et al. 2022). For the resulting immature B cells, absence of self-reactivity is ensured in the bone marrow and periphery, yielding mature naïve B cells circulating the body (Murphy et al. 2012). Upon binding of a specific antigen, usually including additional T cell help, naïve B cells are activated and differentiate into antibody-secreting plasmablasts and plasma cells (Murphy et al. 2012). The resulting antibodies can neutralize small antigens (like toxins), opsonize pathogens for uptake by macrophages, or activate the complement system to form a membrane-attack complex harming the pathogen (Murphy et al. 2012). The surface marker CD19, a co-receptor for BCR signal transduction, is expressed in nearly all stages of B cell development, starting at VDJ recombination (Li et al. 2017).

A proportion of activated B cells migrates to primary lymphoid organs such as the spleen, where it initiates the GC reaction to improve the antigen affinity of the BCR (Murphy et al. 2012). In the so-called dark zone of the GC, B cells expand clonally (Murphy et al. 2012). The name “dark zone” stems from the observation that the local accumulation of cells makes the tissue seem dark on immunohistochemistry stainings of primary lymphoid organs (Allen et al. 2004). In parallel, B cells undergo somatic hypermutation: In this process, random mutations that alter the V regions of immunoglobulin genes responsible for antigen binding are introduced, a process which is mediated by the enzyme activation-induced cytidine deaminase (AID) (Maul and Gearhart 2010). B cells then wander to the light zone to undergo affinity selection: Only mutated B cells with a comparably high affinity for the antigen, in competition with the other B cells generated in the dark zone, will receive T follicular helper cell help (De Silva and Klein 2015; Young and Brink 2021). B cells with sufficient “help” consisting of stimulation of CD40 and the inducible T-cell costimulator (ICOS) (Dong, Temann, and Flavell 2001), as well as expression of the cytokines IL-4 and IL-21 (Gonzalez et al. 2018), survive to transfer back to the dark zone, where the process begins anew in a cyclic reentry model (Young and Brink 2021; De Silva and Klein 2015). “Optimized” B cells subsequently differentiate into memory B cells or plasma cells (Fig. I2) (Nutt et al. 2015; Inoue et al. 2021).

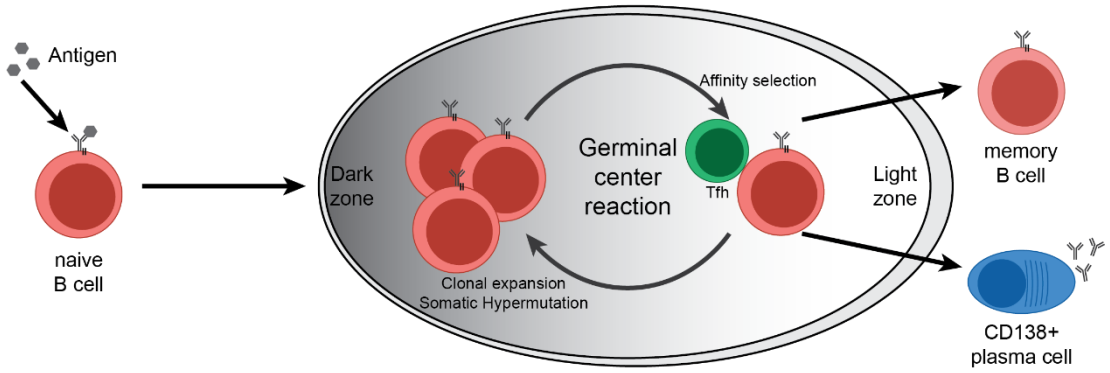

***Figure I2 The GC reaction "optimizes" B cells for the adaptive immune response**. Upon activation of naïve B cells by an antigen, a subset of B cells migrates to primary lymphoid organs to initiate the GC reaction. The bipolar GC has a dark zone, appearing darker on immunohistochemistry stainings due to high cell density, and a light zone. In the dark zone, B cells undergo rapid proliferation (clonal expansion) while simultaneously altering their antigen-binding site with AID-driven somatic hypermutation. Expanded B cells relocate to the dark zone, where they undergo affinity selection by competing for T follicular helper cell (Tfh) help. B cells without help undergo apoptosis, while B cells receiving sufficient Tfh interaction move back to the dark zone in a continuous cycle. Throughout the GC reaction, B cells also differentiate into memory B cells or CD138⁺ plasma cells secreting antibodies to fight the GC-initiating infection.*

AID also allows for class switch recombination, exchanging the BCR immunoglobulin: While naïve B cells express IgM and IgD, as do the first antibody-expressing plasma cells in an immune response, class-switched B cells express either IgA, IgE, or an IgG class (IgG1-IgG4) (Murphy et al. 2012; Schroeder and Cavacini 2010). Each immunoglobulin class has a specialized function and distribution: While IgE is relevant for mast cells in allergic reactions, IgA antibodies are mainly secreted at mucosae to be transported across the epithelium (Schroeder and Cavacini 2010). IgG antibodies are efficient in antigen neutralization, opsonizing pathogens, activating the complement system and sensitizing other immune cells. IgG is usually the most abundant antibody in human serum (Justiz Vaillant et al. 2024).

The BCR responsible for B-cell activation consists of a surface immunoglobulin of the respective type associated with a heterodimer of CD79A and CD79B (Fig. I3) (Murphy et al. 2012; Tanaka and Baba 2020). When a specific antigen is bound, tyrosines in the immunoreceptor tyrosine-based activation motifs (ITAMs) of CD79A and CD79B are phosphorylated by Src-family kinases such as LYN (Bojarczuk et al. 2015). These phosphorylated ITAMs recruit the kinase SYK, which is also activated by phosphorylation (Y532, YY535/536) (Bohnenberger et al. 2011), and subsequently transmits signaling via Bruton's tyrosine kinase (BTK), phospholipase Cγ2 (PLCγ2), phosphatidylinositol 3-kinase (PI3K) and AKT (Bojarczuk et al. 2015; Young et al. 2019). Activated PLCγ2 generates downstream second messengers, which in turn induce the release of intracellular calcium, triggering calcium-dependent signaling (Engelke et al. 2007). These second messengers also activate protein kinase Cβ (PKCβ), which recruits caspase recruitment domain 11 protein (CARD11), B-cell lymphoma 10 (BCL10) and mucosa-associated lymphoid tissue lymphoma translocation protein 1 (MALT1), forming the so-called "CBM complex", which activates NF-κB signaling (Bohnenberger et al. 2011). In this manner, BCR signaling activation promotes B-cell proliferation via PI3K, MAPK and NF-κB signaling (Bojarczuk et al. 2015).

Negative regulation is believed to be mediated by phosphorylation of immunoreceptor tyrosine-based inhibitory motifs (ITIM) of BCR-associated proteins induced by LYN, leading to BCR internalization and signal inhibition (Wen et al. 2019).

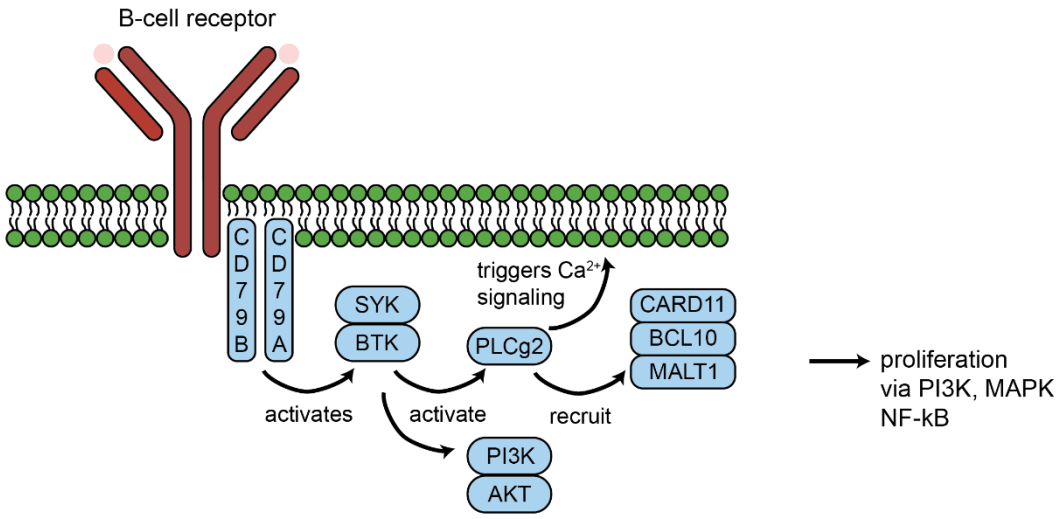

***Figure I3 Classical BCR signaling activates proliferative cascades and downstream effector pathways**. In this simplified scheme, a transmembrane immunoglobulin is activated by binding antigens (pink), phosphorylating ITAMs of CD79A and CD79B. These in turn recruit and activate the kinases SYK and BTK by phosphorylation. BTK phosphorylates the phospholipase PLCγ2 which mediates the generation of second messengers triggering Ca^{2+} signaling and the recruitment of the CBM complex (CARD11, BCL10, MALT1). Simultaneously, BTK activates PI3K and AKT. Together, BCR activation induces B-cell activation and proliferation via PI3K, MAPK and NF-κB signaling cascades.*

In the setting of B-cell malignancies, another mode for BCR signaling was recently described by Phelan et al.: Signaling via the My-T-BCR supercomplex. In this context, BCR signaling seems to synergize with Toll-like receptor (TLR) signaling (Fig. I4)(Phelan et al. 2018). TLRs are innate immune receptors recognizing typical pathogen patterns such as unmethylated CpG DNA found in viruses (in the case of TLR9) (Balka and Nardo 2019). Upon activation, TLR9 recruits MYD88, IRAK1/4, and TRAF6 (Murphy et al. 2012; Balka and Nardo 2019). It was shown that in the endosome of lymphoma cells, the BCR can form a complex with TLR9, amplifying pro-oncogenic signaling (Phelan et al. 2018; Mandato et al. 2023). To our knowledge, this mechanism was only reported in malignancy and might be irrelevant for in healthy B cells.

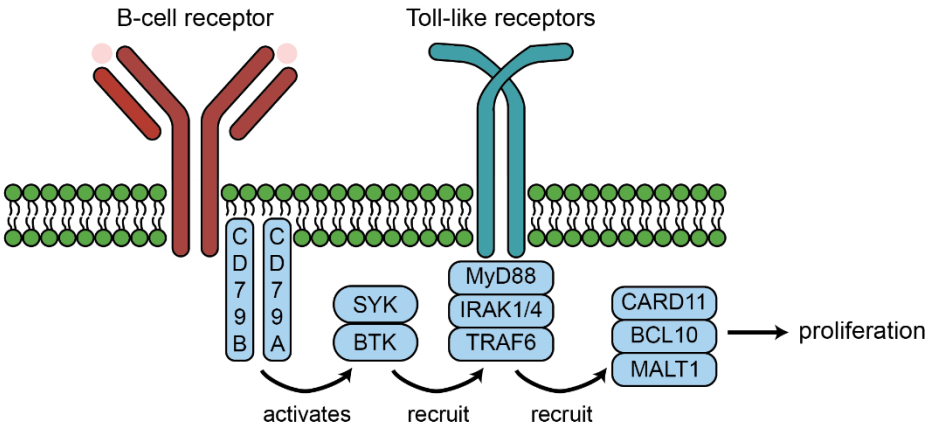

Figure I4 Malignant BCR signaling via the My-T-BCR supercomplex. *In the context of lymphoma, it has been reported that the BCR forms a complex with TLR9 and signaling adaptors in the endosome, leading to enhanced BCR activation benefitting the lymphoma.*

3.3 B cell lymphoma is an age-associated disease

Several factors seem to contribute to cancer development in B cells, making B cell lymphoma one of the 10 most frequently diagnosed cancers worldwide (Bray et al. 2024). On the one hand, the GC reaction promotes cancer development: High B-cell proliferation rates and active alteration of genetic material via AID-driven somatic hypermutation, which does not always target solely the desired BCR antigen-binding site, can lead to unintended effects (Leeman-Neill, Bhagat, and Basu 2024). In fact, AID targets non-Ig genes with a low frequency, which can lead to pro-oncogenic genetic alterations, and signatures of aberrant AID-induced mutations are commonly found in lymphoma (Chapuy et al. 2018; Chaudhuri et al. 2014). On the other hand, ageing is a relevant factor for lymphoma development: Not only does the risk to develop lymphoma increase with age (Wallace and Reagan 2022), patient age is also a major determinant of lymphoma biology in diffuse large B-cell lymphoma (DLBCL), such as subtype and cytogenic complexity (Klapper et al. 2012). Furthermore, age-related spontaneous somatic cytidine deamination (C>T mutation) was found to be the predominant mutational signature in DLBCL (Sarkozy, Salles, and Falandry 2015; Chapuy et al. 2018).

Lymphomas are a heterogeneous group of cancers and are classically subdivided into Hodgkin's lymphoma (HL) and Non-Hodgkin's lymphoma (NHL) (Paquin et al. 2023). While HL carries a low number of tumor cells in a hyperactive microenvironment, showing a defective B-cell program, NHLs comprise a large family of indolent and aggressive lymphomas (Alaggio et al. 2022). The most frequently diagnosed lymphoma is DLBCL, a B-NHL which has a large-cell morphology and a mature B-cell phenotype (Smith et al. 2015; Alaggio et al. 2022).

3.3.1 DLBCL is the most common NHL

DLBCL is an aggressive and heterogeneous disease, shown to have a 5-year survival rate of about 60% following standard first-line treatment with R-CHOP (rituximab, cyclophosphamide, doxorubicin, vincristine and prednisolone) (Horvat et al. 2018; Jakobsen et al. 2022). Two DLBCL subgroups are distinguished by cell-of-origin (COO) classification: Germinal center B cell-like (GCB) and activated B cell-like (ABC) DLBCL (Alizadeh et al. 2000). GCB DLBCLs express GC markers, harbor a GC gene expression profile and are thus thought to arise from GC B cells. ABC DLBCLs are characterized by a higher expression of plasma cell genes, chronic BCR and NF-κB activation, and show a lower overall 5-year survival rate compared to GCB DLBCL (Wright et al. 2003; Sehn and Salles 2021). Although the original COO classification was based on gene expression profiling, immunohistochemistry-based algorithms like the Hans algorithm are often used clinically to distinguish GCB and non-GCB cases (Alizadeh et al. 2000; Hans et al. 2004; Sehn and Salles 2021). Currently, there is no stratified treatment protocol based on COO classification, rendering it mainly relevant for patient prognosis and as starting point for further downstream analyses (Sehn and Salles 2021).

3.3.2 The C5/MCD DLBCL shows a poor prognosis

Recently, the genetic alterations of primary DLBCLs were analyzed by several independent studies, using consensus clustering to identify distinct DLBCL subsets largely overlapping between studies (Chapuy et al. 2018; Wright et al. 2020; Schmitz et al. 2018). These investigations described the cluster 5 or MCD subtype (C5/MCD), a subtype mainly consisting of ABC DLBCLs and defined by frequent co-occurrence of gain-of-function *CD79B* and *MYD88* mutations (Chapuy et al. 2018; Wright et al. 2020; Schmitz et al. 2018). This subtype showed an especially poor progression-free survival (Chapuy et al. 2018; Schmitz et al. 2018). *CD79B* mutations mainly included ITAM mutations, most often mutating Y196, driving BCR signaling (Phelan et al. 2018; Mandato et al. 2023; Davis et al. 2010). *MYD88* mutations in C5/MCD DLBCL selectively involved the activating L265P mutation, which also amplifies BCR and NF-κB signaling (Phelan et al. 2018; Mandato et al. 2023; Munshi et al. 2020; Ngo et al. 2011). Oncogenic BCR signaling in lymphoma cells carrying these two mutations is induced via the My-T-BCR supercomplex (Fig. I5A) (Phelan et al. 2018; Mandato et al. 2023). BCR signaling is essential for B-cell survival and pathogenic proliferative BCR signaling is critical in many DLBCL cases (Young et al. 2019; Srinivasan et al. 2009).

Another characterizing genetic alteration was the amplification of the chromosomal arm *18q* carrying the *BCL2* gene (Chapuy et al. 2018), which is associated with overexpression of BCL2 (Monni et al. 1997). BCL2 is an anti-apoptotic protein of the BCL2 family that was shown to inhibit tumor cell death in lymphomas and other types of cancers (Fig. I5B) (Youle and Strasser 2008).

Additionally, MCD/C5 DLBCLs also carry genetic alterations of genes involved in plasma cell differentiation, among them loss-of-function mutations of *PRDM1* (6q21) (Chapuy et al. 2018), a transcription factor necessary for plasma cell differentiation (Fig. I5C) (Tunyaplin et al. 2004; Shaffer et al. 2002); and the amplification of *SPIB* (*19q*), a transcription factor suppressing plasma cell differentiation (Horiuchi et al. 2023).

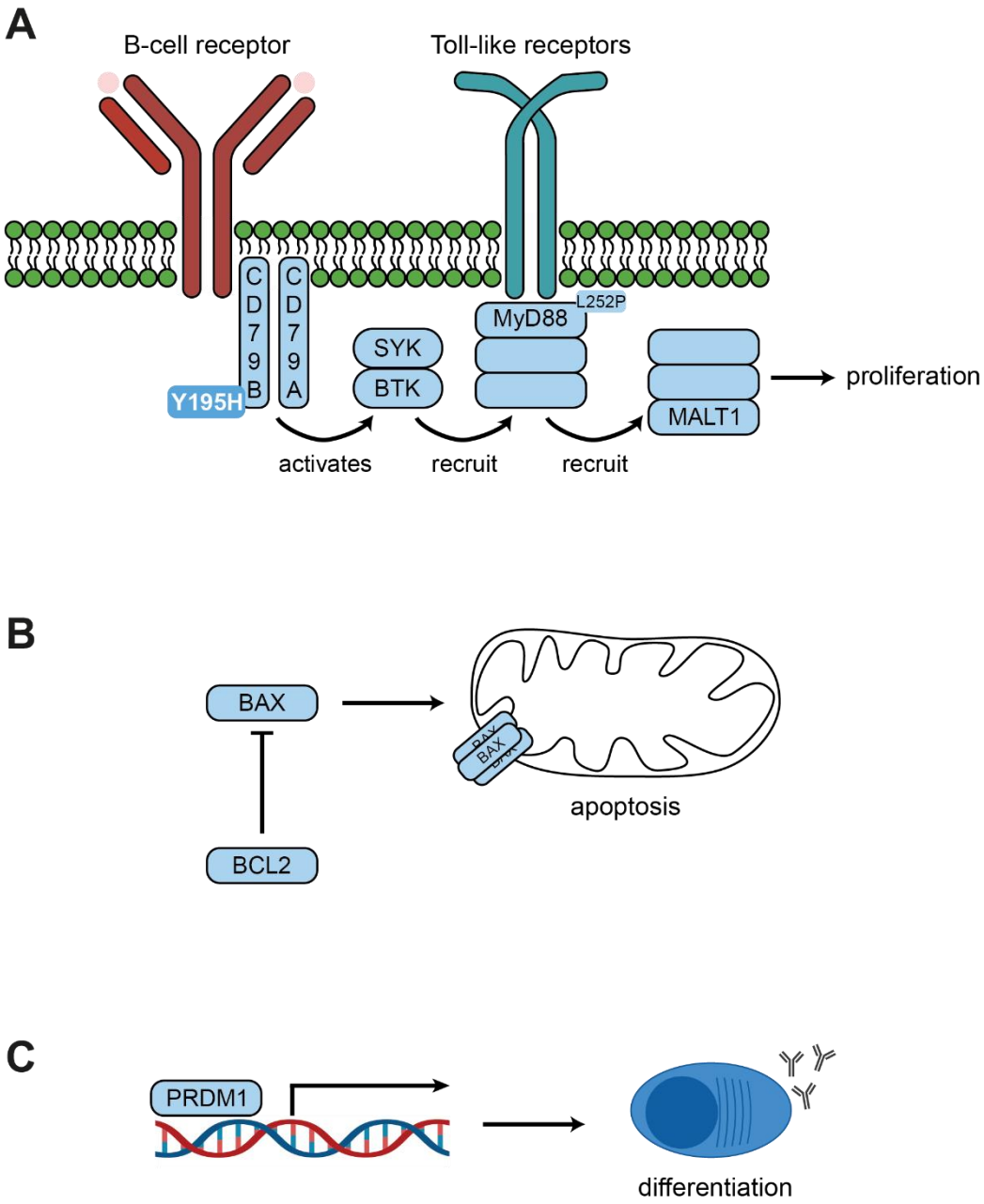

Figure I5 Genetic alterations drive malignant signaling in C5/MCD DLBCL. *(A) Mutations of* MYD88 *and* CD79B *synergize to induce proliferative My-T-BCR supercomplex signaling. Murine homologues of the respective mutations are annotated. (B) Amplification of* 18q*, where the* BCL2 *gene is located, leads to increased level of BCL2, which inhibits apoptosis. (C)* PRDM1*, a transcription factor necessary for plasma cell differentiation, displays loss-of-function mutations in C5/MCD DLBCL.*

It was recently shown that another characteristic genetic alteration of C5/MCD DLBCL, the gain-of-function mutation of *BTG1*, increases competitiveness of B cells in lymphoma development (Mlynarczyk et al. 2023). C5/MCD DLBCL also recurrently harbors *TBL1XR1* loss-of-function mutations, which promote GC reentry skewing B cell fates to memory B cells and can drive lymphomagenesis (Venturutti et al. 2020).

C5/MCD DLBCL was speculated to be sensitive to treatment by agents inhibiting BCR signaling. In line with this, a phase 1/2 clinical trial demonstrated that the BTK inhibitor ibrutinib prolonged survival of ABC DLBCL patients carrying a *CD79B* ITAM mutation, and strikingly 5 out of 5 *CD79B*/*MYD88*-comutant cases responded, suggesting ibrutinib as a potential therapy for these genetically defined cases (Wilson et al. 2015). In a randomized phase 3 trial for the combination of ibrutinib with standard first-line immunochemotherapy (R-CHOP), a survival advantage for ibrutinib-co-treated patients was only found in patients below 60 years (Younes et al. 2019). An additional retrospective analysis found a *BCL2/MYC*-coexpressing patient subset to be preferentially sensitive to ibrutinib treatment, hinting at additional molecular mechanisms at play (Johnson et al. 2023). In the recently published GUIDANCE-1 trial, addition of ibrutinib to R-CHOP in frontline therapy increased response rates in MCD-like DLBCL (Zhang et al. 2023). However, even in responding patients, resistance to ibrutinib is frequent, often induced by BTK mutations (Nakhoda, Vistarop, and Wang 2022), although other mechanisms like metabolic rewiring, suppression of autophagy or the unfolded protein response were suggested as well (Choueiry, Singh, Sircar, et al. 2021; Zhang et al. 2020; Phelan et al. 2024). Further research is required to determine if and when ibrutinib might be a viable and long-term treatment strategy for DLBCL patients.

3.3.3 Mouse models mimic DLBCL *in vivo*

Mouse models are frequently used as pre-clinical tools to study cancers and test treatment options (Ireson et al. 2019). While some models are based on the injection of tumor cells or pro-oncogenic substances, many researchers work with genetically engineered mouse models (Zitvogel et al. 2016). These are often based on genetic alterations specifically activated in target tissues to initiate the intended cancer by using the Cre/loxP system: The Cre recombinase recognizes a certain locus (locus of x-over, loxP) and mediates deletion of genetic material between two loxP sites, for example leading to a gene knockout or removing a stop locus enabling the expression of a gene of interest (Kim, Kim, et al. 2018).

For lymphoma models, B-cell specific expression of Cre is usually achieved by expressing the recombinase from B-cell specific genes heterozygously. For instance, *Cd19*^{Cre} and *Mb1*^{Cre} are expressed in early B-cell stages, while *Cg1*^{Cre} and *Aicda*^{Cre} are expressed in GC stages (Tabatabai et al. 2023; Casola et al. 2006; Rickert, Roes, and Rajewsky 1997; Robbiani et al. 2008; Hobeika et al. 2006). Several DLBCL mouse models for GCB- and ABC-DLBCL have been established:

1. One of the most frequently altered genes in GCB DLBCL is the GC gene *BCL6*, which is often hyperactivated by amplification, translocation, or structural variation (Basso and Dalla-Favera 2012b; Chapuy et al. 2018; Schmitz et al. 2018). Mice carrying a mimicked *BCL6* translocation develop a lymphoproliferative disease, culminating in lymphoma, giving insight into the role of *BCL6* alterations in GCB DLBCL (Cattoretti et al. 2005).
2. Another frequent characteristic of GCB DLBCL is the genetic alteration of chromatin modifiers such as *EZH2* or *KMT2D* (Chapuy et al. 2018; Schmitz et al. 2018). Several mouse models have investigated the promoting effect of *EZH2* mutations on lymphoma proliferation, also in combination with *BCL6* or *BCL2* (Béguelin et al. 2013; Béguelin et al. 2016; Béguelin et al. 2020). Concomitant *BCL2* overexpression and *Kmt2d* or *Crebbp* loss have also led to lymphoma development in mouse models (Zhang et al. 2017; Zhang et al. 2015).
3. The Reinhardt laboratory previously established the so-called MBC mouse model (Flümann et al. 2021; Knittel et al. 2016). *Myd88*^{L252P}, the murine orthologue of *MYD88*^{L265P}, and an overexpression allele of *BCL2*, *Rosa26*$^{LSL.BCL2\text{-}IRES\text{-}GFP}$, were conditionally expressed using *Cd19*^{Cre} (***M****yd88*$^{cond.p.L252P/wt}$*; Rosa26*$^{LSL.\mathbf{B}CL2.IRES.GFP/wt}$*;* ***C****d19*$^{Cre/wt}$). Mice developed lymphomas with a median overall survival of 179 days. Lymphomas were assigned as ABC-DLBCLs by immunohistochemistry staining, gene expression and mutational profiling. These autochthonous mice were successfully used as preclinical tools for testing combined BCL2- and PD-1 blockade. One shortcoming of the model is lack of expression of the B-cell markers B220 and CD19, which are typically expressed in DLBCL tumor samples. Instead, the tumors express the plasma cell marker CD138. This close relation to the plasma cell lineage might hamper interpretability of results for DLBCL patients, necessitating adaptions to faithfully mimic patient DLBCL (Flümann et al. 2021; Knittel et al. 2016).

3.4 Altered tumor metabolism in DLBCL

3.4.1 Deregulated cellular energetics are a hallmark of cancer

Understanding intra- and intercellular signaling is integral to comprehending the complex mechanisms of life (Nair et al. 2019). One major influence on cell signaling is metabolism (Miyazawa and Aulehla 2018). Some intermediates of major catabolic and anabolic pathways serve directly as cell signaling intermediates, such as acetyl-CoA, which acts as second messenger by influencing acetylation profiles (Pietrocola et al. 2015). Many secondary effects induced by metabolic changes also lead to cell signaling alterations, for example in the insulin signaling pathway (Castiello, Heileman, and Tabrizian 2016). Generally, cell signaling strongly controls cell metabolism and vice versa (Natalya and Craig 2016). Disruptions in either metabolic or signaling pathways lead to alterations in the other, impacting the whole system due to the complex network of feedback loops and regulation mechanisms (Lin et al. 2022).

Metabolic alterations can be caused by natural developments like ageing (López-Otín et al. 2013), but also malignant signaling and genetic aberrations, which is why deregulated cellular energetics were named a Hallmark of Cancer (Hanahan and Weinberg 2011; Hanahan 2022). The Warburg effect was the first reported reprogramming of cancer cell energy metabolism, which shifts glucose metabolism to “aerobic glycolysis” (Warburg 1956). To date, the function of this metabolic change is still not fully understood: While some hypothesize it to be the effect of aberrant signaling, it may also promote cancer by maintaining normoxia or producing pro-oncogenic metabolites (Jaworska et al. 2023; Galicia-Vazquez and Aloyz 2019). In fact, the oncometabolite lactate as product of the Warburg effect was proposed to promote pro-oncogenic tumor microenvironment (TME) (Kato et al. 2013), metastasis (Pennington et al. 2019), and tumor-associated cachexia (Liu et al. 2024; Kumagai et al. 2022).

Many other metabolic alterations have been described in cancer cells, which seem to affect tumor fitness and performance, metastasis, and treatment response (Bergers and Fendt 2021). For instance, it was recently described that the metabolite methylglyoxal, a byproduct of glycolysis, inactivates the tumor suppressor protein BRCA2, allowing for tumorigenesis relevant for several cancer types (Kong et al. 2024). Specific lipids have also been known to act as cellular second messengers, making their emerging role in tumor biology seem likely (Vasseur and Guillaumond 2022). For example, prostaglandin E2, sphingosine phosphates and fatty acids were demonstrated to exert crucial roles in metastasis of several cancers (Wang et al. 2020; Patmanathan et al. 2016; Luo et al. 2018). Targeting a lipid kinase phosphorylating phosphoinositolphosphate led to increased targetable antigen presentation in several tumor types (Bao et al. 2023).

Other studies investigated the possibility of dietary interventions in cancer treatment. While the first therapeutic activity of the folic acid antagonist aminopterin was described decades ago (Farber and Diamond 1948), the notion of taking adiposity under consideration for treatment choice (Fournier et al. 2023) or the role of high-fat diet in cancer progression (Labbe et al. 2019), were recently reinforced.

Recent advances in -omics technologies now allow for a comprehensive analysis of metabolism in the context of a cell’s genetic and epigenetic background, promising to improve our understanding of their interplay, impact on cell signaling, as well as treatment outcomes. Integration of metabolic data into tumor characterization could even improve tumor subtyping, improving diagnosis and treatment choice, as illustrated by studies integrating -omics data into subtyping different cancers (Qu et al. 2024; Xiao et al. 2022; Wang et al. 2023).

3.4.2 DLBCL shows deregulated metabolism

Like many other cancers, DLBCL exhibits an increased metabolic activity compared to other somatic cells. Clinical tests for DLBCL diagnosis and staging therefore include ^{18}F-fluorodeoxyglucose-positron

(FDG-PET) emission tomography as readout for glucose uptake, as well as lactate dehydrogenase (LDH) level testing (Kluckova, D'Avola, and Riches 2022).

Within the tumor, the impact of signaling pathway alterations such as BCR or PI3K signaling have been studied extensively, but little is known about their effect on cellular metabolism (Young et al. 2019; Bojarczuk et al. 2019; Pfeifer et al. 2013). Inhibition of the BCR signaling kinase SYK was associated with a decrease in cholesterol biosynthesis in cell lines (Chen, Monti, et al. 2013). By classifying DLBCL cell lines by their metabolic signatures, they are distinguishable into BCR- and OxPhos-dependent cell lines reprogramming their fatty acid metabolism, the latter predominantly using palmitate as respiratory fuel while reducing glucose and increasing glutamine usage (Caro et al. 2012; Wei et al. 2022). Patients also seem classifiable by a metabolism-associated gene signature which impacts the TME (He et al. 2022). Other studies have identified CD37 as prognostic marker for DLBCL and demonstrated its inhibitory role for fatty acid metabolism (Peeters et al. 2022; Xu-Monette et al. 2016). The *SHMT2* gene, which is frequently amplified in B-cell lymphomas, is involved in the mitochondrial folate cycle shown to contribute to cancer metastasis (Lee, Vousden, and Hennequart 2024). Altered metabolism in DLBCL seems to be predictive for treatment response to R-CHOP (Chiche et al. 2019; Fornecker et al. 2019) and chimeric antigen receptor (CAR) T cells (Linguanti et al. 2022; Derlin et al. 2021). MYC as recurrent oncogene in DLBCL seems to drive oxidative phosphorylation, sensitizing to an inhibitor of oxidative phosphorylation (Donati, Ravà, et al. 2022). Furthermore, inhibition of glycolysis and oxidative phosphorylation was found to be a promising therapeutic strategy for DLBCL treatment in cell lines and xenograft models (Noble et al. 2022), but clinical trials testing inhibition of oxidative phosphorylation in advanced solid tumors or acute myeloid leukemia demonstrated high toxicity (Machado et al. 2023; Janku et al. 2021; Yap et al. 2023). Notably, while many studies were performed *in vitro* or on preserved DLBCL patient samples, little is known about metabolic alterations within an *in vivo* system, which will be integral to gain a comprehensive picture interpreting the many reports indicating the role of metabolic alterations in DLBCL.

3.5 Aims of the project

C5/MCD DLBCL is a DLBCL subtype with poor prognosis under standard frontline immunochemotherapy (Chapuy et al. 2018; Schmitz et al. 2018). Therefore, a testing tool for novel treatment options is highly needed.

This research project consists of three parts.

As a foundation, we aimed to establish an improved mouse model mirroring C5/MCD DLBCL biologically in morphology, cell surface marker expression and gene expression (Fig. I6A). Specifically, we hypothesized that a close relation to the plasma cell lineage could be avoided by introducing a plasma cell differentiation block with a conditional knockout of *Prdm1* (generating the PPMBC mouse model) or overexpression of *Spib* (generating the SMBC mouse model) into the previously published

MBC mouse model (Knittel et al. 2016). These models were characterized by flow cytometry, immunohistochemistry, MRI, serum analysis, WES and transciptomics. The preferred model was used as preclinical testing tools for several treatment options, among them CAR-T cell treatment.

The established mouse model was then applied in two clinically relevant research questions:

Firstly, which effects do the frequently occurring *CD79B*^{Y196X} mutations mediate which might be targetable (Fig. I6B)? To this end, a conditional mutation (murine orthologue, *Cd79b*^{Y195H}) was introduced into the model and compared to the *Cd79b*^{wt} counterpart using flow cytometry, immunohistochemistry, MRI, WES, transcriptomics, and proximity ligation assays. Furthermore, response to ibrutinib inhibiting BCR signaling was tested in this model.

Secondly, what metabolic alterations can be found in the different available C5/MCD mouse models that might give rise to additional treatment options (Fig. I6C)? For this purpose, transcriptomic and metabolomic data from different genotypes and after treatment with ibrutinib was analyzed. Metabolic measurements of cell lines treated with ibrutinib were conducted by SeaHorse experiments. Lastly, combination therapy with an inhibitor of oxidative phosphorylation, IACS-010759, was tested in murine cell lines.

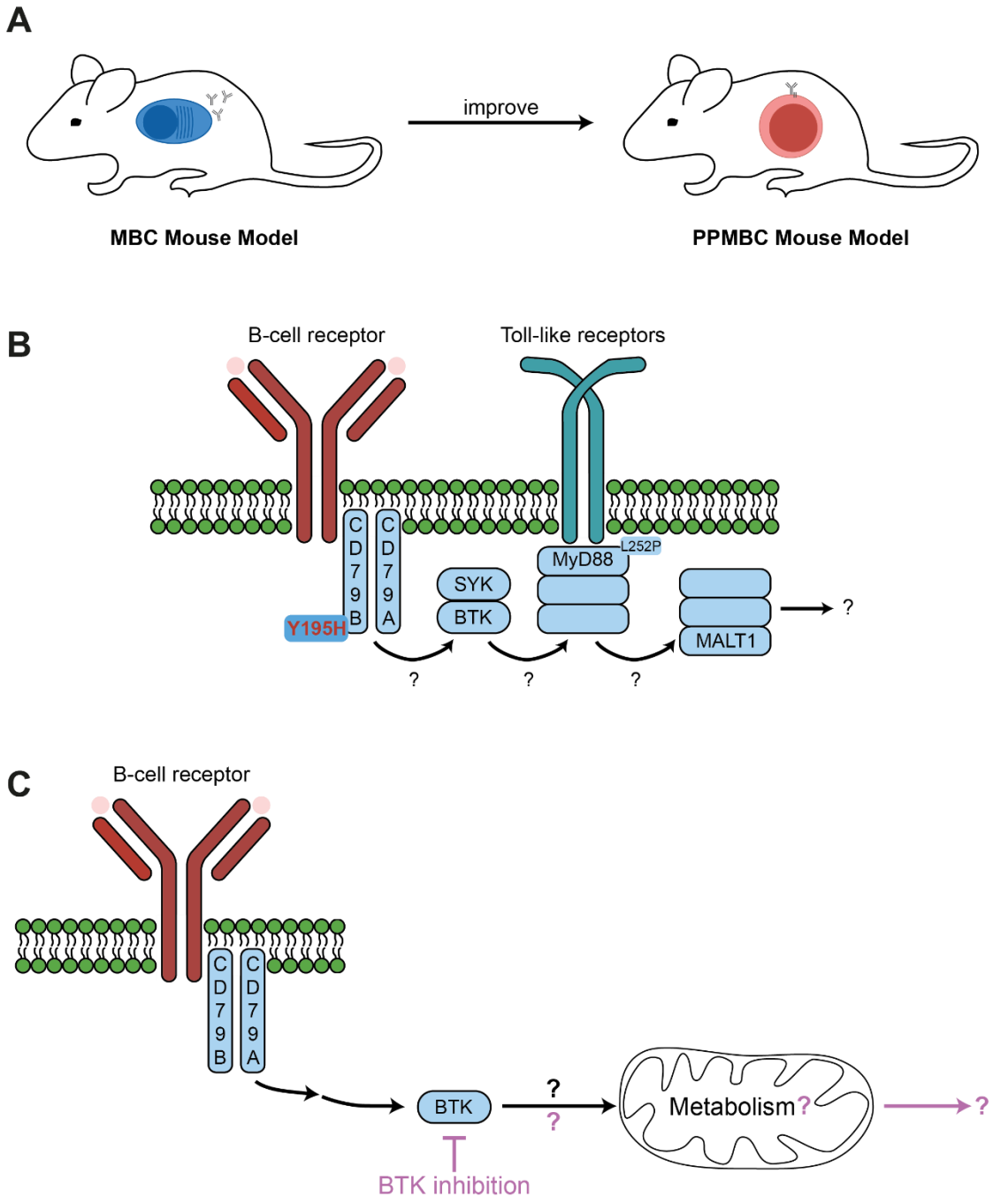

Figure I6 Aims of this project. *(A) First, an improved autochthonous mouse model of C5/MCD DLBCL was to be established by removing the plasmablastic-like phenotype via introduction of a plasma cell differentiation block with a conditional knockout of* Prdm1 *into the previously published MBC mouse model, generating the PPMBC mouse model. This model was subsequently applied to (B) investigate the role of recurring* CD79B *ITAM mutations in C5/MCD DLBCL and to (C) analyze metabolic alterations in different genetic backgrounds and after BTK inhibition.*

4 Materials and methods

4.1 Experimental mice

For chapter 5.2: “For survival analyses, animals were recorded as events that succumbed to disease or that had to be sacrificed due to predefined termination criteria. Animals that died due to genotype-unrelated reasons (appendicitis, abnormal teeth, injuries inflicted by cage mates) were censored.” (Flumann et al. 2023)

To minimize animal suffering, these humane termination criteria were predefined in collaboration with the animal welfare office and approved by the local authorities (Landesamt für Natur, Umwelt und Verbraucherschutz Nordrhein-Westfalen). These criteria included a body condition score of 1 and 2 (Ullman-Cullere and Foltz 1999) indicating poor mouse fitness, weight reduction of ≥5%, abnormal scratch wounds, clotted orifices, pronounced coordination issues, paralysis of extremities, a sustained cowering position, a tightened abdomen, abnormal stereotypical behavior, apathy, self-isolation, automutilation, respiratory problems, epilepsy, prolonged diarrhea or constipation, rectal prolapse. If mice had to be sacrificed solely due to one or more of these reasons, data and samples were not used for further analyses except for causes of death in Fig. R6B and R19B, but some of these criteria could accompany the following “lymphoma-provoked” symptoms. Animals were sacrificed and data and samples were used for the analyses reported in this thesis if they met one or more of the following criteria: Palpable tumor(s) with a diameter >1cm, lymphadenopathy in the neck region, strongly enlarged spleen (3.5-fold), detectable enlargement of the abdomen accompanied with altered walking style.

“In treatment studies, onset of lymphoma was defined by a lesion larger than 150µl or splenomegaly larger than 50 µl detectable by MRI, with a robust volume increase in two consecutive scans. Venetoclax (MedChem Tronica) was administered as a suspension in 0.4% Methylcellulose by oral gavage at 200mg/kg daily. Ibrutinib (MedChem Tronica) was administered as a suspension in 0.4% Methylcellulose by oral gavage at 30mg/kg daily for three weeks as a single agent or in combination with venetoclax, then via drinking water until death. For preparation of drinking water, ibrutinib was resolved in 5% HP-Cyclodextrin (PanReac Applichem) at 0.16mg/ml. Mice were allowed to drink liberally with no other source of water. Mice receiving ibrutinib drinking water received approximately 30 mg/kg ibrutinib per day (Woyach et al. 2014). Upon relapse or progression, animals were re-challenged with venetoclax for three weeks, with or without concurrent treatment with ibrutinib via drinking water.” (Flumann et al. 2023)

“For anti-CD19 CAR-T cell experiments, T cells were isolated from spleens of C57BL/6 wt mice using the Mouse CD3 T cell isolation kit (Biolegend, Cat. No. 480031), cultured and activated as previously described (Kochenderfer et al. 2010). In brief, T cells were activated *in vitro* by anti-mouse CD3e (200

ng/mL, Biolegend, clone 145-2C11), mu-rine IL-2 (100 U/mL, Novartis, 17152.00.00) and anti-mouse CD28 (100 ng/mL, Bio-legend, clone 37.51), and subsequently transduced with CAR-retrovirus. Retrovirus for transduction of T-cells was produced by HEK 293T cells co-transfected with the retroviral Moloney murine leukemia virus (MMLV)-based helper plasmids coding for the gag, pol, and env genes together with the CAR. After transduction, T-cells were stained with a polyclonal goat anti-rat IgG antibody (Biotin, Jackson Immuno, Cat. No. 112-066-072), counter-stained with Streptavidin (APC, Biolegend, Cat. No. 405207) and anti-mouse CD3 (APC, Biolegend, clone 145-2C11) to analyze transduction efficacy. To treat CD19+ lymphomas with antigen-specific T cell therapy, $2x10^6$ engineered CAR-T cells were intravenously injected into lymphoma-bearing C57BL/6 PPMBC mice (identified by MRI). Tumor response was subsequently monitored by weekly MRI and overall survival was recorded." (Flumann et al. 2023)

"For transplantation experiments, *Rag1*$^{-/-}$ mice (C57BL6/J background from Jackson Laboratories 002216) or syngeneic C57BL/6 mice (Cre-negative *Prdm1*$^{fl/fl}$; *Myd88*$^{cond.p.L252P/cond.p.L252P}$; *Rosa26*$^{LSL.BCL2\text{-}IRES\text{-}GFP/LSL.BCL2\text{-}IRES\text{-}GFP}$ breeder animals) were used as recipients. $5x10^6$ cells suspended in PBS were transplanted intraperitoneally (*Rag1*$^{-/-}$) or intravenously (syngeneic mice). All animals were housed in a specific-pathogen-free facility and animal breedings and experiments were approved by the local animal care committee and the relevant authorities (Landesamt für Natur, Umwelt und Verbraucherschutz Nordrhein-Westfalen, AZ: 84-02.04.2014.A146, 84-02.04.2017.A131, 81-02.04.2019.A009, 81-02.04.2020.A395)." (Flumann et al. 2023)

Addition for chapter 5.2 and chapter 5.3: "For samples collected from acutely treated mice, ibrutinib was administered daily by oral gavage for three days at 30mg/kg body weight, then mice were sacrificed for sample collection on the fourth day." (Flumann et al. 2024)

4.1.1 Generation of alleles

For chapter 5.1: "The generation of the *Cd19*^{Cre}, *Myd88*$^{cond.p.L252P}$ and *Rosa26*$^{LSL.BCL2\text{-}IRES\text{-}GFP}$ alleles has been described previously (Flümann et al. 2021). The *Prdm1*^{flox} allele was purchased from the Jackson Laboratory on a C57BL/6J background (Stock No: 008100) (Shapiro-Shelef et al. 2005). To generate the *Rosa26*$^{LSL.Spib.IRES.GFP}$ allele, murine *Spib* cDNA was cloned into a *Rosa26* locus-targeting vector, in which a CAGGS (cytomegalovirus early enhancer/chicken β actin) promoter drives expression of the transgene (*Spib*) as well as an internal ribosomal entry site–driven green fluorescent protein (IRES-GFP). Expression of these genes is prevented by a *LoxP*-flanked STOP cassette. This targeting vector was electroporated into BRUCE4 embryonic stem cells, which were then screened for correct integration by standard Southern blot methods. Correctly targeted ES cells were used to generate chimeras, which were backcrossed onto a pure C57BL/6J back-ground and examined for germ line transmission." (Flumann et al. 2023)

For chapter 5.2: "Generation of the *Cd79b*$^{c\text{-}p.Y195H}$ allele: The targeting vector was generated using standard techniques. The *Cd79b* wildtype sequence was based on the NCBI transcript NM_008339.2. Wildtype exons 3 to 6 were flanked by loxP sites. A polyadenylation signal (hGHpA) was inserted between the 3' UTR and the distal loxP site. Downstream of the distal loxP site, copies of exons 3 to 6 harboring the p.Y195H mutation were inserted. Additionally, a FRT-site flanked neomycin resistance cassette and an F3-flanked puromycin resistance cassette were inserted into the targeting vector, which was then electroporated into C57BL/6NTac embryonic stem cells. Positive clones were derived by dual selection with G418 and puromycin. Correct integration was verified by Southern blotting before blastocyst injection. Germline-transmitting founder animals were received and crossbred with a FlpDel line to remove the puromycin and neomycin resistance cassettes." (Flumann et al. 2024)

4.1.2 Genotyping

For all chapters: To determine the genotypes of experimental mice, PCRs from murine ear punch DNA were performed using GoTaq (Promega, M7845) according to manufacturer's instructions with the following primers (all annotated 5' → 3'):

Target allele	**Forward primer**	**Reverse primer**
Prdm1^{fl}	CAATGCTTGTCTAGTGTC	AGTAGTTGAATGGGAGC
Cd79b$^{c\text{-}p.Y195H}$	GTCTTATTAGAAACCCAACAAACC	GGTTGGGTACTTTTAACTCTTTCC
Rosa26$^{LSL.Spib.IRES.GFP}$ *Rosa26*$^{LSL.BCL2\text{-}IRES\text{-}GFP}$	GCAGGAAGCACTTGCTCTC	CGACAAGGCGTCTAGTTTATGTG
Rosa26^{wt}	GCAGGAAGCACTTGCTCTC	GATAAGGCTGCAGAAGGAGC
Cd19^{Cre}	ACAGAGGGAGGCAATGTTGT	CCCAGAAATGCCAGATTACG
Cd19^{wt}	ACAGAGGGAGGCAATGTTGT	TGCCAGACCAAAGAACTTCC
Myd88$^{cond.p.L252P}$	GCCCTTCTGACATTCAATCC	ATGGCTCTACAAACTAACACTTCC

To determine the genotypes of murine cell lines, PCRs were performed analogously from genomic DNA (see 4.2).

4.2 Generation of murine cell lines

For chapters 5.2 and 5.3: To generate murine cell lines from primary tumors, 10^7 splenocytes from autochthonous lymphomas or secondary lymphomas derived in transplanted *Rag1*$^{-/-}$ mice (see 4.1) were seeded in murine cell line medium (see 4.3). Medium was exchanged weekly until outgrowth of tumor cells was detected. As soon as reliable tumor cell proliferation was observed (cell number doubling in a week or less for at least four consecutive weeks), cells were sorted by flow cytometry to remove residual non-tumor cells and, if more than one proliferative tumor clone distinguishable by surface markers detected by flow cytometry emerged, to separate tumor clones. Cell sorting was

performed using the surface markers annotated in 4.6 on a BD FACSAria Fusion. DNA was extracted (Qiagen, 51306) and genotyped as in 4.1.2.

4.3 Tissue culture

For chapters 5.2 and 5.3: Murine cell lines of genotypes PPMBC (BWQ_296, BWQ_234, BWQ_379, BWQ_379), MBC (BIN_291, BIN_292, BIN_256), 79-PPMBC (CBU_84) and 79-MBC (BSQ_12) were cultured in mouse medium consisting of DMEM (ThermoFisher Scientific, 11960044) supplemented with 1mM Sodium Pyruvate (Thermo Fisher Scientific, 11360039), 1x MEM Non Essential Amino Acid Solution (PAN Biotech, P08-32100), 2mM L-Glutamine (Gibco, 11539876), 10% heat-inactivated FCS (Thermofisher, 10270106), 10mM HEPES (Carl Roth, 6763.2), 33µM β-Mercaptoethanol (Sigma Aldrich, SML0430), 50U/mL Penicillin and 0.05mg/mL Streptomycin. Cells were prepared for experiments by harmonizing cell density, seeding cell lines at a concentration of 250 000 cells/mL and grown at 37°C at 5% CO2 for 48 hours before each experiment.

4.4 MR imaging

For chapters 5.1 and 5.2: “Mouse MR imaging was performed as described previously (Flümann et al. 2021). In brief, mice were anesthetized with 2.5% isoflurane and scanned on a 3.0T MRI system (Igenia, Philips) with a small rodent solenoid coil (diameter 40mm, Philips Research Europe). Axial T2-weighted images of the abdomen were acquired (TSE factor: 10, TR: 2674ms, TE: 65ms, slice thickness: 1.0 mm. Images were exported in DICOM format and spleen and tumor volumes were measured by segmentation using the Horos software.” (Flumann et al. 2023)

4.5 Immunohistochemistry

For chapters 5.1 and 5.2: “Mouse tissue was Formalin-fixed and paraffin-embedded (FFPE). 4µm sections were stained for B220 (BD, clone RA3-6B2), CD138 (BD, Cat. No. 553712), Ki67 (Cell Marque), CD3 (Thermo Fisher, clone RM-9107), biotinylated PNA (Vector Laborato-ries, B-1075-5), BCL6 (CST clone D65C10) and MUM1/IRF4 (Proteintech, Cat. No. 11247-2-AP). Germinal centers were quantified from PNA stainings using the soft-ware ImageJ. Ki67+ cells per total cell count was quantified using the ImmunoRatio plugin for ImageJ.” (Flumann et al. 2023)

For chapter 5.2, the “quantification of Ki67 positive cells was performed using the QuPath software.” (Flumann et al. 2024)

4.6 Flow cytometry

For chapters 5.1 and 5.2: Single-cell suspensions from mouse spleen, lymphomas or peritoneal cavity cells were either stained immediately after collection (Fig. R3C) or collected and preserved at -80°C in FCS+10% DMSO until staining (all other figures). For flow cytometry, these samples were thawed, washed in DPBS (Thermo Fisher, 14190169) and filtered through a 35µm (Falcon, 352235) or 40µm nylon mesh (Corning, 2121462) to exclude cell clumps. To enable exclusion of dead cells, a

Zombie NIR Fixable Viability Kit (Biolegend, Cat. No. 423105) was used by incubating the samples for 15min at 4°C with diluted Zombie NIR™ dye diluted 1:2000 in 100µL DPBS, which was previously determined to be the optimal concentration. Cells were simultaneously treated with 0.25µg Mouse BD Fc Block™ (BD, 553142) to minimize unspecific binding. Then, samples were washed in DPBS and stained for 15min at 4°C "with the following fluorescent-labeled antibodies: BD Biosciences: CD45 (APC-Cy7 and Alexa Fluor700, clone 30-F11), B220 (Pacific-Blue and BV786, clone RA3-6B2), CD95/Fas (BV510, clone Jo2), CD5 (BUV496, clone 53-7.3), IgD (BUV496, clone 217-170), IgA (BV650, clone C10-1), IgM (BV711, clone II/41), CD19 (BUV395, clone 1D3), CXCR4 (PE, clone 2B11), CD38 (BUV395, clone clone 90/CD38), IgG2b (BV650, 28.0clone R12-3), IgG3 (BV650, clone R40-82), IgG1 (BV650, clone RMG1-1), BioLegend: CD3 (PerCP-Cy5.5, clone 281-2), CD138 (PE/Cy7 and PerCP-Cy5.5, clone 281.2), MHCII (AF700, clone M5-1142), CD21/CD35 (PE/Cy7, clone 7E9), CD23 (BV510, clone B3B4), CD86 (PE/Cy7, clone GL1), PLCg2 (PE, biorbyt, Cat. No. orb504888), Invitrogen: CD93 (PE, clone AA4.1), GL-7 (eFluor660, clone GL7), pPLCg2 (APC, clone 4NPRN4). Cell Signaling: pSyk (AF488, clone C87C1), Syk (AF488, clone D3Z1E). Biozol: IgG2c (AF647, Cat. No. SBA-1079-31)." (Flumann et al. 2023)

Subsequently, cells were washed in DPBS and resuspended in FACS buffer (1% BSA (Sigma, A7906) in DPBS) including 2% PFA for signal preservation, and stored at 4°C until FACS analysis within the week.

For phospho flow cytometry experiments (Fig. R13B, Fig. R25, Fig. R26B, Fig. R29D), samples were first stained for extracellular markers as above, then washed in DPBS and permeabilized using the eBioscience FoxP3/Transcription Factor Staining Buffer Set (Invitrogen, 00-5523-00), before staining for intracellular markers at 4°C overnight (pPLCg2, PLCg2, pSyk, Syk). Subsequently, cells were washed in DPBS and resuspended in FACS buffer and stored at 4°C until FACS analysis within the week.

"Flow cytometry was conducted on a Gallios flow cytometer (Beckman Coulter) or LSRFortessa cell analyzer (BD Biosciences) and data was analyzed with the FlowJo software (version 10.6.1; BD Biosciences)." (Flumann et al. 2023)

Analysis of peritoneal cavity cells was performed analogously.

The gating strategies are depicted in Fig. SR1.

For comparison of data collected in different datasets (dataset no. 1 MBC and C; dataset no. 2 79-MBC, MC, 79-C, 79-MC) as performed in Fig. R16, Fig. R17, Fig. R18, data was acquired as indicated above and B cell subsets were determined using the gating strategies in Fig. SR1. Then, data was normalized by dividing the resulting B cell subset percentages by the corresponding cell subset percentage of a wt reference sample measured in both data sets, and multiplied with the cell subset percentage of the wt reference from dataset no. 1. For Fig. R26, data was standardized by division with the respective bulk protein level of each sample, then compared.

4.7 Serum Ig analysis

For chapter 5.1: “Serum was collected from 10-week-old mice and subjected to measurement of IgA, IgM or whole IgG via ELISA, which was performed according to manufacturer’s in-structions (Thermo Fisher, Cat. No. 88-50450-22, 88-50470-88 and 88-50400-22).” (Flumann et al. 2023)

Serum collection was performed by carefully pricking the mouse cheek or tail vein and collecting the needed amount of blood in a Microvette® (Sarstedt, 20.1282). The blood was centrifuged for 10min at 2,000g before transferring the supernatant (serum) into a fresh microtube. Blood was stored at -20°C for short-term storage and then transferred to -80°C for long-term storage before usage.

4.8 3’-RNA-sequencing analysis

For chapter 5.1: “RNA was isolated from cryo-frozen tissue using a commercial kit (Qiagen). Libraries were prepared with the Lexogen QuantSeq kit according to the standard protocol. After validation (2200 TapeStation; Agilent Technologies) and quantification (Qubit System; Invitrogen, Waltham, USA) pools of cDNA libraries were generated. The pools were quantified using the KAPA Library Quantification kit (Peqlab, Erlangen, Germany) and the 7900HT Sequence Detection System (Applied Biosystems, Waltham, USA) and subsequently sequenced on an Illumina HiSeq4000 sequencer using a 1x50 bp protocol. Reads were mapped to the murine genome (mm10) and quantified using Salmon. Data was normalized and statistics were calculated using DESeq2.

Murine B cells were isolated from the peripheral blood, purified with a commercial kit (Miltenyi Biotec, 130-090-862) and treated with 10µg/ml anti-CD40 (FGK45.5, Miltenyi), 10µg/ml anti-IgM (Jackson ImmunoResearch) and 40ng/ml IL-4 (130-094-061, Miltenyi) for 24h. Germinal center cells were purified from murine spleens by a commercial kit targeting PNA (130-110-479, Miltenyi). RNA was isolated using a commercial kit (Qiagen), sequencing was performed as described above. To generate gene sets for blood activated B and germinal center B cells, differentially expressed genes between the two groups were identified. A minimum fold change of 2 and a minimum p value of 0.01 were used as thresholds. Gene set analysis was then performed using the FGSEA package (R). ssGSEA scores were calculated with the corto R package.” (Flumann et al. 2023)

For chapter 5.2 and 5.3: “RNA was isolated from cryopreserved tissue using a commercial kit (Qiagen, 74004). RNA samples were processed and sequenced as previously described (Flümann et al. 2021). For the purpose of data analysis, we initially measured the RNA levels using kallisto (Bray et al. 2016), which involved pseudoaligning the reads to the mm10 reference genome. The variant annotation was performed using the Varian Effect Predictor (VEP), based on the gene definitions from the GRCm38.p6 mouse reference genome as represented in the Ensembl database version 96. To ensure uniformity, MGI Gene symbols were converted using tximport (Soneson, Love, and Robinson 2015), and the counts were imported as length-scaled transcripts per million. To account for

normalization factors related to batch, tissue type, and genotype, as well as perform subsequent differential analyses, we employed DeSeq2." (Flumann et al. 2024)

4.9 BCR sequencing

For chapter 5.1: "PNA$^+$ cells were isolated by MACS-sorting (Germinal Center B Cell (PNA) MicroBead Kit, mouse, Miltenyi Biotec, 130-110-479). The BCR sequencing of PNA$^+$ cells was performed using a commercial kit (NEB, NEBNext immune sequencing kit mouse). To assemble the raw sequencing data into unique sequences (unique combinations of barcodes and BCR sequence), the pRESTO package (Vander Heiden et al. 2014) was employed, according to the kit manufacturer's recommendations. Individual deduplicated sequences were then processed using the IgBlast software (Ye et al. 2013) and the output analyzed for V, D, J gene usage as well as somatic hypermutation rate. The isotype of each read is given in the pRESTO output and determined by aligning the C gene-specific primer sequences used during library preparation.

The library preparation for the BCR receptor sequencing data in Fig. R7 was performed as described previously (Flümann et al. 2021). Sample demultiplexing and assembly was performed employing the published MIGEC pipeline. To assess clone sizes, the MIGEC output was further processed using a custom R script. Clones were assembled by connecting subclonal sequences that differ by only a single mismatch. The resulting networks were visualized with the software Gephi. Gini coefficients were calculated for the dominant clones of each sample with the R package 'reldist'.

For SHM and isotype analysis in lymphoma samples, a commercial kit for full-length Ig sequencing was employed (NEBNext immune sequencing kit mouse). The reads were process using the pRESTO package. The assembled and deduplicated reads were processed with a custom R script to define individual clones by connecting sub-clonal sequences with a distance of 1bp. The dominant clone sequences were analyzed using IgBlast to determine nucleotide and amino acid changes from germline." (Flumann et al. 2023)

For chapter 5.2: "RNA was isolated from cryo-preserved lesions that were histologically characterized as lymphoma (Qiagen, 74004). PNA$^+$ germinal center B cells were isolated using a commercial kit for magnetic separation (Miltenyi, 130-110-479) and served as controls. Libraries were then produced with the NEBNext Immune Sequencing kit (NEB, E6330), following the manufacturer's protocol. Libraries were sequenced on an Illumina MiSeq device (MiSeq Reagent Kit v3, 600 cycles). The derived sequences were processed with the pRESTO toolkit (Vander Heiden et al. 2014). Samples with less than 1,000 unique molecular identifiers (UMIs) or unproductive rearrangements were excluded from further analysis. Heavy and light chain consensus sequences were further processed separately. Individual consensus sequences were combined to one clone if they differed by two or less nucleotides. The clone size was determined by the number of associated UMIs. Circular clonality plots were generated with the software Gephi." (Flumann et al. 2024)

4.10 Whole exome sequencing (WES)

For chapter 5.1: “DNA was isolated from cryo-preserved PPMBC, SMBC and MBC tumors, as well as human FFPE samples, after written informed consent was provided by the patients. Whole exome sequencing was performed on an Illumina NovaSeq6000 according to previously published protocols (Flumann et al. 2023; Herling et al. 2018). By means of the BWA mem aligner, we aligned raw sequencing reads of the mouse samples to the reference genome mm10 and the human samples to the reference genome hg19. Identical read pairs that rep-resent possible PCR duplicates were masked out after alignment. All overlapping regions between the read pairs are considered only once in the analysis. Due to a lack of matched normal for some tumor specimens, we generated a representative non-tumor sample by combining normals matching to some tumor samples. Our in-house cancer genome analysis pipeline is used for mutation and copy number alteration calling (Cun et al. 2018; Peifer et al. 2012). To correct for genotypes that are not captured by representative normal, we filtered out called mutations that were exactly the same in more than one tumor sample.” (Flumann et al. 2023)

For chapter 5.2: “DNA was isolated from cryopreserved tissue using a commercial kit (Qiagen, 69504). Whole exome sequencing was performed on an Illumina NovaSeq6000, as previously published (Flümann et al. 2021). FASTQ files were trimmed using cutadapt (Martin 2011) and subsequently mapped to the mm10 reference genome using Burrows-Wheeler aligner (Li and Durbin 2009). Mapped BAM files were cleaned using Picard tools [Broad Institute]. We followed the GATK best practices recommendations (DePristo et al. 2011; McKenna et al. 2010). Briefly, raw DNA sequence data (SAM files) were initially cleaned using Picard tools using a 'LENIENT' validation stringency. Additional steps included storing read group information and marking duplicates. Consistently, SAMtools (Danecek et al. 2021) were used to sort/index reads. Base calibration was performed using the GATK toolkit (Danecek et al. 2021). Reference files were used as described previously (Lange et al. 2020). For calling a normal reference file, we used a matching normal described previously (Flumann et al. 2023). Further analysis of tumor purity estimations, copy number analysis, and mutation calling involved ABSOLUTE (Carter et al. 2012), Manta (Carter et al. 2012), Copywriter (Kuilman et al. 2015), Mutect2 (McKenna et al. 2010), and Strelka2 (Kim, Scheffler, et al. 2018). Variants were annotated using VEP (McLaren et al. 2016), and visualizations were partially used from maftools (Mayakonda et al. 2018).” (Flumann et al. 2024)

4.11 CAR-T co-culture experiments

For chapter 5.2: “For co-culture experiments, anti-CD19 CAR-T cells were co-cultured with a CD19+ PPMBC lymphoma cell line for 48 hours [see 4.3]. Subsequently, cell counts were analyzed by flow cytometry after staining for CD3 (PE, Biolegend, clone 145-2C11) and CD19 (V500, BD Biosciences, Clone 1D3) after gating for Zombie-negative live cells.” (Flumann et al. 2023)

4.12 B cell receptor internalization

For chapter 5.2: Goat F(ab')2 Anti-Mouse IgM-LE/AF (Southern Biotech, 1023-14) was biotinylated using the EZ-Link Sulfo-NHS-Biotinylation Kit (Thermo Scientific, 21425) following manufacturer's instructions. Using a commercial CD43 magnetic separation kit (Miltenyi, 130-049-801), $CD43^-$ naïve B cells were isolated using LD columns (Miltenyi, 130-042-901) from splenocytes of $Cd19^{Cre/wt}$ and $Cd19^{Cre/wt};Cd79b^{c\text{-}p.Y195H/wt}$ mice following manufacturer's instructions. 500 000 cells per condition were kept at 4˚C in 200µL murine cell line media (see 4.3) and surface BCR was labeled with biotin-conjugated anti-IgM Fab (Jackson ImmunoResearch, 115-067-020) at a dilution of 1:200 or with biotin-conjugated anti-IgM F(ab')2 (see above) at a dilution of 1:133.3 for 30 min. After staining, cells were incubated for 0, 5, 10, 20, 30, 40, 50 and 60min at 37˚C, fixed with 0.5% PFA and stored on ice. Surface-accessible BCR was subsequently stained with 1:200 streptavidin Alexa Fluor 647 (Thermo Fisher, S32357) and 1:200 BUV395 CD19 (BD Biosciences, clone 1D3). Cells were analyzed on a LSRFortessa cell analyzer (BD Biosciences) and data was analyzed with the FlowJo software (version 10.6.1; BD Biosciences).

4.13 Proximity ligation assays

For chapter 5.2: "Formalin-fixed and paraffin-embedded spleen or tumor tissues from mice were cut into 4 µm sections and used for proximity ligation assays (PLAs) with Duolink® In Situ Detection Reagents Red according to the manufacturer's instructions (Sigma, DUO92008). Briefly, FFPE sections were deparaffinized in xylene and subsequently rehydrated in graded alcohol and distilled water. After heat-induced antigen retrieval at pH 6.0 for 30 minutes, slides were placed in PBS and tissue was permeabilized for 10 minutes in ice cold methanol, briefly washed in PBS and then blocked for 30 minutes at room temperature using Duolink® blocking buffer. Tissue was then incubated with the antibody mix overnight at 4°C. Primary antibodies were previously conjugated according to the Duolink® PLA probemaker protocol to PLUS (MYD88, abcam, ab2064; Probemaker Plus, DUO92009) and MINUS (BTK, Cell Signaling, 94988; MALT1, Thermo Fisher, PA5-114500; CD79B, abcam, ab240083; Probemaker Minus, DUO92010) PLA oligonucleotides and diluted 1:50 with Probemaker Assay Reagent and Assay Diluent to generate the antibody mix. For the isotype controls, a rabbit IgG isotype control (abcam, ab37415) was conjugated to PLUS and MINUS PLA oligonucleotides and applied using the same protocol. On the following day, slides were washed in PBS, then ligation and rolling circle amplification steps were performed using the Duolink® In Situ Detection Reagent Red following the manufacturer's protocol. 79-MBC and MBC tissue was counterstained with DAPI (BD Pharmingen, 564907, 1µg/mL), 79-PPMBC and PPMBC tissue was counterstained with 1:50 BV421 rat-anti mouse CD45R/B220 (BD Horizon, Cat. No. 562922). Tissue slices were mounted in Prolong Diamond Antifade Mountant (Invitrogen, P36961). Imaging was performed using a Leica SP8-DLS Confocal microscope. Four images per slide were acquired, each capturing at least 100 cells. PLA spots were counted using

FIJI software (Version 2.9.0/1.53t) and normalized either to total cell count (MBC/ 79-MBC) or count of $B220^+$ -cells (PPMBC/ 79-PPMBC). PLA counts from different batches were compared by normalizing to a reference sample that was included in both batches. This batch normalization was performed on the data sets visualized in Fig. R29A,B**."** (Flumann et al. 2024)

4.14 Metabolomics

For chapter 5.3: For metabolomics analysis of spleen and lymphoma tissue, tissue samples of ~300mg were snap-frozen and stored at -80°C before usage. Samples were disintegrated to a fine powder while frozen using a TissueLyser (Qiagen) for 2 runs, each 2mins at 30Hz. Then, 1 mL of -20°C-cold extraction buffer containing 50% methyl-tert-butyl-ether (Sigma, 306975), 30% methanol (Fisher Chemical, A456-212) and 20% MS-grade water (Honeywell, 14263) supplemented with internal standards (0.25µM U-$^{13}C^{15}N$ amino acids, Cambridge isotopes, 79248; 0.1µg/mL $^{13}C_{10}$ ATP, Sigma, 710695; 10ng/mL citric acid D_4, Sigma, 485438; 10ng/mL EquiSPLASH^{TM} LIPIDOMIX standard, Avanti Polar lipids, 30731) was added to each sample. Samples were sonicated until disintegration and incubate for 30mins in a thermomixer (Eppendorf), at 4°C and 1500rpm. Samples were then centrifuged for 10min at 21000g at 4°C before transferring the supernatant to a fresh tube. 200 µL methyl-tert-butyl-ether and 150 µL LC-grade water were added and the suspension was incubated for another 10mins at 15°C, 1500rpm in a thermomixer. Samples were centrifuged (5min, 15°C, 16000g) and the liquid phases were separated into fresh tubes (upper phase containing lipids, lower phase containing polar metabolites). Liquid was evaporated in a Speed Vac concentrator (Eppendorf) at 20°C and 1000rpm and samples were stored at -80°C until MS analysis. MS analysis was performed by the Metabolomics core facility of the Max Planck Institute for Biology of Ageing. The following detailed descriptions were provided courtesy of Patrick Giavalisco, head of the Metabolomics core facility.

Data was analyzed using R 4.3.2.

4.14.1 Anion-Exchange Chromatography Mass Spectrometry (AEX-MS) for the analysis of anionic metabolites

"Extracted metabolites were re-suspended in 150µl of UPLC/MS grade water (Biosolve), of which 100 µl were transferred to polypropylene autosampler vials (Chromatography Accessories Trott, Germany) before AEX-MS analysis.

The samples were analysed using a Dionex ionchromatography system (Integrion Thermo Fisher Scientific) as described previously (Schwaiger et al. 2017). In brief, 5µL of the resuspended polar metabolite extract were injected in push-partial mode, using an overfill factor of 1, onto a Dionex IonPac AS11-HC column (2mm × 250mm, 4µm particle size, Thermo Fisher Scientific) equipped with a Dionex IonPac AG11-HC guard column (2mm × 50mm, 4µm, Thermo Fisher Scientific). The column temperature was held at 30°C, while the auto sampler temperature was set to 6°C. A potassium

hydroxide gradient was generated using a potassium hydroxide cartridge (Eluent Generator, Thermo Scientific), which was supplied with deionized water (Milli-Q IQ 7000, Millipore). The metabolite separation was carried at a flow rate of 380 µL/min, applying the following gradient conditions: 0-3min, 10mM KOH; 3-12min, 10−50mM KOH; 12-19min, 50-100mM KOH; 19-22min, 100mM KOH, 22-23min, 100-10mM KOH. The column was re-equilibrated at 10mM for 3min.

For the analysis of metabolic pool sizes the eluting compounds were detected in negative ion mode using full scan measurements in the mass range m/z 77 – 770 on a Q-Exactive HF high resolution MS (Thermo Fisher Scientific). The heated electrospray ionization (ESI) source settings of the mass spectrometer were: Spray voltage 3.2kV, capillary temperature was set to 300°C, sheath gas flow 50AU, aux gas flow 20AU at a temperature of 330°C and a sweep gas glow of 2AU. The S-lens was set to a value of 60.

The IC-MS data analysis was performed using the open-source software El Maven (Agrawal et al. 2019) (Version 0.12.0). For this purpose, Thermo raw mass spectra files were converted to mzML format using MSConvert (Chambers et al. 2012) (Version 3.0.22060, Proteowizard). The identity of each compound was validated by authentic reference compounds, which were measured at the beginning and the end of the sequence. For data analysis the area of the deprotonated $[M\text{-}H^{+}]^{-1}$ or doubly deprotonated $[M\text{-}2H]^{-2}$ mass peaks of every required compound was extracted and integrated using a mass accuracy <5 ppm and a retention time (RT) tolerance of <0.05 min as compared to the independently measured reference compounds.

Peak areas were then normalized to internal standards, followed by a normalization to the protein content or the cell number of the analyzed samples." – Patrick Giavalisco

4.14.2 Semi-targeted liquid chromatography-high-resolution mass spectrometry-based (LC-HRS-MS) analysis of amine-containing metabolites

"The LC-HRMS analysis of amine-containing compounds was performed using a QE-Plus high-resolution mass spectrometer coupled to a Vanquish UHPLC chromatography system (Thermo Fisher Scientific). In brief: 50µL of the available 150µL of the above mentioned (AEX-MS method) polar phase were mixed with 25µl of 100mM sodium carbonate (Sigma), followed by the addition of 25µl 2% [v/v] benzoylchloride (Sigma) in acetonitrile (UPC/MS-grade, Biosove, Valkenswaard, Netherlands), as reported previously (Wong et al. 2016). The derivatized samples were thoroughly mixed and kept at a temperature of 20°C until analysis.

For the LC-HRMS analysis, 1µl of the derivatized sample was injected onto a 100 x 2.1mm HSS T3 UPLC column (Waters). The flow rate was set to 400µl/min using a binary buffer system consisting of buffer A (10 mM ammonium formate (Sigma), 0.15% [v/v] formic acid (Sigma) in UPC-MS-grade water (Biosove, Valkenswaard, Netherlands). Buffer B consisted of acetonitrile (IPC-MS grade, Biosove, Valkenswaard, Netherlands). The column temperature was set to 40°C, while the LC gradient was: 0%

B at 0min, 0-15% B 0- 4.1min; 15-17% B 4.1 – 4.5min; 17-55% B 4.5-11min; 55-70% B 11 – 11.5min, 70-100% B 11.5 - 13min; B 100% 13 - 14min; 100-0% B 14 -14.1min; 0% B 14.1-19min; 0% B. The mass spectrometer (Q-Exactive Plus) was operating in positive ionization mode recording the mass range m/z 100-1000. The heated ESI source settings of the mass spectrometer were: Spray voltage 3.5kV, capillary temperature 300°C, sheath gas flow 60AU, aux gas flow 20AU at 330°C and the sweep gas was set to 2 AU. The RF-lens was set to a value of 60.

The LC-MS data analysis was performed using the open-source software El Maven (Agrawal et al. 2019) (Version 0.12.0). For this purpose, Thermo raw mass spectra files were converted to mzML format using MSConvert (Chambers et al. 2012) (Version 3.0.22060, Proteowizard). The identity of each compound was validated by authentic reference compounds, which were measured at the beginning and the end of the sequence. For data analysis the area of the protonated [M + nBz + H]+ (nBz stands for the number of benzoyl moieties attached to each compound). Extracted ion chromatograms were generated with a mass accuracy of <5ppm and a retention time (RT) tolerance of <0.05 min as compared to the independently measured reference compounds. These areas were then normalized to the internal standards, which were added to the extraction buffer, followed by a normalization to the protein content or the cell number of the analyzed samples." – Patrick Giavalisco

4.14.3 Liquid Chromatography-High Resolution Mass Spectrometry-based (LC-HRMS) analysis of lipids

"The stored (-80°C) lipid extracts were re-suspended in 300µL of a UPLC-grade acetonitrile: isopropanol (70:30 [v:v]) mixture, followed by vortexing and 10min incubation on a thermomixer at 4°C. The re-suspended samples were cleared by a 5min centrifugation at 10.000xg and the supernatants were transferred to 2ml glass vials with 200µl glass inserts (Chromatography Zubehör Trott, Germany), which were placed in an Acquity iClass UPLC (Waters) sample manager at 6°C. The UPLC was connected to a Tribrid Orbitrap HRMS, equipped with a heated ESI (HESI) source (ID-X, Thermo Fischer Scientific).

Of each lipid sample 2µl were injected onto a 100 x 2.1mm CSH C18 UPLC column, packed with 1.7µm particles (Waters). The flow rate of the UPLC was set to 350µl/min and the buffer system consisted of buffer A (10mM ammonium acetate, 0.1% acetic acid in water/acetonitrile [4:6] and buffer B (10mM ammonium acetate, 0.1% acetic acid in UPLC-grade acetonitrile/isopropanol 1:9 [v/v]). The UPLC gradient was as follows: 0-1min 75% A, 1-2min 75-60% A, 2-4min 60-42% A, 4-6min 42-38% A, 6-9min 38-30% A, 9-11min 30-27% A, 11-13min 27-22%, 13-15.8min 22-0% A, , 15.8-16min 0% A, 16-16.10-75% A and 16.1-20min 75% A. This leads to a total runtime of 20min per sample.

The ID-X mass spectrometer was operating either for the first injection in positive ionization mode or for the second injection in negative ionization mode. In both cases, the analyzed mass range was between m/z 150-1500. The resolution was set to 120.000, leading to approximately 4 scans per

second. The RF lens was set to 40%, while the AGC target was set to 100%. The maximal ion time was set to 100ms and the HESI source was operating with a spray voltage of 3.5kV in positive ionization mode, while 3.2kV were applied in negative ionization mode. The ion tube transfer capillary temperature was 300°C, the sheath gas flow 60 arbitrary units (AU), the auxiliary gas flow 20AU and the sweep gas flow was set to 1AU at 330°C.

All samples were analyzed in a randomized run-order.

Targeted data analysis was performed using the quan module of the TraceFinder 5.1 software (Thermo Fischer Scientific) in combination with a sample-specific in-house generated compound database. For the analysis of untargeted lipidomic data mMZmine (version 2.3) was used (Pluskal et al. 2010)." – Patrick Giavalisco

4.15 SeaHorse

For chapter 5.3: For SeaHorse experiments, the Agilent Seahorse XF Real-Time ATP Rate Assay Kit (Agilent, 103593) was used according to manufacturer's instructions. Briefly, 250,000cells/well were seeded in DPBS (Thermo Fisher, 14190169) on a SeaHorse plate and allowed to attach for 30min at room temperature. In the meantime, treatment compounds were prepared in a sensor cartridge hydrated overnight on SeaHorse XF Calibrant (Agilent, 100840-000) using SeaHorse DMEM (Agilent, 103680-100) supplemented with 1mM Pyruvate (Agilent, 103578-100), 10mM Glucose (Agilent, 103577-100) and 2mM Glutamine (Agilent 103579-100). SeaHorse measurement was performed using a Seahorse XFe96 Analyzer and normalized using cell counts via Cytation 5 (Fig. R33A, Fig. SR7A) or by protein amounts (Fig. R33B&C). For normalization by protein amounts, SeaHorse medium was removed and cells were resuspended in 10µL 4% SDS (Carl Roth, 2326.2) in DPBS per well and frozen at -20°C. The next day, protein amounts were determined using a Pierce™ BCA Protein Assay Kit (Thermo Fisher, 26619) according to manufacturer's instructions in a Tecan Spark plate reader.

4.16 Ibrutinib sensitivity and combination screen

For chapter 5.3: To determine ibrutinib sensitivity of murine cell lines, 10 000 cells/well per cell line were seeded on a 96-well plate and treated with DMSO or ibrutinib at concentrations of 0.0512nM to 20mM in triplicates. After 3 days of incubation at 37°C, cell viability was determined using alamarBlue™ cell viability reagent (Invitrogen, A50101) according to manufacturer's instructions in a Tecan Spark plate reader.

For the combination screen of ibrutinib and IACS-010759 (sellekchem, S8731), 2500 cells/well per cell line were seeded in a 365-well-plate. Cells were treated with ibrutinib of concentrations of 1nM to 20mM and IACS-010759 at concentrations of 0.6nM to 12.5mM in quadruplicates. After 3 days of incubation at 37°C, cell viability was determined using alamarBlue™ cell viability reagent (Invitrogen, A50101) according to manufacturer's instructions in a Tecan Spark plate reader.

Cell viability data was analyzed by normalizing fluorescence data to the DMSO-treated controls and modeling it to a Hill function (Gesztelyi et al. 2012), using R 4.3.2. For the combination screen, the CIcomputeR package (Zhang, Fu, and Chou 2016) was used.

5 Results

5.1 Distinct genetically determined origins of *Myd88/BCL2*-driven aggressive lymphoma rationalize targeted therapeutic intervention strategies

5.1.0 Contributions

Chapter 5.1 is based on the following publication in *Blood Cancer Discovery*:

Flumann, R., J. Hansen, B. W. Pelzer, P. Nieper, T. Lohmann, I. Kisis, T. Riet, V. Kohlhas, P. H. Nguyen, M. Peifer, N. Abedpour, G. Bosco, R. K. Thomas, M. Kochanek, J. Knufer, L. Jonigkeit, F. Beleggia, A. Holzem, R. Buttner, P. Lohneis, J. Meinel, M. Ortmann, T. Persigehl, M. Hallek, D. P. Calado, M. Chmielewski, S. Klein, J. R. Gothert, B. Chapuy, B. Zevnik, F. T. Wunderlich, B. von Tresckow, R. D. Jachimowicz, A. M. Melnick, H. C. Reinhardt and G. Knittel (2023). "Distinct Genetically Determined Origins of Myd88/BCL2-Driven Aggressive Lymphoma Rationalize Targeted Therapeutic Intervention Strategies." Blood Cancer Discov 4(1): 78-97.

The following figures were retrieved from the publication: Fig. R1A, R1B, R2, R3, R4, R5, R6, R7, R8, R9, R10, R11, R12, R13B except for rightmost panel, R14; and Appendix SR1

The following figures were generated solely for this thesis: R1C, R13B rightmost panel; and Appendix SR2, SR3B

Detailed author contributions relevant for experiments shown in this thesis are as following:

R. Flümann, H.C. Reinhardt, G. Knittel, P. Nieper, M. Chmielewski conceptualized and designed the project.

R. Flümann and F. T. Wunderlich generated the novel *Spib* allele and confirmed its function. R. Flümann coordinated breeding of all mice.

R. Flümann, J. Hansen and J. Knüfer monitored the mice, performed autopsies, and took all mouse samples.

R. Flümann, J. Hansen, L. Jonigkeit performed MRI analyses.

J. Hansen and B. Pelzer designed the flow cytometry panels. J. Hansen established and optimized flow cytometry panels and acquired flow cytometry data. J. Hansen and R. Flümann analyzed the flow cytometry data.

R. Flümann analyzed immunohistochemistry stainings.

R. Flümann measured serum immunoglobulin levels by ELISA.

R. Flümann, J. Hansen and J. Knüfer prepared samples for transcriptomic analyses and whole-exome sequencing (WES). G. Knittel and S. Klein analyzed transcriptomes and WES.

G. Knittel and R. Flümann prepared BCR sequencing. G. Knittel analyzed BCR sequencing.

J. Hansen and J. Knüfer performed *Rag1*$^{-/-}$ engraftment experiments.

T. Riet prepared the CAR-T construct, performed *in vitro* CAR-T experiments and supplied CD19 CAR-T cells. J. Hansen and J. Knüfer performed *in vivo* CAR-T experiments.

R. Flümann performed treatment experiments with venetoclax and ibrutinib.

G. Knittel and R. Flümann performed statistical analyses of all experiments.

Resources were contributed by T. Lohmann, G. Bosco, R.K. Thomas, R. Büttner, T. Persigehl, M. Hallek, D.P. Calado, M. Chmielewski, J.R. Göthert, B. Chapuy, B. Zevnik, F.T. Wunderlich, B. von Tresckow, R.D. Jachimowicz, A.M. Melnick, H.C. Reinhardt.

A complete list of contributions, including for publication aspects not part of this thesis, is found in chapter 7.

5.1.1 Genetic alterations predispose for lymphomas with different dependencies

Our previously published MBC mouse model recapitulated many characteristics of human DLBCL and could be used for pre-clinical treatment testing (Flümann et al. 2021; Knittel et al. 2016). However, MBC lymphomas were found to be $CD138^{+}B220^{-}$, hinting at a close relationship to the plasmablastic lineage, which is rarely seen in DLBCL patients. Therefore, we reanalyzed available patient whole-exome sequencing (WES) data (Chapuy et al. 2018; Schmitz et al. 2018), and found that the majority of cases carrying characteristic *MYD88* mutations displayed additional genetic alterations conferring a plasma cell differentiation block (Fig. R1A). *PRDM1*, which is the master regulator of plasma cell differentiation (Shapiro-Shelef et al. 2005), was frequently lost via *PRDM1* loss-of-function mutations and deletions of the *PRDM1* locus (*6q* or *6q21*). Another observed mechanism leading to plasma cell differentiation arrest was the amplification of the locus of *SPIB* (located on *19q*), a transcription factor suppressing plasma cell differentiation by inhibiting the expression of *PRDM1* (Horiuchi et al. 2023). Additionally, mutations of *TBLXR1* and increased activation of *BCL6* by fusion or structural variation have been shown to prevent GC B cell differentiation (Basso and Dalla-Favera 2012a; Venturutti et al. 2020). Taken together, 90% (46/51) of *MYD88*-mutant MCD cases and 79% (19/24) of *MYD88*-mutant C5 cases carried at least one of these genetic alterations, prompting us to investigate the role of a plasma cell differentiation block in our MBC mouse model.

To this end, a loxP-flanked *Prdm1* allele (Shapiro-Shelef et al. 2005) to conditionally delete *Prdm1* in B cells carrying $Cd19^{Cre}$ was acquired (Fig. R1B). Additionally, a novel *Spib* overexpression allele by inserting a *Spib.IRES.GFP* site with a *loxP.STOP.loxP* cassette into the *Rosa26* locus was generated (Fig. R1B), mediating *Spib* overexpression dependent on Cre-mediated excision of the STOP cassette (Flumann et al. 2023). Both alleles were combined with our existing MBC mouse model, generating

- The PPMBC mouse model (***P****rdm1*$^{fl/fl}$*; **M**yd88*$^{cond.p.L252P/wt}$*; Rosa26*$^{LSL.\mathbf{B}CL2.IRES.GFP/wt}$*; **C**d19*$^{Cre/wt}$*)*
- The SMBC mouse model (***M****yd88*$^{cond.p.L252P/wt}$*; Rosa26*$^{LSL.\mathbf{B}CL2.IRES.GFP/LSL.\mathbf{S}pib.IRES.GFP}$*; **C**d19*$^{Cre/wt}$)

(Please note that the genetic generation of the PPMBC and SMBC mouse models took place without involvement by J. Hansen and is described here for explanatory reasons.)

To characterize both mouse models before and after onset of malignancy, we investigated two cohorts of mice. To analyze the premalignant phenotype, we sacrificed 10-week-old mice, an age at which no signs of lymphoma could be detected yet. For in depth analysis of the terminal phenotype, we monitored mice longitudinally up to an age of 100 weeks and sacrificed them at predefined termination criteria (such as highly enlarged spleens or tumors, see 4.1, Fig. R1C).

Chapter 5.1 begins with the characterization of the PPMBC and SMBC mouse models, first before signs of malignancy (premalignant phenotype, 5.1.2), followed by analysis of animal and tumor phenotype upon lymphoma development (5.1.3-5.1.6). Subsequently, several treatment options are tested in the PPMBC model (5.1.7-5.1.8).

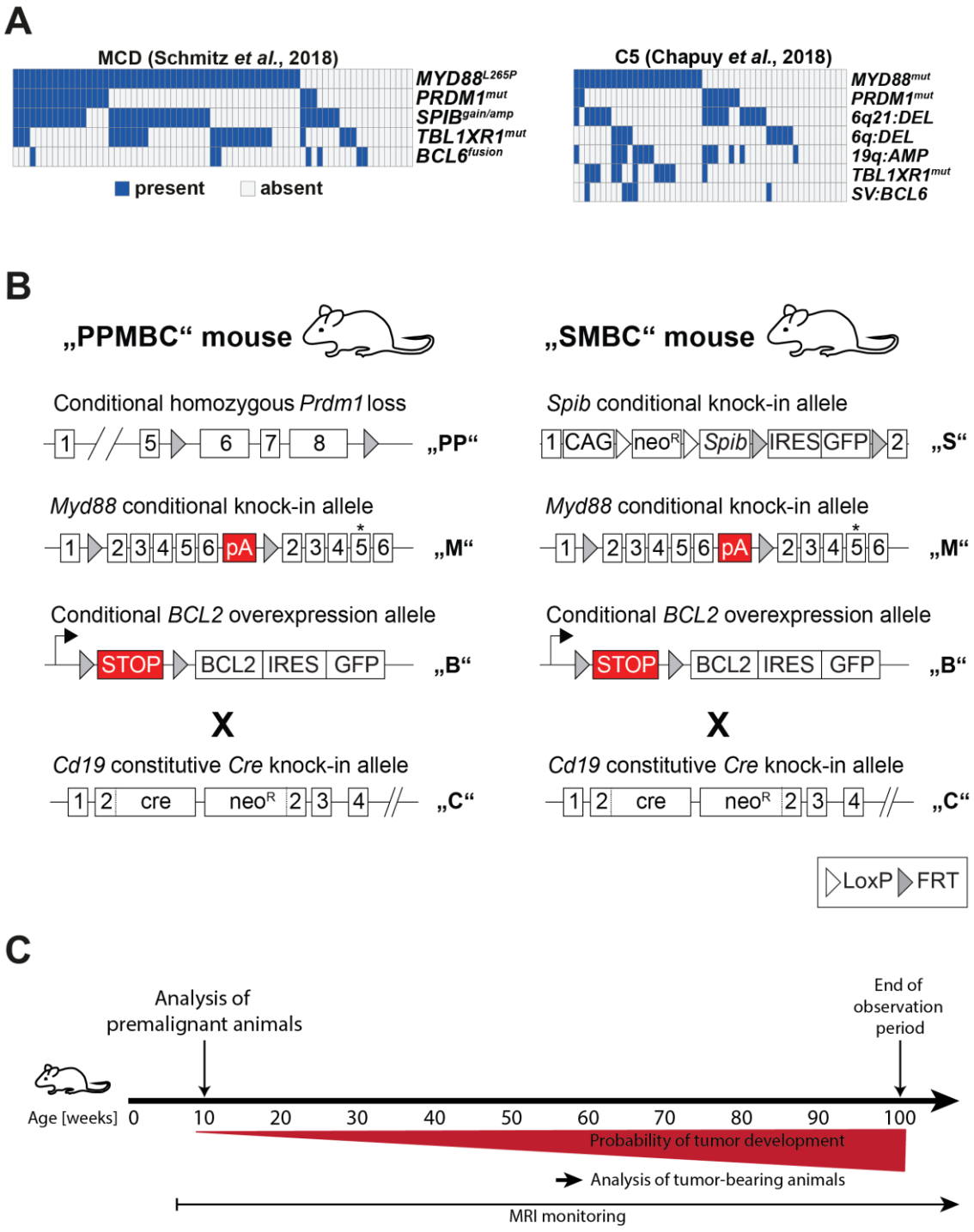

Figure R1 MCD/C5 DLBCL frequently carries a plasma cell differentiation block. *(A) Analysis of genetic data from (Chapuy et al. 2018; Schmitz et al. 2018) reveals high incidence of genetic alterations mediating a plasma cell differentiation block in* MYD88*-mutated DLBCL patients. (B) Alleles used to generate the PPMBC and SMBC mouse models for modeling DLBCL with a plasma cell differentiation block. (C) SMBC and PPMBC mice were analyzed at two time points, premalignant animals at an age of 10 weeks and tumor-bearing animals upon tumor development, see text and section 4.1. loxP locus-of x-over, FRT flippase recognition target, MRI Magnetic resonance imaging, pA polyadenylation site, * mutation, STOP stop codon, neo^R neomycin resistance cassette, IRES internal ribosome entry site.*

5.1.2 Deletion of *Prdm1* and overexpression of *Spib* block plasma cell differentiation

Already at 10 weeks of age, first effects of *Prdm1* deletion and *Spib* overexpression could be observed in PPMBC and SMBC mice. Using magnetic resonance imaging (MRI), we observed significantly increased spleen volumes in SMBC and PPMBC mice compared to MBC and *Cd19*$^{cre/wt}$ (C) controls (Fig. R2). This change became more pronounced at 20 weeks of age, when SMBC and PPMBC demonstrated ~2-fold increased spleen volumes compared to MBC mice, which in turn had ~2-fold increased spleen volumes compared to C mice. This hints at an increased lymphocyte pool leading to accelerated spleen growth, reinforced by the additional genetic alterations induced in the SMBC and PPMBC mouse model.

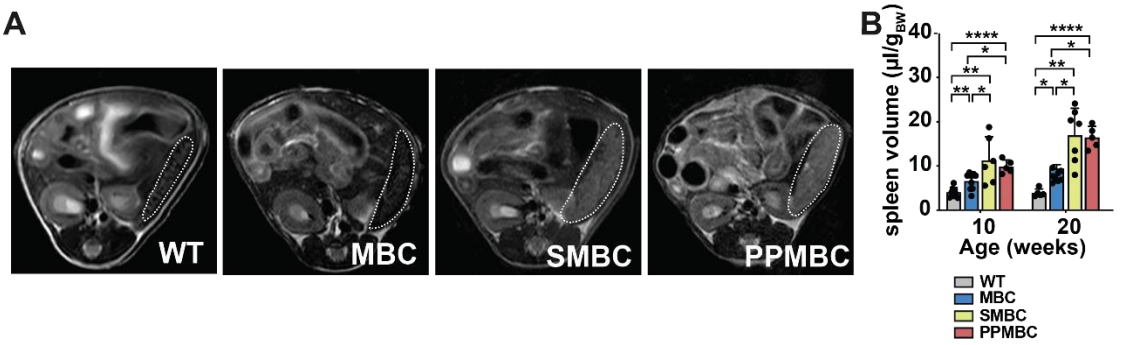

Figure R2 SMBC and PPMBC mice display splenomegaly early-on*. (A) Representative MRI sections of the abdomen of 10-week-old mice of the respective genotypes. The spleen is outlined in white. (B) Quantification of spleen volumes of 10- and 20-week-old mice by MRI (wt, n ≥ 5; MBC, n = 6; SMBC, n ≥ 6; and PPMBC, n = 5). *p≤0.05, **p≤0.01, ***p≤0.001, ****p≤0.0001. Welch unpaired two-tailed t test, error bars represent SD.*

To further investigate this first indication of expedited malignant lymphoproliferation, we sacrificed mice at 10 weeks of age and extracted splenocytes and peritoneal cavity cells to study present B-cell subsets. An increased B cell subset could indicate the potential lymphoma founder population in our model, providing insight into murine lymphomagenesis. To characterize the immune cell populations, we used flow cytometry to investigate the following B cell populations: CD19^{+}B220^{-} B-1 cells (B1), innate-like B cells involved in rapid infection response and mainly found in the peritoneal cavity, with CD5^{+} effector B1a cells and CD5^{-} B1b cells with memory function in immune protection (Haas 2015); CD23^{-}CD21^{+} marginal zone B cells (MZB) residing adjacent to the splenic sinus involved in response to T cell-independent antigens; CD23^{+}CD21^{+} follicular B cells (FoB), the dominant mature B cell subset located in lymphoid follicles; and CD138^{+} plasmablasts (PBs) which secrete antibodies (Wong et al. 2019; Nutt et al. 2015). For flow cytometry gating strategies see Fig. SR1.

MBC and SMBC splenocytes displayed significantly decreased CD19^{+}B220^{-} B1 levels compared to C mice (*Cd19*$^{Cre/wt}$), while PPMBC splenic CD19^{+}B220^{-} B1 levels were significantly increased (Fig. R3A). Interestingly, the ratio between CD5^{+} B1a and CD5^{-} B1b cells was altered as well: While CD5^{+} B1a cell levels were decreased, CD5^{-} B1b cells showed significantly increased levels in MBC, SMBC and PPMBC mice compared to C mice (Fig. R3A). When looking at B-cell subsets in general, all three models showed increased CD19^{+}B220^{+} B cell levels, as expected from the induced malignant genetic alterations (Fig.

R3B). However, $CD23^{-}CD21^{+}$ MZB pools were significantly decreased in MBC and SMBC, but not PPMBC spleens. $CD23^{+}CD21^{+}$ FoB populations, on the other hand, were increased in MBC and SMBC spleens (Fig. R3B).

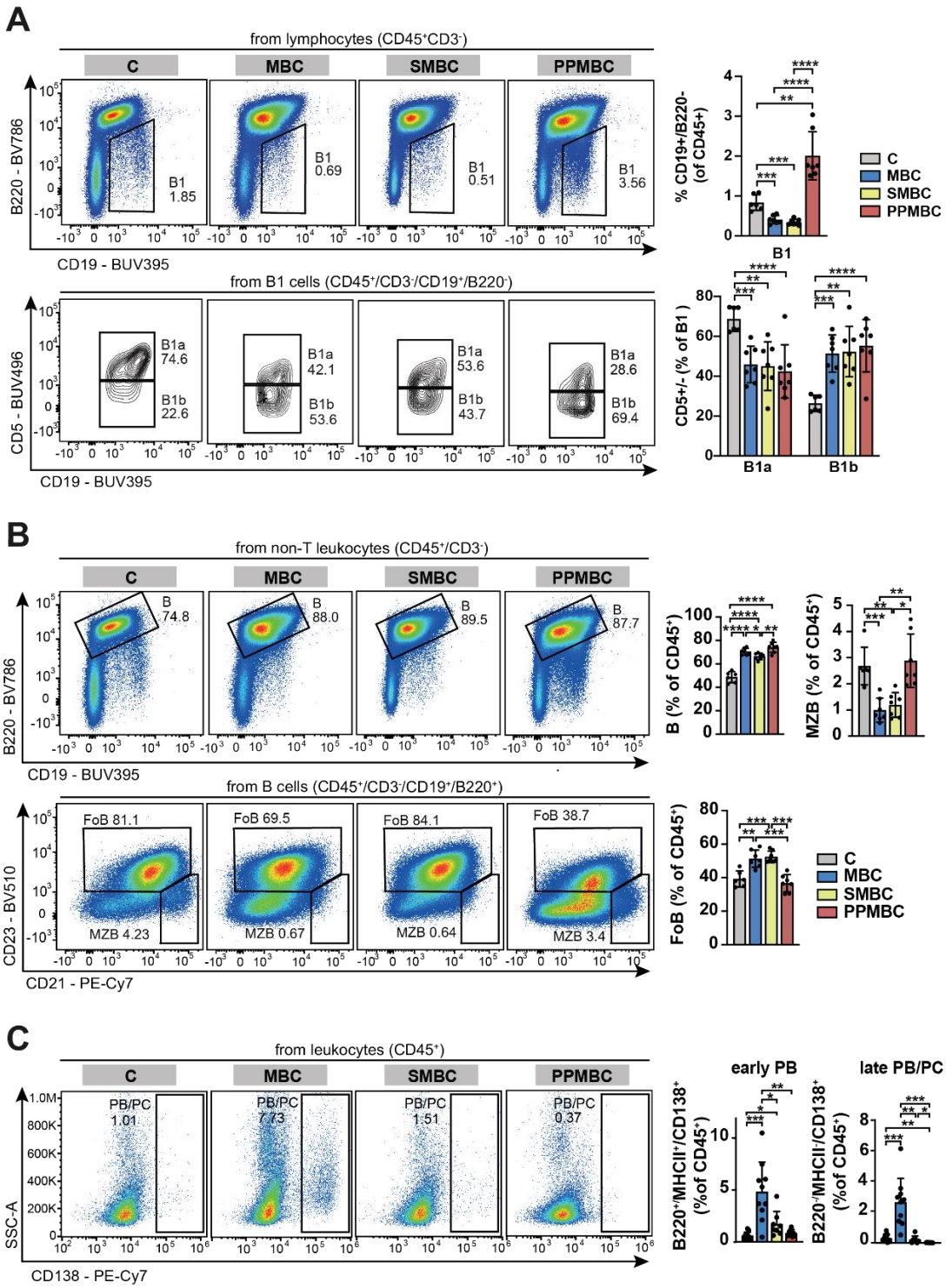

Figure R3 Flow cytometry analysis of premalignant PPMBC and SMBC mice show altered splenic B-cell subsets. *(A) $CD19^{+}B220^{-}$ B1 cells (B1), including B1a and B1b subsets. (B) $CD19^{+}B220^{+}$ B cells including follicular B (FoB) and marginal zone B cells (MZB) of 10-week old C (n = 6), MBC (n = 7), SMBC (n = 7) and PPMBC (n = 7) mice. (C) Splenic $CD138^{+}$ Plasmablasts (PB) and plasma cells (PC) from 10-week-old C (n = 11), MBC (n = 10), SMBC (n = 8), or PPMBC (n = 9) mice. *p≤0.05, **p≤0.01, ***p≤0.001, ****p≤0.0001. Welch unpaired two-tailed t test, error bars SD.*

Lastly, we investigated levels of splenic CD138$^+$ cells, indicating the plasmablast and plasma cell compartments. As expected, overexpression of *Spib* or deletion of *Prdm1* strongly reduced both subsets in premalignant SMBC and PPMBC mice compared to MBC mice. Reduction of late plasmablast/plasma cell levels was significantly more pronounced in PPMBC mice compared to SMBC mice, suggesting a more thorough plasma cell differentiation block (Fig. R3C).

Peritoneal cavity cells were analyzed analogously with comparable results (Fig. SR2).

Taken together, the induced genetic alterations show varying impacts on B-cell subsets in spleen and peritoneal cavity of premalignant mice. In many investigated subsets, MBC and SMBC cell ratios seemed more similar to each other compared to PPMBC mice. PPMBC mice revealed B-cell levels more comparable to C mice for peritoneal cavity B cells, splenic marginal zone B cells and follicular B cells.

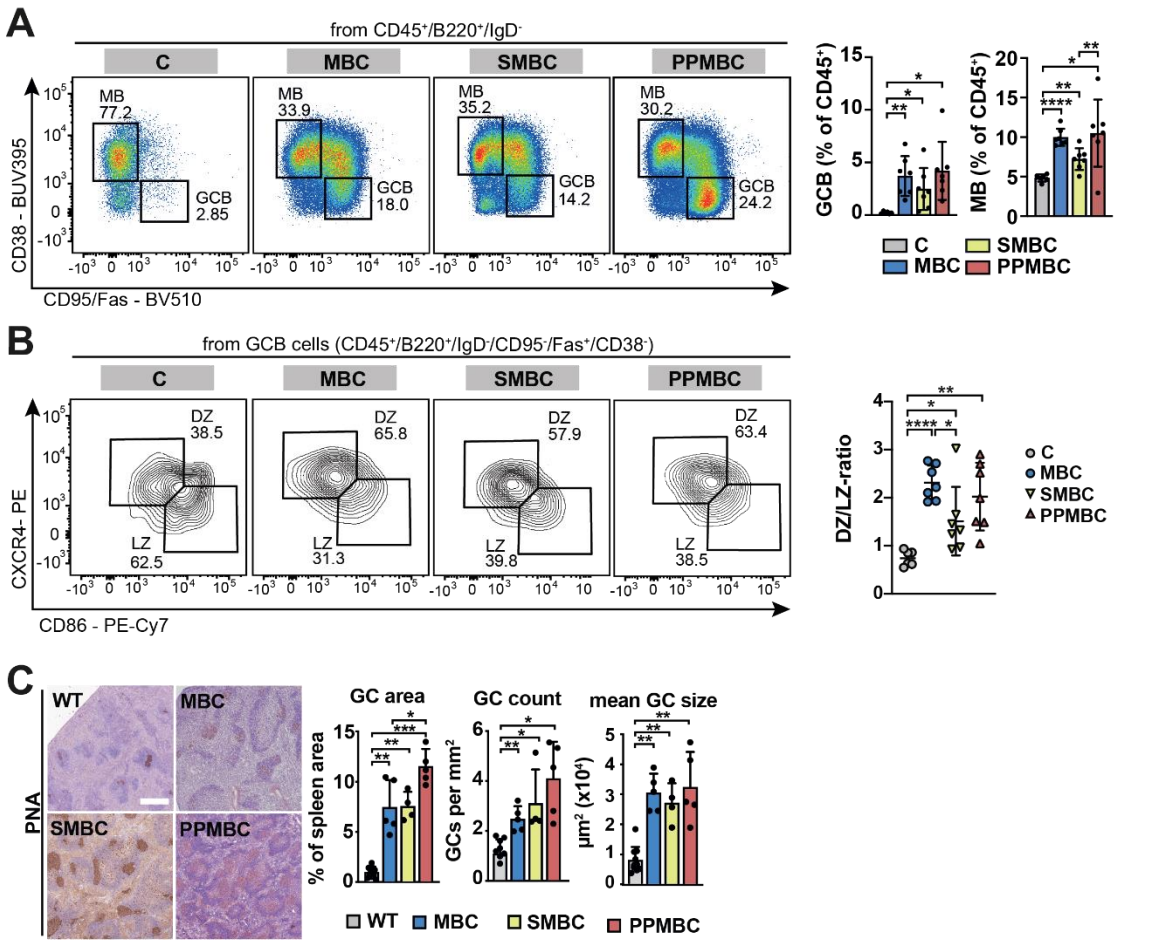

Figure R4 Autochthonous mouse models, especially PPMBC mice, showed increased GC development at 10 weeks of age. *(A, B) Flow cytometry analysis of splenic B cells subsets of 10-week old C (n = 6), MBC (n = 7), SMBC (n = 7) and PPMBC (n = 7) mice. (A) memory B (MB) cell subsets and GCB cell subsets. (B) Flow cytometry analysis of GC light zone (LZ) and dark zone (DZ) polarity. (C) Immunohistochemistry analysis of PNA$^+$ GCs in FFPE tissue of spleens of 10-week-old wt (n = 10), MBC (n = 5), SMBC (n = 5) and PPMBC (n = 5) mice. Scale bar represents 500µm. *p≤0.05, **p≤0.01, ***p≤0.001, ****p≤0.0001. Welch unpaired two-tailed t test, error bars SD. PNA peanut agglutinin.*

Since many lymphomas originate from the GC reaction (Mlynarczyk, Fontán, and Melnick 2019), we examined GC B cell subsets and consequences from the GC reaction in more detail (Fig. R4, Gating Strategies Fig. SR1). All three mouse models displayed increased levels of $CD38^{-}CD95^{+}$ GCB cells and $CD38^{+}CD95^{-}$ memory B (MB) cells in flow cytometry analyses (Fig. R4A). GC DZ/LZ ratio was significantly altered as well: All three models showcased an increased DZ/LZ ratio, hinting at increased proliferation in the dark zone (Fig. R4B). As observed in histology samples of splenic tissue when staining for GCs with peanut agglutinin (PNA), GC area, count and mean size was increased in all three mouse models as well (Fig. R4C). This increased level of GC reaction might drive lymphomagenesis in these mice.

BCR signaling is highly relevant for C5/MCD DLBCL, rendering removal of surface BCR expression synthetically lethal for this DLBCL subset (Chapuy et al. 2018; Davis et al. 2010; Young et al. 2015). Interestingly, MBC and SMBC mice demonstrated significantly decreased levels of surface IgM on splenic naïve B cells (Fig. R5A), hinting at a decreased dependency on BCR signaling. When investigating serum Ig titers via ELISA, we observed decreased immunoglobulin titers for SMBC and PPMBC mice compared to MBC mice (Fig. R5B), as expected by the lack of plasma cells. This was again more pronounced in PPMBC mice, highlighting the decreased permissiveness for plasma cell development in this genotype.

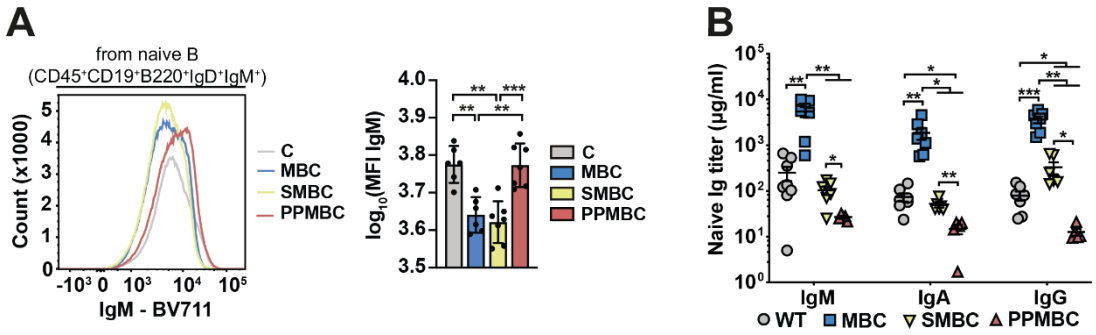

Figure R5 Analysis of immunoglobulins in autochthonous mouse models of DLBCL. *(A) Surface IgM levels on splenic naïve B cells of 10-week-old mice C (n = 6), MBC (n = 6), SMBC (n = 7) and PPMBC (n = 7) mice, representative flow cytometry analysis and quantification. (B) Serum Ig titers of IgM, IgA and IgG from 10-week-old wt (n = 8), MBC (n = 7), SMBC (n = 6), PPMBC (n = 5) mice by ELISA. *p≤0.05, **p≤0.01, ***p≤0.001. Welch unpaired two-tailed t test, error bars SD.*

5.1.3 Deletion of *Prdm1* and *Spib* overexpression accelerate lymphomagenesis

To determine the effect of B cell-specific *Prdm1* deletion or *Spib* overexpression in MBC animals on overall survival, we monitored mice until they reached predefined termination criteria (see 4.1), such as development of large tumors. As previously reported for MBC mice (Flümann et al. 2021), animals succumbed to lymphoma stochastically. While MBC animals demonstrated a median overall survival of 49 weeks, survival was significantly reduced in PPMBC and SMBC mice (median overall survival of 34.1 and 37.1 weeks, respectively), suggesting an additional pro-oncogenic effect mediated by these genetic alterations (Fig. R6A). As previously described, most MBC animals died from $B220^{-}CD138^{+}$ lymphomas (Fig. R6B, C). PPMBC animals consistently developed $B220^{+}CD138^{-}$ lymphomas (Fig. R6B, C). When considering SMBC animals, however, some developed $B220^{-}CD138^{+}$ lymphomas, while others developed $B220^{+}CD138^{-}$ lymphomas, again hinting at increased permissiveness for the plasma cell lineage (Fig. R6B). Note that a small proportion of animals died from non-malignant causes such as scratch wounds (Fig. R6B). Interestingly, SMBC and PPMBC showed detectable infiltration of $CD3^{+}$ T cells (Fig. R6C). Due to the emerging role of the TME in lymphoma biology, a further in-depth investigation of infiltrating T cells might give novel insights into C5/MCD biology (Steen et al. 2021).

As expected from an aggressive lymphoma like DLBCL, high proliferation rates were detected in MBC, SMBC and PPMBC tissue samples, revealed by high positivity for the proliferation marker Ki67. Ki67 positivity was comparable between all three genotypes (Fig. R6C, D).

For SMBC and PPMBC mice, lesions occurred mainly in spleen and lymph nodes and could be detected with magnetic resonance imaging (Fig. R6E).

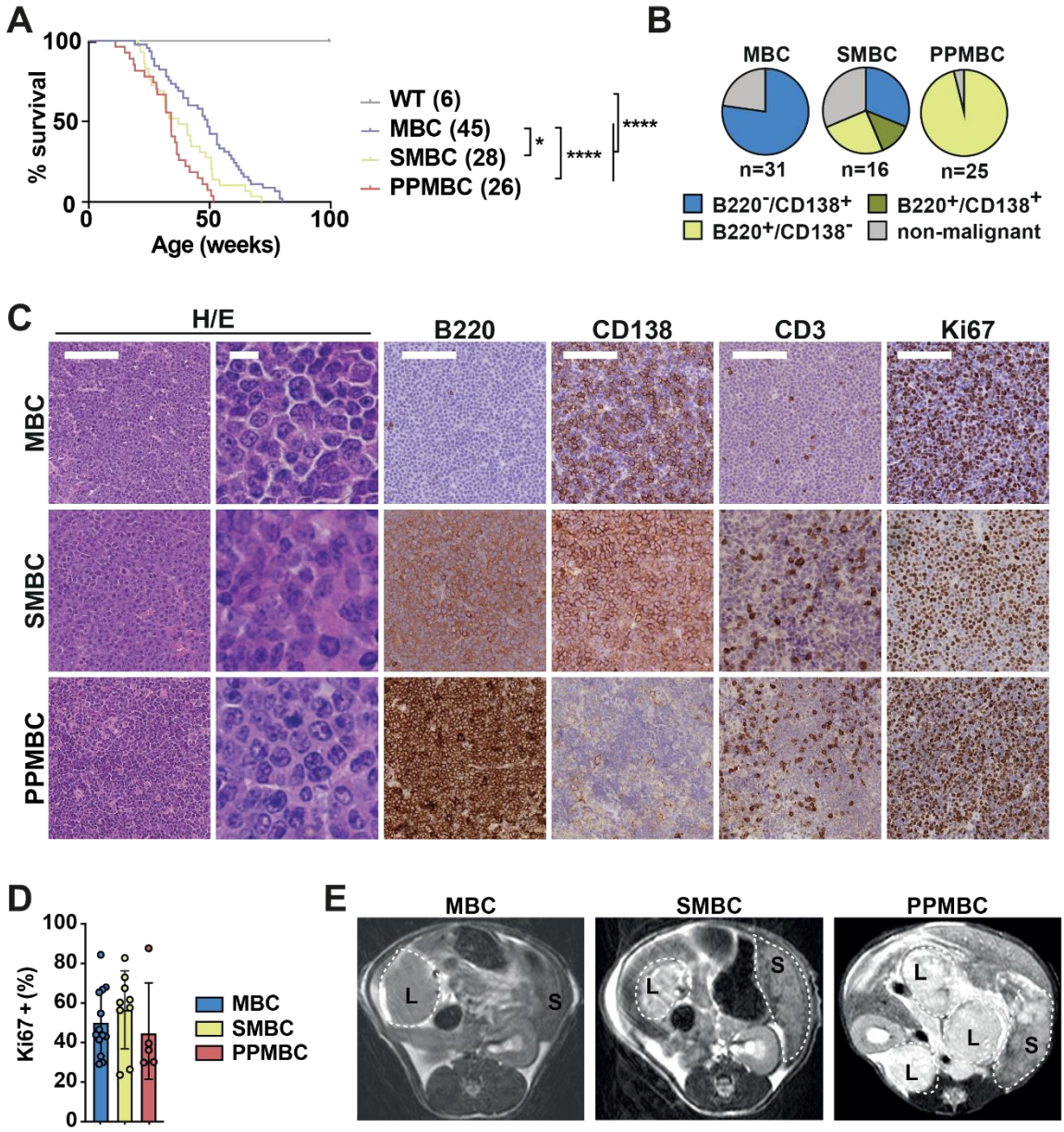

Figure R6 SMBC and PPMBC mice develop lymphomas. *(A) Overall survival of wild-type (n=6), MBC (n=45), SMBC (n=28) and PPMBC (n=26) mice. (B) Terminal phenotypes of MBC, SMBC and PPMBC animals. (C) Representative immunohistochemistry stainings of FFPE tumor tissue from MBC, SMBC and PPMBC animals. (D) Quantification of cells positive for the proliferation marker Ki67 by immunohistochemistry staining of FFPE tumor tissue from MBC (n = 13), SMBC (n = 9) and PPMBC (n = 5) animals. (E) Representative MRIs of lymphoma-bearing MBC, SMBC and PPMBC animals. *p≤0.05, ****p≤0.0001. Log-rank test (A) and Welch unpaired two-tailed t test (D), error bars SD.*

To confirm that not only B cell proliferation was increased in general, but tumors originated from one or several malignant clones, we investigated clonality by RNA-based BCR sequencing (Shugay et al. 2014). While splenocytes from wild-type mice showed a clonally highly diverse BCR repertoire, MBC, SMBC and PPMBC tumor cells demonstrated one or few dominant clones making up to more than 90% of the B cell subset in the majority of cases (Fig. R7A, B). From this, we determined the Gini coefficient used to assess the evenness of clonal distribution, ranging from 0 to 1 (Wright Muelas et al. 2019). A Gini coefficient of 1 would represent a maximally inequal distribution, meaning a perfectly monoclonal tumor (Wright Muelas et al. 2019). The Gini coefficients for MBC samples were close to 1, representing nearly monoclonal samples where one clone dominates the distribution. SMBC samples showed a comparatively high variance for the Gini coefficient, while PPMBC tumors had a high, but significantly lower Gini coefficient compared to MBC tumor samples, indicating a less stringent clonality (Fig. R7C). On the other hand, we observed an expectable usage of *Ighv* genes, indicating that dominant clones differed between lymphoma samples (Fig. R7D). If all tumors were driven by the same specific set of (auto-)antigens in different animals, this could be indicated by usage of the same *Ighv* genes as seen in some DLBCLs (Young et al. 2015). Our data discourages this hypothesis in our models (Fig. R7D).

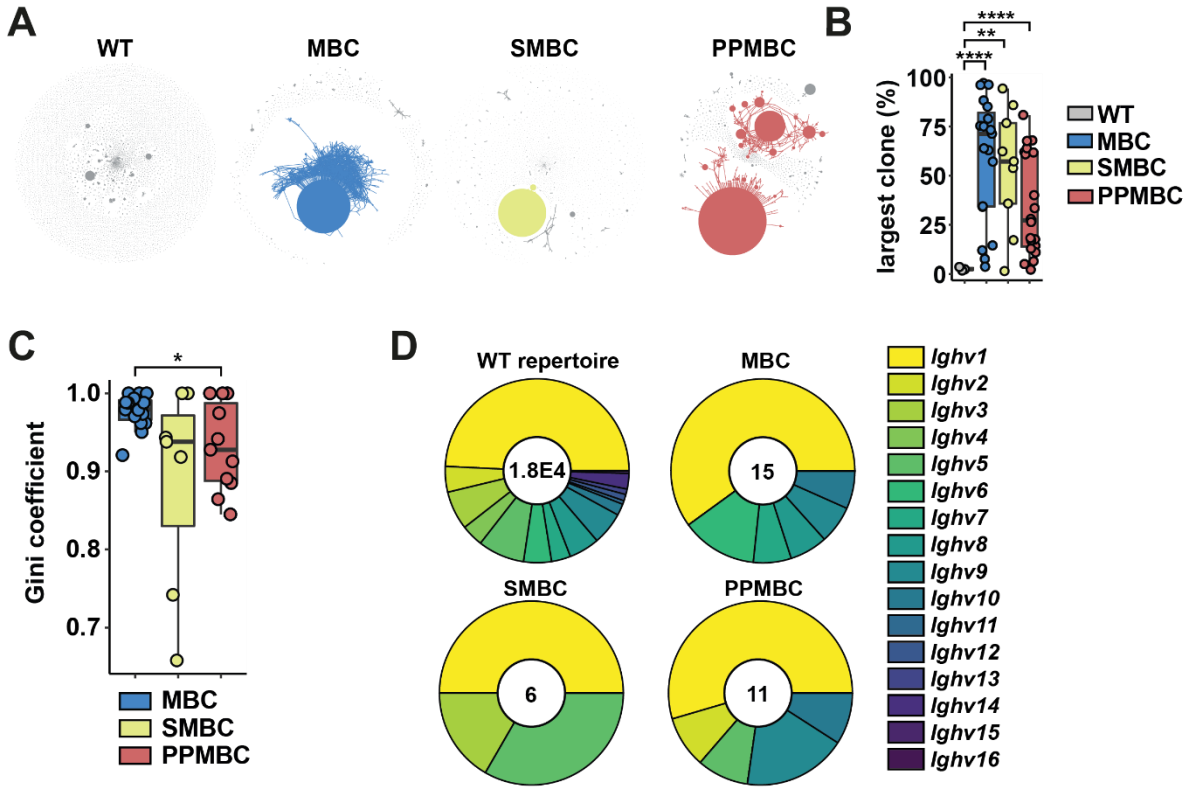

***Figure R7 MBC, SMBC and PPMBC mice develop (oligo-)clonal lymphomas**. (A) Representative clonality plots generated from BCR sequencing data. Main clones are displayed as colorful circles connecting to sequences with one mismatch. Individual circles represent a specific V(D)J sequence. The circle size represents the respective readout count. (B) Proportion of the largest clone per sample in MBC (n =18), SMBC (n = 9) and PPMBC (n = 18) tumors compared to the polyclonal B cells of wt spleens (n = 3). (C) Gini coefficient as readout for clone size. (D) Usage of* Ighv *genes in splenic B cells of WT (pool of 3 independent spleen samples) or in malignant clones of MBC, SMBC and PPMBC tumor samples. Indicated numbers in the middle represent number of clones analyzed (1 clone/sample in MBC, SMBC and PPMBC samples). *p≤0.05, **p≤0.01, ***p≤0.001, ****p≤0.0001. Welch unpaired two-tailed t test, error bars represent SD.*

As previously mentioned, BCR signaling was shown to be highly relevant for C5/MCD DLBCL and different immunoglobulin isotypes confer distinct types of BCR signaling (Chapuy et al. 2018; Maity et al. 2018; James 2022). We therefore investigated isotype choice in MBC, SMBC and PPMBC tumor samples, revealing different proportions of MBC, SMBC and PPMBC tumors to express IgA, IgG or IgM, although sample sizes were notably small (Fig. SR3A). Similarly, we observed different isotype positivity for different samples in our flow cytometry data (Fig. SR3B).

5.1.4 SMBC and PPMBC tumors show propagative capacity outside of lymphatic tissue and in engrafted *Rag1*$^{-/-}$ mice

Extranodal disease is observed frequently in B-cell lymphoma patients (Sehn and Salles 2021). In SMBC and PPMBC mice, extranodal infiltration into the liver and the lung was significantly more prevalent than in MBC mice, as detected by immunohistochemistry staining for B220^{+} B cells (Fig. R8A, B). At mouse autopsy, we also noticed increased lymphoma dissemination into different lymph node regions in PPMBC and SMBC mice, compared to MBC mice (Fig. R8B). Interestingly, while most MBC mice displayed affected mesenteric lymph nodes, the spleen seemed to be the most affected organ in SMBC and PPMBC mice (Fig. R8B).

Next, we tested the engraftment capacity into immunodeficient *Rag1*$^{-/-}$ mice. Due to the loss of the genome-editing nuclease RAG1 responsible for VDJ recombination (Mombaerts et al. 1992), these mice lack mature T and B cells, allowing for adoptive transfer of splenocytes from immunocompetent mice without rejection by the intrinsic adaptive immune system (Ganesan et al. 2007). After injecting tumor cells into *Rag1*$^{-/-}$ mice, we observed engraftment in a majority of cases, comparable between genotypes (Fig. R8C). Engrafted PPMBC tumors were similar to primary tumors in expression of the surface markers B220 and CD3, as well as positivity for the proliferation marker Ki67, as seen in immunohistochemistry stainings (Fig. R8D). We further applied the technique of injecting lymphoma cells into *Rag1*$^{-/-}$ mice to derive cell lines from tumor tissue for future studies *in vitro* (see 4.2 and 5.3).

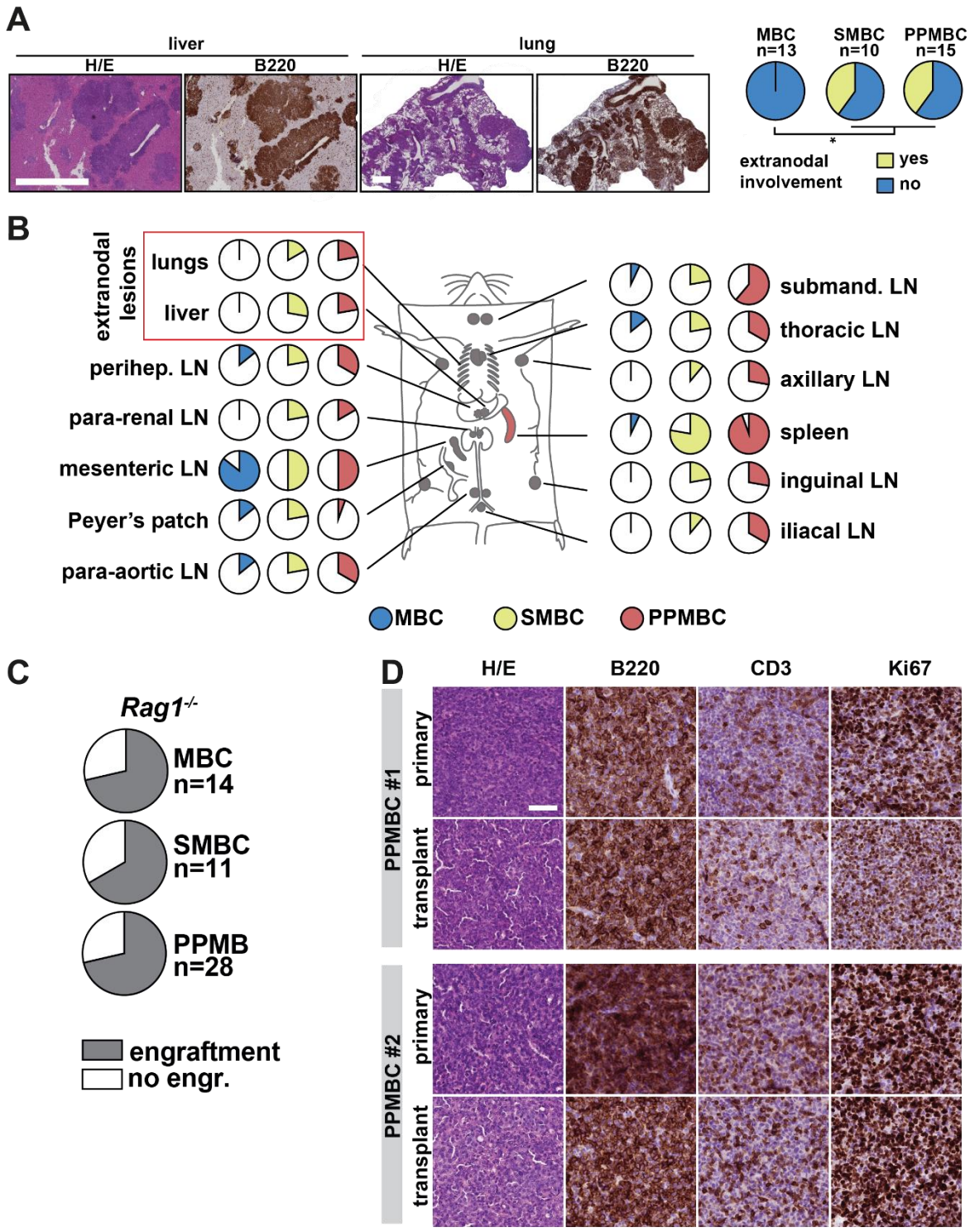

Figure R8 High aggressivity of MBC, SMBC and PPMBC lymphomas as determined by metastasis and engraftment rate into* Rag1$^{-/-}$ *animals. *(A) Representative immunohistochemistry stainings of extranodal lesions in PPMBC animals. Quantification of extranodal lesions in MBC, SMBC and PPMBC animals. (B) Quantification of lymphoma-affected sites in MBC (n = 14), SMBC (n = 10) and PPMBC (n = 10) animals as determined at autopsy. (C) Quantification of engraftment of tumor cells of the respective genotype after injection into* Rag1$^{-/-}$ *animals. (D) Representative immunohistochemistry stainings of lymphoma tissue of primary PPMBC tumors and secondary tumors derived in* Rag1$^{-/-}$ *animals by engraftment of cells from the respective primary tumor. Scale bars represent 500µm. *p≤0.05, **p≤0.01, ***p≤0.001, ****p≤0.0001. Welch unpaired two-tailed t test, error bars SD.*

5.1.5 A plasma cell differentiation block predisposes for ongoing somatic hypermutation

The decreased clonal dominance observed in SMBC and PPMBC mice (Fig. R7B) could be caused by ongoing somatic hypermutation increasing mutation rate and genetic heterogeneity within the tumor. In line with this, we found *Aicda*, the transcript for the enzyme AID initiating the process of mutating immunoglobulin gene variable regions (Martin and Scharff 2002), to be significantly upregulated in the transcriptomes in SMBC and PPMBC tumor samples (Fig. R9A). Complementary determining region mutation frequency was increased as well (Flumann et al. 2023) and we detected several newly emerged genetic alterations in the investigated tumor samples (Fig. R9B). Several of these genetic alterations were previously shown to be recurrently altered in DLBCL and often relevant for C5/MCD DLBCL (Chapuy et al. 2018; Schmitz et al. 2018; Reddy et al. 2017; Wright et al. 2020), such as mutations in the genes for *Irf2bp2*, *Pim1*, *Pou2f2* and *H2-Ab1* (Fig. R9C). This indicates our model to be a useful representation of C5/MCD DLBCL even recapitulating the genetic heterogeneity of clinical C5/MCD DLBCL.

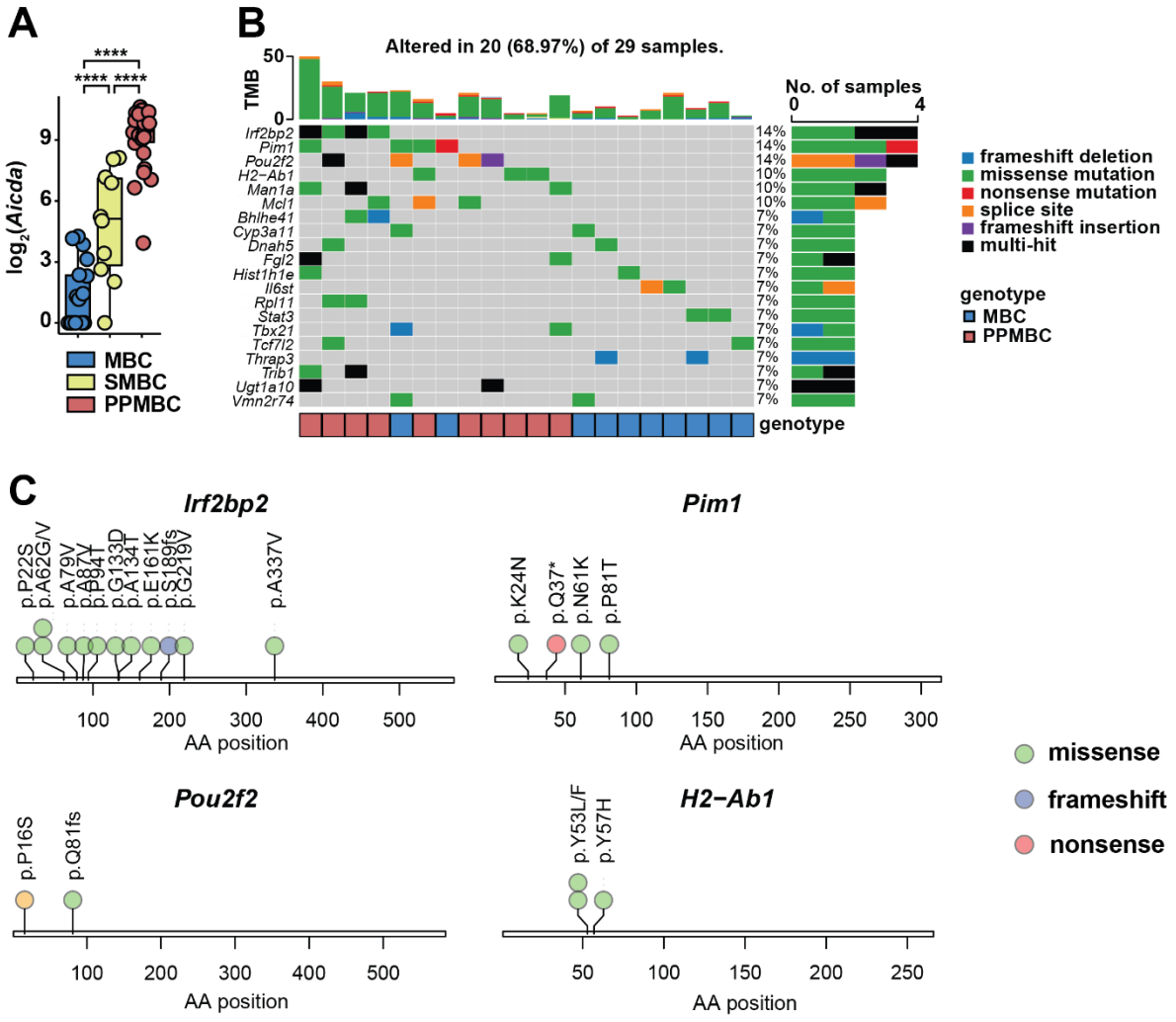

Figure R9 Ongoing AID-driven somatic hypermutation generates additional genetic alterations in MBC and PPMBC mice. *(A) RNA levels of* Aicda *determined by RNA-seq. (B) Genetic alterations in WES data of MBC and PPMBC lymphomas. (C) Lollipop plots of genetic alterations in genes shown to be relevant for C5/MCD DLBCL (WES data). ****p≤0.0001. Welch unpaired two-tailed t test, error bars SD.*

5.1.6 PPMBC and SMBC models allow for conclusions on DLBCL lineage

DLBCL is classically subdivided into GCB- and ABC-like by COO classification (Alizadeh et al. 2000), C5/MCD DLBCL mostly consists of ABC DLBCL (Chapuy et al. 2018; Schmitz et al. 2018). We confirmed our mouse tumor samples to be IRF4^{+} (Fig. R10A), which is a defining characteristic of non-GCB DLBCL based on Hans algorithm (Hans et al. 2004). To further specify the cell of origin of our modeled lymphomas, we generated 3'-RNA-seq reference data from GC B and AB cells from wild-type animals for gene set analysis (GCB^{up} and AB^{up}). Transcriptomes from the published GCB-DLBCL mouse model *Kmt2d*$^{fl/fl}$;*VavP-Bcl2*;*Cγ1*$^{Cre/wt}$ (Zhang et al. 2015), referenced as KBC model, were significantly enriched for genes belonging to the GCB^{up} gene set and depleted for the AB^{up} genes, when compared to our C5/MCD lymphoma models. The PPMBC, MBC and SMBC mouse models all appeared enriched for AB^{up} genes and depleted for GCB^{up} genes when compared to the KBC reference data. When considering single-sample enrichment scores, SMBC scored highest for AB^{up}, followed by MBC and then PPMBC, all clearly on the AB^{up} side (Fig. R10B). Hence, we conclude that our three mouse models develop a disease comparable to ABC DLBCL based on transcriptome analysis.

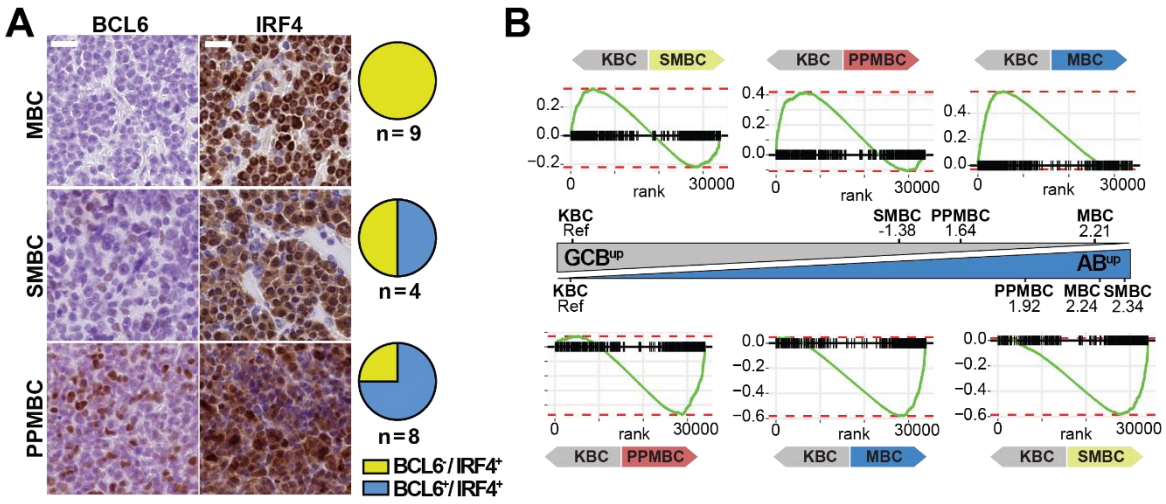

Figure R10 MBC, SMBC and PPMBC mice develop ABC DLBCL. *(A) Representative immunohistochemistry stainings of MBC, SMBC and PPMBC lesions and quantification. (B) Gene set enrichment analysis (GSEA) for AB and GCB gene sets in KBC, SMBC, PPMBC and MBC lesions. The middle graphic displays single-sample GSEA scores representing the degree to which genes of the GCB^{up}/ABC^{up} gene sets are coordinately upregulated compared to KBC as a reference.*

The origin of malignant genetic alterations in lymphoma is believed to lie at least partially in AID-driven somatic hypermutation within the GC reaction (Chapuy et al. 2018). On the other hand, ABC DLBCLs were previously found to be related to plasmablast or plasma cells based on gene expression (Alizadeh et al. 2000; Dekker et al. 2016). More recently, memory B cells with an aged/autoimmune B-cell program were proposed as possible cell of origin (Venturutti and Melnick 2020; Venturutti et al. 2022). In line with the latter hypothesis, our B220^{+} PPMBC and SMBC lymphomas showed expression of memory B cell markers (Fig. R11). Interestingly, while the expression of the GC dark zone marker CXCR4 was increased in our premalignant animals (see Fig. R4B), we observed decreased CXCR4 expression levels compared to healthy splenocytes (Fig. R11). This might hint at further malignant events altering cell surface marker expression during lymphomagenesis in the PPMBC model.

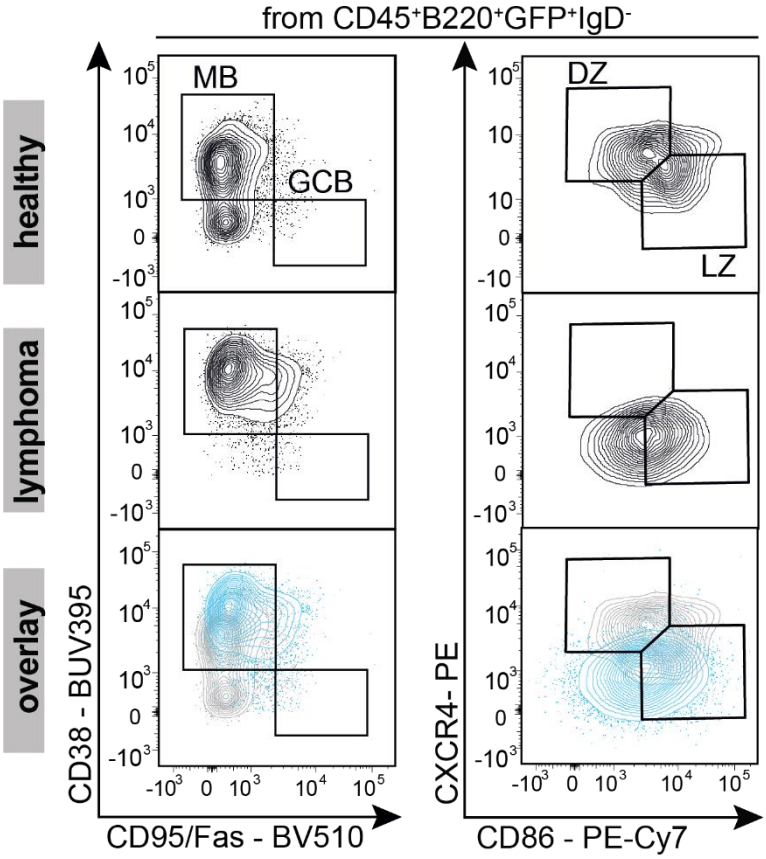

Figure R11 PPMBC mice develop DLBCLs related to the MB lineage. *Representative comparison of flow cytometry analyses of a PPMBC lymphoma ("lymphoma", blue) with spleen cells from a 10-week-old healthy C mouse ("healthy", grey) and overlay. MB memory B cells, GCB germinal center B cells, DZ dark zone, LZ light zone.*

5.1.7 The PPMBC model as a platform to assess immunotherapeutic approaches

An immunotherapy rapidly gaining importance in the lymphoma field is treatment with CD19-targeting chimeric antigen receptor (CAR) T cells. Several CAR-T cell products were recently approved for treatment of lymphomas and other hematologic malignancies in Europe and the United States, achieving overall response rates ranging between 53 to 83% in DLBCL (Cappell and Kochenderfer 2023). To generate a CAR-T construct, an antigen-binding domain (commonly anti-CD19 for DLBCL) is combined with the CD3 T cell activation chain CD3ζ, additionally carrying a hinge region, a transmembrane domain and a co-stimulatory domain for higher efficiency (Cappell and Kochenderfer 2023). This construct is integrated in autologous T cells, to allow these patient-derived genetically modified T cells to target the lymphoma (Cappell and Kochenderfer 2023). In our simplified approach, a domain binding murine CD19 was combined with murine CD28 as transmembrane domain and the murine CD3ζ, which was used to transfect splenic T cells (Fig. R12A). *In vitro*, CAR-T cells efficiently eliminated $CD19^+$ PPMBC lymphoma cells at all investigated effector cell to target cell ratios down to 0.25:1, while mock-transduced T cells demonstrated little to no anti-malignant capacity (Fig. R12B). Anti-tumor competence was confirmed *in vivo,* where treatment of lymphoma-bearing PPMBC mice decreased tumor volume and prolonged survival compared to untreated mice (Fig. R12C and R12D). Upon closer inspection, CAR-T cells seemed to be mainly active in mice carrying a low tumor burden (spleen volume between 500 and 699 µL) at treatment initiation, while mice with a high tumor burden (spleen size ≥700 µL) benefitted little from CAR-T treatment (Fig. R12C and D). Consistently, lymphoma burden was previously indicated to be predictive for CAR-T response in clinical trials (Locke et al. 2020).

Treatment with a murine PD-L1 antibody (Schofield et al. 2021) was also tested in PPMBC mice, not reducing tumor volume by more than 25%, but prolonging overall survival of mice by a few months. (Flumann et al. 2023)

In both approaches, the PPMBC mouse model served as a useful proxy for preclinical treatment testing, corroborating its value for future research.

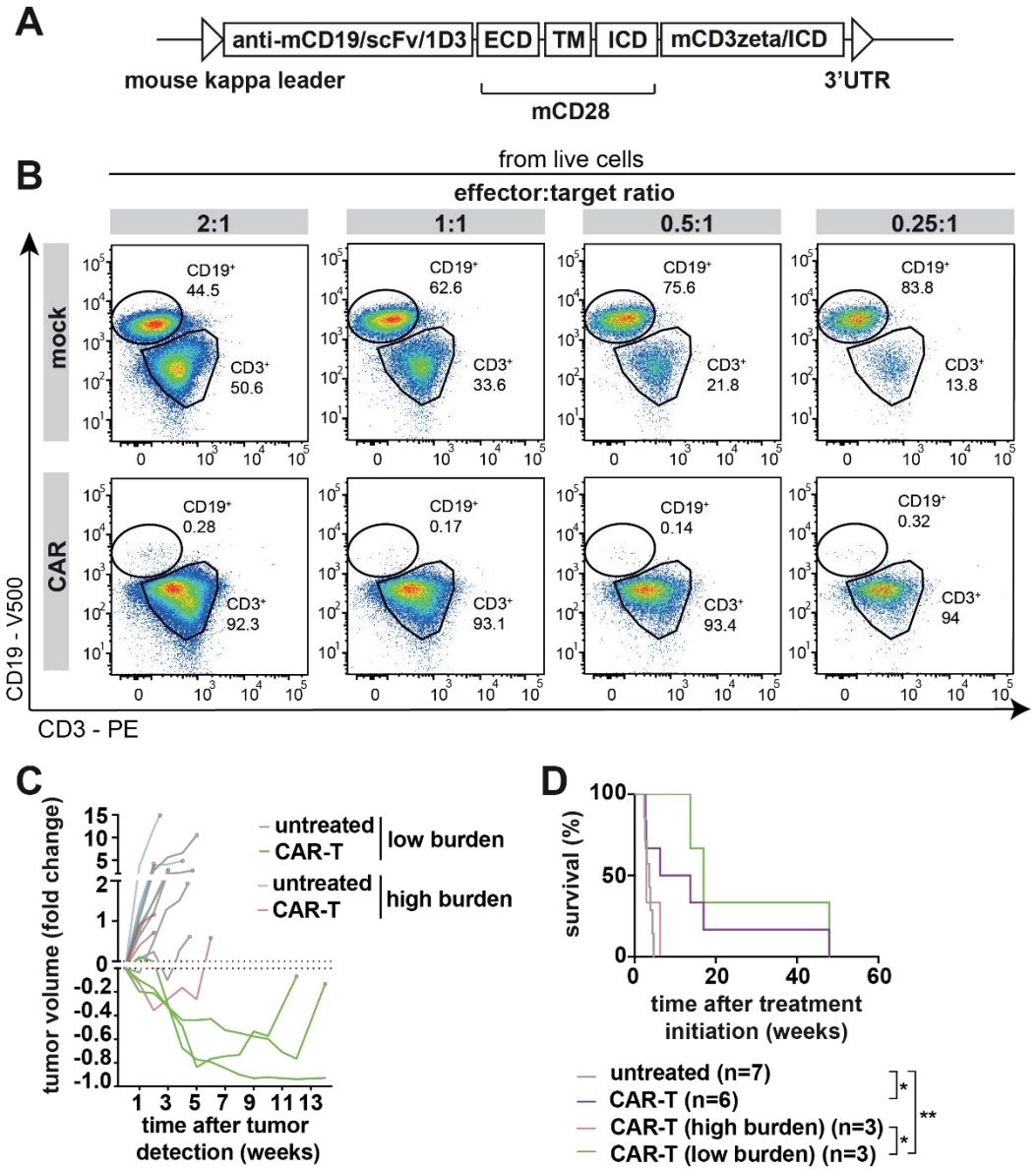

Figure R12 CAR-T cell treatment of lymphoma-bearing PPMBC mice reveals the role of tumor size for treatment response. *(A) Schematic of the used CAR construct to transfect murine T cells. (B) Population sizes of B and T cells after 48h of* in vitro *coculture of CD19⁺ cells (PPMBC lymphoma cell line) with mock-treated T cells or CAR-T cells at different effector:target cell ratios. (C) Changes of tumor volume in lymphoma-bearing PPMBC mice untreated or treated with CAR-T cells with high or low tumor burden. (D) Survival of lymphoma-bearing PPMBC mice untreated or treated with CAR-T cells with high or low tumor burden. *p≤0.05, **p≤0.01. Log-rank test.*

5.1.8 Increased BCR signaling reveals a therapeutic vulnerability for PPMBC lymphomas

Our transcriptomic data revealed signs of elevated BCR signaling in PPMBC lymphomas leading to increased pro-oncogenic downstream signaling like activation of the NF-κB and PI3K pathways (Fig. R13A). When investigating phosphorylation levels of BCR signaling adaptors, we also found increased activating phosphorylation levels of PLCγ2 (Y759) and SYK (Y525/526) in PPMBC compared to MBC lymphomas (Fig. R13B). When normalizing this data to bulk protein levels, the latter showing high variation, ratios of phosphorylated to total protein levels differed significantly only for SYK, but not PLCγ2 (Fig. R13B-right). Nevertheless, we conclude that proximal BCR signaling activity is elevated in PPMBC lymphomas.

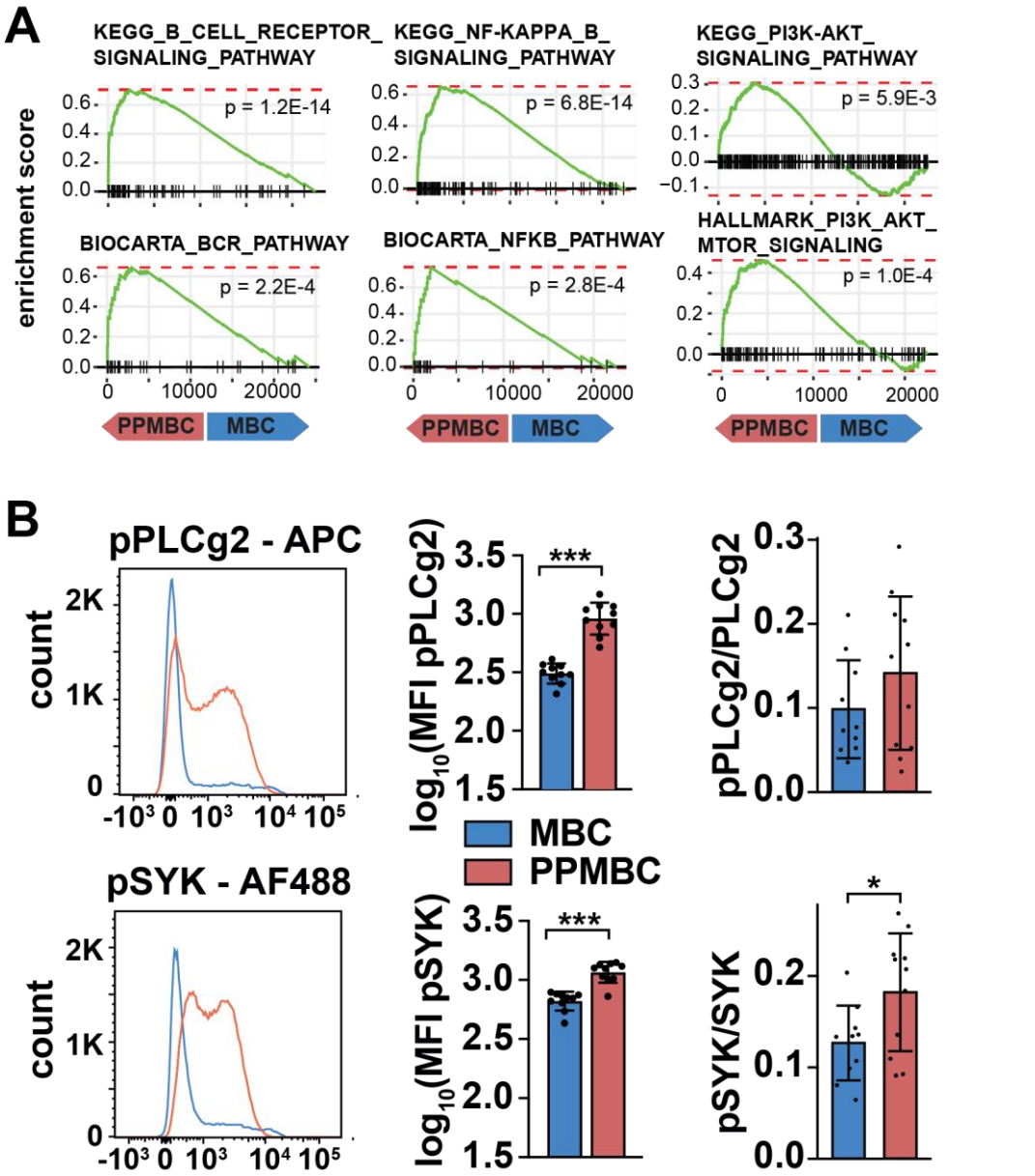

Figure R13 BCR signaling is elevated in PPMBC lymphomas. *(A) Gene set enrichment analysis of BCR-relevant signaling pathways in MBC and PPMBC lymphomas. (B) Flow cytometry analysis of phosphorylated BCR signaling adaptors PLCγ2 and SYK in MBC (n = 10) and PPMBC (n =10) lymphomas. Representative and quantification of median fluorescence intensity (MFI), also normalized to bulk unphosphorylated protein levels. *p≤0.05, **p≤0.01, ***p≤0.001, ****p≤0.0001. Welch unpaired two-tailed t test, error bars SD.*

Therefore, we asked whether BTK inhibition via ibrutinib targeting BCR signaling might be therapeutically active in PPMBC mice. Since we previously demonstrated efficacy of targeting BCL2 using the BCL2 inhibitor venetoclax in our BCL2-dependent MBC mouse model (Flümann et al. 2021), venetoclax, ibrutinib, and a combination of both was tested in PPMBC mice. Both agents alone led to a tumor volume reduction in treated mice, upon which animals soon relapsed and regained tumor growth (Fig. R14A). Combining venetoclax and ibrutinib, however, led to near-disappearance of tumors and significantly prolonged response rates (Fig. R14A). This was reflected in the maximal tumor volume change per treated mouse (Fig. R14B) and increased progression-free and overall survival of mice treated with both agents compared to untreated or single-agent-treated animals (Fig. R14C and D). Taken together, this *in vivo* experiment displayed high therapeutic potential for the combination of ibrutinib and venetoclax for treatment of ABC DLBCL. These findings were transferred to the clinic in an off-label setting, presenting high response rates in five out of six ABC DLBCL patients (Flumann et al. 2023), revealing the combination as potential bridging treatment method and confirming our model as suitable pre-clinical testing tool.

(Please note that mouse treatment with venetoclax and ibrutinib (Fig. R14), as well as patient treatment, was performed without involvement of J. Hansen and is described here to illustrate the relevance of the preceding sections.)

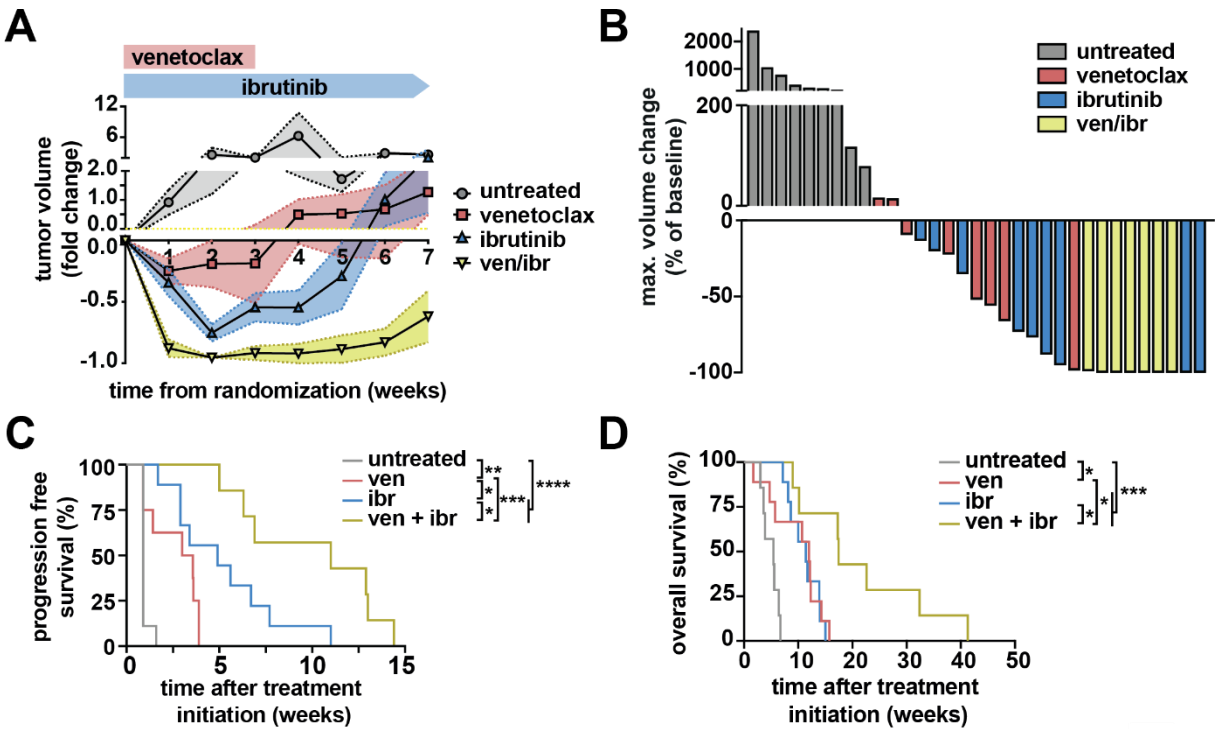

Figure R14 Combination treatment with ibrutinib and venetoclax is highly effective in lymphoma-bearing PPMBC mice. *(A) Tumor volume change in untreated, single-agent-treated or combination-treated PPMBC mice. (B) Maximum tumor volume change in untreated, single-agent-treated or combination-treated PPMBC mice. (C) Progression-free survival and (D) overall survival of untreated (n = 7), single-agent venetoclax-treated (n = 8) or ibrutinib-treated (n = 9) or combination-treated (n = 7) PPMBC mice. *p≤0.05, **p≤0.01, ***p≤0.001, ****p≤0.0001. Log-rank test.*

5.2 An inducible *Cd79b* mutation confers ibrutinib sensitivity in mouse models of *Myd88*-driven diffuse large B-cell lymphoma

5.2.0 Contributions

Chapter 5.2 is based on the following publication in *Blood Advances*:

R. Flumann*, J. Hansen*, J. Meinel, P. Pfeiffer, H. Goldfarb Wittkopf, A. Lutz, J. Wirtz, M. Mollmann, T. Zhou, A. Tabatabai, T. Lohmann, M. Jauch, F. Beleggia, B. Pelzer, F. Ullrich, S. Hofmann, A. Arora, T. Persigehl, R. Buttner, B. von Tresckow, S. Klein*, R. D. Jachimowicz*, H. C. Reinhardt* and G. Knittel* (2024). "An inducible Cd79b mutation confers ibrutinib sensitivity in mouse models of Myd88-driven diffuse large B-cell lymphoma." Blood Adv 8(5): 1063-1074.

*R.F., J.H., S.K., R.D.J., H.C.R., and G.K. contributed equally to this study.

The following figures were retrieved from the publication: Fig. R15A, R19, R20, R21, R22, R23, R24, R25, R27, R28, R29

The following figures were generated solely for this thesis: Fig. R15B, R16, R17, R18, R26

Detailed author contributions relevant for experiments shown in this thesis are as following:

R. Flümann, J. Hansen, S. Klein, R.D. Jachimowicz, H.C. Reinhardt, and G.Knittel conceived and designed experiments.

R. Flümann, J. Hansen, H. Goldfarb Wittkopf and A. Lütz monitored the mice, performed autopsies, and took all mouse samples.

R. Flümann, J. Hansen, A. Lütz and J. Wirtz performed and analyzed MRI.

J. Hansen acquired flow cytometry data. J. Hansen and R. Flümann analyzed the flow cytometry data.

R. Flümann analyzed immunohistochemistry stainings.

R. Flümann, J. Hansen, H. Goldfarb Wittkopf and A. Lütz prepared samples for transcriptomic analyses and WES. G. Knittel and S. Klein analyzed transcriptomes and WES data.

G. Knittel and R. Flümann prepared BCR sequencing. G. Knittel analyzed BCR sequencing.

J. Hansen performed and analyzed BCR internalization experiments.

R. Flümann and J. Hansen performed and analyzed proximity ligation assay experiments.

J. Hansen, H. Goldfarb Wittkopf, A. Lütz and R. Flümann performed treatment experiments with ibrutinib.

G. Knittel performed statistical analyses of all published experiments. J. Hansen performed statistical analyses of experiments analyzed for this thesis.

Resources were contributed by B. Pelzer, T. Persigehl, R. Büttner.

The novel conditional *Cd79b*^{Y195H} allele was generated by an external company (Taconic Biosciences) and function was confirmed experimentally by R. Flümann.

A complete list of contributions, including for publication aspects not part of this thesis, is found in chapter 7.

5.2.1 *CD79B* is associated with C5/MCD DLBCL biology

Mutation of the immunoreceptor tyrosine-based activation motif (Y196X) of the BCR component *CD79B* is one of the predominant genetic alterations for C5/MCD DLBCL (Chapuy et al. 2018; Schmitz et al. 2018). While BCR signaling dependency was shown to be characterizing for C5/MCD DLBCL (Chapuy et al. 2018; Young et al. 2019) and the *CD79B*^{Y196X} mutation supposedly increases BCR signaling by decreasing interaction with the Lyn-mediated negative feedback loop (Davis et al. 2010), its exact role is incompletely understood.

To elucidate the mechanisms mediated by the *CD79B* ITAM mutation and especially its effect on therapy response, we employed our previously published MBC and PPMBC mouse models (Flumann et al. 2023; Flümann et al. 2021; Knittel et al. 2016). To this end, a Cre-inducible *Cd**79b***$^{cond.p.Y195H}$ allele (hereafter *Cd79b*^{Y195H}) was generated, where the murine orthologue Y195 of the ITAM tyrosine frequently mutated in patient DLBCL (Y196) is exchanged to histidine (Chapuy et al. 2018; Schmitz et al. 2018). We crossed this allele into our MBC and PPMBC mouse models to develop the 79-MBC and 79-PPMBC mouse models, respectively (Fig. R15A).

(Please note that the Cd79b^{Y195H} *allele was generated by an external company without involvement by J. Hansen and is described here for explanatory reasons.)*

To investigate early effects of the *Cd79b* ITAM mutation on B cell development, we analyzed a cohort of premalignant 10-week-old mice (79-MBC and MBC). For in-depth analysis of the malignant impact of the mutation immediately before onset of lymphoma, 30-week-old animals were investigated (79-PPMBC and PPMBC). After lymphoma development throughout life, mice were sacrificed and inspected to determine the malignant phenotype (Fig. R15B).

Chapter 5.2 begins with the characterization of the 79-MBC and 79-PPMBC mouse models, first before signs of malignancy (premalignant phenotype, 5.2.2), followed by in-depth analysis of animal and tumor phenotype upon lymphoma development (5.2.3-5.2.4). Subsequently, BCR signaling and treatment with ibrutinib is investigated in the 79-MBC and 79-PPMBC models (5.2.5-5.2.6).

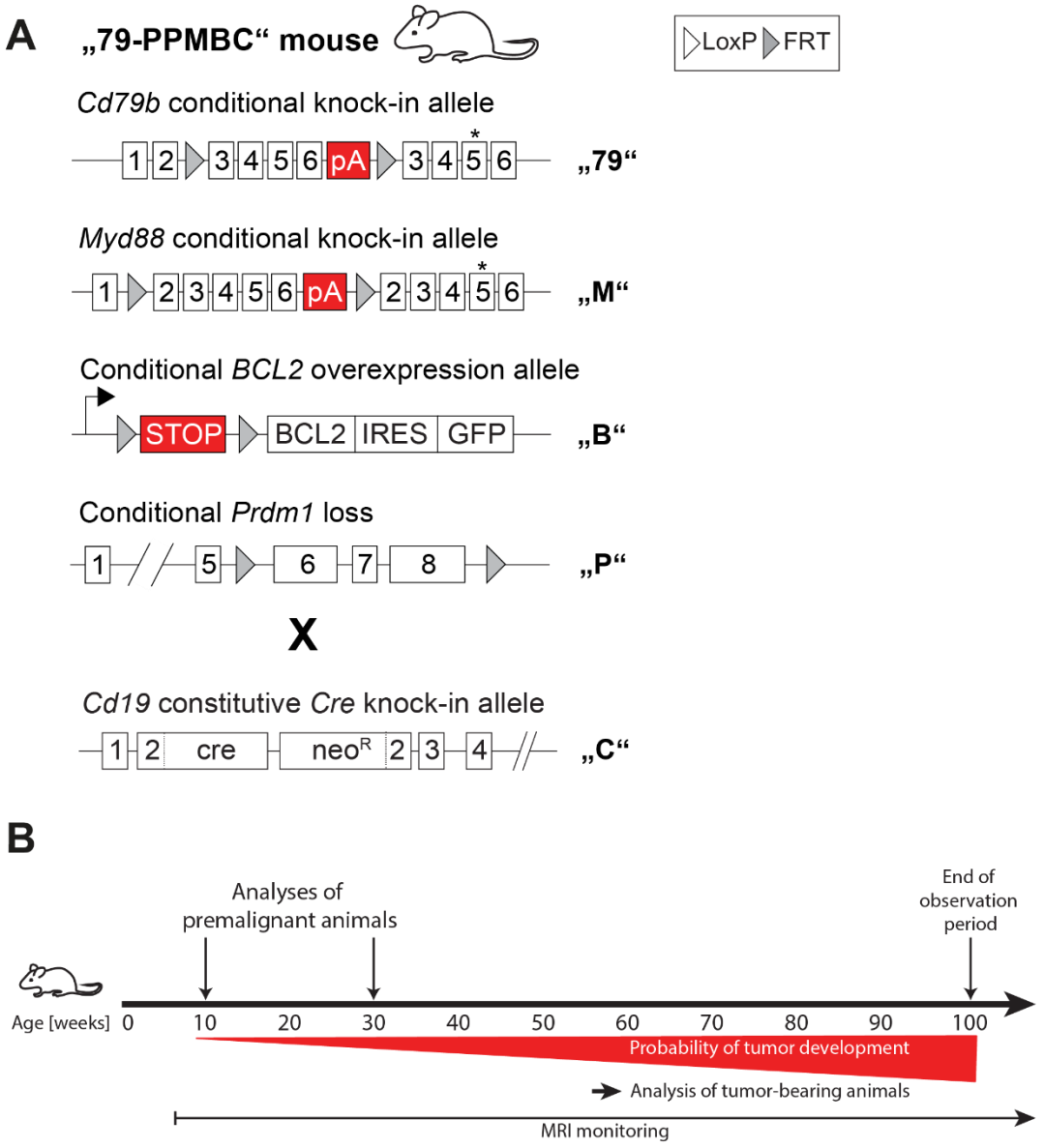

Figure R15 Experimental setup to investigate the role of* CD79B^{Y195H} *in an autochthonous mouse model. *(A) Alleles used to generate the 79-PPMBC and 79-MBC mouse models. (B) 79-MBC and 79-PPMBC mice were analyzed at an age of 10 or 30 weeks and tumor-bearing animals were investigated upon tumor development. loxP locus-of x-over, FRT flippase recognition target, MRI Magnetic resonance imaging, pA polyadenylation site, * mutation, STOP stop codon, neo^R neomycin resistance cassette, IRES internal ribosome entry site.*

5.2.2 The *Cd79b*^{Y195H} mutation demonstrated little effect on general B-cell development

To investigate whether the putatively pro-oncogenic *Cd79b*^{Y195H} mutation impacts the B-cell compartment before detectable signs of lymphoma, we studied premalignant mice at 10 weeks (MBC and 79-MBC) and 30 weeks (PPMBC and 79-PPMBC) of age by flow cytometry analyses of splenocytes. Due to animal availability, it was not possible to analyze both the 10- and the 30-week time points in all genotypes.

Surprisingly, we observed no significant alteration in B cell subset levels of CD19^{+}B229^{-} B1, CD19^{+}B220^{+} B, CD23^{+}CD21^{+} FoB or CD23^{-}CD21^{+} MZB cells when comparing 79-MBC to MBC mice (Fig. R16). When comparing 79-PPMBC to PPMBC mice, CD19^{+}B229^{-} B1 and CD23^{+}CD21^{+} FoB cell levels were unaltered, while CD19^{+}B220^{+} B and CD23^{-}CD21^{+} MZB cell levels were decreased by ~1/5 in 79-PPMBC mice (Fig. R16).

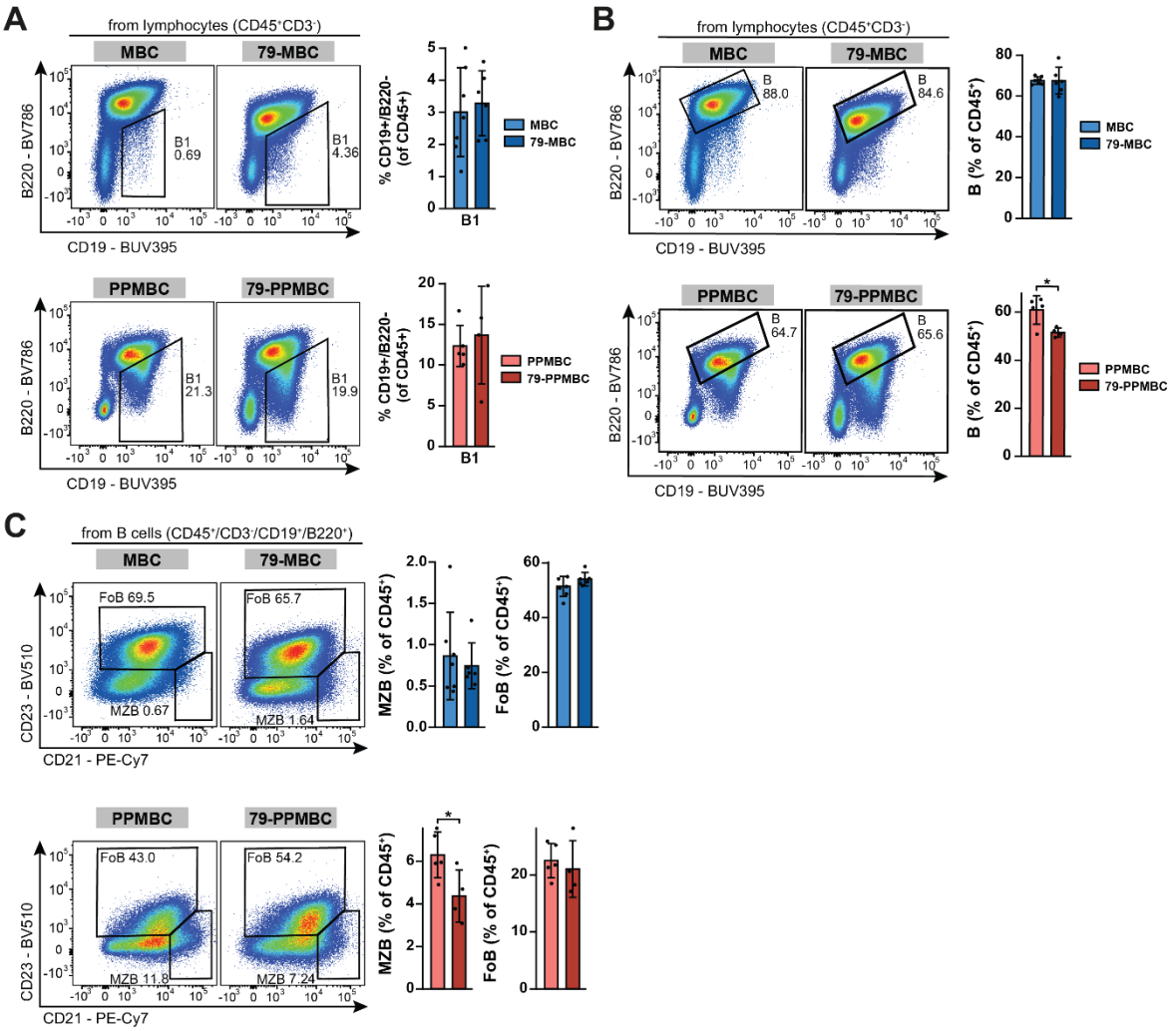

Figure R16 Splenic B cell subsets analyzed by flow cytometry are largely comparable between* Cd79b^{Y195H} *and* Cd79b^{mut} *premalignant animals*.*** *(A) CD19^{+}B220^{-} B1 cells. (B) CD19^{+}B220^{+} B cells. (C) CD23^{+}CD21^{+} FoB and CD23^{-}CD21^{+} MZB cells. *p≤0.05, **p≤0.01, ***p≤0.001, ****p≤0.0001. Welch unpaired two-tailed t test, error bars SD. Note that MBC data was acquired in a different sample set than 79-MBC, PPMBC or 79-PPMBC and comparison is based on normalizing the data to a wt reference sample acquired in both data sets (see 4.6).*

Furthermore, the populations of potential lymphoma precursor cells, $CD38^{-}CD95^{+}$ GCB and $CD38^{+}CD95^{-}$ MB cells, were similar or reduced by the *Cd79b*^{Y195H} mutation. Splenic MB cells were nearly halved in 79-MBC compared to MBC mice, while splenic GCB cell levels in 79-PPMBC mice were roughly a third of the ones in PPMBC mice (Fig. R17).

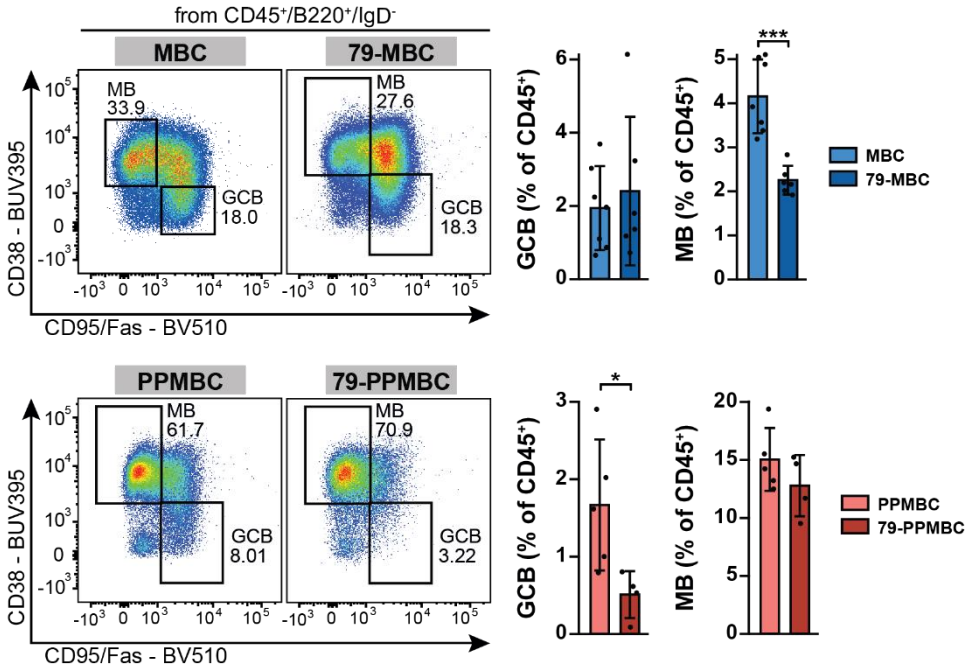

Figure R17 Splenic MB and GCB subsets analyzed by flow cytometry are largely comparable between* Cd79b^{Y195H} *and* Cd79b^{mut} ***premalignant animals. **p≤0.05, **p≤0.01, ***p≤0.001, ****p≤0.0001. Welch unpaired two-tailed t test, error bars SD. Note that MBC data was acquired in a different sample set than 79-MBC, PPMBC or 79-PPMBC and comparison is based on normalizing the data to a wt reference sample acquired in both data sets (see 4.6).*

It might initially be surprising to not observe increased lymphoma progenitor cell levels in the B-cell developmental stages with *Cd79b*^{Y195H} as additional prooncogenic alteration. The lab previously showed that for instance the *MYD88*^{L252P} mutation alone did not affect B cell levels, but overexpression of *BCL2* present in all genotypes investigated in Fig. R16 and Fig. R17 was determining to increase B cell levels (Flümann et al. 2021). Similarly, we observed comparable B cell levels between C, MC, 79-C and 79-MC mice, indicating that *BCL2* overexpression is the basis for increased B cell levels in our MBC and PPMBC lymphoma models (Fig. R18).

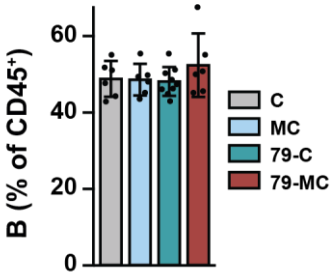

***Figure R18 B cell levels are unaltered in the absence of overexpressed* BCL2.** *Splenic $CD19^{+}B220^{+}$ B cell levels of 10-week-old C (n = 6), MC (n = 6), 79-C (n = 9) and 79-MC (n = 6) animals as determined by flow cytometry.*

5.2.3 *Myd88* and *Cd79b* comutant murine lymphomas closely resemble human ABC-DLBCL

In line with the unaltered amount of lymphoma progenitor cells, addition of *Cd79b*^{Y195H} to the MBC or PPMBC background did not alter median survival of the mice (Fig. R19A), further hinting that the additional pro-oncogenic genetic alteration does not affect lymphoma development itself. As previously demonstrated (Fig. R6A), mice with PPMBC background died earlier than mice with MBC background: PPMBC mice showed a median survival of 37.0 weeks and 79-PPMBC mice of 37.4 weeks, while MBC mice survived 44.0 and 43.2 weeks, respectively (Fig. R19A).

The terminal phenotype was comparable for the MBC or PPMBC background independent of the *Cd79b* status: While most MBC and 79-MBC mice succumbed to B220^{-}CD138^{+} lymphoma, PPMBC and 79-PPMBC mice mostly passed away due to B220^{+}CD138^{-} lymphoma (Fig. R19B). For MBC and 79-MBC mice, several animals died due to non-malignant reasons such as excessive scratch wounds (Fig. R19B). 79-PPMBC mice showed a slightly larger proportion of non-malignant causes of death compared to PPMBC mice as well (Fig. R19B).

When investigating tissue samples using immunohistochemistry, we also observed a similar tumor cell composition independently of *Cd79b* status. Lymphoma structure seemed unaltered, B220 or CD138 expression patterns were comparable, as well as proliferation rates indicated by Ki67 expression (Fig. R19C, D). MRI analysis of lymphoma-bearing animals displayed large lesions affecting spleen, lymph nodes and other organs (Fig. R19E).

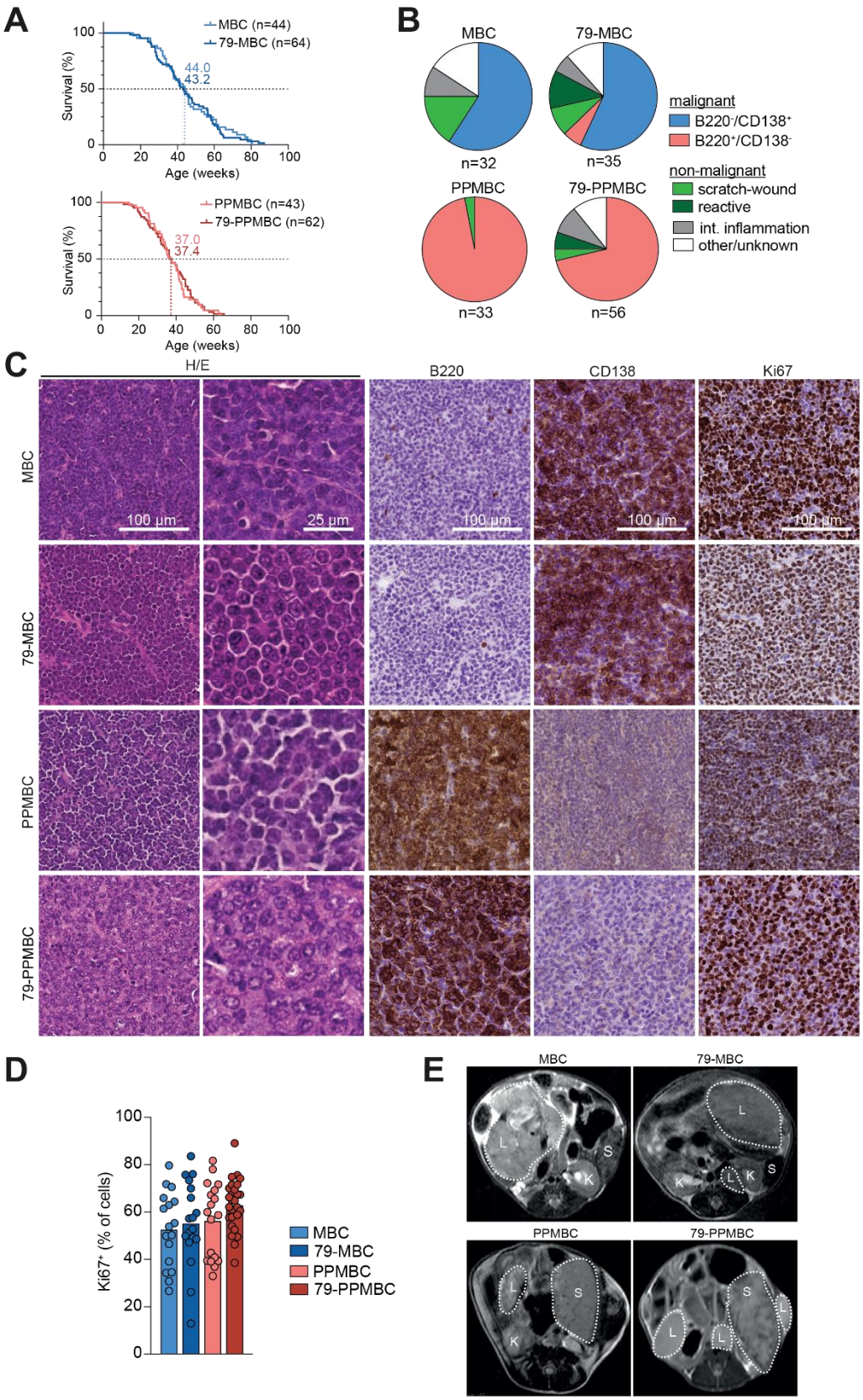

Figure R19* Cd79b^{wt} *and* Cd79b^{Y195H} *lymphomas seem largely comparable. *(A) Overall survival of MBC, 79-MBC, PPMBC and 79-PPMBC mice. (B) Terminal phenotype of MBC, 79-MBC, PPMBC and 79-PPMBC mice. (C) Representative immunohistochemistry stainings of MBC, 79-MBC, PPMBC and 79-PPMBC lymphomas. (D) Quantification of Ki67$^+$ cells in immunohistochemistry stainings of FFPE tissue of MBC, 79-MBC, PPMBC and 79-PPMBC lesions. (E) Representative MRIs of MBC, 79-MBC, PPMBC and 79-PPMBC mice.*

Infiltration patterns of lymphomas seemed largely unaffected by *Cd79b* status, although minor differences were observed: 79-MBC mice presented less involvement of abdominal lymph nodes compared to MBC mice, while 79-PPMBC mice presented less involvement of the submandibular lymph nodes compared to PPMBC mice (Fig. R20).

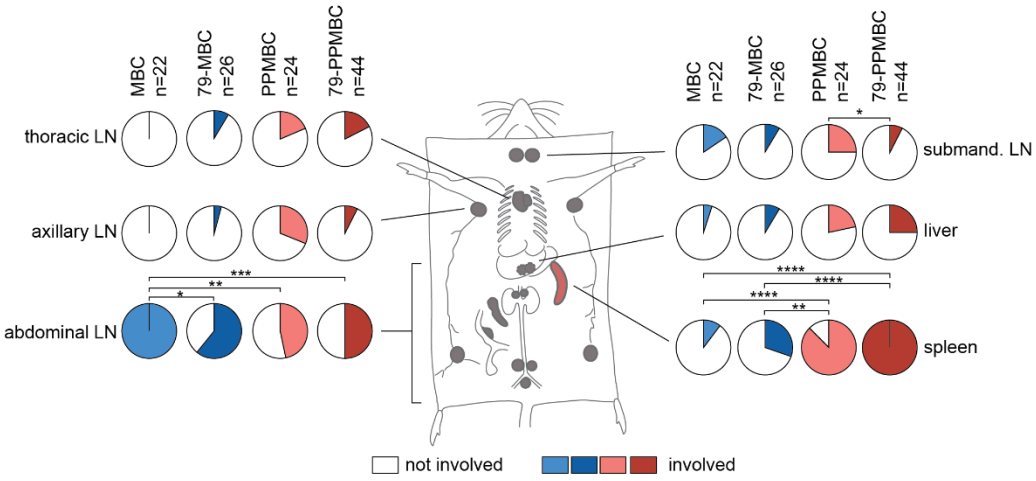

Figure R20* Cd79b^{Y195H} *animals show increased levels of splenic lesions. *Quantification of lymphoma-affected sites at autopsy in MBC, 79-MBC, PPMBC and 79-PPMBC animals. *p≤0.05, **p≤0.01, ***p≤0.001, ****p≤0.0001. Fisher's exact test, corrected for multi-hypothesis testing.*

Also, clonality of the tumor fraction seemed unchanged by *Cd79b* status as determined by BCR sequencing: Investigated tumors demonstrated expansion of one or several clones (Fig. R21A). Clonality fraction was significantly increased for all investigated genotypes compared to PNA$^+$ GC wild-type B cells. Interestingly, when analyzing BCR isotype, we observed a higher fraction of IgM$^+$ lymphomas in 79-PPMBC animals compared to other genotypes (Fig. R21C), which is frequently seen in DLBCL patients (Lenz et al. 2007). To summarize, many features of our autochthonous mouse models are unaffected by *Cd79b*^{Y195H} (survival, cause of death, tumor morphology, B220 expression, CD138 expression, Ki67 expression), but the mutation has a minor effect on lymph node involvement and immunoglobulin expression.

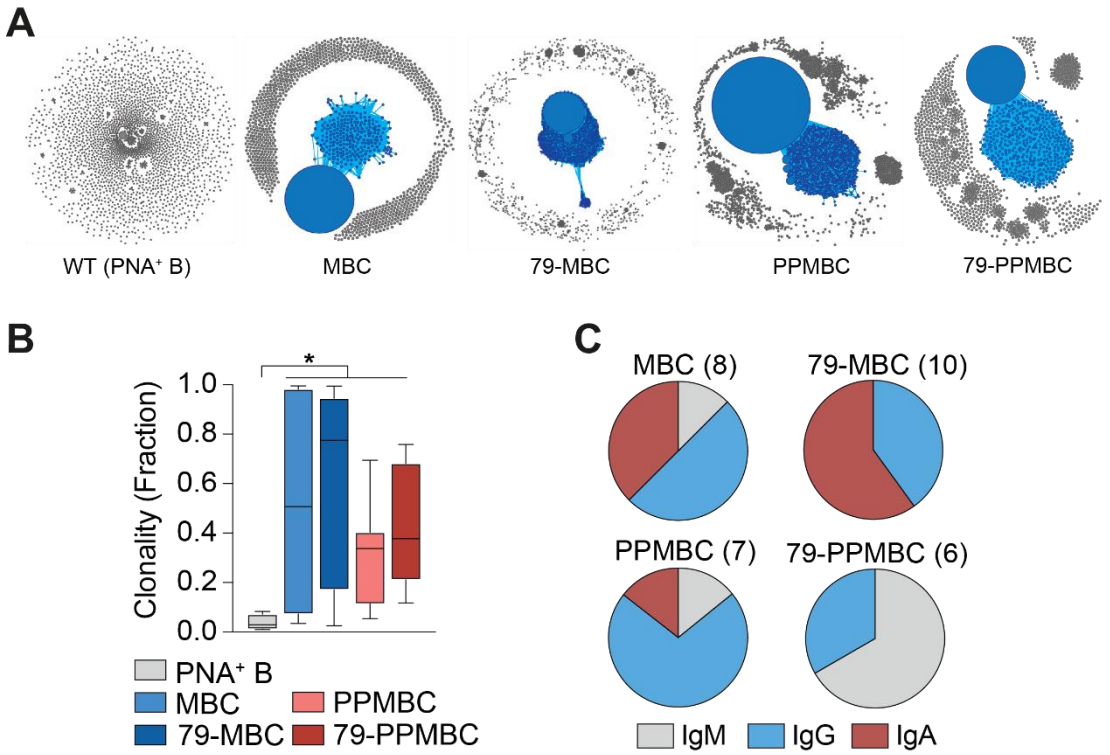

Figure R21 79-PPMBC tumors are (oligo-)clonal and largely IgM+. *(A) Representative clonality plots generated from BCR sequencing data. Main clones are displayed as blue circles connecting to sequences with one mismatch. Individual circles represent a specific V(D)J sequence. The circle size represents the respective readout count. (B) Fraction of the largest clone in each analyzed sample (MBC, n = 8; 79-MBC, n = 10; PPMBC, n = 5; and 79-PPMBC, n = 6) compared to splenic PNA+ B cells from wt animals (n = 4). (C) Immunoglobulin heavy chains identified from BCR sequencing data. *p≤0.05. Welch unpaired two-tailed t test, Benjamini-Hochberg-correction for multihypothesis testing.*

5.2.4 Genetic and transcriptomic features of *Myd88* and *Cd79b* commutant murine lymphomas match human ABC-DLBCLs

To explore our murine *Cd79b* wild-type and mutant lymphomas more deeply, we performed WES and 3'-RNA-sequencing of bulk lymphoma tisue. We previously showed increased expression levels of *Aicda*, the transcript of AID, for PPMBC compared to MBC lymphomas, indicative of ongoing somatic hypermutation (Flumann et al. 2023). This increased level was retained in 79-PPMBC lymphomas. We also observed a trend of increased *Aicda* expression in 79-MBC lymphomas compared to MBC lymphomas (Fig. R22).

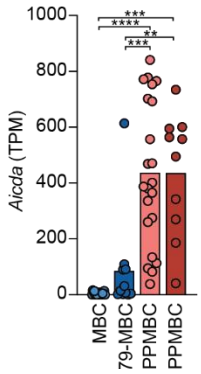

Figure R22* Aicda *expression is increased in PPMBC and 79-PPMBC lymphomas as determined from transcriptome data. **p≤0.05, **p≤0.01, ***p≤0.001, ****p≤0.0001. Welch unpaired two-tailed t test, Benjamini-Hochberg-correction for multihypothesis testing. TPM transcript per million (proportion of a transcript in a pool of all transcripts).*

Independently of *Aicda* expression, lymphomas of all four genotypes presented with acquired mutations in addition to the Cre-induced genetic alterations. Especially 79-PPMBC mice frequently harbored lesions commonly seen in human MCD DLBCL: Mutations in *Pim1*, *Irf2bp2*, *Etv6, Pim2, Vmp1, Bcl2, Nfkbia, Mpeg1, Socs3, Ciita*. Many of the enriched genetic alterations are likely pro-oncogenic and could be relevant for lymphoma biology, warranting further investigation (Fig. R23).

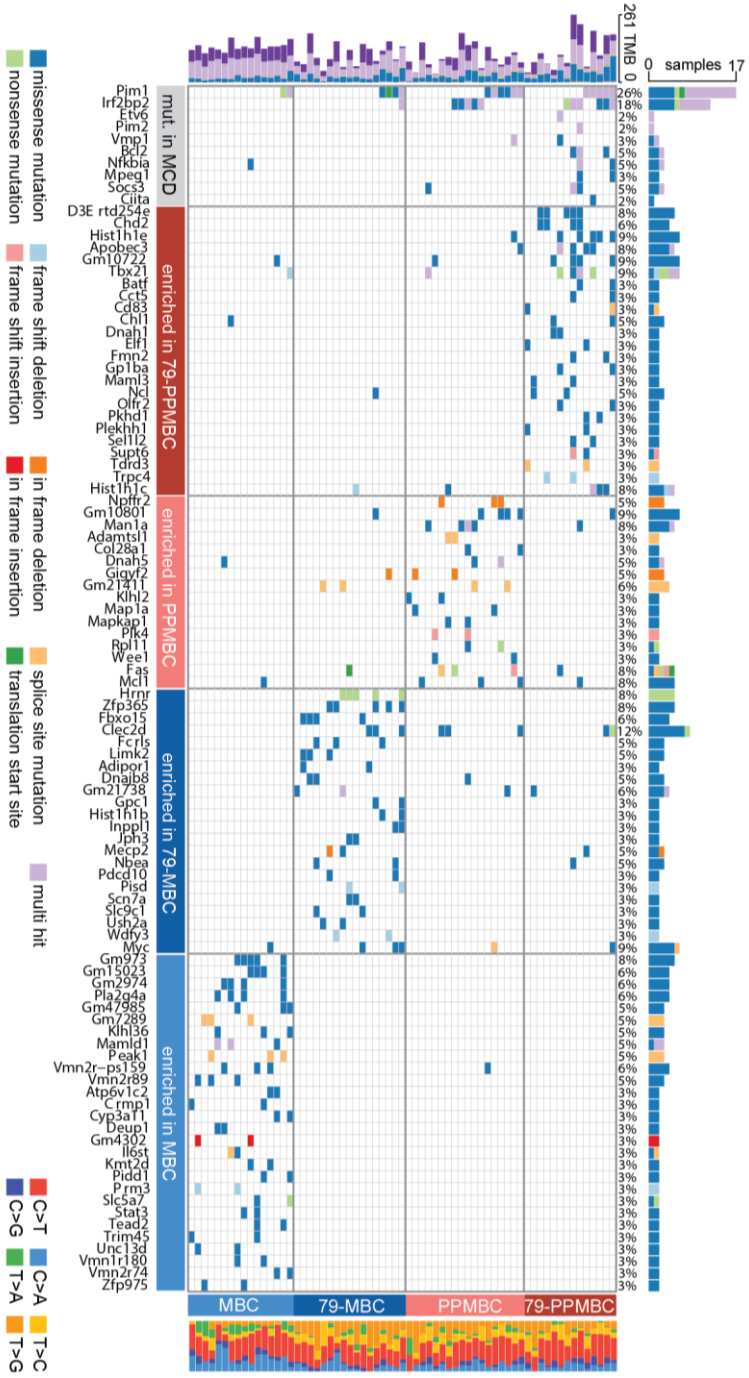

Figure R23 Autochthonous mouse models acquire additional genetic alterations. *Oncoplot displaying recurrently mutated genes from MBC, 79-MBC, PPMBC, and 79-PPMBC lymphomas (WES data). Genes indicated "mut. In MCD" have previously been reported to commonly occur in MCD DLBCL .*

Delving deeper into the origin of these lymphomas in our autochthonous mice, we explored gene set enrichments and surface marker expression for putative founder populations. As previously demonstrated for PPMBC lymphomas (Fig. R11), we again support the notion of the memory B cell lineage as relevant for lymphomagenesis: 79-PPMBC lymphomas expressed memory B cell surface markers (Fig. R24A) and both PPMBC and 79-PPMBC lymphomas had a significantly increased memory B cell score (Fig. R24B). Due to the plasma cell differentiation block mediated by loss of *Prdm1*, these cells are unable to terminally differentiate and likely cycle between GCB and MB stages, facilitating the path to lymphomagenesis.

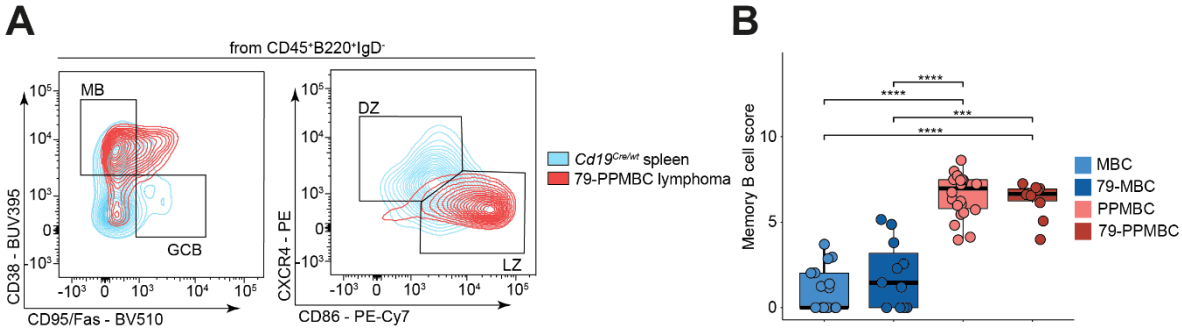

***Figure R24 79-PPMBC lymphomas are related to memory B cells**. (A) Overlay of representative flow cytometry analyses of healthy splenic C cells (blue) and 79-PPMBC lymphoma cells (red) with indicated memory B cell (MB) and GC B cell (GCB) gates. (B) A memory B cell score was derived from the estimated memory B cell count determined by mMCP-counter in gene expression data (n = 60). *p≤0.05, **p≤0.01, ***p≤0.001, ****p≤0.0001. Welch unpaired two-tailed t test, Benjamini-Hochberg-correction for multihypothesis testing.*

5.2.5 *Myd88* and *Cd79b* co-mutant murine lymphomas harbor amplified BCR signaling

When probing *Cd79b*^{Y195H} lymphoma cells for BCR signaling activation by flow cytometry analyses of lymphoma cell suspensions, we observed significantly increased levels of activating phosphorylation of the BCR signaling adaptors PLCg2 and SYK in 79-MBC compared to MBC, and 79-PPMBC compared to PPMBC lymphomas, respectively (Fig. R25). The *Cd79b*^{Y195H} mutation seemed to amplify BCR signaling in these lymphomas, offering up a potential treatment strategy (see 5.2.6).

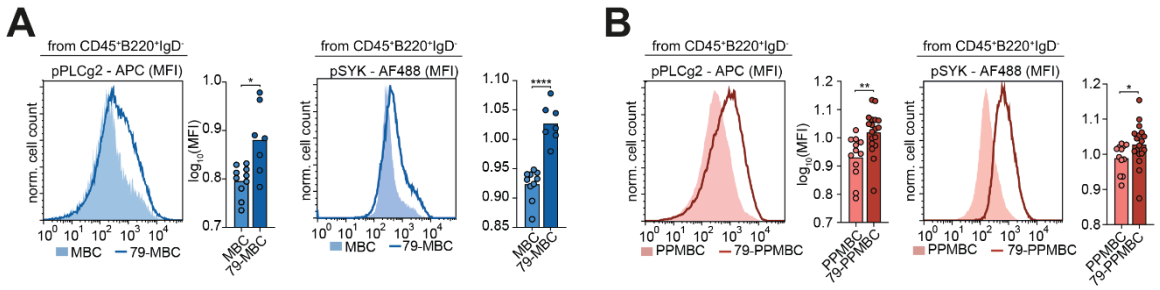

***Figure R25 Phosphorylation of BCR signaling adaptors is increased in* Cd79b^{Y195H} *lymphomas**. Flow cytometry analysis of phosphorylated BCR signaling adaptors PLCg2 and SYK. Representative and quantification for the comparison of (A) MBC (n = 10) and 79-MBC (n = 7) lymphomas or (B) PPMBC (n = 12) and 79-PPMBC (n = 18) lymphomas. *p≤0.05, **p≤0.01, ***p≤0.001, ****p≤0.0001. Welch unpaired two-tailed t test.*

In contrast to this notion, when comparing healthy B cells extracted from spleens between 79-C and C mice, we found no indication of increased BCR signaling (Fig. R26). Although it was previously assumed that ITAM mutations of *Cd79b* decrease internalization of the BCR complex upon stimulation (Gazumyan, Reichlin, and Nussenzweig 2006), we found no similar evidence of this for the single *Cd79b*^{Y195H} mutation in nonmalignant B cells investigated here (Fig. R26A). Likewise, in phospho flow cytometry data, activating phosphorylation levels for SYK and PLCg2 were comparable between 79-C and C mice (Fig. R26B). To summarize, although *Cd79b*^{Y195H} amplified BCR signaling in lymphoma samples of autochthonous C5/MCD mouse models, healthy spleen cells of mice carrying *Cd79b*^{Y195H} without additional pro-oncogenic alterations showed no indication of increased BCR signaling levels.

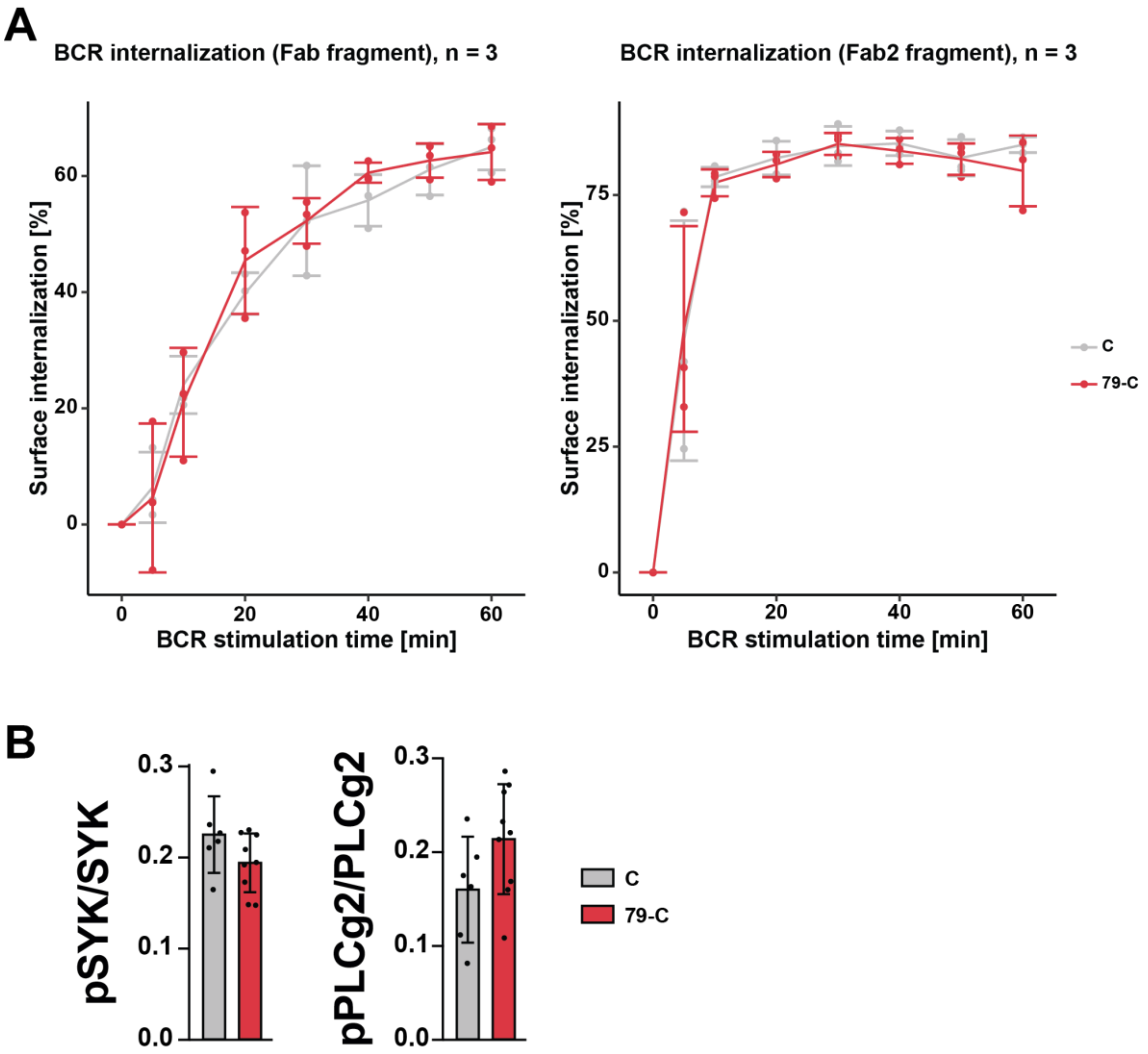

Figure R26* Cd79b^{Y195H} *alone is insufficient to increase BCR signaling. *(A) Splenic naïve B cells from healthy C and 79-C mice were stimulated for the indicated time points with IgM-binding Fab or F(ab)$_2$ fragments. Surface BCR was subsequently quantified by flow cytometry to determine the fraction of internalized BCR, normalizing to time point 0 (unstimulated). (B) Quantification of flow cytometry analysis of phosphorylated BCR signaling adaptors PLCg2 and SYK normalized to bulk protein levels in splenic B cells of 10-week-old C (n = 6) and 79-C (n = 9) mice. *p≤0.05, **p≤0.01, ***p≤0.001, ****p≤0.0001. Welch unpaired two-tailed t test.*

5.2.6 The *Cd79b*^{Y195H} mutation confers a targetable reliability on BCR signaling

MYD88 and *CD79B* co-mutant lymphomas were previously reported to initiate the My-T-BCR supercomplex driving malignant BCR signaling in C5/MCD DLBCLs (Phelan et al. 2018; Mandato et al. 2023). To investigate the occurrence of this complex in our lymphoma model, we used proximity ligation assays (PLAs) to test for interaction of MYD88 as TLR signaling adaptor and several BCR components (Fig. R27). Using probes for two proteins of interest at a time, PLA uses an *in situ* rolling circle amplification of DNA only possible if both probes are in close proximity (Hegazy et al. 2020). Subsequent staining for the amplified DNA enables highly sensitive detection, visualizing protein colocalization within 40nm (Hegazy et al. 2020). As a control, we demonstrated significantly increased PLA signal when using probes specific for our proteins of interest compared to IgG isotype controls (Fig. R27C).

In line with the presence of a signaling complex formed by TLR and BCR components, we observed increased colocalization of MYD88 with the BCR signaling components CD79B, MALT1 and BTK in *Cd79b*^{Y195H} compared to *Cd79b*^{wt} lymphoma sections both in the PPMBC and the MBC background (Fig. R27A, B). Intriguingly, when we treated animals for three days with ibrutinib and took samples on the fourth day, this acute ibrutinib treatment abolished colocalization to *Cd79b*^{wt} baseline levels in both backgrounds (Fig. 27A, B). Hence, inhibition of BTK by ibrutinib appears to perturb this signaling complex, potentially interrupting the proliferative BCR signaling required by the lymphoma.

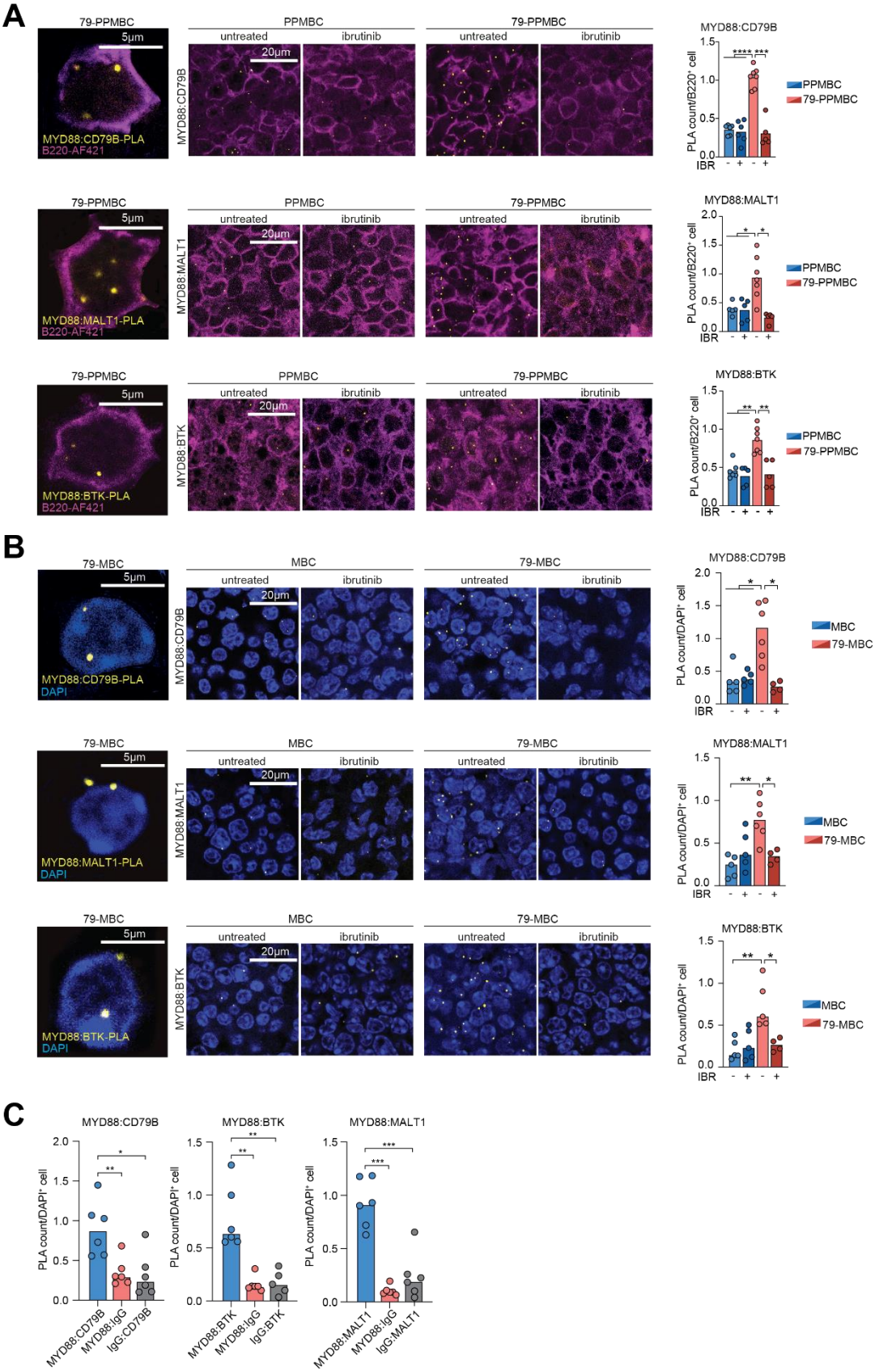

Figure R27* Cd79b^{Y195H} *promotes the formation of a MYD88-BCR complex which can be disrupted by acute ibrutinib treatment. *(A, B) PLAs targeting MYD88 and BCR signaling components in FFPE tissue from (A) PPMBC and 79-PPMBC or (B) MBC and 79-MBC lymphomas, as well as from animals acutely treated with ibrutinib of the respective genotype. (C) Control PLA of the indicated target proteins with an IgG isotype control. *p≤0.05, **p≤0.01, ***p≤0.001, ****p≤0.0001. Welch unpaired two-tailed t test, Benjamini-Hochberg multihypothesis correction.*

To investigate the long-term effects of this BCR signaling inhibition, we treated lymphoma-bearing animals orally with ibrutinib for several weeks. We had previously demonstrated ibrutinib treatment to prolong survival of PPMBC mice (Fig. R18) and again demonstrated a survival benefit of several weeks for PPMBC mice, while survival of MBC mice was comparable between untreated and ibrutinib-treated animals (Fig. R28). The *Cd79b*^{Y195H} mutation, however, enhanced the response to ibrutinib in both MBC and PPMBC backgrounds, leading to an astonishing lymphoma regression especially in 79-PPMBC mice, increasing survival by several months (Fig. R28). We therefore conclude the *Cd79b*^{Y195H} mutation to be indicative for ibrutinib response in *Myd88*- and *Bcl2*-driven lymphomas.

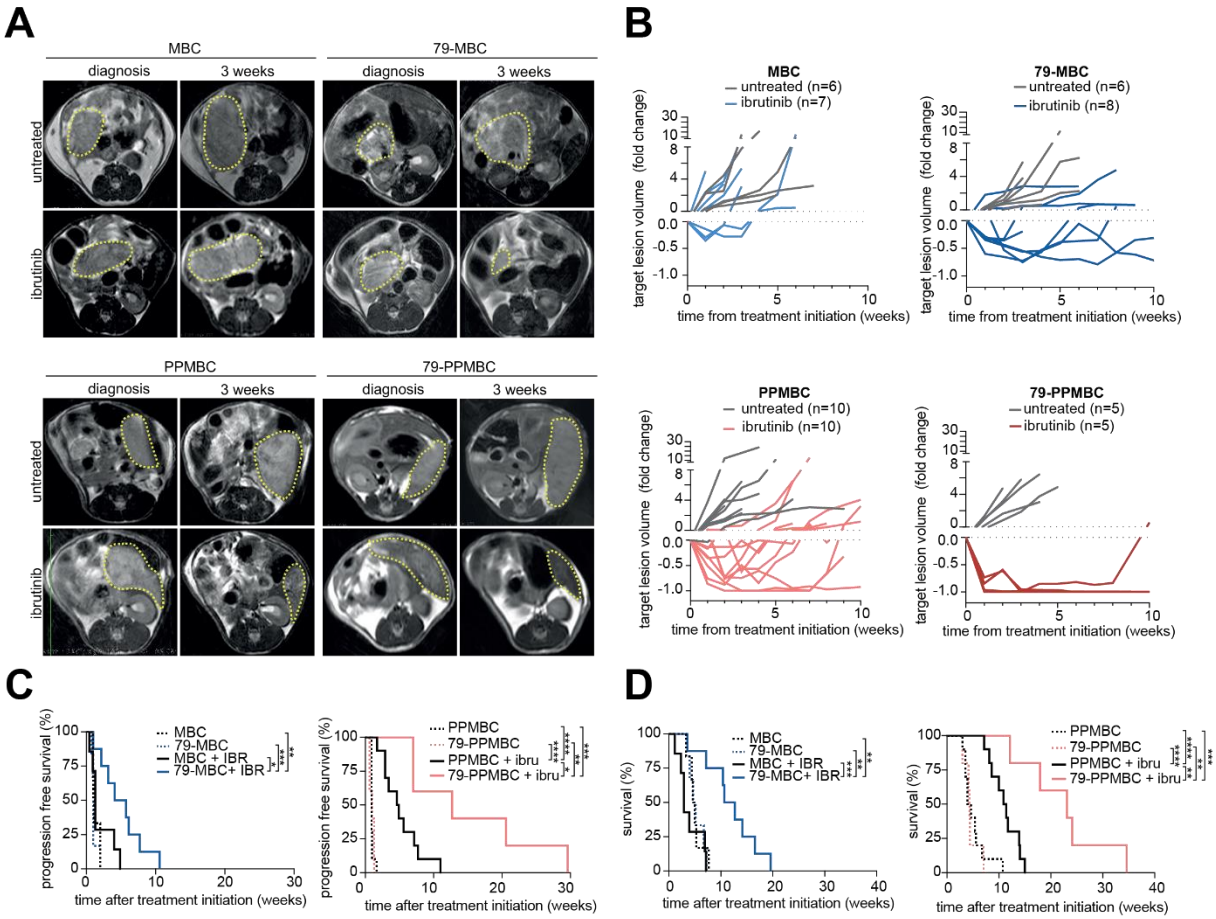

Figure R28 Mice carrying the* Cd79b^{Y195H} *have an enhanced response to ibrutinib. *(A) Representative MRI images of lymphoma-bearing animals at diagnosis and after 3 weeks of ibrutinib treatment. (B) Tumor volume development as determined by MRI in untreated and ibrutinib-treated animals. (C) Progression-free survival and (D) overall survival of animals left untreated or treated with ibrutinib. *p≤0.05, **p≤0.01, ***p≤0.001, ****p≤0.0001. Log-rank test.*

This astounding result notwithstanding, all mice eventually relapsed under continuous ibrutinib treatment and succumbed to the disease (Fig. R28C, D). Interestingly, when performing PLA for MYD88 and CD79B on FFPE samples from relapsed 79-MBC and 79-PPMBC mice, we found the colocalization of the two signaling complex components to be significantly increased compared to the acutely treated samples, even restored to naïve levels in 79-MBC samples (Fig. R29A, B). Consistently, levels of activating phosphorylation of the BCR signaling adaptors SYK and PLCg2 did not differ between naïve and relapsed 79-PPMBC samples (Fig. R29D), although it is necessary to highlight that only two

relapsed samples were available for phospho flow cytometry analysis. We observed a significant decrease of B cell levels in relapsed compared to treatment-naïve 79-PPMBC lymphoma samples, hinting at novel tumor-driving mechanisms in relapsed 79-PPMBC mice (Fig. R29C). When performing WES on relapsed 79-MBC and 79-PPMBC lymphoma samples, we did not observe canonical resistance-conferring BTK mutations as frequently seen in patients (Nakhoda, Vistarop, and Wang 2022), but genetic alterations in other genes whose relevance for ibrutinib resistance needs to be investigated further (Fig. R29E). Taken together, we present additional autochthonous mouse models of C5/MCD DLBCL, the 79-MBC and 79-PPMBC models. We demonstrated a targetable dependency on increased BCR signaling in the *Cd79b* mutant setting and explored ibrutinib resistance mechanisms.

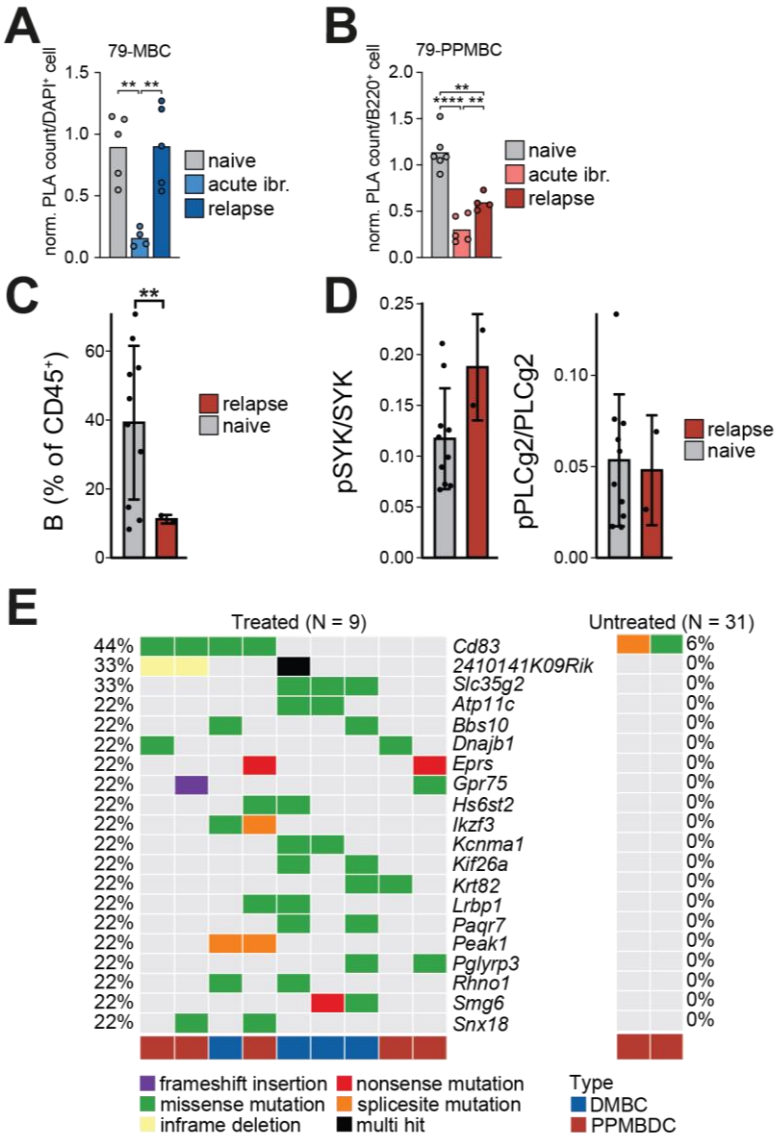

Figure R29 Relapse under continuous ibrutinib exposure seems associated with partially restored BCR signaling. *(A, B) PLA counts of colocalized MYD88 and CD79B in FFPE lymphoma tissue from naïve, acutely ibrutinib-treated and relapsed (A) 79-MBC and (B) 79-PPMBC lymphomas. (C) Quantification of B220⁺CD19⁺ B cell fraction in lymphomas of treatment-naïve (n = 10) and ibrutinib-relapsed (n = 2) 79-PPMBC mice analyzed by flow cytometry. (D) Quantification of phosphorylated SYK and PLCg2 normalized to bulk protein levels in lymphomas of treatment-naïve (n = 10) and ibrutinib-relapsed (n = 2) 79-PPMBC mice analyzed by flow cytometry. (E) Genetic alterations determined by WES of lymphomas from 79-MBC and 79-PPMBC mice relapsed under continuous ibrutinib treatment. Genes with a significantly higher mutation frequency in the relapsed cohort than in naïve samples (Fisher's exact test) are visualized. **p≤0.01, ***p≤0.001, ****p≤0.0001. Welch unpaired two-tailed t test, Benjamini-Hochberg multihypothesis correction.*

5.3 Autochthonous mouse models show metabolic distinctions

5.3.0 Contributions

Chapter 5.3 contains unpublished data.

The following figure was retrieved from the publication for 5.2 (Flumann et al. 2024): Fig. R30

The following figures were generated solely for this thesis: Fig. R31, R32, R33, R34, R35; SR4, SR5, SR6, SR7

Detailed contributions relevant for this thesis are as following:

J. Hansen, R. Flümann, R. Jachimowicz, H.C. Reinhardt and G. Knittel conceptualized and designed the project.

R. Flümann, J. Hansen, H. Goldfarb Wittkopf and A. Lütz prepared samples for transcriptomic analyses and WES. G. Knittel and S. Klein analyzed transcriptomes and WES.

J. Hansen and R. Flümann performed metabolomics experiments. Mass spectrometry analysis was executed by the metabolomics core facility of the MPI for Biology of Ageing. J. Hansen analyzed metabolomics data.

J. Hansen conducted and analyzed SeaHorse experiments.

J. Hansen performed and analyzed viability assays under ibrutinib treatment.

J. Hansen, R. Flümann, M. Hützen and Y. Elkis carried out the ibrutinib/IACS combination screen. J. Hansen analyzed screen data.

Resources were contributed by R. Jachimowicz, T. Langer, A. Trifunovic.

5.3.1 Genetic alterations shape tumor metabolism in autochthonous DLBCL mouse models

To uncover the molecular mechanisms driving lymphomagenesis in our different autochthonous mouse models, we employed bulk RNA-sequencing of lymphoma tissue of the four different genotypes MBC, 79-MBC, PPMBC and 79-PPMBC (see also 5.2.4). Unsupervised clustering using a Partitioning Around Medoids approach segregated samples from all four genotypes into two distinct clusters, apparently dictated by the loss of *Prdm1*. While all PPMBC and 79-PPMBC samples were assigned to cluster 1, the MBC and 79-MBC samples (except for one case) were assigned to cluster 2. Each cluster was defined by overexpression of genes in the respective genotypes (Fig. R30A).

"To uncover gene sets that were associated with each cluster, we applied an overrepresentation analysis, using enrichr (Chen, Tan, et al. 2013). In line with our previously published data (Flumann et al. 2023) this overrepresentation analysis revealed that PPMBC and 79-PPMBC lymphomas displayed a significantly higher expression of genes associated with the "BCR Signaling Pathway," "TNF-alpha Signaling via NF-κB," "NF-kappaB complex," and "B cell receptor complex" gene sets from the Jensen, Hallmark, and WikiPathways reference gene sets, respectively." (Flumann et al. 2024)

Further analysis of the enriched gene sets revealed an overrepresentation of genes involved in the fatty acid synthase complex in PPMBC and 79-PPMBC mice (cluster 1), as well as overrepresentation of glycolysis genes in MBC and 79-MBC mice (cluster 2), hinting at metabolic distinctions between the genotypes (Fig. R30A).

"We next performed an additional overrepresentation analysis, using enrichr. However, this time, we included genes that were recurrently mutated for each individual genotype to evaluate our observation regarding the enrichment of genes frequently mutated in C5/MCD DLBCL. Through this analysis, we discovered that the recurrently mutated genes in our 79-PPMBC genotype were significantly associated with "B-cell activation" and "DLBCL ABC subtype," among other factors." (Fig. 30B) (Flumann et al. 2024)

In addition, the ceramide signaling pathway was significantly affected in our 79-PPMBC genotype (Fig. R30B). Ceramides are biologically active lipids involved in several cellular signal transduction pathways (Shalaby et al. 2021). A ceramide disbalance might affect signaling in 79-PPMBC lymphomas. On the other hand, both 79-MBC and MBC mice scored for genetic alterations in the oxidative stress response (Fig. R30B). This could induce a targetable imbalance between the production of reactive oxygen species and the tumor's ability to detoxify these reactive intermediates (Bhatti, Bhatti, and Reddy 2017). The metabolic distinctions in our different mouse models might affect lymphomagenesis and/or treatment response as well, prompting us to investigate the metabolism of tumors and cell lines in more detail.

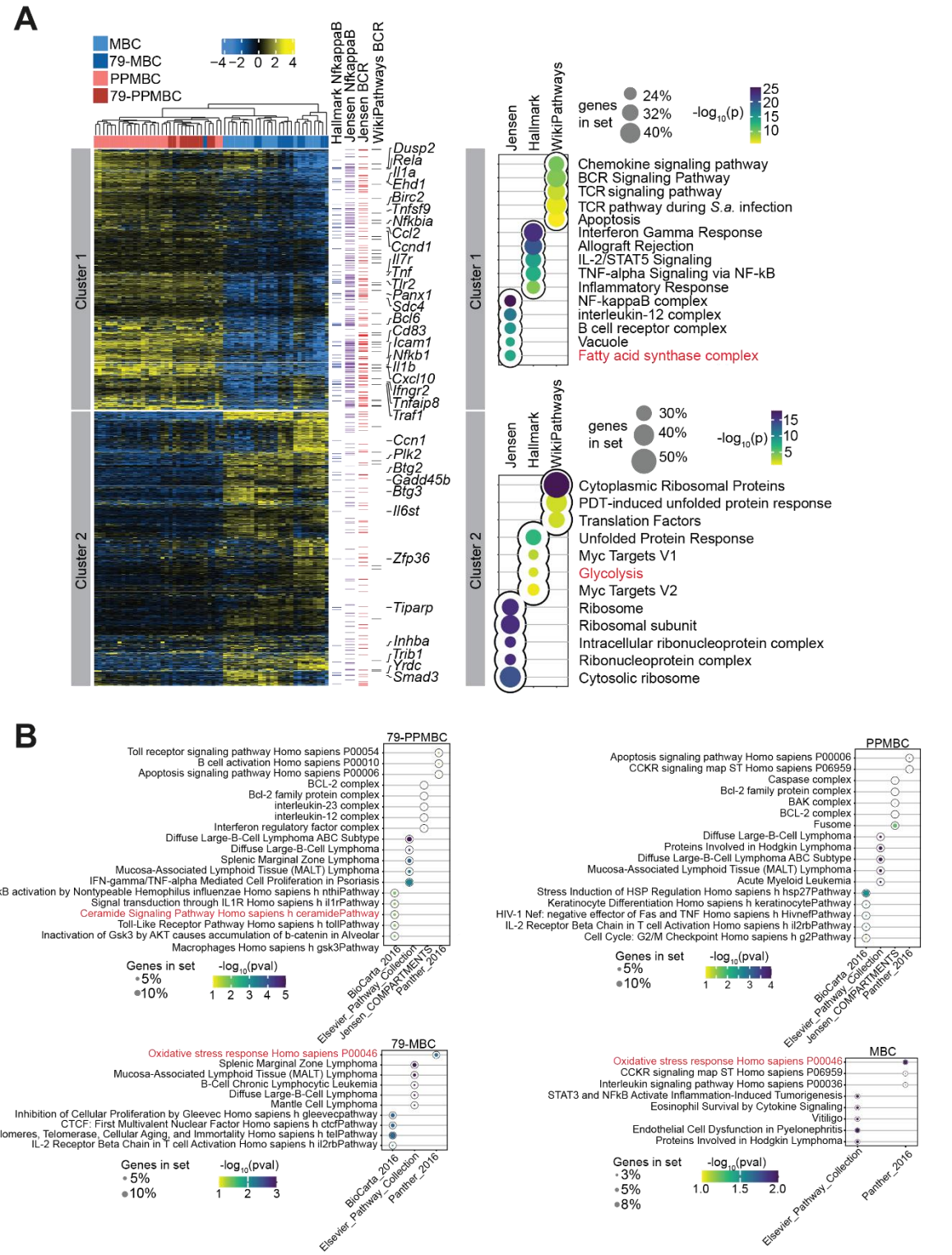

Figure R30 MBC, 79-MBC, PPMBC and 79-PPMBC lymphomas display distinct transcriptomic signatures, among them metabolic differences. *(A) Transcriptomic data for the different genotypes was acquired and two clusters were assigned by unsupervised clustering of gene expression data, dividing MBC and 79-MBC versus PPMBC and 79-PPMBC samples (with one MBC sample intruding into the latter cluster). Genes expressed differentially between the clusters are displayed in a heatmap with color-coded logarithmic fold changes. "Highlighted MGI Gene Symbols were extracted from the Hallmark NfkappaB signature, Jensen compartments of NfkappaB, Jensen B-cell receptor (BCR) complex, and WikiPathways BCR, which were also significantly enriched in cluster 1. […] The size of the dot corresponds to the number of genes overlapping between the given cluster and the gene set, whereas the adjusted p value is visualized following a color code with an individual legend being provided." (Flumann et al. 2024) (B) "Gene set enrichment analyses were performed on the list of significantly mutated genes in lymphomas of the indicated genotypes." (Flumann et al. 2024) (A, B) Gene sets directly involved in metabolic alterations are highlighted in red.*

5.3.2 Metabolite levels differ between genotypes and treatment groups

To investigate the metabolic differences between tumors of different genotypes, we extracted bulk metabolites (polar metabolites including amino acids, lipids) from cryo-conserved tumor tissue. Metabolites were analyzed by chromatography followed by mass spectrometry, and metabolites were normalized using heavy ion-labeled standards (see 4.14). From the resulting metabolite quantities, samples were grouped by genotype and treatment. Significant differences between groups were determined by t test followed by Benjamini-Hochberg multiple hypothesis testing correction, then depicted in a volcano plot (Fig. R31).

Interestingly, we observed several metabolites to be significantly different when comparing 79-MBC and MBC tumors. For polar metabolites (Fig. R31A), dCTP and dTTP were upregulated in 79-MBC tumors compared to MBC tumors. The increased levels of these DNA precursors suggest alterations in the nucleotide biosynthesis pathway, which could be indicative of increased cell proliferation or alterations in DNA repair processes (Sobanski et al. 2021; Diehl et al. 2022).

When comparing lipid levels (Fig. R31B), a high number of specific lipids differed between genotypes as well:

4 species of acylcarnitines (AcCa) were significantly upregulated in MBC tumors compared to 79-MBC tumors. These metabolites primarily facilitate the transport of long-chain fatty acids into the mitochondria for fatty acid oxidation (Dambrova et al. 2022). Increased levels might hint at augmented fatty acid metabolism.

2 phosphocholines (PCh) were significantly upregulated in 79-MBC tumors compared to MBC tumors, and 8 species of PChs were significantly increased in MBC tumors compared to 79-MBC tumors. PChs are a major component of cell membranes, regulating their physical properties, and also relevant for the biosynthesis of other lipids (van der Veen et al. 2017).

2 lysophosphocholines (LPC) were significantly increased in MBC tumors compared to 79-MBC tumors. LPCs are degradation products of PChs, but also involved in cell signaling such as regulation of inflammation (Liu et al. 2020). Altered levels implicate differing PCh degradation and/or cellular signaling.

6 species of phosphoethanolamines (PE) were significantly upregulated in 79-MBC tumors compared to MBC tumors. Comparably to PChs, PEs are abundant in cellular membranes, and the PCh/PE ratio affects membrane properties like dynamics of lipid droplets (van der Veen et al. 2017).

2 species of triglycerides (TG) were significantly increased in MBC tumors. TGs are classical lipids for cellular energy storage (Alves-Bezerra and Cohen 2017).

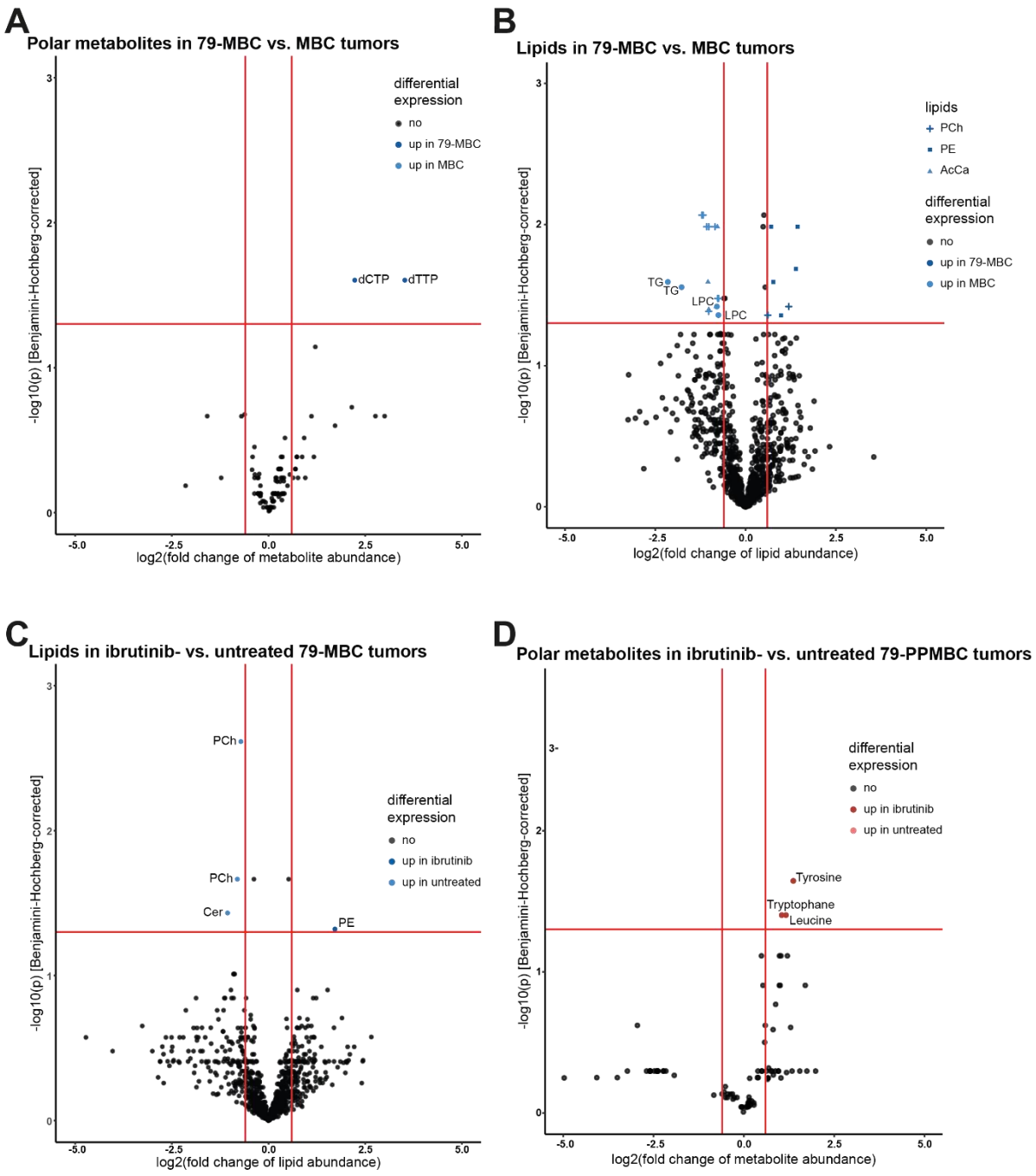

Figure R31 Lymphomas from different genotypes and treatment groups show individually altered metabolites in metabolomics data*. Comparison of polar metabolites (A) and lipids (B) between 79-MBC (n = 3) and MBC (n = 6) tumors. (C) Comparison of lipids in ibrutinib-treated (n = 5) vs. untreated 79-MBC tumors (n = 3). (D) Comparison of polar metabolites between or 79-PPMBC (n = 6) and PPMBC (n = 6) tumor samples. Unpaired two-samples t-test, Benjamini-Hochberg-corrected for multi hypothesis testing.*

When further dissecting each significantly altered lipid (Supplementary Table 1), little was known about their individual role and function in distinction to other, closely related lipids from the same lipid class that were not significantly altered. This makes interpretation of lipidomics data challenging, since the relevance of a single altered lipid species is unclear. While our results do give indications for altered metabolic pathways in 79-MBC versus MBC tumors, the specific pathways and the significance of potentially minor differences remain undetermined.

Surprisingly, when performing the same analysis comparing 79-PPMBC and PPMBC tumor tissues, we did not observe any significantly altered polar metabolite or lipid between the two genotypes (Fig. SR4A, B). This indicates that alterations between 79-MBC and MBC tumors likely do not originate solely from the mutation of *Cd79b* and further underlying mechanisms might play into them. Since we previously demonstrated the PPMBC and 79-PPMBC models to be more closely related to human ABC DLBCL than the MBC and 79-MBC models (see also 5.1, 5.2), the relevance for differences between the two latter models for patient care is uncertain. Therefore, dissecting the underlying metabolic differences between all four investigated mouse models is beyond the scope of this project, although follow-up experiments might still give valuable insight into lymphomagenesis and the biology of these mouse models in the future.

The BTK inhibitor ibrutinib was previously reported to affect cell metabolism in mantle cell lymphoma and chronic lymphocytic leukemia (Zhang et al. 2019; Galicia-Vázquez and Aloyz 2018). Additionally, ibrutinib-resistant cell line models shifted their metabolism from glycolysis to oxidative phosphorylation (Choueiry, Singh, Sircar, et al. 2021). After previously demonstrating efficacy of the BTK inhibitor ibrutinib in 79-MBC and 79-PPMBC mice (see 5.2.6), we decided to investigate our mouse models for metabolic changes upon ibrutinib treatment. To this end, we collected tumor tissue from mice treated with ibrutinib for 3 days and acquired metabolomics data (acutely ibrutinib-treated, see 4.1). When comparing metabolite levels of tumor tissue from acutely treated MBC and 79-MBC mice with tissue from untreated animals, we again observed metabolic alterations (Fig. R31C, Fig. SR5):

In 79-MBC tissue, no significantly altered polar metabolites were found when comparing ibrutinib-treated and untreated tumor tissue (Fig. SR5A), but 2 PCh and 1 Cer were upregulated in the untreated setting, while 1 PE was upregulated in ibrutinib-treated tumor tissue (Fig. 32C). These individual lipids were again of unknown significance (Supplementary table 3).

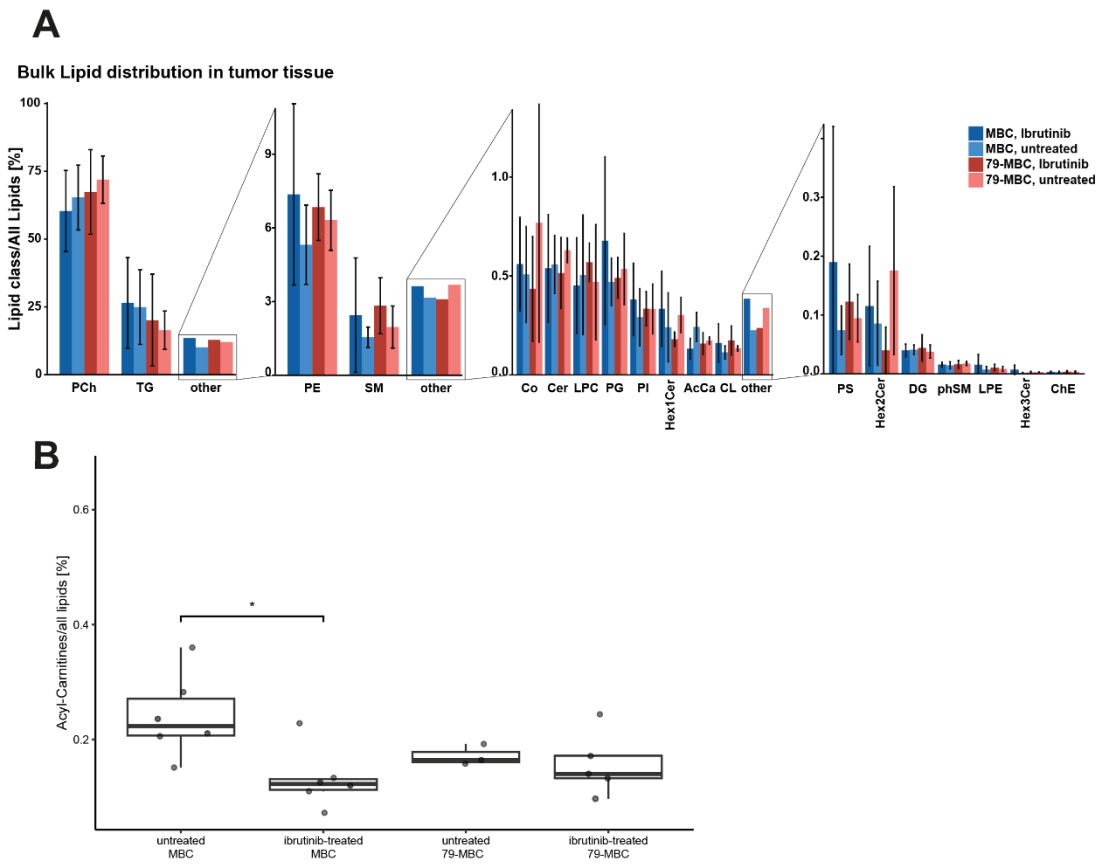

Figure R32 Bulk lipid classes do not differ between MBC and 79-MBC tumors, but AcCa levels differ between untreated and ibrutinib-treated MBC samples*. (A) Comparison of all lipid classes between MBC and 79-MBC tumor samples, untreated and acutely ibrutinib-treated. PCh phospphocholine, TG triacylglycerols, PE phospholethanolamine, SM sphingomyelin, Co coenzyme Q, Cer ceramide, LPC lysophoshphocholine, PG phosphoglycerol, PI phosphoinositol, Hex1,2,3Cer Mono-/Di-/Trihexosylceramide, AcCa acylcarnitine, CL cardiolipin, PS phosphoserine, DG diacylglycerol, phSM phytosphingomyelin, LPE lysophosphoethanolamine, ChE cholesterol ester. Note that when comparing untreated with treated groups or MBC with 79-MBC data using unpaired two-samples t-test with Benjamini-Hochberg-correction for multi hypothesis testing, all p>0.05. (B) Focused comparison of bulk acyl-carnitine levels between MBC and 79-MBC tumor samples, untreated and acutely ibrutinib-treated. *p<0.05, ANOVA with Tukey's post-hoc test.*

In untreated MBC tumor tissue, creatine, which is important for recycling of ATP in energy-intense tissue (Bonilla et al. 2021), was overrepresented when comparing to ibrutinib-treated tissue, indicating altered energy metabolism (Fig. SR5B). A multitude of lipids was affected in ibrutinib- versus untreated MBC tumor tissue, namely 7 AcCas, 9 ceramides (Cer) and 2 hexylceramides (Hex3Cer), 2 diglycerides (DG), 1 LPC, 42 PChs, and 5 PEs (Figure SR5C, Supplementary Table 2). Again, bulk lipid class levels seem unaffected (Fig. R32A), except for AcCas: Ibrutinib-treated MBC tumor tissue displayed a significant reduction of bulk AcCa levels compared to untreated MBC tumor tissue (Fig. R32B). The role of this alteration is unclear, and interpretation of these results is impeded by the fact that it is impossible to distinguish a metabolic response to ibrutinib and the metabolic alterations induced by tumor apoptosis which might be initiated by ibrutinib, especially in the responding 79-MBC genotype. Further experiments, such as sampling at different time points or performing metabolic flux analyses, would be necessary to clarify this distinction.

This uncertainty is given further substance by data comparing ibrutinib-treated with untreated PPMBC and 79-PPMBC tumor tissue (Fig. 31D, Fig. SR6). Lipids were not significantly altered between treatment groups, neither were polar metabolites in PPMBC tumor tissue. 79-PPMBC tumor tissue displayed a significant increase of three amino acids in ibrutinib-treated mice compared to untreated mice (Fig. R31D), namely tyrosine, leucine and tryptophane. While leucin and tryptophane are considered nonpolar amino acids, tyrosine has a polar alcohol group. The three amino acids do not originate from the same biosynthesis pathway, again complicating explanation of this phenomenon.

Taken together, we observed differences in metabolite levels between tumor tissue from different genotypes and treatment groups in our autochthonous mouse models. MBC and 79-MBC tumor tissue differed in the abundance of deoxy-nucleotides and several individual lipid species with unclear function. In contrast, when comparing PPMBC and 79-PPMBC tumor tissue, no significantly altered metabolites were detected. Ibrutinib treatment, on the other hand, altered individual metabolite abundance in MBC, 79-MBC, and 79-PPMBC tumors. Abundance of bulk AcCas was significantly decreased in ibrutinib-treated compared to untreated MBC tumors, hinting at an altered fatty acid metabolism, and several amino acids were increased when comparing ibrutinib-treated with untreated 79-PPMBC tumors. However, no clear picture or mechanism explaining these alterations emerges, making interpretation of our data challenging. Additionally, the low sample size of 3-6 tumors per genotype and treatment group might render the study underpowered. Further investigation will be required to draw meaningful conclusions.

5.3.3 Ibrutinib treatment does not significantly affect ATP production by glycolysis and oxidative phosphorylation in murine cell lines

To determine whether the altered metabolite levels seen in our metabolomics data might be related to differential activation of metabolic pathways such as glycolysis or oxidative phosphorylation, we decided to perform SeaHorse experiments using cell lines derived from tumors obtained from our autochthonous mouse models. Using SeaHorse experiments, automatic, real-time measurements of cellular oxygen consumption rate (OCR) and extracellular acidification rate (ECAR) can be conducted, enabling the derivation of ATP production rates of live cells for analysis of mitochondrial respiration and glycolysis (Agilent website). While preliminary experiments indicated alterations induced by ibrutinib-treatment of our cell lines (data not shown), appropriate normalization and experiment standardization abolished these differences. Specifically, we observed no significant alteration of ATP production rates by glycolysis or mitochondrial respiration by pre-treating the 79-MBC cell line BSQ_12 with DMSO or different concentrations of ibrutinib ranging from 1-100nM (Fig. R33A and Fig. SR7). *In vivo* setting, we had treated mice with 30mg ibrutinib per kg body weight, corresponding to ~68µM given orally, which with a bioavailability of ~10% (De Vries et al. 2016) corresponds to an order of magnitude of µM as maximal therapeutic concentration. Note that the IC50 for ibrutinib is >5µM in

BSQ_12 (Fig. R34D), which is unexpected since we previously observed 79-MBC mice to respond to ibrutinib treatment (Fig. 28), implicating differences between the *in vivo* tumor compared to the *in vitro* cell line.

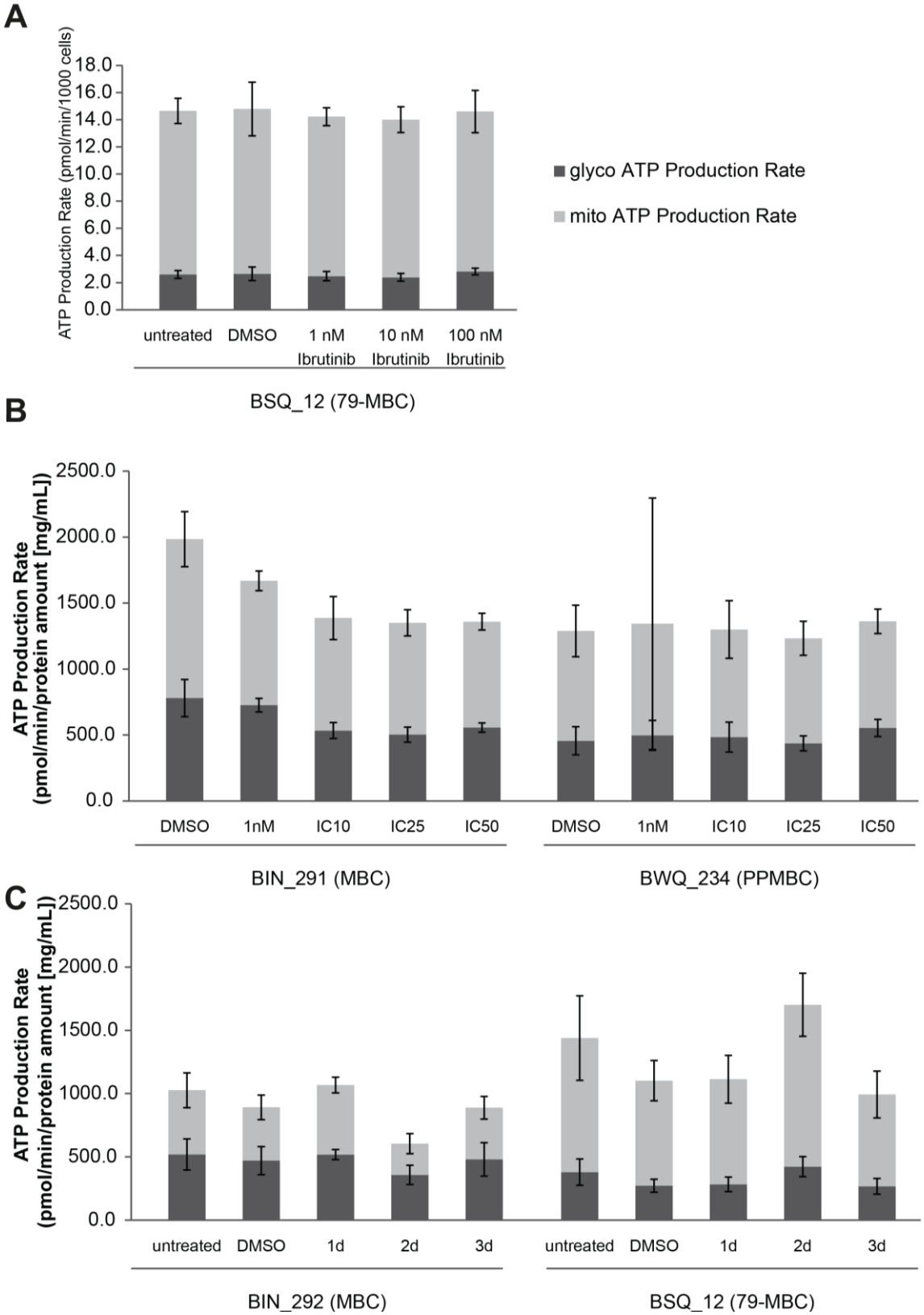

Figure R33 SeaHorse Analysis of DMSO- and ibrutinib-treated murine cell lines does not reveal significant differences*. (A) 79-MBC cell line BSQ_12 was treated for 1 day with DMSO or ibrutinib. (B) MBC cell line BIN_291 and PPMBC cell line BWQ_234 were treated for 1 day with DMSO or ibrutinib. (C) MBC cell line BIN_292 and 79-MBC cell line BSQ_12 were treated for 3 days with DMSO or for 1-3 days with ibrutinib.*

Since concentrations of 1-100nM were far below the observed IC50 of BSQ_12 of >5µM, they might be too low to have any discernible effect on glycolysis and oxidative phosphorylation. On the other hand, concentrations of ibrutinib >100nM are known to exert off-target effects on other proteins (Nicolson et al. 2018; Byrd et al. 2016), limiting the specificity of our assay with high ibrutinib concentrations. Therefore, we chose cell lines with lower IC50s of ibrutinib for the next assay: We treated the MBC cell line BIN_291 and the PPMBC cell line BWQ_234 for one day with 1nM ibrutinib, as well as concentrations close to their respective IC10, IC25 and IC50 (determined in a 3-day viability assay, Fig. R34A, B). Concentrations were chosen in their respective range, but for technical reasons not diluted exactly to the respective ICs (Supplementary Table 4). In this setup, we again observed little changes between the DMSO-treated and ibrutinib-treated conditions (Fig. R33B).

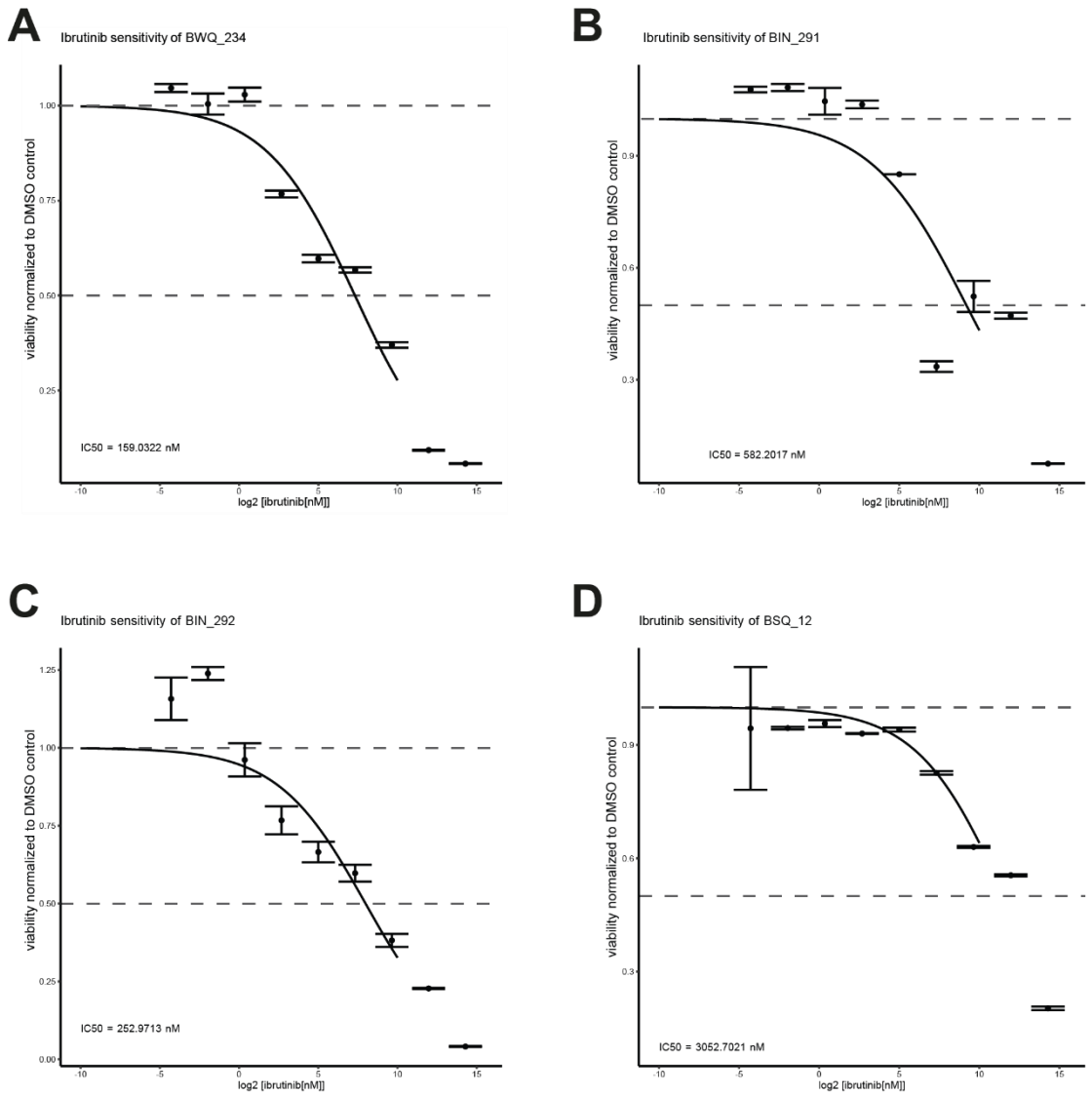

Figure R34 Murine cell lines display differential sensitivity to ibrutinib. *Ibrutinib sensitivity assays for murine cell lines (A) BWQ_234, (B) BIN_291, (C) BIN_292, (D) BSQ_12. Cell lines were treated for three days with ibrutinib (concentration range 0.0512nM-20mM), viability determined by alamarBlue™ assay and normalized to the DMSO-treated condition before modeling data to a Hill function.*

Lastly, we looked into potential metabolic alterations induced by ibrutinib treatment for different durations, comparing the MBC cell line BIN_292 and the 79-MBC cell line BSQ_12. While the ATP production rate differed between untreated, DMSO-treated and cells treated with ibrutinib for different times, no clear trend was apparent (Fig. R33C). Although further experiments would be required to exclude the possibility completely, from this data, it seems unlikely that ibrutinib affects the gross metabolism of our murine lymphoma cell lines.

As previously mentioned, a potential explanation for this phenomenon might originate from in the differences between 2D-grown *in vitro* cell lines, and primary tumor tissue. We attempted to circumvent this issue by performing SeaHorse experiments with cells extracted freshly from primary tumor tissue (Fig. SR7B). However, when comparing the MBC cell line BIN_291, the PPMBC cell line BWQ_234, and data from the 79-MBC primary tumor cells BSQ_197, freshly extracted tumor cells showed little to no metabolic activity and appeared quiescent (Fig. SR7B), limiting analysis with SeaHorse experiments.

5.3.4 Ibrutinib treatment acts synergistically with inhibition of oxidative phosphorylation on murine cell lines

As we previously observed a significant enrichment of mutations in genes annotated for the oxidative stress response gene set in MBC and 79-MBC lesions (Fig. 30), we set out to investigate whether this might elicit a targetable vulnerability. Challenging oxidative phosphorylation in cell lines with inhibitors such as IACS-010759 increases levels of reactive oxygen species (Molina et al. 2018), which are responsible for oxidative stress (Forman and Zhang 2021). Other studies proposed a synergistic effect of ibrutinib treatment and inhibition of oxidative phosphorylation: Ibrutinib-resistant DLBCL cell lines shifted their metabolism from glycolysis to oxidative phosphorylation (Choueiry, Singh, Sircar, et al. 2021), and targeting DNMT3A-mediated oxidative phosphorylation sensitized mantle cell lymphoma cell lines and PDX models to ibrutinib (Hoang et al. 2024). We therefore decided to investigate the interaction of ibrutinib treatment with inhibition of oxidative phosphorylation.

To this end, we performed a combination screen using ibrutinib and the OxPhos-inhibitor IACS-010759, which was previously shown to be effective in MYC-driven lymphoma models (Donati, Nicoli, et al. 2022). Murine cell lines cell lines derived from tumors obtained from our autochthonous mouse models were treated for three days with ibrutinib (concentration range 0.0512nM-20mM), IACS-010759 (concentration range 0.6nM-12.5mM), or combinations of the two. Cell viability was determined by alamarBlue™ assay and normalized to DMSO-treated cells of the same cell line.

By analyzing the resulting viability data using the Chou-Talalay combination index (Chou 2010), we observed synergism (combination index CI <1) in 8 of 9 murine cell lines (table R1) and synergism at all but the two lowest effect levels (Fa) in the 9th cell line (BSQ_12, resulting plots in Fig. R35). Synergism seemed independent of single-agent ibrutinib or IACS-010759 sensitivity (table R1). This combined

efficacy was quite surprising as we did not observe metabolic alterations in oxidative phosphorylation induced by ibrutinib (see 5.3.2). This promising result warrants further research into the effectivity of the combination *in vitro* and *in vivo*, as well as in-detail analysis of potential mechanisms for the observed synergy.

Cumulatively, our data on metabolic alterations in autochthonous mouse models of C5/MCD DLBCL do not present a clear picture of genetic or treatment-induce metabolic pathway changes relevant for patient treatment, but opens up potential routes for further investigation.

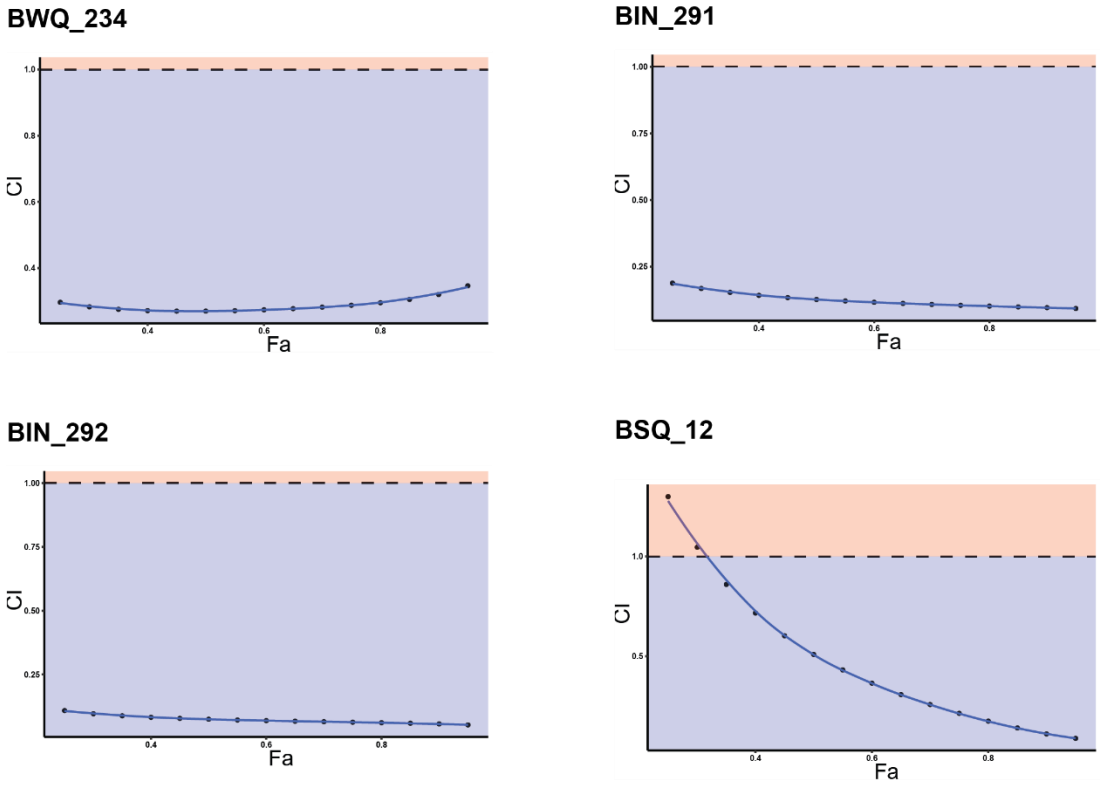

***Figure R35 ibrutinib and IACS-010759 act synergistically in murine C5/MCD cell lines**. Representative illustrations of the combination index (CI) as determined by Chou-Talalay model for the combination of ibrutinib and IACS-010759, tested at several Fa (fraction affected, effect level).*

Table R1 CI for the tested murine cell lines. IC50s as determined from combination screen. Note that the exact IC50 can vary between experiments, therefore numbers do not exactly match IC50s determined in Fig. R34.

cell_line	genotype	CI	IC50(Ibrutinib) [nM]	IC50(IACS-010759) [nM]
BWQ_269	PPMBC	<1	0.4	13.9
BWQ_234	PPMBC	<1	529.9	2547.1
BWQ_379	PPMBC	<1	231.5	4195.0
BIN_291	MBC	<1	536.6	706.4
BIN_292	MBC	<1	1282.5	6240.6
BIN_256	MBC	<1	2386.8	5276.8
CBU_84	79-PPMBC	<1	6771.1	1671.1
BSQ_12	79-MBC	mostly <1	4920.6	77.0

6 Discussion

DLBCL is a frequently diagnosed cancer (Bray et al. 2024). The poor prognosis for patients relapsing or refractory to standard frontline therapy requires additional knowledge about the disease (Sehn and Salles 2021). C5/MCD DLBCL consists of a subgroup of DLBCL patients characterized by genetic alterations including mutations of *MYD88* and *CD79B*, amplification of the *BCL2* locus and alterations conveying a plasma cell differentiation block (Chapuy et al. 2018; Schmitz et al. 2018). This subgroup was demonstrated to have an especially poor outcome, amplifying the need for innovative treatment options (Chapuy et al. 2018; Schmitz et al. 2018).

In this project, the PPMBC mouse model, which is mimicking the clinically relevant features of C5/MCD DLBCL, was established. By comparing with patient data and testing several treatment options, this model was validated as a powerful preclinical tool for investigation of C5/MCD DLBCL. The success of the combination of venetoclax and ibrutinib in mouse and the off-label clinical treatment of a small patient cohort broadens the options for bridging therapies for DLBCL patients. Furthermore, application of the PPMBC mouse model in investigating the commonly occurring *CD79B* mutation in C5/MCD DLBCL indicated the mutation to serve as a biomarker for response to ibrutinib treatment. In another approach, the model was applied to research cell metabolism in C5/MCD DLBCL, revealing metabolic differences mediated by genetic alterations and a synergistic response in derived cell lines treated with ibrutinib and an inhibitor of oxidative phosphorylation. However, to fully comprehend the scope of metabolic alterations in C5/MCD DLBCL, further research is required.

6.1 The PPMBC mouse model serves as a preclinical testing tool

By investigating the role of a plasma cell differentiation block in C5/MCD DLBCL, we not only revealed its relevance for lymphomagenesis, but also generated a mouse model mirroring clinically relevant features of C5/MCD DLBCL on a cellular level (Flumann et al. 2023). While plasmablastic lymphoma is a distinct entity, it was proposed that also ABC DLBCL such as C5/MCD DLBCL is derived from B cells in the process of differentiating into plasma cells (Frick, Dörken, and Lenz 2011), which is blocked in our model system. Although the frequent occurrence of plasma cell differentiation blocks was observed, it was mainly noted to increase aggressivity of the disease (Montes-Moreno et al. 2010). Here, we showed that a plasma cell differentiation block was necessary to faithfully recapture C5/MCD DLBCL in our autochthonous mouse model. Specifically, we obtained two different alleles conferring this block, generating the SMBC and PPMBC mouse models. While both the overexpression of the transcription factor *SpiB* and the loss of the transcription factor *Prdm1* block B cell differentiation into plasma cells (Horiuchi et al. 2023; Boi et al. 2015; Shapiro-Shelef et al. 2005), we observed different qualities of the intended differentiation block, with lower levels of residual plasmablasts and plasma cells in the PPMBC model. Additionally, the PPMBC model exhibited a higher reliability in terms of

consistent phenotype, tumor localization, lymphoma surface marker expression, and other characteristics. “These differences between SMBC and PPMBC mice might be at least partially explained by the fact that *Prdm1* deletion in our model prevents any protein expression, whereas *Spib* overexpression from the *Rosa26* locus might be counter regulated by mechanisms leading to SPIB degradation or through partial silencing of the *Rosa26* locus.

Next to mutational and epigenetic inactivation, *PRDM1* is also transcriptionally repressed by BCL6 (Shaffer et al. 2000; Tunyaplin et al. 2004), which itself is a target of PRDM1-mediated repression, thus constituting a negative feedback loop (Shaffer et al. 2002). In addition to its role in blocking terminal plasma cell differentiation via *PRDM1* repression, SPIB also plays an important role for proper BCR signaling in mature B cells. In contrast to *Spib*-proficient B cells, *Spib*-deficient B cells display reduced proliferation in response to BCR cross-linking and an impaired ability to form GCs (Su et al. 1997; Garrett-Sinha et al. 1999). The oncogenic role of *SPIB* in ABC-DLBCL is further underscored by the observation that the ABC-DLBCL cell line OCI-Ly3 harbors a rearrangement, which juxtaposes *SPIB* to *Ig* enhancers leading to enforced *SPIB* expression (Lenz et al. 2007). Altogether, it is conceivable that the similar lymphomagenesis-enhancing effects of *Spib* overexpression and *Prdm1* deletion in the MBC model are the result of different molecular mechanisms, namely, a potent plasma cell differentiation block in the *Prdm1*-deficient setting and a slightly less pronounced block in terminal differentiation together with augmented BCR signaling in the *Spib*-overexpressing scenario.” (Flumann et al. 2023)

For our further studies, we therefore focused on the PPMBC mouse model. Many characteristics seem shared between C5/MCD DLBCL patients and the PPMBC mouse model, but in contrast to patient data (Lenz et al. 2007), the majority of PPMBC-derived lymphomas were class-switched. This factor was remedied in the 79-PPMBC model, which showed an increased rate of non-class switched, IgM^+ lymphomas (Fig. R21C), indicating that the 79-PPMBC model might mimic DLBCL patient lymphoma even better than other genotypes. Besides this, there are likely other details differing between the mouse model and the human scenario which could be improved by adding additional genetic alterations. For the sake of simplicity in terms of breeding and for preserving the variety of additional, naturally developing genetic alterations seen in the PPMBC model mirroring the human genetics, we opted to continue our research with the PPMBC mouse model. We believe that it reflects substantial aspects of C5/MCD DLBCL.

In our mouse models, we used $Cd19^{Cre}$ to drive the expression of conditional genetic alterations relevant for lymphomagenesis, where the *Cre* expression cassette was inserted into exon 2 of the endogenous murine *Cd19* allele (Rickert, Roes, and Rajewsky 1997). CD19 is expressed upon VDJ recombination early-on in the B cell lineage. In this setup, due to the concomitant broad expression of *Cre*, nearly all B cells in the autochthonous mouse model carried the desired genetic alterations. While this ensured expression of the desired alleles in all potential lymphoma precursor cells, it potentially

affected more B cells than necessary for lymphomagenesis and limited the possibilities to investigate the roles of healthy, nonmalignant B cells in the TME or the systemic immune response. While the infiltration of nonmalignant B cells into DLBCL tissue has been observed before (Liu et al. 2023; Ye et al. 2022), their relevance for tumor characteristics and treatment response remains unclear. In the PPMBC mouse model, genetic alteration of all mature B cells likely prohibits investigation of nonmalignant B cells. We occasionally observed scratch wounds and other indications of autoimmune reactions in our autochthonous mice, which could be explained by the manipulation of non-tumor cells mediating self-reactivity as well. On the other hand, usage of *Cd19*^{Cre} generated a reliable mouse model with faithful tumor development in an agreeable time frame.

In an orthogonal approach, *Aicda*^{Cre} expressed in GC B cells was used to drive the expression of conditional *BCL2* overexpression, *Myd88* and *Cd79b* mutation and *Prdm1* loss alleles in a bone marrow transplantation approach (Pindzola et al. 2022). At an age of 6-8 months, only 5 out of 8 animals showed signs of lymphoma development (expansion of white pulp in the spleen) and were far from succumbing to the disease (Pindzola et al. 2022), indicating a delayed lymphoma onset compared to our PPMBC mouse model (Fig. R19). In contrast, combining conditional *BCL2* overexpression, *MYD88* mutation and/or *Prdm1* loss alleles with *Cr2*^{Cre}, which expresses Cre in mature B cells, gave additional insights into the early, premalignant phenotype of these mice: Comparably to our models, increased GC development was observed with amplified output of plasmablasts and plasma cells in the presence of functional *Prdm1,* while loss of *Prdm1* promoted GC expansion and the generation of potential precursor cells (Pindzola et al. 2022).

The combination of the mentioned alleles with other *Cre* alleles was, to our knowledge, not tested yet. It is conceivable that the usage of more restricted alleles such as *Cγ1*^{Cre}, expressed in GC B cells (Casola et al. 2006), or *Cd21*^{Cre}, expressed during the differentiation of transitional B cells into mature B cells (Kraus et al. 2004), might yield mouse models capturing an advanced spectrum of the DLBCL TME, while likely delaying lymphoma onset as well.

When considering expensive and laborious mouse models for preclinical studies, the possibility of other model systems potentially sufficient to answer specific research questions should be deliberated as well. A plethora of human DLBCL cell lines was established in the past which can be easily handled *in vitro*, capture most recurrent genetic alterations of patient DLBCL, and could be used to make impactful discoveries on cellular signaling alterations, metabolism and other features (Kubacz et al. 2022; Li, Ning, et al. 2019; Young et al. 2019; Yanguas-Casás et al. 2021). We ourselves frequently apply murine cell lines derived from our mouse models for *in vitro* experiments, but discerned notable differences when comparing data: For instance, while 79-MBC animals respond strongly to ibrutinib treatment (Fig. R28), the 79-MBC cell line BSQ_12 did not seem to be sensitive to ibrutinib treatment (Fig. R24, table R1), and similarly for the 79-PPMBC cell line CBU_84 (table R1). It is known that cancer

cell lines often differ from tumors, as was found for instance for genetic alterations and gene expression profiles of ovarian cancer cell lines (Domcke et al. 2013). Also, cell lines can evolve over time *in vitro*, sometimes changing drug response (Ben-David et al. 2018). A study comparing canine lymphoma cell lines with canine lymphoma tissue previously found that gene expression is altered in these *in vitro* models and some therapeutic targets are not similarly expressed between the two, among them *GSK3B* and *PIK3CD*, which are relevant for cell metabolism (Taher et al. 2018). These and other limitations highlight the need for *in vivo* models.

Another approach for modeling DLBCL is the usage of primary human GC cells that can be genetically manipulated and immortalized for tissue culture (Caeser et al. 2021). 3D organoids attempt to include the complex TME into their modeling, can be used for high-throughput drug screening and have been used to test antibody therapy and chemotherapy in lymphoma (Foxall et al. 2021; Tebon et al. 2023; Sullivan et al. 2024). However, even these models cannot capture the full complexity of a living organism, emphasizing mouse models to be an important tool especially in the context of treatment testing (Tabatabai et al. 2023).

6.2 The *Cd79b*^{Y195H} mutation amplifies BCR signaling and targetability

Applying our PPMBC mouse model to study the role of the *CD79B* ITAM mutation in DLBCL, we were surprised to note no significant disease acceleration and no advanced lethality when introducing the *Cd79b*^{Y195H} allele into our model. “This observation is in line with a recent report showing that the cytotoxic effect of RNAi-mediated *CD79B* depletion in the DLBCL cell line HBL1 (harboring a *CD79B*$^{p.Y196F}$ mutation) could be rescued by both, *CD79B* wildtype and various ITAM-mutant cDNAs (Davis et al. 2010). Importantly, there was no quantitative difference in the ability to rescue the *CD79B* depletion phenotype between wildtype and mutant cDNAs, possibly indicating that *CD79B* ITAM mutants do not provide a proliferative advantage per se (Davis et al. 2010). Based on this observation, it was proposed that the selection of *CD79B* ITAM mutations might be an early event during lymphomagenesis, enabling supraphysiological responses to self or foreign antigen (Davis et al. 2010; Shaffer, Young, and Staudt 2012). […] However, it is important to note that in our *Cd19*^{Cre}driven model system, *Cd79b* ITAM mutations are induced at the same time as *Myd88* and *BCL2* aberrations, which by themselves promote self-reactivity (Flümann et al. 2021).” (Flumann et al. 2024)

In fact, we observed reduced values of splenic B220^{+}CD19^{+} B cells in premalignant 79-PPMBC compared to PPMBC mice (Fig. R16B), corroborating the possibility of increased elimination of self-reactive B cells in this background.

It is long known that negative feedback mechanisms induce cell death in active B cells to prevent self-reactivity, mediating a complex balance between survival and death signals upon B cell activation (Donjerković and Scott 2000). Therefore, another explanation for the comparable survival rates of *Cd79b*^{Y195H} and *Cd79b*^{wt} mice could be that initiating anti-apoptotic signaling by *BCL2* overexpression is

the limiting step of lymphomagenesis in our mouse models, rendering the role of *CD79B* secondary. In fact, most DLBCLs seem to express antiapoptotic proteins, commonly BCL-2, but also BCL-XL or MCL-1 (Klanova et al. 2022; de Jong et al. 2019).

The *CD79B*^{Y196X} ITAM mutation has previously been described to reduce BCR inhibition mediated by LYN leading to BCR internalization and signal reduction (Gazumyan, Reichlin, and Nussenzweig 2006; Xu et al. 2005; Davis et al. 2010). However, this raises a seeming contradiction: If *CD79B* mutations decreased BCR internalization in C5/MCD DLBCL, how could B cells depend on My-T-BCR signaling initiated by internalized BCRs in DLBCL endosomes? We here observed no altered BCR internalization levels upon BCR activation in primary B cells carrying the *Cd79b*^{Y195H} mutation (Fig. R26), providing a possible answer. Further research needs to be conducted to solve this paradox.

On the other hand, our results again raise the question on the exact mechanism of increased BCR signaling mediated by *Cd79b*^{Y195H}: If the mutation does not reduce inhibition of BCR signaling, which mechanism of action driving increased BCR signaling is it promoting instead? Its relevance for My-T-BCR signaling has been demonstrated repeatedly (Phelan et al. 2018; Mandato et al. 2023) and we have observed significantly increased rates of colocalization with MYD88 as well, which might be the main outcome of *Cd79b*^{Y195H}.

6.3 Ibrutinib as treatment option for C5/MCD DLBCL

Within this project, several treatment options for C5/MCD DLBCL were tested successfully on autochthonous mouse models.

Ibrutinib is a BTK inhibitor approved as monotherapy treatment for chronic lymphocytic leukemia (Timofeeva and Gandhi 2021), relapsed/refractory mantle cell lymphoma (Radhakrishnan et al. 2022) and other lymphatic malignancies (Xue et al. 2020). We here identified the *Cd79b* ITAM mutation to be a strong factor for response to ibrutinib monotherapy in our autochthonous mouse models. While MBC and PPMBC mice responded little to ibrutinib treatment, 79-MBC and 79-PPMBC mice demonstrated a striking survival benefit of multiple months under continuous ibrutinib treatment (Fig. R28). Our data supports the previously proposed notion of *CD79B* as determining factor in ibrutinib response (Wilson et al. 2015) and contradicts other claims of *CD79B* limiting ibrutinib response (Kim et al. 2016).

In a recent report, no significant increase in overall survival by the addition of ibrutinib to frontline therapy was found in non-GCB patients, although detailed analyses claim to find survival advantages in subgroups like younger patients or *BCL2/MYC* co-expressors (Younes et al. 2019; Johnson et al. 2023). In the GUIDANCE-01 trial, patients were treated with R-CHOP plus an additional agent according to their DLBCL subgroup, with ibrutinib for MCD-like patients, increasing response rates significantly (Zhang et al. 2023). In line with this, a recent report found promising BTK inhibition responses in

patients with *MYD88* and/or *CD79B* mutations (Deng et al. 2024). It is likely that ibrutinib only benefits this patient subgroup, in line with our findings.

Nevertheless, ibrutinib responses in our mouse model were not durable and the evolving resistance mechanisms remain speculation. While our WES analysis did not return typical mutations of *Btk* or *Plcg2* associated with BTK inhibitor resistance in CLL patients (Woyach et al. 2014), we found an accumulation of *Cd83* mutations in relapsed tumors. CD83 is known to be expressed on activated immune cells and to play a role in immune response regulation (Li, Ju, et al. 2019; Riaz et al. 2023). Moreover, CD83 seems to negatively attenuate B-cell function upon BCR activation and CD83 inhibition leads to increased B-cell responses to immunization *in vivo* (Kretschmer et al. 2007; Kretschmer et al. 2009). Further research might show the relation of *Cd83* mutations and ibrutinib resistance.

The combination of venetoclax and ibrutinib was shown to be effective in chronic lymphocytic leukemia (Niemann et al. 2021) and Waldenström's macroglobulinemia with *MYD88* mutations (Castillo et al. 2024). Due to the dependence of our mouse model on antiapoptotic BCL2 and malignant BCR signaling, the high response rates of PPMBC mice treated with a combination of ibrutinib and venetoclax (Fig. R14) were anticipated. When translating these results to DLBCL patients in an off-label setting, several non-GCB patients responded to this bridging treatment, prolonging survival and offering the opportunity to undergo other subsequent treatments (Flumann et al. 2023). In DLBCL, there is emerging data for the combination as a promising treatment option in non-GCB DLBCL (Zhou et al. 2021). Importantly, this combination therapy could be beneficial in patients without *CD79B* ITAM mutations, as we showed efficacy in our *Cd79b*^{wt} PPMBC model (Fig. R14). However, since responses do not seem durable in patients or our mouse models, additional research needs to be conducted to determine resistance mechanisms and/or favorable follow-up therapies.

Another promising therapy option for DLBCL is adoptive cell therapy with CD19-targeting CAR-T cells. Several products are already approved for treatment of lymphomas in Europe and the United States with overall response rates ranging between 53 to 83% in DLBCL (Cappell and Kochenderfer 2023). In fact, based on the results of recent clinical trials, CAR-T-cell therapy has been recommended as second-line therapy for DLBCL patients refractory to or relapsing under initial chemoimmunotherapy (Lutfi et al. 2023; Westin and Sehn 2022). When treating PPMBC mice with mCD19-targeting CAR-T cells, we observed striking response rates in mice with a low tumor burden, leading to a survival benefit of numerous months (Fig. R12). This long remission phase underscores the high hopes for CAR-T cell treatment in DLBCL.

However, response to CAR-T cell treatment was poor in PPMBC mice with a high tumor burden (Fig. R12). Although this is in line with patient data (Locke et al. 2020), it is possible that other factors affect CAR-T cell response which could be further analyzed using the PPMBC mouse model in the future.

It is also worth mentioning that recent reports on T-cell malignancies arising after CAR-T cell treatment has elicited worries about this therapy option (Ghilardi et al. 2024; Verdun and Marks 2024). We have observed no indication for secondary cancers in CAR-T-treated PPMBC mice, which is expected based on the low incidence numbers observed in the human setting. Nevertheless, PPMBC mice should be tested for malignant T-cell proliferation in future CAR-T cell experiments.

Another concern of CAR-T cell therapy is the occurrence of serious adverse events accompanying therapy (Brudno and Kochenderfer 2016). Acute adverse events include damaging of tissues expressing the CAR-targeted antigen, the toxic cytokine release syndrome, cross-reactivity with nontargeted proteins, allergic reactions, neurologic toxicities, and graft-versus-host disease (for allogeneic CAR-T cells)(Brudno and Kochenderfer 2016; Cappell and Kochenderfer 2023). Long-term effects encompass long-lasting B-cell depletion accompanied by immunoglobulin depletion, impairing immune reactions and vaccine responses (Cappell and Kochenderfer 2023). A more specific on-tumor, off-target CAR-T activity could overcome these risks (Rafiq, Hackett, and Brentjens 2020). In fact, when a collaborating group tested a switch CAR/CCR T cell construct in our PPMBC mouse model with higher specificity, tumor growth was inhibited while an intact $CD80^{-}CD19^{+}$ B cell population was retained, indicating this approach to be promising for reducing adverse events (Prinz et al. 2024).

6.4 The metabolic landscape of C5/MCD DLBCL remains complex

We determined that genetic backgrounds shape metabolic alterations in autochthonous mouse models of C5/MCD DLBCL, although the impact of this finding remains unclear. It is conceivable that the observed differences by introducing the *Cd79b*^{Y195H} mutation might stem from alterations of other cellular pathways and be secondary effects. In fact, BCR signaling itself was previously indicated to alter B-cell metabolism, promoting glucose uptake and glycolysis (Doughty et al. 2006) and BCR-DLBCLs seem to exhibit less oxidative phosphorylation and dependence on fatty acid oxidation (Caro et al. 2012). While our data could not show a stratified pattern, we do see increased BCR signaling in *Cd79b*^{Y195H} lymphoma samples concomitantly with oxidative stress in the MBC background, as well as altered lipid metabolism (Fig. R30). These metabolic changes might be accessory phenomena induced by BCR signaling alterations, but might be targetable all the same, as indicated by the synergy of ibrutinib treatment with IACS-010759, an inhibitor of oxidative phosphorylation (Fig. R34).

Interpretation of our metabolomics data was impeded by the sheer quantity of polar metabolites and especially lipids whose individual function is unclear in the majority of cases. When comparing PPMBC and 79-PPMBC samples, this high number of comparisons of individual metabolites quickly led to p level saturation by Benjamini-Hochberg correction for multiple hypothesis testing, rendering

potentially interesting differences insignificant. A higher number of samples and a more targeted approach, only comparing specific metabolites of interest, might render similar analyses more meaningful in future experiments. Another approach that could be upscaled more easily would be the usage of cell line models, but metabolic profiles of cell lines only partially overlap with primary tissue, as was shown for colon cancer cell lines (Rombouts et al. 2021), and cell lines can acquire atypical genetic or gene expression alterations as seen in breast cancer cell lines (Liu et al. 2019). Here, we also observed the differences in ibrutinib response (see below), indicating that our *in vitro* models cannot recapitulate the *in vivo* setting in all aspects.

It was previously reported that ibrutinib response and resistance development could be affected by metabolic alterations in lymphomas and chronic lymphocytic leukemia (Choueiry, Singh, Sun, et al. 2021; Galicia-Vázquez and Aloyz 2018; Zhang et al. 2019). After illustrating the pivotal role of *Cd79b*^{Y195H} in ibrutinib response, we set out to investigate whether metabolic alterations might be the driving force for the distinguishing ibrutinib response between mice of different genotypes, and whether ibrutinib itself affects cellular metabolism. In our cell line model, we could neither detect significant metabolic differences between cell lines derived from murine lymphomas with different genetic backgrounds, nor between untreated and ibrutinib-treated samples of the same cell line (Fig. R33). A possible explanation could be differences between the *in vitro* and *in vivo* setting, as we observed neither the 79-MBC BSQ_12 nor the 79-PPMBC CBU_84 cell line to be sensitive to ibrutinib treatment (table R1), although animals of these genotypes responded to ibrutinib treatment (Fig. 28). The synergy of treatment with ibrutinib and IACS-010759 (Fig. R34), however, does hint at an interplay between BCR inhibition and metabolism in the cell line model. Further research is required to elucidate this mechanism and its significance.

Another confounding factor when analyzing the relationship of BCR inhibition and metabolism is the recently reported link between ibrutinib response in *MYD88*^{L265P} lymphomas and autophagy (Phelan et al. 2024). *MYD88*^{L265P} lymphomas seem to selectively inhibit an autophagic tumor suppressive pathway degrading MYD88^{L265P} necessary for lymphoma survival which can be reactivated by BTK inhibition (Phelan et al. 2024). If this pathway is attenuated, ibrutinib response might be hindered or resistance mechanisms could emerge. Autophagy and tumor metabolism have long been known to interact, with autophagy sustaining glycolysis and mitochondrial metabolism by delivering key metabolites in cancer cells (Pandey, Yadav, and Shukla 2021). Taken together, a complex picture of the role of metabolic alterations in lymphoma biology and treatment emerges, warranting further investigation to draw meaningful conclusions.

6.5 Conclusion

Within this thesis, three chapters of lymphoma biology were studied. First, autochthonous mouse models of C5/MCD DLBCL were analyzed, optimized and validated comprehensively. In our PPMBC

mice, C5/MCD DLBCL seems to develop from the B-cell lineage of memory B-cell differentiation, supporting this lineage as potential origin for C5/MCD DLBCL as previously suggested (Venturutti and Melnick 2020). The comparability to patient DLBCL cells and availability for treatment testing makes our PPMBC mouse model a valuable preclinical testing tool for C5/MCD DLBCL research (Fig. D1A). Looking forward, the PPMBC mouse model will likely emerge as a powerful tool in DLBCL research. The MBC mouse model could already be applied by us and our collaborators to study a plethora of research questions (Flumann et al. 2024; Tabatabai et al. 2023; Pindzola et al. 2022; Venturutti et al. 2022) and we believe the PPMBC mouse model to be used even more broadly, generating new knowledge about C5/MCD DLBCL and validating treatments pre-clinically. The PPMBC mouse model was already employed in DLBCL research by us (see below), and our collaborators to test a switch CAR/CCR T cell treatment approach (Prinz et al. 2024).

In a second angle, the PPMBC model was applied to gain deeper insights into the effect of the commonly occurring *CD79B* ITAM mutation, presenting it as determining factor for BCR signaling and response to BTK inhibition (Fig. D1B). Identifying *Cd79b*^{Y195H} to distinguish ibrutinib response will facilitate treatment of C5/MCD DLBCL patients in the future. Additionally, further analysis of the model to ascertain the modes of ibrutinib resistance manifestation might enable resistance prevention in the future.

Lastly, different mouse models were used to investigate C5/MCD DLBCL metabolism, demonstrating differences between genotypes and synergism of ibrutinib treatment and inhibition of oxidative phosphorylation (Fig. D1C). Additional research will be required to interpret the relevance of this data in full.

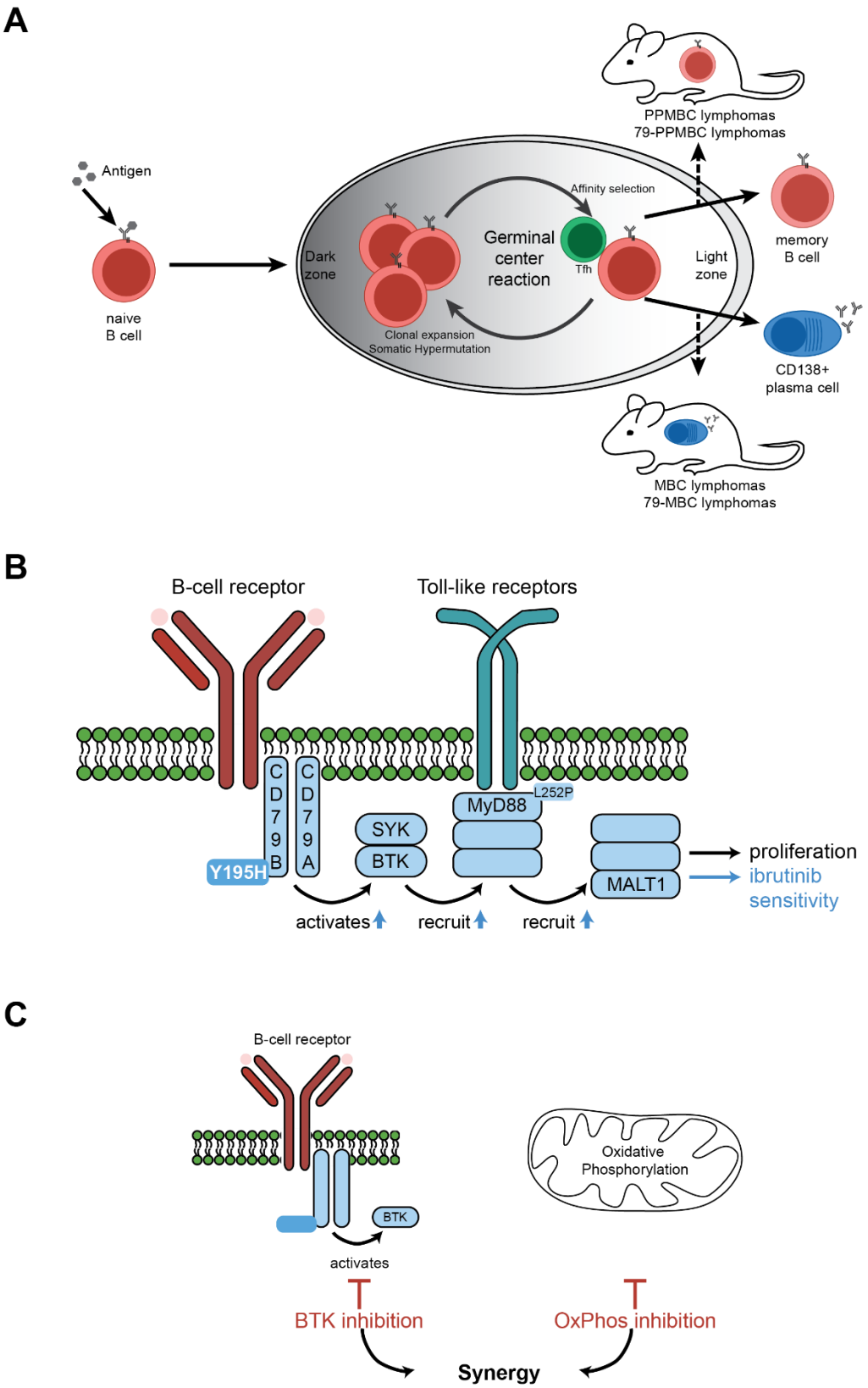

Figure D1 This thesis investigated DLBCL from three angles. (A) To obtain a powerful preclinical testing tool, the PPMBC mouse model was generated and validated by comparison with human data and treatment testing, showing improvement over the previously published MBC model. Note that the indicated lymphomas only share some characteristics of memory B cells or plasma cells and are not fully differentiated to either cell type. (B) By applying the PPMBC mouse model to investigate the role of Cd79b^{Y195H}*, we determined an increased and targetable dependency on BCR signaling. (C) The metabolic differences in our mouse models prompted us to analyze the interplay of BCR signaling and oxidative phosphorylation, finding synergy of targeting both in our murine cell lines.*

7 Publications

Title: “An inducible Cd79b mutation confers ibrutinib sensitivity in mouse models of Myd88-driven diffuse large B-cell lymphoma”

Published in: Blood Advances, Vol. 8, Issue 5

Publishing date: 28 February 2024

Accession: (Flumann et al. 2024)

DOI: 10.1182/bloodadvances.2023011213

Authors: R. Flumann*, J. Hansen*, J. Meinel, P. Pfeiffer, H. Goldfarb Wittkopf, A. Lutz, J. Wirtz, M. Mollmann, T. Zhou, A. Tabatabai, T. Lohmann, M. Jauch, F. Beleggia, B. Pelzer, F. Ullrich, S. Hofmann, A. Arora, T. Persigehl, R. Buttner, B. von Tresckow, S. Klein*, R. D. Jachimowicz*, H. C. Reinhardt* and G. Knittel*; *R.F., J.H., S.K., R.D.J., H.C.R., and G.K. contributed equally to this study.

Author contributions: R.F., J.H., P.P., H.G.W., A.L., J.W., M.M., T.Z., A.T., T.L., M.J., S.H., A. A., and G.K. conducted experiments and collected the data; R.F., J.H., J.M., P.P., T.L., F.B., B.P., F.U., B.v.T., S.K., and G.K. performed analyses; R.F., J.H., S.K., R.D.J, H.C.R., and G.K. conceived and designed experiments; T.P. and R.B. contributed data; B.P., T.P., and R.B. contributed analysis tools; R.F., J.H., B.v.T., S.K., R.D.J., H.C.R., and G.K. wrote the manuscript.

Title: “Distinct Genetically Determined Origins of Myd88/BCL2-Driven Aggressive Lymphoma Rationalize Targeted Therapeutic Intervention Strategies”

Published in: Blood Cancer Discovery, Vol. 4, Issue 1

Publishing date: 6 January 2023

Accession: (Flumann et al. 2023)

DOI: 10.1158/2643-3230.BCD-22-0007

Authors: Flumann, R., J. Hansen, B. W. Pelzer, P. Nieper, T. Lohmann, I. Kisis, T. Riet, V. Kohlhas, P. H. Nguyen, M. Peifer, N. Abedpour, G. Bosco, R. K. Thomas, M. Kochanek, J. Knufer, L. Jonigkeit, F. Beleggia, A. Holzem, R. Buttner, P. Lohneis, J. Meinel, M. Ortmann, T. Persigehl, M. Hallek, D. P. Calado, M. Chmielewski, S. Klein, J. R. Gothert, B. Chapuy, B. Zevnik, F. T. Wunderlich, B. von Tresckow, R. D. Jachimowicz, A. M. Melnick, H. C. Reinhardt and G. Knittel

Author contributions: R. Flümann: Conceptualization, data curation, formal analysis, validation, investigation, visualization, methodology, writing–original draft, project administration. J. Hansen: Investigation. B.W. Pelzer: Investigation. P. Nieper: Conceptualization, data curation, formal analysis, investigation, visualization, methodology. T. Lohmann: Resources, software, formal analysis, visualization. I. Kisis: Investigation. T. Riet: Data curation, formal analysis, investigation, visualization. V. Kohlhas: Investigation, methodology. P.-H. Nguyen: Methodology. M. Peifer: Software, investigation. N. Abedpour: Software, investigation. G. Bosco: Resources, methodology. R.K. Thomas:

Resources. M. Kochanek: Investigation. J. Knüfer: Investigation. L. Jonigkeit: Investigation. F. Beleggia: Software. A. Holzem: Investigation, methodology. R. Büttner: Resources, methodology. P. Lohneis: Investigation. J. Meinel: Investigation. M. Ortmann: Investigation. T. Persigehl: Resources, methodology. M. Hallek: Resources. D.P. Calado: Resources. M. Chmielewski: Conceptualization, resources, supervision. S. Klein: Software, formal analysis, visualization, methodology. J.R. Göthert: Resources. B. Chapuy: Resources, software. B. Zevnik: Resources, methodology. F.T. Wunderlich: Resources, methodology. B. von Tresckow: Resources. R.D. Jachimowicz: Resources. A.M. Melnick: Resources, supervision, methodology. H.C. Reinhardt: Conceptualization, resources, supervision, funding acquisition, writing–original draft, project administration. G. Knittel: Conceptualization, software, formal analysis, supervision, validation, investigation, visualization, methodology, writing–original draft, project administration.

Contributions to:

Tabatabai, A., A. Arora, S. Hofmann, M. Jauch, B. von Tresckow, **J. Hansen**, R. Flumann, R. D. Jachimowicz, S. Klein, H. C. Reinhardt and G. Knittel (2023). "Mouse models of diffuse large B cell lymphoma." Front Immunol 14: 1313371.

DOI: 10.3389/fimmu.2023.1313371

Venturutti, L., M. A. Rivas, B. W. Pelzer, R. Flumann, **J. Hansen**, I. Karagiannidis, M. Xia, D. R. McNally, Y. Isshiki, A. Lytle, M. Teater, C. R. Chin, C. Meydan, G. Knittel, E. Ricker, C. E. Mason, X. Ye, Q. Pan-Hammarstrom, C. Steidl, D. W. Scott, H. C. Reinhardt, A. B. Pernis, W. Beguelin and A. M. Melnick (2022). "An Aged/Autoimmune B-cell Program Defines the Early Transformation of Extranodal Lymphomas." Cancer Discov. (2023) 13 (1): 216–243.

DOI: 10.1158/2159-8290.CD-22-0561

8 Acknowledgements

Thanks to Ruth Flümann, for supervising and training me, and working alongside me. Thank you also to my other lab members for their friendship and optimism!

Many thanks to my thesis advisory committee Hamid Kashkar, Niels Gehring and Alexander Tarakhovsky for their feedback and support. Thank you to Tobias Bollenbach for agreeing to chair my PhD Defense.

Thank you to all collaborators and colleagues involved in the projects, especially to the coauthors of the herein mentioned publications. Thank you to the animal caretakers and MPI core facility members for helping me each step of the way. Thank you to Ron Jachimowicz, the Universität zu Köln, the Uniklinik Köln and the Max Planck Institute for Biology of Ageing for hosting me. Thank you to the Graduate School for Biological Sciences for organizational help. Thanks to Daniela Morick for all your advice.

For financial aid and intellectual support, I thank the Cologne Graduate School of Ageing and the Studienstiftung des deutschen Volkes.

For proofreading the thesis, I thank Ruth Flümann, Melanie Thelen and Leon Seeger.

Thank you to my family and friends for your encouragement and the fun we have.

Thank you to my husband Leon. For everything!

9 Eidesstaatliche Erklärung

„Hiermit versichere ich an Eides statt, dass ich die vorliegende Dissertation selbstständig und ohne die Benutzung anderer als der angegebenen Hilfsmittel und Literatur angefertigt habe. Alle Stellen, die wörtlich oder sinngemäß aus veröffentlichten und nicht veröffentlichten Werken dem Wortlaut oder dem Sinn nach entnommen wurden, sind als solche kenntlich gemacht. Ich versichere an Eides statt, dass diese Dissertation noch keiner anderen Fakultät oder Universität zur Prüfung vorgelegen hat; dass sie - abgesehen von unten angegebenen Teilpublikationen und eingebundenen Artikeln und Manuskripten - noch nicht veröffentlicht worden ist sowie, dass ich eine Veröffentlichung der Dissertation vor Abschluss der Promotion nicht ohne Genehmigung des Promotionsausschusses vornehmen werde. Die Bestimmungen dieser Ordnung sind mir bekannt. Darüber hinaus erkläre ich hiermit, dass ich die Ordnung zur Sicherung guter wissenschaftlicher Praxis und zum Umgang mit wissenschaftlichem Fehlverhalten der Universität zu Köln gelesen und sie bei der Durchführung der Dissertation zugrundeliegenden Arbeiten und der schriftlich verfassten Dissertation beachtet habe und verpflichte mich hiermit, die dort genannten Vorgaben bei allen wissenschaftlichen Tätigkeiten zu beachten und umzusetzen. Ich versichere, dass die eingereichte elektronische Fassung der eingereichten Druckfassung vollständig entspricht.“

Teilpublikationen: Teile dieser Doktorarbeit wurden in den folgenden Publikationen veröffentlicht:

Flumann, R., J. Hansen, B. W. Pelzer, P. Nieper, T. Lohmann, I. Kisis, T. Riet, V. Kohlhas, P. H. Nguyen, M. Peifer, N. Abedpour, G. Bosco, R. K. Thomas, M. Kochanek, J. Knufer, L. Jonigkeit, F. Beleggia, A. Holzem, R. Buttner, P. Lohneis, J. Meinel, M. Ortmann, T. Persigehl, M. Hallek, D. P. Calado, M. Chmielewski, S. Klein, J. R. Gothert, B. Chapuy, B. Zevnik, F. T. Wunderlich, B. von Tresckow, R. D. Jachimowicz, A. M. Melnick, H. C. Reinhardt and G. Knittel (2023). "Distinct Genetically Determined Origins of Myd88/BCL2-Driven Aggressive Lymphoma Rationalize Targeted Therapeutic Intervention Strategies." Blood Cancer Discov 4(1): 78-97.

R. Flumann*, J. Hansen*, J. Meinel, P. Pfeiffer, H. Goldfarb Wittkopf, A. Lutz, J. Wirtz, M. Mollmann, T. Zhou, A. Tabatabai, T. Lohmann, M. Jauch, F. Beleggia, B. Pelzer, F. Ullrich, S. Hofmann, A. Arora, T. Persigehl, R. Buttner, B. von Tresckow, S. Klein*, R. D. Jachimowicz*, H. C. Reinhardt* and G. Knittel* (2024). "An inducible Cd79b mutation confers ibrutinib sensitivity in mouse models of Myd88-driven diffuse large B-cell lymphoma." Blood Adv 8(5): 1063-1074. *R.F., J.H., S.K., R.D.J., H.C.R., and G.K. contributed equally to this study.

Datum, Ort, Unterschrift

10 References

Agrawal, S., S. Kumar, R. Sehgal, S. George, R. Gupta, S. Poddar, A. Jha, and S. Pathak. 2019. 'El-MAVEN: A Fast, Robust, and User-Friendly Mass Spectrometry Data Processing Engine for Metabolomics', *Methods Mol Biol*, 1978: 301-21.

Alaggio, Rita, Catalina Amador, Ioannis Anagnostopoulos, Ayoma D. Attygalle, Iguaracyra Barreto De Oliveira Araujo, Emilio Berti, Govind Bhagat, Anita Maria Borges, Daniel Boyer, Mariarita Calaminici, Amy Chadburn, John K. C. Chan, Wah Cheuk, Wee-Joo Chng, John K. Choi, Shih-Sung Chuang, Sarah E. Coupland, Magdalena Czader, Sandeep S. Dave, Daphne De Jong, Ming-Qing Du, Kojo S. Elenitoba-Johnson, Judith Ferry, Julia Geyer, Dita Gratzinger, Joan Guitart, Sumeet Gujral, Marian Harris, Christine J. Harrison, Sylvia Hartmann, Andreas Hochhaus, Patty M. Jansen, Kennosuke Karube, Werner Kempf, Joseph Khoury, Hiroshi Kimura, Wolfram Klapper, Alexandra E. Kovach, Shaji Kumar, Alexander J. Lazar, Stefano Lazzi, Lorenzo Leoncini, Nelson Leung, Vasiliki Leventaki, Xiao-Qiu Li, Megan S. Lim, Wei-Ping Liu, Abner Louissaint, Andrea Marcogliese, L. Jeffrey Medeiros, Michael Michal, Roberto N. Miranda, Christina Mitteldorf, Santiago Montes-Moreno, William Morice, Valentina Nardi, Kikkeri N. Naresh, Yasodha Natkunam, Siok-Bian Ng, Ilske Oschlies, German Ott, Marie Parrens, Melissa Pulitzer, S. Vincent Rajkumar, Andrew C. Rawstron, Karen Rech, Andreas Rosenwald, Jonathan Said, Clémentine Sarkozy, Shahin Sayed, Caner Saygin, Anna Schuh, William Sewell, Reiner Siebert, Aliyah R. Sohani, Reuben Tooze, Alexandra Traverse-Glehen, Francisco Vega, Beatrice Vergier, Ashutosh D. Wechalekar, Brent Wood, Luc Xerri, and Wenbin Xiao. 2022. 'The 5th edition of the World Health Organization Classification of Haematolymphoid Tumours: Lymphoid Neoplasms', *Leukemia*, 36: 1720-48.

Alizadeh, Ash A., Michael B. Eisen, R. Eric Davis, Chi Ma, Izidore S. Lossos, Andreas Rosenwald, Jennifer C. Boldrick, Hajeer Sabet, Truc Tran, Xin Yu, John I. Powell, Liming Yang, Gerald E. Marti, Troy Moore, James Hudson, Lisheng Lu, David B. Lewis, Robert Tibshirani, Gavin Sherlock, Wing C. Chan, Timothy C. Greiner, Dennis D. Weisenburger, James O. Armitage, Roger Warnke, Ronald Levy, Wyndham Wilson, Michael R. Grever, John C. Byrd, David Botstein, Patrick O. Brown, and Louis M. Staudt. 2000. 'Distinct types of diffuse large B-cell lymphoma identified by gene expression profiling', *Nature*, 403: 503-11.

Allen, Christopher D. C., K. Mark Ansel, Caroline Low, Robin Lesley, Hirokazu Tamamura, Nobutaka Fujii, and Jason G. Cyster. 2004. 'Germinal center dark and light zone organization is mediated by CXCR4 and CXCR5', *Nature Immunology*, 5: 943-52.

Alves-Bezerra, M., and D. E. Cohen. 2017. 'Triglyceride Metabolism in the Liver', *Compr Physiol*, 8: 1-8.

Balka, Katherine R., and Dominic Nardo. 2019. 'Understanding early TLR signaling through the Myddosome', *Journal of Leukocyte Biology*, 105: 339-51.

Bao, Y., Y. Qiao, J. E. Choi, Y. Zhang, R. Mannan, C. Cheng, T. He, Y. Zheng, J. Yu, M. Gondal, G. Cruz, S. Grove, X. Cao, F. Su, R. Wang, Y. Chang, I. Kryczek, M. Cieslik, M. D. Green, W. Zou, and A. M. Chinnaiyan. 2023. 'Targeting the lipid kinase PIKfyve upregulates surface expression of MHC class I to augment cancer immunotherapy', *Proc Natl Acad Sci U S A*, 120: e2314416120.

Basso, K., and R. Dalla-Favera. 2012a. 'Roles of BCL6 in normal and transformed germinal center B cells', *Immunol Rev*, 247: 172-83.

Basso, Katia, and Riccardo Dalla-Favera. 2012b. 'Roles of BCL6 in normal and transformed germinal center B cells', *Immunological Reviews*, 247: 172-83.

Béguelin, Wendy, Relja Popovic, Matt Teater, Yanwen Jiang, Karen, Monica Rosen, Hao Shen, Shao, Ling Wang, Teresa Ezponda, Eva Martinez-Garcia, Haikuo Zhang, Yupeng Zheng, Sharad, Michael, Heidi, Glenn, Ryan, Yan Liu, Charles, David, Young, Neil Kelleher, Rita Shaknovich, Caretha, Randy, Kwok-Kin Wong, Leandro Cerchietti, Ross, Omar Abdel-Wahab, Jonathan, Olivier Elemento, and Ari. 2013. 'EZH2 Is Required for Germinal Center Formation and Somatic EZH2 Mutations Promote Lymphoid Transformation', *Cancer Cell*, 23: 677-92.

Béguelin, Wendy, Matt Teater, Micah D. Gearhart, María Teresa Calvo Fernández, Rebecca L. Goldstein, Mariano G. Cárdenas, Katerina Hatzi, Monica Rosen, Hao Shen, Connie M. Corcoran, Michelle Y. Hamline, Randy D. Gascoyne, Ross L. Levine, Omar Abdel-Wahab, Jonathan D. Licht, Rita Shaknovich, Olivier Elemento, Vivian J. Bardwell, and Ari M. Melnick. 2016. 'EZH2 and BCL6 Cooperate to Assemble CBX8-BCOR Complex to Repress Bivalent Promoters, Mediate Germinal Center Formation and Lymphomagenesis', *Cancer Cell*, 30: 197-213.

Béguelin, Wendy, Matt Teater, Cem Meydan, Kenneth B. Hoehn, Jude M. Phillip, Alexey A. Soshnev, Leandro Venturutti, Martín A. Rivas, María T. Calvo-Fernández, Johana Gutierrez, Jeannie M. Camarillo, Katsuyoshi Takata, Karin Tarte, Neil L. Kelleher, Christian Steidl, Christopher E. Mason, Olivier Elemento, C. David Allis, Steven H. Kleinstein, and Ari M. Melnick. 2020. 'Mutant EZH2 Induces a Pre-malignant Lymphoma Niche by Reprogramming the Immune Response', *Cancer Cell*, 37: 655-73.e11.

Ben-David, Uri, Benjamin Siranosian, Gavin Ha, Helen Tang, Yaara Oren, Kunihiko Hinohara, Craig A. Strathdee, Joshua Dempster, Nicholas J. Lyons, Robert Burns, Anwesha Nag, Guillaume Kugener, Beth Cimini, Peter Tsvetkov, Yosef E. Maruvka, Ryan O'Rourke, Anthony Garrity, Andrew A. Tubelli, Pratiti Bandopadhayay, Aviad Tsherniak, Francisca Vazquez, Bang Wong, Chet Birger, Mahmoud Ghandi, Aaron R. Thorner, Joshua A. Bittker, Matthew Meyerson, Gad Getz, Rameen Beroukhim, and Todd R. Golub. 2018. 'Genetic and transcriptional evolution alters cancer cell line drug response', *Nature*, 560: 325-30.

Bergers, Gabriele, and Sarah-Maria Fendt. 2021. 'The metabolism of cancer cells during metastasis', *Nature Reviews Cancer*, 21: 162-80.

Bhatti, J. S., G. K. Bhatti, and P. H. Reddy. 2017. 'Mitochondrial dysfunction and oxidative stress in metabolic disorders - A step towards mitochondria based therapeutic strategies', *Biochim Biophys Acta Mol Basis Dis*, 1863: 1066-77.

Bohnenberger, Hanibal, Thomas Oellerich, Michael Engelke, He-Hsuan Hsiao, Henning Urlaub, and Jürgen Wienands. 2011. 'Complex phosphorylation dynamics control the composition of the Syk interactome in B cells', *European Journal of Immunology*, 41: 1550-62.

Boi, M., E. Zucca, G. Inghirami, and F. Bertoni. 2015. 'PRDM1/BLIMP1: a tumor suppressor gene in B and T cell lymphomas', *Leuk Lymphoma*, 56: 1223-8.

Bojarczuk, Kamil, Malgorzata Bobrowicz, Michal Dwojak, Nina Miazek, Piotr Zapala, Anders Bunes, Marta Siernicka, Maria Rozanska, and Magdalena Winiarska. 2015. 'B-cell receptor signaling in the pathogenesis of lymphoid malignancies', 55: 255-65.

Bojarczuk, Kamil, Kirsty Wienand, Jeremy A. Ryan, Linfeng Chen, Mariana Villalobos-Ortiz, Elisa Mandato, Joanna Stachura, Anthony Letai, Lee N. Lawton, Bjoern Chapuy, and Margaret A. Shipp. 2019. 'Targeted inhibition of PI3Kα/δ is synergistic with BCL-2 blockade in genetically defined subtypes of DLBCL', *Blood*, 133: 70-80.

Bonilla, Diego A., Richard B. Kreider, Jeffrey R. Stout, Diego A. Forero, Chad M. Kerksick, Michael D. Roberts, and Eric S. Rawson. 2021. 'Metabolic Basis of Creatine in Health and Disease: A Bioinformatics-Assisted Review', *Nutrients*, 13: 1238.

Bray, Freddie, Mathieu Laversanne, Hyuna Sung, Jacques Ferlay, Rebecca L. Siegel, Isabelle Soerjomataram, and Ahmedin Jemal. 2024. 'Global cancer statistics 2022: GLOBOCAN estimates of incidence and mortality worldwide for 36 cancers in 185 countries', *CA: A Cancer Journal for Clinicians*.

Bray, N. L., H. Pimentel, P. Melsted, and L. Pachter. 2016. 'Near-optimal probabilistic RNA-seq quantification', *Nat Biotechnol*, 34: 525-7.

Brudno, J. N., and J. N. Kochenderfer. 2016. 'Toxicities of chimeric antigen receptor T cells: recognition and management', *Blood*, 127: 3321-30.

Byrd, John C., Bonnie Harrington, Susan O'Brien, Jeffrey A. Jones, Anna Schuh, Steve Devereux, Jorge Chaves, William G. Wierda, Farrukh T. Awan, Jennifer R. Brown, Peter Hillmen, Deborah M. Stephens, Paolo Ghia, Jacqueline C. Barrientos, John M. Pagel, Jennifer Woyach, Dave Johnson, Jane Huang, Xiaolin Wang, Allard Kaptein, Brian J. Lannutti, Todd Covey, Maria Fardis, Jesse McGreivy, Ahmed Hamdy, Wayne Rothbaum, Raquel Izumi, Thomas G. Diacovo, Amy J. Johnson, and Richard R. Furman. 2016. 'Acalabrutinib (ACP-196) in Relapsed Chronic Lymphocytic Leukemia', *New England Journal of Medicine*, 374: 323-32.

Caeser, Rebecca, Jie Gao, Miriam Di Re, Chun Gong, and Daniel J. Hodson. 2021. 'Genetic manipulation and immortalized culture of ex vivo primary human germinal center B cells', *Nature Protocols*, 16: 2499-519.

Cappell, K. M., and J. N. Kochenderfer. 2023. 'Long-term outcomes following CAR T cell therapy: what we know so far', *Nat Rev Clin Oncol*, 20: 359-71.

Caro, Pilar, Amar, Erik Norberg, Illana A. Stanley, Bjoern Chapuy, Scott, Klaudia Polak, Daniel Tondera, John Gounarides, Hong Yin, Feng Zhou, Michael, Linfeng Chen, Stefano Monti, Jarrod, Margaret, and Nika. 2012. 'Metabolic Signatures Uncover Distinct Targets in Molecular Subsets of Diffuse Large B Cell Lymphoma', *Cancer Cell*, 22: 547-60.

Carsetti, R. 2000. 'The development of B cells in the bone marrow is controlled by the balance between cell-autonomous mechanisms and signals from the microenvironment', *J Exp Med*, 191: 5-8.

Carter, S. L., K. Cibulskis, E. Helman, A. McKenna, H. Shen, T. Zack, P. W. Laird, R. C. Onofrio, W. Winckler, B. A. Weir, R. Beroukhim, D. Pellman, D. A. Levine, E. S. Lander, M. Meyerson, and G. Getz. 2012. 'Absolute quantification of somatic DNA alterations in human cancer', *Nat Biotechnol*, 30: 413-21.

Casola, S., G. Cattoretti, N. Uyttersprot, S. B. Koralov, J. Segal, Z. Hao, A. Waisman, A. Egert, D. Ghitza, and K. Rajewsky. 2006. 'Tracking germinal center B cells expressing germ-line immunoglobulin 1 transcripts by conditional gene targeting', *Proceedings of the National Academy of Sciences*, 103: 7396-401.

Castiello, F. Rafael, Khalil Heileman, and Maryam Tabrizian. 2016. 'Microfluidic perfusion systems for secretion fingerprint analysis of pancreatic islets: applications, challenges and opportunities', *Lab on a Chip*, 16: 409-31.

Castillo, J. J., A. R. Branagan, D. Sermer, C. A. Flynn, K. Meid, M. Little, K. Stockman, T. White, A. Canning, M. L. Guerrera, A. Kofides, S. Liu, X. Liu, K. Richardson, N. Tsakmaklis, C. J. Patterson, Z. R. Hunter, S. P. Treon, and S. Sarosiek. 2024. 'Ibrutinib and venetoclax as primary therapy in symptomatic, treatment-naive Waldenstrom macroglobulinemia', *Blood*, 143: 582-91.

Cattoretti, Giorgio, Laura Pasqualucci, Gianna Ballon, Wayne Tam, Subhadra V. Nandula, Qiong Shen, Tongwei Mo, Vundavalli V. Murty, and Riccardo Dalla-Favera. 2005. 'Deregulated BCL6 expression recapitulates the pathogenesis of human diffuse large B cell lymphomas in mice', *Cancer Cell*, 7: 445-55.

Chambers, M. C., B. Maclean, R. Burke, D. Amodei, D. L. Ruderman, S. Neumann, L. Gatto, B. Fischer, B. Pratt, J. Egertson, K. Hoff, D. Kessner, N. Tasman, N. Shulman, B. Frewen, T. A. Baker, M. Y. Brusniak, C. Paulse, D. Creasy, L. Flashner, K. Kani, C. Moulding, S. L. Seymour, L. M. Nuwaysir, B. Lefebvre, F. Kuhlmann, J. Roark, P. Rainer, S. Detlev, T. Hemenway, A. Huhmer, J. Langridge, B. Connolly, T. Chadick, K. Holly, J. Eckels, E. W. Deutsch, R. L. Moritz, J. E. Katz, D. B. Agus, M. MacCoss, D. L. Tabb, and P. Mallick. 2012. 'A cross-platform toolkit for mass spectrometry and proteomics', *Nat Biotechnol*, 30: 918-20.

Chapuy, Bjoern, Chip Stewart, Andrew J. Dunford, Jaegil Kim, Atanas Kamburov, Robert A. Redd, Mike S. Lawrence, Margaretha G. M. Roemer, Amy J. Li, Marita Ziepert, Annette M. Staiger, Jeremiah A. Wala, Matthew D. Ducar, Ignaty Leshchiner, Ester Rheinbay, Amaro Taylor-Weiner, Caroline A. Coughlin, Julian M. Hess, Chandra S. Pedamallu, Dimitri Livitz, Daniel Rosebrock, Mara Rosenberg, Adam A. Tracy, Heike Horn, Paul Van Hummelen, Andrew L. Feldman, Brian K. Link, Anne J. Novak, James R. Cerhan, Thomas M. Habermann, Reiner Siebert, Andreas

Rosenwald, Aaron R. Thorner, Matthew L. Meyerson, Todd R. Golub, Rameen Beroukhim, Gerald G. Wulf, German Ott, Scott J. Rodig, Stefano Monti, Donna S. Neuberg, Markus Loeffler, Michael Pfreundschuh, Lorenz Trümper, Gad Getz, and Margaret A. Shipp. 2018. 'Molecular subtypes of diffuse large B cell lymphoma are associated with distinct pathogenic mechanisms and outcomes', *Nature Medicine*, 24: 679-90.

Chaudhuri, Jayanta, Todd Evans, Ritu Kumar, and Laurenj Dimenna. 2014. 'Biological function of activation-induced cytidine deaminase (AID)', *Biomedical Journal*, 37: 269.

Chen, E. Y., C. M. Tan, Y. Kou, Q. Duan, Z. Wang, G. V. Meirelles, N. R. Clark, and A. Ma'ayan. 2013. 'Enrichr: interactive and collaborative HTML5 gene list enrichment analysis tool', *BMC Bioinformatics*, 14: 128.

Chen, Linfeng, Stefano Monti, Przemyslaw Juszczynski, Jing Ouyang, Bjoern Chapuy, Donna Neuberg, John, Agata, Thomas, Ahmet Dogan, Thomas, Jeffery, Scott, Todd Golub, and Margaret. 2013. 'SYK Inhibition Modulates Distinct PI3K/AKT- Dependent Survival Pathways and Cholesterol Biosynthesis in Diffuse Large B Cell Lymphomas', 23: 826-38.

Chiche, Johanna, Julie Reverso-Meinietti, Annabelle Mouchotte, Camila Rubio-Patiño, Rana Mhaidly, Elodie Villa, Jozef P. Bossowski, Emma Proics, Manuel Grima-Reyes, Agnès Paquet, Konstantina Fragaki, Sandrine Marchetti, Josette Briere, Damien Ambrosetti, Jean-François Michiels, Thierry Jo Molina, Christiane Copie-Bergman, Jacqueline Lehmann-Che, Isabelle Peyrottes, Frederic Peyrade, Eric De Kerviler, Bruno Taillan, Georges Garnier, Els Verhoeyen, Véronique Paquis-Flucklinger, Laetitia Shintu, Vincent Delwail, Celine Delpech-Debiais, Richard Delarue, André Bosly, Tony Petrella, Gabriel Brisou, Bertrand Nadel, Pascal Barbry, Nicolas Mounier, Catherine Thieblemont, and Jean-Ehrland Ricci. 2019. 'GAPDH Expression Predicts the Response to R-CHOP, the Tumor Metabolic Status, and the Response of DLBCL Patients to Metabolic Inhibitors', *Cell Metabolism*, 29: 1243-57.e10.

Chou, T. C. 2010. 'Drug combination studies and their synergy quantification using the Chou-Talalay method', *Cancer Res*, 70: 440-6.

Choueiry, Fouad, Satishkumar Singh, Anuvrat Sircar, Georgios Laliotis, Xiaowei Sun, Evangelia Chavdoula, Shiqi Zhang, Jobeth Helmig-Mason, Amber Hart, Narendranath Epperla, Philip Tsichlis, Robert Baiocchi, Lapo Alinari, Jiangjiang Zhu, and Lalit Sehgal. 2021. 'Integration of Metabolomics and Gene Expression Profiling Elucidates IL4I1 as Modulator of Ibrutinib Resistance in ABC-Diffuse Large B Cell Lymphoma', *Cancers*, 13: 2146.

Choueiry, Fouad, Satishkumar Singh, Xiaowei Sun, Shiqi Zhang, Anuvrat Sircar, Hart Amber, Lapo Alinari, Epperla Narendranath, Robert Baiocchi, Jiangjiang Zhu, and Lalit Sehgal. 2021. "Multiomics Integration Elucidates Metabolic Modulators of Drug Resistance in Lymphoma." In.: Cold Spring Harbor Laboratory.

Cun, Y., T. P. Yang, V. Achter, U. Lang, and M. Peifer. 2018. 'Copy-number analysis and inference of subclonal populations in cancer genomes using Sclust', *Nat Protoc*, 13: 1488-501.

Dambrova, M., M. Makrecka-Kuka, J. Kuka, R. Vilskersts, D. Nordberg, M. M. Attwood, S. Smesny, Z. D. Sen, A. C. Guo, E. Oler, S. Tian, J. Zheng, D. S. Wishart, E. Liepinsh, and H. B. Schioth. 2022. 'Acylcarnitines: Nomenclature, Biomarkers, Therapeutic Potential, Drug Targets, and Clinical Trials', *Pharmacol Rev*, 74: 506-51.

Danecek, P., J. K. Bonfield, J. Liddle, J. Marshall, V. Ohan, M. O. Pollard, A. Whitwham, T. Keane, S. A. McCarthy, R. M. Davies, and H. Li. 2021. 'Twelve years of SAMtools and BCFtools', *Gigascience*, 10.

Davis, R. Eric, Vu N. Ngo, Georg Lenz, Pavel Tolar, Ryan M. Young, Paul B. Romesser, Holger Kohlhammer, Laurence Lamy, Hong Zhao, Yandan Yang, Weihong Xu, Arthur L. Shaffer, George Wright, Wenming Xiao, John Powell, Jian-Kang Jiang, Craig J. Thomas, Andreas Rosenwald, German Ott, Hans Konrad Muller-Hermelink, Randy D. Gascoyne, Joseph M. Connors, Nathalie A. Johnson, Lisa M. Rimsza, Elias Campo, Elaine S. Jaffe, Wyndham H. Wilson, Jan Delabie, Erlend B. Smeland, Richard I. Fisher, Rita M. Braziel, Raymond R. Tubbs, J. R. Cook, Dennis D. Weisenburger, Wing C. Chan, Susan K. Pierce, and Louis M. Staudt. 2010. 'Chronic active B-cell-receptor signalling in diffuse large B-cell lymphoma', *Nature*, 463: 88-92.

de Jong, M. R. W., M. Langendonk, B. Reitsma, M. Nijland, A. van den Berg, E. Ammatuna, L. Visser, and T. van Meerten. 2019. 'Heterogeneous Pattern of Dependence on Anti-Apoptotic BCL-2 Family Proteins upon CHOP Treatment in Diffuse Large B-Cell Lymphoma', *Int J Mol Sci*, 20.

De Silva, N. S., and U. Klein. 2015. 'Dynamics of B cells in germinal centres', *Nat Rev Immunol*, 15: 137-48.

De Smet, Kris, and Roland Contreras. 2005. 'Human Antimicrobial Peptides: Defensins, Cathelicidins and Histatins', *Biotechnology Letters*, 27: 1337-47.

De Vries, Ronald, Johan W. Smit, Peter Hellemans, James Jiao, Joseph Murphy, Donna Skee, Jan Snoeys, Juthamas Sukbuntherng, Maarten Vliegen, Loeckie De Zwart, Erik Mannaert, and Jan De Jong. 2016. 'Stable isotope-labelled intravenous microdose for absolute bioavailability and effect of grapefruit juice on ibrutinib in healthy adults', *British Journal of Clinical Pharmacology*, 81: 235-45.

Dekker, J. D., D. Park, A. L. Shaffer, 3rd, H. Kohlhammer, W. Deng, B. K. Lee, G. C. Ippolito, G. Georgiou, V. R. Iyer, L. M. Staudt, and H. O. Tucker. 2016. 'Subtype-specific addiction of the activated B-cell subset of diffuse large B-cell lymphoma to FOXP1', *Proc Natl Acad Sci U S A*, 113: E577-86.

Deng, Ting, Shiyuan Zhang, Min Xiao, Jia Gu, Liang Huang, and Xiaoxi Zhou. 2024. 'A single-centre, real-world study of BTK inhibitors for the initial treatment of MYD88mut CD79Bmut diffuse large B-cell lymphoma', *Cancer Medicine*, 13.

DePristo, M. A., E. Banks, R. Poplin, K. V. Garimella, J. R. Maguire, C. Hartl, A. A. Philippakis, G. del Angel, M. A. Rivas, M. Hanna, A. McKenna, T. J. Fennell, A. M. Kernytsky, A. Y. Sivachenko, K. Cibulskis, S. B. Gabriel, D. Altshuler, and M. J. Daly. 2011. 'A framework for variation discovery and genotyping using next-generation DNA sequencing data', *Nat Genet*, 43: 491-8.

Derlin, Thorsten, Christian Schultze-Florey, Rudolf A. Werner, Nora Möhn, Thomas Skripuletz, Sascha David, Gernot Beutel, Matthias Eder, Tobias L. Ross, Frank M. Bengel, Arnold Ganser, and Christian Koenecke. 2021. '18F-FDG PET/CT of

off-target lymphoid organs in CD19-targeting chimeric antigen receptor T-cell therapy for relapsed or refractory diffuse large B-cell lymphoma', *Annals of Nuclear Medicine*, 35: 132-38.

Diehl, Frances F., Teemu P. Miettinen, Ryan Elbashir, Christopher S. Nabel, Alicia M. Darnell, Brian T. Do, Scott R. Manalis, Caroline A. Lewis, and Matthew G. Vander Heiden. 2022. 'Nucleotide imbalance decouples cell growth from cell proliferation', *Nature Cell Biology*, 24: 1252-64.

Domcke, Silvia, Rileen Sinha, Douglas A. Levine, Chris Sander, and Nikolaus Schultz. 2013. 'Evaluating cell lines as tumour models by comparison of genomic profiles', *Nature Communications*, 4.

Donati, Giulio, Paola Nicoli, Alessandro Verrecchia, Veronica Vallelonga, Ottavio Croci, Simona Rodighiero, Matteo Audano, Laura Cassina, Aya Ghsein, Giorgio Binelli, Alessandra Boletta, Nico Mitro, and Bruno Amati. 2022. "Oxidative stress potentiates the therapeutic action of a mitochondrial complex I inhibitor in MYC-driven B-cell lymphoma." In.: Cold Spring Harbor Laboratory.

Donati, Giulio, Micol Ravà, Marco Filipuzzi, Paola Nicoli, Laura Cassina, Alessandro Verrecchia, Mirko Doni, Simona Rodighiero, Federica Parodi, Alessandra Boletta, Christopher P. Vellano, Joseph R. Marszalek, Giulio F. Draetta, and Bruno Amati. 2022. 'Targeting mitochondrial respiration and the BCL2 family in high-grade MYC-associated B-cell lymphoma', *Molecular Oncology*, 16: 1132-52.

Dong, C., U. A. Temann, and R. A. Flavell. 2001. 'Cutting edge: critical role of inducible costimulator in germinal center reactions', *J Immunol*, 166: 3659-62.

Donjerković, Dubravka, and David W. Scott. 2000. 'Activation-induced cell death in B lymphocytes', *Cell Research*, 10: 179-92.

Doughty, C. A., B. F. Bleiman, D. J. Wagner, F. J. Dufort, J. M. Mataraza, M. F. Roberts, and T. C. Chiles. 2006. 'Antigen receptor-mediated changes in glucose metabolism in B lymphocytes: role of phosphatidylinositol 3-kinase signaling in the glycolytic control of growth', *Blood*, 107: 4458-65.

Engelke, M., N. Engels, K. Dittmann, B. Stork, and J. Wienands. 2007. 'Ca(2+) signaling in antigen receptor-activated B lymphocytes', *Immunol Rev*, 218: 235-46.

Farber, Donna L., Naomi A. Yudanin, and Nicholas P. Restifo. 2014. 'Human memory T cells: generation, compartmentalization and homeostasis', *Nature Reviews Immunology*, 14: 24-35.

Farber, S., and L. K. Diamond. 1948. 'Temporary remissions in acute leukemia in children produced by folic acid antagonist, 4-aminopteroyl-glutamic acid', *N Engl J Med*, 238: 787-93.

Flumann, R., J. Hansen, J. Meinel, P. Pfeiffer, H. Goldfarb Wittkopf, A. Lutz, J. Wirtz, M. Mollmann, T. Zhou, A. Tabatabai, T. Lohmann, M. Jauch, F. Beleggia, B. Pelzer, F. Ullrich, S. Hofmann, A. Arora, T. Persigehl, R. Buttner, B. von Tresckow, S. Klein, R. D. Jachimowicz, H. C. Reinhardt, and G. Knittel. 2024. 'An inducible Cd79b mutation confers ibrutinib sensitivity in mouse models of Myd88-driven diffuse large B-cell lymphoma', *Blood Adv*, 8: 1063-74.

Flumann, R., J. Hansen, B. W. Pelzer, P. Nieper, T. Lohmann, I. Kisis, T. Riet, V. Kohlhas, P. H. Nguyen, M. Peifer, N. Abedpour, G. Bosco, R. K. Thomas, M. Kochanek, J. Knufer, L. Jonigkeit, F. Beleggia, A. Holzem, R. Buttner, P. Lohneis, J. Meinel, M. Ortmann, T. Persigehl, M. Hallek, D. P. Calado, M. Chmielewski, S. Klein, J. R. Gothert, B. Chapuy, B. Zevnik, F. T. Wunderlich, B. von Tresckow, R. D. Jachimowicz, A. M. Melnick, H. C. Reinhardt, and G. Knittel. 2023. 'Distinct Genetically Determined Origins of Myd88/BCL2-Driven Aggressive Lymphoma Rationalize Targeted Therapeutic Intervention Strategies', *Blood Cancer Discov*, 4: 78-97.

Flümann, Ruth, Tim Rehkämper, Pascal Nieper, Pauline Pfeiffer, Alessandra Holzem, Sebastian Klein, Sanil Bhatia, Moritz Kochanek, Ilmars Kisis, Benedikt W. Pelzer, Heinz Ahlert, Julia Hauer, Alexandra Da Palma Guerreiro, Jeremy A. Ryan, Maurice Reimann, Arina Riabinska, Janica Wiederstein, Marcus Krüger, Martina Deckert, Janine Altmüller, Andreas R. Klatt, Lukas P. Frenzel, Laura Pasqualucci, Wendy Béguelin, Ari M. Melnick, Sandrine Sander, Manuel Montesinos-Rongen, Anna Brunn, Philipp Lohneis, Reinhard Büttner, Hamid Kashkar, Arndt Borkhardt, Anthony Letai, Thorsten Persigehl, Martin Peifer, Clemens A. Schmitt, Hans Christian Reinhardt, and Gero Knittel. 2021. 'An Autochthonous Mouse Model of Myd88- and BCL2-Driven Diffuse Large B-cell Lymphoma Reveals Actionable Molecular Vulnerabilities', *Blood Cancer Discovery*, 2: 70-91.

Forman, Henry Jay, and Hongqiao Zhang. 2021. 'Targeting oxidative stress in disease: promise and limitations of antioxidant therapy', *Nature Reviews Drug Discovery*, 20: 689-709.

Fornecker, Luc-Matthieu, Leslie Muller, Frédéric Bertrand, Nicodème Paul, Angélique Pichot, Raoul Herbrecht, Marie-Pierre Chenard, Laurent Mauvieux, Laurent Vallat, Seiamak Bahram, Sarah Cianférani, Raphaël Carapito, and Christine Carapito. 2019. 'Multi-omics dataset to decipher the complexity of drug resistance in diffuse large B-cell lymphoma', *Scientific Reports*, 9.

Fournier, F., R. Diaz-Marin, F. Pilon, M. Neault, R. Juneau, G. Girouard, A. M. Wilson, B. Larrivee, F. A. Mallette, S. Crespo-Garcia, and P. Sapieha. 2023. 'Obesity triggers tumoral senescence and renders poorly immunogenic malignancies amenable to senolysis', *Proc Natl Acad Sci U S A*, 120: e2209973120.

Foxall, Russell, Priyanka Narang, Bridget Glaysher, Elin Hub, Emma Teal, Mark C. Coles, Margaret Ashton-Key, Stephen A. Beers, and Mark S. Cragg. 2021. 'Developing a 3D B Cell Lymphoma Culture System to Model Antibody Therapy', *Frontiers in Immunology*, 11.

Freedman, H. I., and J. A. Gatica. 1977. 'A threshold model simulating humoral immune response to replicating antigens', *Mathematical Biosciences*, 37: 113-34.

Frick, Mareike, Bernd Dörken, and Georg Lenz. 2011. 'The molecular biology of diffuse large B-cell lymphoma', *Therapeutic Advances in Hematology*, 2: 369-79.

Galicia-Vazquez, Gabriela, and Raquel Aloyz. 2019. 'Metabolic rewiring beyond Warburg in chronic lymphocytic leukemia: How much do we actually know?', *Critical Reviews in Oncology/Hematology*, 134: 65-70.

Galicia-Vázquez, Gabriela, and Raquel Aloyz. 2018. 'Ibrutinib Resistance Is Reduced by an Inhibitor of Fatty Acid Oxidation in Primary CLL Lymphocytes', *Frontiers in Oncology*, 8.

Ganesan, Priyadarshini L., Stephen I. Alexander, Debbie Watson, Grant J. Logan, Geoff Y. Zhang, and Ian E. Alexander. 2007. 'Robust anti-tumor immunity and memory in Rag-1-deficient mice following adoptive transfer of cytokine-primed splenocytes and tumor CD80 expression', *Cancer Immunology, Immunotherapy*, 56: 1955-65.

Garrett-Sinha, Lee Ann, Gloria H. Su, Sridhar Rao, Shara Kabak, Zengping Hao, Marcus R. Clark, and M. Celeste Simon. 1999. 'PU.1 and Spi-B Are Required for Normal B Cell Receptor–Mediated Signal Transduction', *Immunity*, 10: 399-408.

Gazumyan, Anna, Amy Reichlin, and Michel C. Nussenzweig. 2006. 'Igβ tyrosine residues contribute to the control of B cell receptor signaling by regulating receptor internalization', *The Journal of Experimental Medicine*, 203: 1785-94.

Gesztelyi, Rudolf, Judit Zsuga, Adam Kemeny-Beke, Balazs Varga, Bela Juhasz, and Arpad Tosaki. 2012. 'The Hill equation and the origin of quantitative pharmacology', *Archive for History of Exact Sciences*, 66: 427-38.

Ghilardi, Guido, Joseph A. Fraietta, James N. Gerson, Vivianna M. Van Deerlin, Jennifer J. D. Morrissette, Gabriel C. Caponetti, Luca Paruzzo, Jaryse C. Harris, Elise A. Chong, Sandra P. Susanibar Adaniya, Jakub Svoboda, Sunita D. Nasta, Ositadimma H. Ugwuanyi, Daniel J. Landsburg, Eugenio Fardella, Adam J. Waxman, Emeline R. Chong, Vrutti Patel, Raymone Pajarillo, Irina Kulikovskaya, David B. Lieberman, Adam D. Cohen, Bruce L. Levine, Edward A. Stadtmauer, Noelle V. Frey, Dan T. Vogl, Elizabeth O. Hexner, Stefan K. Barta, David L. Porter, Alfred L. Garfall, Stephen J. Schuster, Carl H. June, and Marco Ruella. 2024. 'T cell lymphoma and secondary primary malignancy risk after commercial CAR T cell therapy', *Nature Medicine*, 30: 984-89.

Gonzalez, D. G., C. M. Cote, J. R. Patel, C. B. Smith, Y. Zhang, K. M. Nickerson, T. Zhang, S. M. Kerfoot, and A. M. Haberman. 2018. 'Nonredundant Roles of IL-21 and IL-4 in the Phased Initiation of Germinal Center B Cells and Subsequent Self-Renewal Transitions', *J Immunol*, 201: 3569-79.

Gros, Piet, Fin J. Milder, and Bert J. C. Janssen. 2008. 'Complement driven by conformational changes', *Nature Reviews Immunology*, 8: 48-58.

Haas, K. M. 2015. 'B-1 lymphocytes in mice and nonhuman primates', *Ann N Y Acad Sci*, 1362: 98-109.

Hanahan, Douglas. 2022. 'Hallmarks of Cancer: New Dimensions', *Cancer Discovery*, 12: 31-46.

Hanahan, Douglas, and Robert Weinberg. 2011. 'Hallmarks of Cancer: The Next Generation', *Cell*, 144: 646-74.

Hans, C. P., D. D. Weisenburger, T. C. Greiner, R. D. Gascoyne, J. Delabie, G. Ott, H. K. Muller-Hermelink, E. Campo, R. M. Braziel, E. S. Jaffe, Z. Pan, P. Farinha, L. M. Smith, B. Falini, A. H. Banham, A. Rosenwald, L. M. Staudt, J. M. Connors, J. O. Armitage, and W. C. Chan. 2004. 'Confirmation of the molecular classification of diffuse large B-cell lymphoma by immunohistochemistry using a tissue microarray', *Blood*, 103: 275-82.

He, Jing, Ziwei Chen, Qingfeng Xue, Pingping Sun, Yuan Wang, Cindy Zhu, and Wenyu Shi. 2022. 'Identification of molecular subtypes and a novel prognostic model of diffuse large B-cell lymphoma based on a metabolism-associated gene signature', *Journal of Translational Medicine*, 20.

Hegazy, M., E. Cohen-Barak, J. L. Koetsier, N. A. Najor, C. Arvanitis, E. Sprecher, K. J. Green, and L. M. Godsel. 2020. 'Proximity Ligation Assay for Detecting Protein-Protein Interactions and Protein Modifications in Cells and Tissues in Situ', *Curr Protoc Cell Biol*, 89: e115.

Herling, Carmen D., Nima Abedpour, Jonathan Weiss, Anna Schmitt, Ron Daniel Jachimowicz, Olaf Merkel, Maria Cartolano, Sebastian Oberbeck, Petra Mayer, Valeska Berg, Daniel Thomalla, Nadine Kutsch, Marius Stiefelhagen, Paula Cramer, Clemens-Martin Wendtner, Thorsten Persigehl, Andreas Saleh, Janine Altmüller, Peter Nürnberg, Christian Pallasch, Viktor Achter, Ulrich Lang, Barbara Eichhorst, Roberta Castiglione, Stephan C. Schäfer, Reinhard Büttner, Karl-Anton Kreuzer, Hans Christian Reinhardt, Michael Hallek, Lukas P. Frenzel, and Martin Peifer. 2018. 'Clonal dynamics towards the development of venetoclax resistance in chronic lymphocytic leukemia', *Nature Communications*, 9.

Hoang, Nguyet-Minh, Yunxia Liu, Paul D. Bates, Alexa R. Heaton, Angelica F. Lopez, Peng Liu, Fen Zhu, Ruoyu Chen, Apoorv Kondapelli, Xiyu Zhang, Paul E. Selberg, Vu N. Ngo, Melissa C. Skala, Christian M. Capitini, and Lixin Rui. 2024. 'Targeting DNMT3A-mediated oxidative phosphorylation to overcome ibrutinib resistance in mantle cell lymphoma', *Cell Reports Medicine*, 5: 101484.

Hobeika, E., S. Thiemann, B. Storch, H. Jumaa, P. J. Nielsen, R. Pelanda, and M. Reth. 2006. 'Testing gene function early in the B cell lineage in mb1-cre mice', *Proceedings of the National Academy of Sciences*, 103: 13789-94.

Horiuchi, Shu, Takuya Koike, Hirofumi Takebuchi, Katsuaki Hoshino, Izumi Sasaki, Yuri Fukuda-Ohta, Tsuneyasu Kaisho, and Daisuke Kitamura. 2023. 'SpiB regulates the expression of B-cell-related genes and increases the longevity of memory B cells', *Frontiers in Immunology*, 14.

Hornef, Mathias W., Mary Jo Wick, Mikael Rhen, and Staffan Normark. 2002. 'Bacterial strategies for overcoming host innate and adaptive immune responses', *Nature Immunology*, 3: 1033-40.

Horvat, M., V. Zadnik, T. Juznic Setina, L. Boltezar, J. Pahole Golicnik, S. Novakovic, and B. Jezersek Novakovic. 2018. 'Diffuse large B-cell lymphoma: 10 years' real-world clinical experience with rituximab plus cyclophosphamide, doxorubicin, vincristine and prednisolone', *Oncol Lett*, 15: 3602-09.

Hughes, A. M., V. Kuek, R. S. Kotecha, and L. C. Cheung. 2022. 'The Bone Marrow Microenvironment in B-Cell Development and Malignancy', *Cancers (Basel)*, 14.

Inoue, T., R. Shinnakasu, C. Kawai, W. Ise, E. Kawakami, N. Sax, T. Oki, T. Kitamura, K. Yamashita, H. Fukuyama, and T. Kurosaki. 2021. 'Exit from germinal center to become quiescent memory B cells depends on metabolic reprograming and provision of a survival signal', *J Exp Med*, 218.

Inoue, Takeshi, and Tomohiro Kurosaki. 2024. 'Memory B cells', *Nature Reviews Immunology*, 24: 5-17.

Ireson, Christopher R., Mo S. Alavijeh, Alan M. Palmer, Emily R. Fowler, and Hazel J. Jones. 2019. 'The role of mouse tumour models in the discovery and development of anticancer drugs', *British Journal of Cancer*, 121: 101-08.

Jakobsen, L. H., A. K. Ovlisen, M. T. Severinsen, J. Baech, K. H. Kragholm, I. Glimelius, A. O. Gang, J. M. Jorgensen, H. Frederiksen, C. B. Poulsen, M. R. Clausen, P. T. Pedersen, R. S. Pedersen, C. Torp-Pedersen, S. Eloranta, and T. C. El-Galaly. 2022. 'Patients in complete remission after R-CHOP(-like) therapy for diffuse large B-cell lymphoma have limited excess use of health care services in Denmark', *Blood Cancer J*, 12: 16.

James, L. K. 2022. 'B cells defined by immunoglobulin isotypes', *Clin Exp Immunol*, 210: 230-39.

Janeway, C. A., Jr. 1992. 'The immune system evolved to discriminate infectious nonself from noninfectious self', *Immunol Today*, 13: 11-6.

Janku, Filip, Patricia Lorusso, Aaron S. Mansfield, Rita Nanda, Alexander Spira, Tianli Wang, Amal Melhem-Bertrandt, Jennifer Sugg, and Howard A. Ball. 2021. 'First-in-human evaluation of the novel mitochondrial complex I inhibitor ASP4132 for treatment of cancer', *Investigational New Drugs*, 39: 1348-56.

Jaworska, Martyna, Julia Szczudło, Adrian Pietrzyk, Jay Shah, Sonia E. Trojan, Barbara Ostrowska, and Kinga A. Kocemba-Pilarczyk. 2023. 'The Warburg effect: a score for many instruments in the concert of cancer and cancer niche cells', *Pharmacological Reports*, 75: 876-90.

Johnson, P. W. M., S. Balasubramanian, B. Hodkinson, S. M. Shreeve, S. Sun, S. Srinivasan, A. J. Steele, J. Vermeulen, L. H. Sehn, and W. H. Wilson. 2023. 'Clinical impact of ibrutinib plus R-CHOP in untreated DLBCL coexpressing BCL2 and MYC in the phase 3 PHOENIX trial', *Blood Adv*, 7: 2008-17.

Justiz Vaillant, A. A., Z. Jamal, P. Patel, and K. Ramphul. 2024. 'Immunoglobulin.' in, *StatPearls* (Treasure Island (FL)).

Kato, Yasumasa, Shigeyuki Ozawa, Chihiro Miyamoto, Yojiro Maehata, Atsuko Suzuki, Toyonobu Maeda, and Yuh Baba. 2013. 'Acidic extracellular microenvironment and cancer', *Cancer Cell International*, 13: 89.

Kim, Hyeonhui, Minki Kim, Sun-Kyoung Im, and Sungsoon Fang. 2018. 'Mouse Cre-LoxP system: general principles to determine tissue-specific roles of target genes', *Laboratory Animal Research*, 34: 147.

Kim, J. H., W. S. Kim, K. Ryu, S. J. Kim, and C. Park. 2016. 'CD79B limits response of diffuse large B cell lymphoma to ibrutinib', *Leuk Lymphoma*, 57: 1413-22.

Kim, S., K. Scheffler, A. L. Halpern, M. A. Bekritsky, E. Noh, M. Kallberg, X. Chen, Y. Kim, D. Beyter, P. Krusche, and C. T. Saunders. 2018. 'Strelka2: fast and accurate calling of germline and somatic variants', *Nat Methods*, 15: 591-94.

Klanova, M., D. Kazantsev, E. Pokorna, T. Zikmund, J. Karolova, M. Behounek, N. Renesova, D. Sovilj, C. D. Kelemen, K. Helman, R. Jaksa, O. Havranek, L. Andera, M. Trneny, and P. Klener. 2022. 'Anti-apoptotic MCL1 Protein Represents Critical Survival Molecule for Most Burkitt Lymphomas and BCL2-negative Diffuse Large B-cell Lymphomas', *Mol Cancer Ther*, 21: 89-99.

Klapper, Wolfram, Markus Kreuz, Christian W. Kohler, Birgit Burkhardt, Monika Szczepanowski, Itziar Salaverria, Michael Hummel, Markus Loeffler, Shoji Pellissery, Wilhelm Woessmann, Carsten Schwänen, Lorenz Trümper, Swen Wessendorf, Rainer Spang, Dirk Hasenclever, and Reiner Siebert. 2012. 'Patient age at diagnosis is associated with the molecular characteristics of diffuse large B-cell lymphoma', *Blood*, 119: 1882-87.

Kluckova, Katarina, Annalisa D'Avola, and John Charles Riches. 2022. 'Advances in Understanding of Metabolism of B-Cell Lymphoma: Implications for Therapy', *Cancers*, 14: 5552.

Knittel, Gero, Paul Liedgens, Darya Korovkina, Jens M. Seeger, Yussor Al-Baldawi, Mona Al-Maarri, Christian Fritz, Katerina Vlantis, Svetlana Bezhanova, Andreas H. Scheel, Olaf-Oliver Wolz, Maurice Reimann, Peter Möller, Cristina López, Matthias Schlesner, Philipp Lohneis, Alexander N. R. Weber, Lorenz Trümper, Louis M. Staudt, Monika Ortmann, Manolis Pasparakis, Reiner Siebert, Clemens A. Schmitt, Andreas R. Klatt, F. Thomas Wunderlich, Stephan C. Schäfer, Thorsten Persigehl, Manuel Montesinos-Rongen, Margarete Odenthal, Reinhard Büttner, Lukas P. Frenzel, Hamid Kashkar, and H. Christian Reinhardt. 2016. 'B-cell–specific conditional expression of Myd88p.L252P leads to the development of diffuse large B-cell lymphoma in mice', *Blood*, 127: 2732-41.

Kochenderfer, J. N., Z. Yu, D. Frasheri, N. P. Restifo, and S. A. Rosenberg. 2010. 'Adoptive transfer of syngeneic T cells transduced with a chimeric antigen receptor that recognizes murine CD19 can eradicate lymphoma and normal B cells', *Blood*, 116: 3875-86.

Kong, L. R., K. Gupta, A. J. Wu, D. Perera, R. Ivanyi-Nagy, S. M. Ahmed, T. Z. Tan, S. L. Tan, A. Fuddin, E. Sundaramoorthy, G. S. Goh, R. T. X. Wong, A. S. H. Costa, C. Oddy, H. Wong, C. P. K. Patro, Y. S. Kho, X. Z. Huang, J. Choo, M. Shehata, S. C. Lee, B. C. Goh, C. Frezza, J. J. Pitt, and A. R. Venkitaraman. 2024. 'A glycolytic metabolite bypasses "two-hit" tumor suppression by BRCA2', *Cell*, 187: 2269-87 e16.

Kraus, M., M. B. Alimzhanov, N. Rajewsky, and K. Rajewsky. 2004. 'Survival of resting mature B lymphocytes depends on BCR signaling via the Igalpha/beta heterodimer', *Cell*, 117: 787-800.

Kretschmer, B., K. Luthje, S. Schneider, B. Fleischer, and M. Breloer. 2009. 'Engagement of CD83 on B cells modulates B cell function in vivo', *J Immunol*, 182: 2827-34.

Kretschmer, Birte, Katja Lüthje, Andreas H. Guse, Svenja Ehrlich, Friedrich Koch-Nolte, Friedrich Haag, Bernhard Fleischer, and Minka Breloer. 2007. 'CD83 Modulates B Cell Function In Vitro: Increased IL-10 and Reduced Ig Secretion by CD83Tg B Cells', *PLoS ONE*, 2: e755.

Kubacz, Matylda, Aleksandra Kusowska, Magdalena Winiarska, and Małgorzata Bobrowicz. 2022. 'In Vitro Diffuse Large B-Cell Lymphoma Cell Line Models as Tools to Investigate Novel Immunotherapeutic Strategies', *Cancers*, 15: 235.

Kuilman, T., A. Velds, K. Kemper, M. Ranzani, L. Bombardelli, M. Hoogstraat, E. Nevedomskaya, G. Xu, J. de Ruiter, M. P. Lolkema, B. Ylstra, J. Jonkers, S. Rottenberg, L. F. Wessels, D. J. Adams, D. S. Peeper, and O. Krijgsman. 2015. 'CopywriteR: DNA copy number detection from off-target sequence data', *Genome Biol*, 16: 49.

Kumagai, Shogo, Shohei Koyama, Kota Itahashi, Tokiyoshi Tanegashima, Yi-tzu Lin, Yosuke Togashi, Takahiro Kamada, Takuma Irie, Genki Okumura, Hidetoshi Kono, Daisuke Ito, Rika Fujii, Sho Watanabe, Atsuo Sai, Shota Fukuoka, Eri Sugiyama, Go Watanabe, Takuya Owari, Hitomi Nishinakamura, Daisuke Sugiyama, Yuka Maeda, Akihito Kawazoe, Hiroki Yukami, Keigo Chida, Yuuki Ohara, Tatsuya Yoshida, Yuki Shinno, Yuki Takeyasu, Masayuki Shirasawa, Kenta Nakama, Keiju Aokage, Jun Suzuki, Genichiro Ishii, Takeshi Kuwata, Naoya Sakamoto, Masahito Kawazu, Toshihide Ueno, Taisuke Mori, Naoya Yamazaki, Masahiro Tsuboi, Yasushi Yatabe, Takahiro Kinoshita, Toshihiko Doi, Kohei Shitara, Hiroyuki Mano, and Hiroyoshi Nishikawa. 2022. 'Lactic acid promotes PD-1 expression in regulatory T cells in highly glycolytic tumor microenvironments', *Cancer Cell*, 40: 201-18.e9.

Labbe, D. P., G. Zadra, M. Yang, J. M. Reyes, C. Y. Lin, S. Cacciatore, E. M. Ebot, A. L. Creech, F. Giunchi, M. Fiorentino, H. Elfandy, S. Syamala, E. D. Karoly, M. Alshalalfa, N. Erho, A. Ross, E. M. Schaeffer, E. A. Gibb, M. Takhar, R. B. Den, J. Lehrer, R. J. Karnes, S. J. Freedland, E. Davicioni, D. E. Spratt, L. Ellis, J. D. Jaffe, A. V. D'Amico, P. W. Kantoff, J. E. Bradner, L. A. Mucci, J. E. Chavarro, M. Loda, and M. Brown. 2019. 'High-fat diet fuels prostate cancer progression by rewiring the metabolome and amplifying the MYC program', *Nat Commun*, 10: 4358.

Lange, S., T. Engleitner, S. Mueller, R. Maresch, M. Zwiebel, L. Gonzalez-Silva, G. Schneider, R. Banerjee, F. Yang, G. S. Vassiliou, M. J. Friedrich, D. Saur, I. Varela, and R. Rad. 2020. 'Analysis pipelines for cancer genome sequencing in mice', *Nat Protoc*, 15: 266-315.

Leceta, Javier, Rosa Del Campo, Stefan Jordan, and Christoph S. N. Klose. 2022. 'Editorial: Immunoregulation at mucosal surfaces', *Frontiers in Immunology*, 13.

Lee, Younghwan, Karen H. Vousden, and Marc Hennequart. 2024. 'Cycling back to folate metabolism in cancer', *Nature Cancer*, 5: 701-15.

Leeman-Neill, R. J., G. Bhagat, and U. Basu. 2024. 'AID in non-Hodgkin B-cell lymphomas: The consequences of on- and off-target activity', *Adv Immunol*, 161: 127-64.

Lenz, Georg, Inga Nagel, Reiner Siebert, Anna V. Roschke, Warren Sanger, George W. Wright, Sandeep S. Dave, Bruce Tan, Hong Zhao, Andreas Rosenwald, Hans Konrad Muller-Hermelink, Randy D. Gascoyne, Elias Campo, Elaine S. Jaffe, Erlend B. Smeland, Richard I. Fisher, W. Michael Kuehl, Wing C. Chan, and Louis M. Staudt. 2007. 'Aberrant immunoglobulin class switch recombination and switch translocations in activated B cell–like diffuse large B cell lymphoma', *The Journal of Experimental Medicine*, 204: 633-43.

Li, H., and R. Durbin. 2009. 'Fast and accurate short read alignment with Burrows-Wheeler transform', *Bioinformatics*, 25: 1754-60.

Li, Haoxin, Shaoyang Ning, Mahmoud Ghandi, Gregory V. Kryukov, Shuba Gopal, Amy Deik, Amanda Souza, Kerry Pierce, Paula Keskula, Desiree Hernandez, Julie Ann, Dojna Shkoza, Verena Apfel, Yilong Zou, Francisca Vazquez, Jordi Barretina, Raymond A. Pagliarini, Giorgio G. Galli, David E. Root, William C. Hahn, Aviad Tsherniak, Marios Giannakis, Stuart L. Schreiber, Clary B. Clish, Levi A. Garraway, and William R. Sellers. 2019. 'The landscape of cancer cell line metabolism', *Nature Medicine*, 25: 850-60.

Li, X., Y. Ding, M. Zi, L. Sun, W. Zhang, S. Chen, and Y. Xu. 2017. 'CD19, from bench to bedside', *Immunol Lett*, 183: 86-95.

Li, Z., X. Ju, P. A. Silveira, E. Abadir, W. H. Hsu, D. N. J. Hart, and G. J. Clark. 2019. 'CD83: Activation Marker for Antigen Presenting Cells and Its Therapeutic Potential', *Front Immunol*, 10: 1312.

Lin, Yuying, Shen Yan, Xiao Chang, Xiaoquan Qi, and Xu Chi. 2022. 'The global integrative network: integration of signaling and metabolic pathways', *aBIOTECH*, 3: 281-91.

Linguanti, Flavia, Elisabetta Maria Abenavoli, Valentina Berti, and Egesta Lopci. 2022. 'Metabolic Imaging in B-Cell Lymphomas during CAR-T Cell Therapy', *Cancers*, 14: 4700.

Liu, Ke, Patrick A. Newbury, Benjamin S. Glicksberg, William Z. D. Zeng, Shreya Paithankar, Eran R. Andrechek, and Bin Chen. 2019. 'Evaluating cell lines as models for metastatic breast cancer through integrative analysis of genomic data', *Nature Communications*, 10.

Liu, Nianping, Chen Jiang, Xinfeng Yao, Minghao Fang, Xiaolong Qiao, Lin Zhu, Zongcheng Yang, Xuyuan Gao, Ying Ji, Chaoshi Niu, Chuandong Cheng, Kun Qu, and Jun Lin. 2023. 'Single-cell landscape of primary central nervous system diffuse large B-cell lymphoma', *Cell Discovery*, 9.

Liu, P., W. Zhu, C. Chen, B. Yan, L. Zhu, X. Chen, and C. Peng. 2020. 'The mechanisms of lysophosphatidylcholine in the development of diseases', *Life Sci*, 247: 117443.

Liu, X., S. Li, Q. Cui, B. Guo, W. Ding, J. Liu, L. Quan, X. Li, P. Xie, L. Jin, Y. Sheng, W. Chen, K. Wang, F. Zeng, Y. Qiu, C. Liu, Y. Zhang, F. Lv, X. Hu, and R. P. Xiao. 2024. 'Activation of GPR81 by lactate drives tumour-induced cachexia', *Nat Metab*, 6: 708-23.

Locke, F. L., J. M. Rossi, S. S. Neelapu, C. A. Jacobson, D. B. Miklos, A. Ghobadi, O. O. Oluwole, P. M. Reagan, L. J. Lekakis, Y. Lin, M. Sherman, M. Better, W. Y. Go, J. S. Wiezorek, A. Xue, and A. Bot. 2020. 'Tumor burden, inflammation, and product attributes determine outcomes of axicabtagene ciloleucel in large B-cell lymphoma', *Blood Adv*, 4: 4898-911.

López-Otín, Carlos, Maria A. Blasco, Linda Partridge, Manuel Serrano, and Guido Kroemer. 2013. 'The Hallmarks of Aging', *Cell*, 153: 1194-217.

Luo, Xiangjian, Xu Zhao, Can Cheng, Namei Li, Ying Liu, and Ya Cao. 2018. 'The implications of signaling lipids in cancer metastasis', *Experimental & Molecular Medicine*, 50: 1-10.

Lutfi, F., A. Patel, J. Mehta, A. Goyal, and S. Dahiya. 2023. 'Second-line treatment with CAR T-cell therapy for large B-cell lymphoma', *Clin Adv Hematol Oncol*, 21: 170-78.

Machado, Nicole D., Lisa C. Heather, Adrian L. Harris, and Geoff S. Higgins. 2023. 'Targeting mitochondrial oxidative phosphorylation: lessons, advantages, and opportunities', *British Journal of Cancer*, 129: 897-99.

Maity, Palash C., Moumita Datta, Antonella Nicolò, and Hassan Jumaa. 2018. 'Isotype Specific Assembly of B Cell Antigen Receptors and Synergism With Chemokine Receptor CXCR4', *Frontiers in Immunology*, 9.

Mandato, E., Q. Yan, J. Ouyang, J. Paczkowska, Y. Qin, Y. Hao, K. Bojarczuk, J. Hansen, B. Chapuy, S. J. Rodig, S. J. Khan, R. A. Redd, and M. A. Shipp. 2023. 'MYD88L265P Augments Proximal B-Cell Receptor Signaling in Large B-Cell Lymphomas Via an Interaction with DOCK8', *Blood*.

Martin, Alberto, and Matthew D. Scharff. 2002. 'Somatic hypermutation of the AID transgene in B and non-B cells', *Proceedings of the National Academy of Sciences*, 99: 12304-08.

Martin, Marcel. 2011. 'Cutadapt removes adapter sequences from high-throughput sequencing reads', *2011*, 17: 3.

Maul, Robert W., and Patricia J. Gearhart. 2010. 'AID and Somatic Hypermutation.' in (Elsevier).

Mayakonda, A., D. C. Lin, Y. Assenov, C. Plass, and H. P. Koeffler. 2018. 'Maftools: efficient and comprehensive analysis of somatic variants in cancer', *Genome Res*, 28: 1747-56.

McKenna, A., M. Hanna, E. Banks, A. Sivachenko, K. Cibulskis, A. Kernytsky, K. Garimella, D. Altshuler, S. Gabriel, M. Daly, and M. A. DePristo. 2010. 'The Genome Analysis Toolkit: a MapReduce framework for analyzing next-generation DNA sequencing data', *Genome Res*, 20: 1297-303.

McLaren, W., L. Gil, S. E. Hunt, H. S. Riat, G. R. Ritchie, A. Thormann, P. Flicek, and F. Cunningham. 2016. 'The Ensembl Variant Effect Predictor', *Genome Biol*, 17: 122.

Miyazawa, Hidenobu, and Alexander Aulehla. 2018. 'Revisiting the role of metabolism during development', *Development*, 145: dev131110.

Mlynarczyk, C., M. Teater, J. Pae, C. R. Chin, L. Wang, T. Arulraj, D. Barisic, A. Papin, K. B. Hoehn, E. Kots, J. Ersching, A. Bandyopadhyay, E. Barin, H. X. Poh, C. M. Evans, A. Chadburn, Z. Chen, H. Shen, H. M. Isles, B. Pelzer, I. Tsialta, A. S. Doane, H. Geng, M. H. Rehman, J. Melnick, W. Morgan, D. T. T. Nguyen, O. Elemento, M. G. Kharas, S. R. Jaffrey, D. W. Scott, G. Khelashvili, M. Meyer-Hermann, G. D. Victora, and A. Melnick. 2023. 'BTG1 mutation yields supercompetitive B cells primed for malignant transformation', *Science*, 379: eabj7412.

Mlynarczyk, Coraline, Lorena Fontán, and Ari Melnick. 2019. 'Germinal center-derived lymphomas: The darkest side of humoral immunity', *Immunological Reviews*, 288: 214-39.

Molina, Jennifer R., Yuting Sun, Marina Protopopova, Sonal Gera, Madhavi Bandi, Christopher Bristow, Timothy McAfoos, Pietro Morlacchi, Jeffrey Ackroyd, Ahmed-Noor A. Agip, Gheath Al-Atrash, John Asara, Jennifer Bardenhagen, Caroline C. Carrillo, Christopher Carroll, Edward Chang, Stefan Ciurea, Jason B. Cross, Barbara Czako, Angela Deem, Naval Daver, John Frederick De Groot, Jian-Wen Dong, Ningping Feng, Guang Gao, Jason Gay, Mary Geck Do, Jennifer Greer, Virginia Giuliani, Jing Han, Lina Han, Verlene K. Henry, Judy Hirst, Sha Huang, Yongying Jiang, Zhijun Kang, Tin Khor, Sergej Konoplev, Yu-Hsi Lin, Gang Liu, Alessia Lodi, Timothy Lofton, Helen Ma, Mikhila Mahendra, Polina Matre, Robert Mullinax, Michael Peoples, Alessia Petrocchi, Jaime Rodriguez-Canale, Riccardo Serreli, Thomas Shi, Melinda Smith, Yoko Tabe, Jay Theroff, Stefano Tiziani, Quanyun Xu, Qi Zhang, Florian Muller, Ronald A. Depinho, Carlo Toniatti, Giulio F. Draetta, Timothy P. Heffernan, Marina Konopleva, Philip Jones, M. Emilia Di Francesco, and Joseph R. Marszalek. 2018. 'An inhibitor of oxidative phosphorylation exploits cancer vulnerability', *Nature Medicine*, 24: 1036-46.

Mombaerts, P., J. Iacomini, R. S. Johnson, K. Herrup, S. Tonegawa, and V. E. Papaioannou. 1992. 'RAG-1-deficient mice have no mature B and T lymphocytes', *Cell*, 68: 869-77.

Monni, O., H. Joensuu, K. Franssila, J. Klefstrom, K. Alitalo, and S. Knuutila. 1997. 'BCL2 overexpression associated with chromosomal amplification in diffuse large B-cell lymphoma', *Blood*, 90: 1168-74.

Montes-Moreno, S., A. R. Gonzalez-Medina, S. M. Rodriguez-Pinilla, L. Maestre, L. Sanchez-Verde, G. Roncador, M. Mollejo, J. F. Garcia, J. Menarguez, C. Montalban, M. C. Ruiz-Marcellan, E. Conde, and M. A. Piris. 2010. 'Aggressive large B-cell lymphoma with plasma cell differentiation: immunohistochemical characterization of plasmablastic lymphoma and diffuse large B-cell lymphoma with partial plasmablastic phenotype', *Haematologica*, 95: 1342-49.

Munshi, Manit, Xia Liu, Jiaji G. Chen, Lian Xu, Nickolas Tsakmaklis, Maria G. Demos, Amanda Kofides, Maria Luisa Guerrera, Cristina Jimenez, Gloria G. Chan, Zachary R. Hunter, M. Lia Palomba, Kimon V. Argyropoulos, Kirsten Meid, Andrew Keezer, Joshua Gustine, Toni Dubeau, Jorge J. Castillo, Christopher J. Patterson, Jinhua Wang, Sara J. Buhrlage, Nathanael S. Gray, Steven P. Treon, and Guang Yang. 2020. 'SYK is activated by mutated MYD88 and drives pro-survival signaling in MYD88 driven B-cell lymphomas', *Blood Cancer Journal*, 10.

Murphy, Kenneth, Paul Travers, Mark Walport, and Charles Janeway. 2012. *Janeway's immunobiology* (Garland Science: New York).

Nagasawa, T. 2006. 'Microenvironmental niches in the bone marrow required for B-cell development', *Nat Rev Immunol*, 6: 107-16.

Nair, Arathi, Prashant Chauhan, Bhaskar Saha, and Katharina F. Kubatzky. 2019. 'Conceptual Evolution of Cell Signaling', *International Journal of Molecular Sciences*, 20: 3292.

Nakhoda, Shazia, Aldana Vistarop, and Y. Lynn Wang. 2022. 'Resistance to Bruton tyrosine kinase inhibition in chronic lymphocytic leukaemia and non-Hodgkin lymphoma', *British Journal of Haematology*.

Natalya, and Craig. 2016. 'The Emerging Hallmarks of Cancer Metabolism', *Cell Metabolism*, 23: 27-47.

Ngo, Vu N., Ryan M. Young, Roland Schmitz, Sameer Jhavar, Wenming Xiao, Kian-Huat Lim, Holger Kohlhammer, Weihong Xu, Yandan Yang, Hong Zhao, Arthur L. Shaffer, Paul Romesser, George Wright, John Powell, Andreas Rosenwald, Hans Konrad Muller-Hermelink, German Ott, Randy D. Gascoyne, Joseph M. Connors, Lisa M. Rimsza, Elias Campo, Elaine S. Jaffe, Jan Delabie, Erlend B. Smeland, Richard I. Fisher, Rita M. Braziel, Raymond R. Tubbs, J. R. Cook, Denny D. Weisenburger, Wing C. Chan, and Louis M. Staudt. 2011. 'Oncogenically active MYD88 mutations in human lymphoma', *Nature*, 470: 115-19.

Nicolson, Phillip L. R., Craig E. Hughes, Stephanie Watson, Sophie H. Nock, Alexander T. Hardy, Callum N. Watson, Samantha J. Montague, Hayley Clifford, Aarnoud P. Huissoon, Jean-Daniel Malcor, Mark R. Thomas, Alice Y. Pollitt, Michael G. Tomlinson, Guy Pratt, and Steve P. Watson. 2018. 'Inhibition of Btk by Btk-specific concentrations of ibrutinib and acalabrutinib delays but does not block platelet aggregation mediated by glycoprotein VI', *Haematologica*, 103: 2097-108.

Niemann, C. U., M. D. Levin, J. Dubois, S. Kersting, L. Enggaard, G. J. Veldhuis, R. Mous, C. H. M. Mellink, J. A. Dobber, C. B. Poulsen, H. Frederiksen, A. Janssens, I. Schjodt, E. C. Dompeling, J. Ranti, M. Mattsson, M. Bellido, H. T. T. Tran, K. Nasserinejad, and A. P. Kater. 2021. 'Venetoclax and ibrutinib for patients with relapsed/refractory chronic lymphocytic leukemia', *Blood*, 137: 1117-20.

Noble, Richard A., Huw Thomas, Yan Zhao, Lili Herendi, Rachel Howarth, Ilaria Dragoni, Hector C. Keun, Christopher P. Vellano, Joseph R. Marszalek, and Stephen R. Wedge. 2022. 'Simultaneous targeting of glycolysis and oxidative phosphorylation as a therapeutic strategy to treat diffuse large B-cell lymphoma', *British Journal of Cancer*, 127: 937-47.

Nutt, Stephen L., Philip D. Hodgkin, David M. Tarlinton, and Lynn M. Corcoran. 2015. 'The generation of antibody-secreting plasma cells', *Nature Reviews Immunology*, 15: 160-71.

Pandey, A., P. Yadav, and S. Shukla. 2021. 'Unfolding the role of autophagy in the cancer metabolism', *Biochem Biophys Rep*, 28: 101158.

Paquin, Ashley R., Emmanuella Oyogoa, Hannah Stowe McMurry, Thomas Kartika, Malinda West, and Joseph J. Shatzel. 2023. 'The diagnosis and management of suspected lymphoma in general practice', *European Journal of Haematology*, 110: 3-13.

Patmanathan, Sathya Narayanan, Steven P. Johnson, Sook Ling Lai, Suthashini Panja Bernam, Victor Lopes, Wenbin Wei, Maha Hafez Ibrahim, Federico Torta, Pradeep Narayanaswamy, Markus R. Wenk, Deron R. Herr, Paul G. Murray, Lee Fah Yap, and Ian C. Paterson. 2016. 'Aberrant expression of the S1P regulating enzymes, SPHK1 and SGPL1, contributes to a migratory phenotype in OSCC mediated through S1PR2', *Scientific Reports*, 6: 25650.

Peeters, Rens, Jorge Cuenca-Escalona, Esther A. Zaal, Anna T. Hoekstra, Anouk C. G. Balvert, Marcos Vidal-Manrique, Niek Blomberg, Sjoerd J. Van Deventer, Rinke Stienstra, Julia Jellusova, Martin Giera, Luciana Hannibal, Ute Spiekerkoetter, Martin Ter Beest, Celia R. Berkers, and Annemiek B. Van Spriel. 2022. 'Fatty acid metabolism in aggressive B-cell lymphoma is inhibited by tetraspanin CD37', *Nature Communications*, 13.

Peifer, M., L. Fernandez-Cuesta, M. L. Sos, J. George, D. Seidel, L. H. Kasper, D. Plenker, F. Leenders, R. Sun, T. Zander, R. Menon, M. Koker, I. Dahmen, C. Muller, V. Di Cerbo, H. U. Schildhaus, J. Altmuller, I. Baessmann, C. Becker, B. de Wilde, J. Vandesompele, D. Bohm, S. Ansen, F. Gabler, I. Wilkening, S. Heynck, J. M. Heuckmann, X. Lu, S. L. Carter, K. Cibulskis, S. Banerji, G. Getz, K. S. Park, D. Rauh, C. Grutter, M. Fischer, L. Pasqualucci, G. Wright, Z. Wainer, P. Russell, I. Petersen, Y. Chen, E. Stoelben, C. Ludwig, P. Schnabel, H. Hoffmann, T. Muley, M. Brockmann, W. Engel-Riedel, L. A. Muscarella, V. M. Fazio, H. Groen, W. Timens, H. Sietsma, E. Thunnissen, E. Smit, D. A. Heideman, P. J. Snijders, F. Cappuzzo, C. Ligorio, S. Damiani, J. Field, S. Solberg, O. T. Brustugun, M. Lund-Iversen, J. Sanger, J. H. Clement, A. Soltermann, H. Moch, W. Weder, B. Solomon, J. C. Soria, P. Validire, B. Besse, E. Brambilla, C. Brambilla, S. Lantuejoul, P. Lorimier, P. M. Schneider, M. Hallek, W. Pao, M. Meyerson, J. Sage, J. Shendure, R. Schneider, R. Buttner, J. Wolf, P. Nurnberg, S. Perner, L. C. Heukamp, P. K. Brindle, S. Haas, and R. K. Thomas. 2012. 'Integrative genome analyses identify key somatic driver mutations of small-cell lung cancer', *Nat Genet*, 44: 1104-10.

Pennington, Z., M. L. Goodwin, E. M. Westbroek, E. Cottrill, A. K. Ahmed, and D. M. Sciubba. 2019. 'Lactate and cancer: spinal metastases and potential therapeutic targets (part 2)', *Ann Transl Med*, 7: 221.

Pfeifer, M., M. Grau, D. Lenze, S. S. Wenzel, A. Wolf, B. Wollert-Wulf, K. Dietze, H. Nogai, B. Storek, H. Madle, B. Dorken, M. Janz, S. Dirnhofer, P. Lenz, M. Hummel, A. Tzankov, and G. Lenz. 2013. 'PTEN loss defines a PI3K/AKT pathway-dependent germinal center subtype of diffuse large B-cell lymphoma', *Proceedings of the National Academy of Sciences*, 110: 12420-25.

Phelan, J. D., S. Scheich, J. Choi, G. W. Wright, B. Haupl, R. M. Young, S. A. Rieke, M. Pape, Y. Ji, H. Urlaub, A. Bolomsky, C. Doebele, A. Zindel, T. Wotapek, M. Kasbekar, B. Collinge, D. W. Huang, Z. A. Coulibaly, V. M. Morris, X. Zhuang, J. C. Enssle, X. Yu, W. Xu, Y. Yang, H. Zhao, Z. Wang, A. D. Tran, C. J. Shoemaker, G. Shevchenko, D. J. Hodson, A. L. Shaffer, 3rd, L. M. Staudt, and T. Oellerich. 2024. 'Response to Bruton's tyrosine kinase inhibitors in aggressive lymphomas linked to chronic selective autophagy', *Cancer Cell*, 42: 238-52 e9.

Phelan, James D., Ryan M. Young, Daniel E. Webster, Sandrine Roulland, George W. Wright, Monica Kasbekar, Arthur L. Shaffer, Michele Ceribelli, James Q. Wang, Roland Schmitz, Masao Nakagawa, Emmanuel Bachy, Da Wei Huang, Yanlong Ji, Lu Chen, Yandan Yang, Hong Zhao, Xin Yu, Weihong Xu, Maryknoll M. Palisoc, Racquel R. Valadez, Theresa Davies-Hill, Wyndham H. Wilson, Wing C. Chan, Elaine S. Jaffe, Randy D. Gascoyne, Elias Campo, Andreas Rosenwald, German Ott, Jan Delabie, Lisa M. Rimsza, Fausto J. Rodriguez, Fayez Estephan, Matthias Holdhoff, Michael J. Kruhlak, Stephen M. Hewitt, Craig J. Thomas, Stefania Pittaluga, Thomas Oellerich, and Louis M. Staudt. 2018. 'A multiprotein supercomplex controlling oncogenic signalling in lymphoma', *Nature*, 560: 387-91.

Pietrocola, Federico, Lorenzo Galluzzi, José, Frank Madeo, and Guido Kroemer. 2015. 'Acetyl Coenzyme A: A Central Metabolite and Second Messenger', *Cell Metabolism*, 21: 805-21.

Pindzola, G. M., R. Razzaghi, R. N. Tavory, H. T. Nguyen, V. M. Morris, M. Li, S. Agarwal, B. Huang, T. Okada, H. C. Reinhardt, G. Knittel, H. Kashkar, R. M. Young, S. Pittaluga, and J. R. Muppidi. 2022. 'Aberrant expansion of spontaneous splenic germinal centers induced by hallmark genetic lesions of aggressive lymphoma', *Blood*, 140: 1119-31.

Pluskal, T., S. Castillo, A. Villar-Briones, and M. Oresic. 2010. 'MZmine 2: modular framework for processing, visualizing, and analyzing mass spectrometry-based molecular profile data', *BMC Bioinformatics*, 11: 395.

Prinz, Lars Fabian, Tobias Riet, Daniel Felix Neureuther, Simon Lennartz, Danuta Chrobok, Hanna Hübbe, Gregor Uhl, Nicole Riet, Petra Hofmann, Marianna Hösel, Adrian Georg Simon, Luis Tetenborg, Paul Segbers, Joji Shimono, Philipp Gödel, Hyatt Balke-Want, Ruth Flümann, Gero Knittel, Hans Christian Reinhardt, Christoph Scheid, Reinhard Büttner, Björn Chapuy, Roland Tillmann Ullrich, Michael Hallek, and Markus Martin Chmielewski. 2024. 'An anti-CD19/CTLA-4 switch improves efficacy and selectivity of CAR T cells targeting CD80/86-upregulated DLBCL', *Cell Reports Medicine*, 5: 101421.

Qu, N., D. Chen, B. Ma, L. Zhang, Q. Wang, Y. Wang, H. Wang, Z. Ni, W. Wang, T. Liao, J. Xiang, Y. Wang, S. Jin, D. Xue, W. Wu, Y. Wang, Q. Ji, H. He, H. L. Piao, and R. Shi. 2024. 'Integrated proteogenomic and metabolomic characterization of papillary thyroid cancer with different recurrence risks', *Nat Commun*, 15: 3175.

Radhakrishnan, Vivek Sulekha, Padmaja Lokireddy, Mayur Parihar, Prashanth Srirangapattana Prakash, and Hari Menon. 2022. 'Mantle cell lymphoma: A clinical review of the changing treatment paradigms with the advent of novel therapies, and an insight into Indian data', *Cancer Reports*, 5.

Rafiq, Sarwish, Christopher S. Hackett, and Renier J. Brentjens. 2020. 'Engineering strategies to overcome the current roadblocks in CAR T cell therapy', *Nature Reviews Clinical Oncology*, 17: 147-67.

Reddy, Anupama, Jenny Zhang, Nicholas S. Davis, Andrea B. Moffitt, Cassandra L. Love, Alexander Waldrop, Sirpa Leppa, Annika Pasanen, Leo Meriranta, Marja-Liisa Karjalainen-Lindsberg, Peter Nørgaard, Mette Pedersen, Anne O. Gang, Estrid Høgdall, Tayla B. Heavican, Waseem Lone, Javeed Iqbal, Qiu Qin, Guojie Li, So Young Kim, Jane Healy, Kristy L. Richards, Yuri Fedoriw, Leon Bernal-Mizrachi, Jean L. Koff, Ashley D. Staton, Christopher R. Flowers, Ora Paltiel, Neta Goldschmidt, Maria Calaminici, Andrew Clear, John Gribben, Evelyn Nguyen, Magdalena B. Czader, Sarah L. Ondrejka, Angela Collie, Eric D. Hsi, Eric Tse, Rex K. H. Au-Yeung, Yok-Lam Kwong, Gopesh Srivastava, William W. L. Choi, Andrew M. Evens, Monika Pilichowska, Manju Sengar, Nishitha Reddy, Shaoying Li, Amy Chadburn, Leo I. Gordon, Elaine S. Jaffe, Shawn Levy, Rachel Rempel, Tiffany Tzeng, Lanie E. Happ, Tushar Dave, Deepthi Rajagopalan, Jyotishka Datta, David B. Dunson, and Sandeep S. Dave. 2017. 'Genetic and Functional Drivers of Diffuse Large B Cell Lymphoma', *Cell*, 171: 481-94.e15.

Riaz, Bushra, S. M. Shamsul Islam, Hye Myung Ryu, and Seonghyang Sohn. 2023. 'CD83 Regulates the Immune Responses in Inflammatory Disorders', *International Journal of Molecular Sciences*, 24: 2831.

Rickert, R. C., J. Roes, and K. Rajewsky. 1997. 'B lymphocyte-specific, Cre-mediated mutagenesis in mice', *Nucleic Acids Res*, 25: 1317-8.

Robbiani, Davide F., Anne Bothmer, Elsa Callen, Bernardo Reina-San-Martin, Yair Dorsett, Simone Difilippantonio, Daniel J. Bolland, Hua Tang Chen, Anne E. Corcoran, André Nussenzweig, and Michel C. Nussenzweig. 2008. 'AID Is Required for the Chromosomal Breaks in c-myc that Lead to c-myc/IgH Translocations', *Cell*, 135: 1028-38.

Rombouts, Caroline, Margot De Spiegeleer, Lieven Van Meulebroek, Lynn Vanhaecke, and Winnok H. De Vos. 2021. 'Comprehensive polar metabolomics and lipidomics profiling discriminates the transformed from the non-transformed state in colon tissue and cell lines', *Scientific Reports*, 11.

Sarkozy, Clémentine, Gilles Salles, and Claire Falandry. 2015. 'The Biology of Aging and Lymphoma: a Complex Interplay', *Current Oncology Reports*, 17.

Schmitz, Roland, George W. Wright, Da Wei Huang, Calvin A. Johnson, James D. Phelan, James Q. Wang, Sandrine Roulland, Monica Kasbekar, Ryan M. Young, Arthur L. Shaffer, Daniel J. Hodson, Wenming Xiao, Xin Yu, Yandan Yang, Hong Zhao, Weihong Xu, Xuelu Liu, Bin Zhou, Wei Du, Wing C. Chan, Elaine S. Jaffe, Randy D. Gascoyne, Joseph M. Connors, Elias Campo, Armando Lopez-Guillermo, Andreas Rosenwald, German Ott, Jan Delabie, Lisa M. Rimsza, Kevin Tay Kuang Wei, Andrew D. Zelenetz, John P. Leonard, Nancy L. Bartlett, Bao Tran, Jyoti Shetty, Yongmei Zhao, Dan R. Soppet, Stefania Pittaluga, Wyndham H. Wilson, and Louis M. Staudt. 2018. 'Genetics and Pathogenesis of Diffuse Large B-Cell Lymphoma', *New England Journal of Medicine*, 378: 1396-407.

Schofield, D. J., J. Percival-Alwyn, M. Rytelewski, J. Hood, R. Rothstein, L. Wetzel, K. McGlinchey, G. Adjei, A. Watkins, L. Machiesky, W. Chen, J. Andrews, M. Groves, M. Morrow, R. A. Stewart, A. Leinster, R. W. Wilkinson, S. A. Hammond, N. Luheshi, C. Dobson, and M. Oberst. 2021. 'Activity of murine surrogate antibodies for durvalumab and tremelimumab lacking effector function and the ability to deplete regulatory T cells in mouse models of cancer', *MAbs*, 13: 1857100.

Schroeder, H. W., Jr., and L. Cavacini. 2010. 'Structure and function of immunoglobulins', *J Allergy Clin Immunol*, 125: S41-52.

Schwaiger, M., E. Rampler, G. Hermann, W. Miklos, W. Berger, and G. Koellensperger. 2017. 'Anion-Exchange Chromatography Coupled to High-Resolution Mass Spectrometry: A Powerful Tool for Merging Targeted and Non-targeted Metabolomics', *Anal Chem*, 89: 7667-74.

Sehn, L. H., and G. Salles. 2021. 'Diffuse Large B-Cell Lymphoma', *N Engl J Med*, 384: 842-58.

Shaffer, A. L., 3rd, R. M. Young, and L. M. Staudt. 2012. 'Pathogenesis of human B cell lymphomas', *Annu Rev Immunol*, 30: 565-610.

Shaffer, A. L., Kuo- I. Lin, Tracy C. Kuo, Xin Yu, Elaine M. Hurt, Andreas Rosenwald, Jena M. Giltnane, Liming Yang, Hong Zhao, Kathryn Calame, and Louis M. Staudt. 2002. 'Blimp-1 Orchestrates Plasma Cell Differentiation by Extinguishing the Mature B Cell Gene Expression Program', *Immunity*, 17: 51-62.

Shaffer, A. L., Xin Yu, Yunsheng He, Jennifer Boldrick, Erick P. Chan, and Louis M. Staudt. 2000. 'BCL-6 Represses Genes that Function in Lymphocyte Differentiation, Inflammation, and Cell Cycle Control', *Immunity*, 13: 199-212.

Shalaby, Y. M., A. Al Aidaros, A. Valappil, B. R. Ali, and N. Akawi. 2021. 'Role of Ceramides in the Molecular Pathogenesis and Potential Therapeutic Strategies of Cardiometabolic Diseases: What we Know so Far', *Front Cell Dev Biol*, 9: 816301.

Shapiro-Shelef, M., K. I. Lin, D. Savitsky, J. Liao, and K. Calame. 2005. 'Blimp-1 is required for maintenance of long-lived plasma cells in the bone marrow', *J Exp Med*, 202: 1471-6.

Shugay, M., O. V. Britanova, E. M. Merzlyak, M. A. Turchaninova, I. Z. Mamedov, T. R. Tuganbaev, D. A. Bolotin, D. B. Staroverov, E. V. Putintseva, K. Plevova, C. Linnemann, D. Shagin, S. Pospisilova, S. Lukyanov, T. N. Schumacher, and D. M. Chudakov. 2014. 'Towards error-free profiling of immune repertoires', *Nat Methods*, 11: 653-5.

Smith, A., S. Crouch, S. Lax, J. Li, D. Painter, D. Howell, R. Patmore, A. Jack, and E. Roman. 2015. 'Lymphoma incidence, survival and prevalence 2004–2014: sub-type analyses from the UK's Haematological Malignancy Research Network', *British Journal of Cancer*, 112: 1575-84.

Sobanski, Thais, Maddison Rose, Amila Suraweera, Kenneth O'Byrne, Derek J. Richard, and Emma Bolderson. 2021. 'Cell Metabolism and DNA Repair Pathways: Implications for Cancer Therapy', *Frontiers in Cell and Developmental Biology*, 9.

Soneson, C., M. I. Love, and M. D. Robinson. 2015. 'Differential analyses for RNA-seq: transcript-level estimates improve gene-level inferences', *F1000Res*, 4: 1521.

Srinivasan, Lakshmi, Yoshiteru Sasaki, Dinis Pedro Calado, Baochun Zhang, Ji Hye Paik, Ronald A. Depinho, Jeffrey L. Kutok, John F. Kearney, Kevin L. Otipoby, and Klaus Rajewsky. 2009. 'PI3 Kinase Signals BCR-Dependent Mature B Cell Survival', *Cell*, 139: 573-86.

Steen, C. B., B. A. Luca, M. S. Esfahani, A. Azizi, B. J. Sworder, B. Y. Nabet, D. M. Kurtz, C. L. Liu, F. Khameneh, R. H. Advani, Y. Natkunam, J. H. Myklebust, M. Diehn, A. J. Gentles, A. M. Newman, and A. A. Alizadeh. 2021. 'The landscape of tumor cell states and ecosystems in diffuse large B cell lymphoma', *Cancer Cell*, 39: 1422-37 e10.

Su, G. H., H. Chen, N. Muthusamy, L. A. Garrett-Sinha, D. Baunoch, D. G. Tenen, and M. C. Simon. 1997. 'Defective B cell receptor-mediated responses in mice lacking the Ets protein, Spi-B', *The EMBO Journal*, 16: 7118-29.

Sullivan, Matthew R., Rachel P. White, Ravi Dashnamoorthy, Ninad Kanetkar, Ilana Berger Fridman, Adam Ekenseair, Andrew M. Evens, and Tania Konry. 2024. 'Characterizing influence of rCHOP treatment on diffuse large B-cell lymphoma microenvironment through in vitro microfluidic spheroid model', *Cell Death & Disease*, 15.

Tabatabai, A., A. Arora, S. Hofmann, M. Jauch, B. von Tresckow, J. Hansen, R. Flumann, R. D. Jachimowicz, S. Klein, H. C. Reinhardt, and G. Knittel. 2023. 'Mouse models of diffuse large B cell lymphoma', *Front Immunol*, 14: 1313371.

Taher, Leila, Julia Beck, Wen Liu, Catrin Roolf, Jan T. Soller, Barbara C. Rütgen, Sabine E. Hammer, Murali Chodisetti, Sina Sender, Katharina A. Sterenczak, Georg Fuellen, Christian Junghanss, Bertram Brenig, Ingo Nolte, Ekkehard Schütz, and Hugo Murua Escobar. 2018. 'Comparative High-Resolution Transcriptome Sequencing of Lymphoma Cell Lines and de novo Lymphomas Reveals Cell-Line-Specific Pathway Dysregulation', *Scientific Reports*, 8.

Tanaka, Shinya, and Yoshihiro Baba. 2020. 'B Cell Receptor Signaling.' in (Springer Singapore).

Tebon, Peyton J., Bowen Wang, Alexander L. Markowitz, Ardalan Davarifar, Brandon L. Tsai, Patrycja Krawczuk, Alfredo E. Gonzalez, Sara Sartini, Graeme F. Murray, Huyen Thi Lam Nguyen, Nasrin Tavanaie, Thang L. Nguyen, Paul C. Boutros, Michael A. Teitell, and Alice Soragni. 2023. 'Drug screening at single-organoid resolution via bioprinting and interferometry', *Nature Communications*, 14.

Timofeeva, Natalia, and Varsha Gandhi. 2021. 'Ibrutinib combinations in CLL therapy: scientific rationale and clinical results', *Blood Cancer Journal*, 11.

Tunyaplin, Chainarong, A. L. Shaffer, Cristina D. Angelin-Duclos, Xin Yu, Louis M. Staudt, and Kathryn L. Calame. 2004. 'Direct Repression of prdm1 by Bcl-6 Inhibits Plasmacytic Differentiation', *The Journal of Immunology*, 173: 1158-65.

Ullman-Cullere, M. H., and C. J. Foltz. 1999. 'Body condition scoring: a rapid and accurate method for assessing health status in mice', *Lab Anim Sci*, 49: 319-23.

van der Veen, J. N., J. P. Kennelly, S. Wan, J. E. Vance, D. E. Vance, and R. L. Jacobs. 2017. 'The critical role of phosphatidylcholine and phosphatidylethanolamine metabolism in health and disease', *Biochim Biophys Acta Biomembr*, 1859: 1558-72.

Vander Heiden, J. A., G. Yaari, M. Uduman, J. N. Stern, K. C. O'Connor, D. A. Hafler, F. Vigneault, and S. H. Kleinstein. 2014. 'pRESTO: a toolkit for processing high-throughput sequencing raw reads of lymphocyte receptor repertoires', *Bioinformatics*, 30: 1930-2.

Vasseur, Sophie, and Fabienne Guillaumond. 2022. 'Lipids in cancer: a global view of the contribution of lipid pathways to metastatic formation and treatment resistance', *Oncogenesis*, 11.

Venturutti, L., M. A. Rivas, B. W. Pelzer, R. Flumann, J. Hansen, I. Karagiannidis, M. Xia, D. R. McNally, Y. Isshiki, A. Lytle, M. Teater, C. R. Chin, C. Meydan, G. Knittel, E. Ricker, C. E. Mason, X. Ye, Q. Pan-Hammarstrom, C. Steidl, D. W. Scott, H. C. Reinhardt, A. B. Pernis, W. Beguelin, and A. M. Melnick. 2022. 'An Aged/Autoimmune B-cell Program Defines the Early Transformation of Extranodal Lymphomas', *Cancer Discov*.

Venturutti, L., M. Teater, A. Zhai, A. Chadburn, L. Babiker, D. Kim, W. Beguelin, T. C. Lee, Y. Kim, C. R. Chin, W. T. Yewdell, B. Raught, J. M. Phillip, Y. Jiang, L. M. Staudt, M. R. Green, J. Chaudhuri, O. Elemento, P. Farinha, A. P. Weng, M. D. Nissen, C. Steidl, R. D. Morin, D. W. Scott, G. G. Prive, and A. M. Melnick. 2020. 'TBL1XR1 Mutations Drive Extranodal Lymphoma by Inducing a Pro-tumorigenic Memory Fate', *Cell*, 182: 297-316 e27.

Venturutti, Leandro, and Ari M. Melnick. 2020. 'The dangers of déjà vu: memory B cells as the cells of origin of ABC-DLBCLs', *Blood*, 136: 2263-74.

Verdun, N., and P. Marks. 2024. 'Secondary Cancers after Chimeric Antigen Receptor T-Cell Therapy', *N Engl J Med*, 390: 584-86.

Wallace, Danielle S., and Patrick M. Reagan. 2022. 'Age is just a number: managing relapsed or refractory diffuse large B-cell lymphoma (DLBCL) in older patients', *Annals of Lymphoma*, 6.

Wang, Jun, Na Sun, Thomas Kunzke, Jian Shen, Philipp Zens, Verena M. Prade, Annette Feuchtinger, Sabina Berezowska, and Axel Walch. 2023. 'Spatial metabolomics identifies distinct tumor-specific and stroma-specific subtypes in patients with lung squamous cell carcinoma', *npj Precision Oncology*, 7.

Wang, Tong, Bo Jing, Dongliang Xu, Yueling Liao, Hongyong Song, Beibei Sun, Wenzheng Guo, Jianhua Xu, Kaimi Li, Min Hu, Shuli Liu, Jing Ling, Yanbin Kuang, Tuo Zhang, Siwei Zhang, Feng Yao, Binhua P. Zhou, and Jiong Deng. 2020. 'PTGES/PGE2 signaling links immunosuppression and lung metastasis in Gprc5a-knockout mouse model', *Oncogene*, 39: 3179-94.

Warburg, O. 1956. 'On respiratory impairment in cancer cells', *Science*, 124: 269-70.

Wei, P., A. J. Bott, A. A. Cluntun, J. T. Morgan, C. N. Cunningham, J. C. Schell, Y. Ouyang, S. B. Ficarro, J. A. Marto, N. N. Danial, R. J. DeBerardinis, and J. Rutter. 2022. 'Mitochondrial pyruvate supports lymphoma proliferation by fueling a glutamate pyruvate transaminase 2-dependent glutaminolysis pathway', *Sci Adv*, 8: eabq0117.

Wen, Y., Y. Jing, L. Yang, D. Kang, P. Jiang, N. Li, J. Cheng, J. Li, X. Li, Z. Peng, X. Sun, H. Miller, Z. Sui, Q. Gong, B. Ren, W. Yin, and C. Liu. 2019. 'The regulators of BCR signaling during B cell activation', *Blood Sci*, 1: 119-29.

Westin, J., and L. H. Sehn. 2022. 'CAR T cells as a second-line therapy for large B-cell lymphoma: a paradigm shift?', *Blood*, 139: 2737-46.

Wilson, Wyndham H., Ryan M. Young, Roland Schmitz, Yandan Yang, Stefania Pittaluga, George Wright, Chih-Jian Lih, P. Mickey Williams, Arthur L. Shaffer, John Gerecitano, Sven De Vos, Andre Goy, Vaishalee P. Kenkre, Paul M. Barr, Kristie A. Blum, Andrei Shustov, Ranjana Advani, Nathan H. Fowler, Julie M. Vose, Rebecca L. Elstrom, Thomas M. Habermann, Jacqueline C. Barrientos, Jesse McGreivy, Maria Fardis, Betty Y. Chang, Fong Clow, Brian Munneke, Davina Moussa, Darrin M. Beaupre, and Louis M. Staudt. 2015. 'Targeting B cell receptor signaling with ibrutinib in diffuse large B cell lymphoma', *Nature Medicine*, 21: 922-26.

Wong, J. M., P. A. Malec, O. S. Mabrouk, J. Ro, M. Dus, and R. T. Kennedy. 2016. 'Benzoyl chloride derivatization with liquid chromatography-mass spectrometry for targeted metabolomics of neurochemicals in biological samples', *J Chromatogr A*, 1446: 78-90.

Wong, Jason B., Susannah L. Hewitt, Lynn M. Heltemes-Harris, Malay Mandal, Kristen Johnson, Klaus Rajewsky, Sergei B. Koralov, Marcus R. Clark, Michael A. Farrar, and Jane A. Skok. 2019. 'B-1a cells acquire their unique characteristics by bypassing the pre-BCR selection stage', *Nature Communications*, 10.

Woyach, J. A., E. Bojnik, A. S. Ruppert, M. R. Stefanovski, V. M. Goettl, K. A. Smucker, L. L. Smith, J. A. Dubovsky, W. H. Towns, J. MacMurray, B. K. Harrington, M. E. Davis, S. Gobessi, L. Laurenti, B. Y. Chang, J. J. Buggy, D. G. Efremov, J. C. Byrd, and A. J. Johnson. 2014. 'Bruton's tyrosine kinase (BTK) function is important to the development and expansion of chronic lymphocytic leukemia (CLL)', *Blood*, 123: 1207-13.

Wright, G., B. Tan, A. Rosenwald, E. H. Hurt, A. Wiestner, and L. M. Staudt. 2003. 'A gene expression-based method to diagnose clinically distinct subgroups of diffuse large B cell lymphoma', *Proceedings of the National Academy of Sciences*, 100: 9991-96.

Wright, George W., Da Wei Huang, James D. Phelan, Zana A. Coulibaly, Sandrine Roulland, Ryan M. Young, James Q. Wang, Roland Schmitz, Ryan D. Morin, Jeffrey Tang, Aixiang Jiang, Aleksander Bagaev, Olga Plotnikova, Nikita Kotlov, Calvin A. Johnson, Wyndham H. Wilson, David W. Scott, and Louis M. Staudt. 2020. 'A Probabilistic Classification Tool for Genetic Subtypes of Diffuse Large B Cell Lymphoma with Therapeutic Implications', *Cancer Cell*, 37: 551-68.e14.

Wright Muelas, Marina, Farah Mughal, Steve O'Hagan, Philip J. Day, and Douglas B. Kell. 2019. 'The role and robustness of the Gini coefficient as an unbiased tool for the selection of Gini genes for normalising expression profiling data', *Scientific Reports*, 9.

Xiao, Yi, Ding Ma, Yun-Song Yang, Fan Yang, Jia-Han Ding, Yue Gong, Lin Jiang, Li-Ping Ge, Song-Yang Wu, Qiang Yu, Qing Zhang, François Bertucci, Qiuzhuang Sun, Xin Hu, Da-Qiang Li, Zhi-Ming Shao, and Yi-Zhou Jiang. 2022. 'Comprehensive metabolomics expands precision medicine for triple-negative breast cancer', *Cell Research*, 32: 477-90.

Xu-Monette, Z. Y., L. Li, J. C. Byrd, K. J. Jabbar, G. C. Manyam, C. Maria de Winde, M. van den Brand, A. Tzankov, C. Visco, J. Wang, K. Dybkaer, A. Chiu, A. Orazi, Y. Zu, G. Bhagat, K. L. Richards, E. D. Hsi, W. W. Choi, J. Huh, M. Ponzoni, A. J. Ferreri, M. B. Moller, B. M. Parsons, J. N. Winter, M. Wang, F. B. Hagemeister, M. A. Piris, J. Han van Krieken, L. J. Medeiros, Y. Li, A. B. van Spriel, and K. H. Young. 2016. 'Assessment of CD37 B-cell antigen and cell of origin significantly improves risk prediction in diffuse large B-cell lymphoma', *Blood*, 128: 3083-100.

Xu, Y., K. W. Harder, N. D. Huntington, M. L. Hibbs, and D. M. Tarlinton. 2005. 'Lyn tyrosine kinase: accentuating the positive and the negative', *Immunity*, 22: 9-18.

Xue, Chao, Xin Wang, Lingyan Zhang, Qingyuan Qu, Qian Zhang, and Yujie Jiang. 2020. 'Ibrutinib in B-cell lymphoma: single fighter might be enough?', *Cancer Cell International*, 20.

Yanguas-Casás, Natalia, Lucía Pedrosa, Ismael Fernández-Miranda, and Margarita Sánchez-Beato. 2021. 'An Overview on Diffuse Large B-Cell Lymphoma Models: Towards a Functional Genomics Approach', *Cancers*, 13: 2893.

Yap, Timothy A., Naval Daver, Mikhila Mahendra, Jixiang Zhang, Carlos Kamiya-Matsuoka, Funda Meric-Bernstam, Hagop M. Kantarjian, Farhad Ravandi, Meghan E. Collins, Maria Emilia Di Francesco, Ecaterina E. Dumbrava, Siqing Fu, Sisi Gao, Jason P. Gay, Sonal Gera, Jing Han, David S. Hong, Elias J. Jabbour, Zhenlin Ju, Daniel D. Karp, Alessia Lodi, Jennifer R. Molina, Natalia Baran, Aung Naing, Maro Ohanian, Shubham Pant, Naveen Pemmaraju, Prithviraj Bose, Sarina A. Piha-Paul, Jordi Rodon, Carolina Salguero, Koji Sasaki, Anand K. Singh, Vivek Subbiah, Apostolia M. Tsimberidou, Quanyun A. Xu, Musa Yilmaz, Qi Zhang, Yuan Li, Christopher A. Bristow, Meenakshi B. Bhattacharjee, Stefano Tiziani, Timothy P. Heffernan, Christopher P. Vellano, Philip Jones, Cobi J. Heijnen, Annemieke Kavelaars, Joseph R. Marszalek, and Marina Konopleva. 2023. 'Complex I inhibitor of oxidative phosphorylation in advanced solid tumors and acute myeloid leukemia: phase I trials', *Nature Medicine*, 29: 115-26.

Ye, J., N. Ma, T. L. Madden, and J. M. Ostell. 2013. 'IgBLAST: an immunoglobulin variable domain sequence analysis tool', *Nucleic Acids Res*, 41: W34-40.

Ye, Xiaofei, Lei Wang, Man Nie, Yuyao Wang, Shichen Dong, Weicheng Ren, Guibo Li, Zhi-Ming Li, Kui Wu, and Qiang Pan-Hammarström. 2022. 'A single-cell atlas of diffuse large B cell lymphoma', *Cell Reports*, 39: 110713.

Youle, Richard J., and Andreas Strasser. 2008. 'The BCL-2 protein family: opposing activities that mediate cell death', *Nature Reviews Molecular Cell Biology*, 9: 47-59.

Younes, Anas, Laurie H. Sehn, Peter Johnson, Pier Luigi Zinzani, Xiaonan Hong, Jun Zhu, Caterina Patti, David Belada, Olga Samoilova, Cheolwon Suh, Sirpa Leppä, Shinya Rai, Mehmet Turgut, Wojciech Jurczak, Matthew C. Cheung, Ronit Gurion, Su-Peng Yeh, Andres Lopez-Hernandez, Ulrich Dührsen, Catherine Thieblemont, Carlos Sergio Chiattone, Sriram Balasubramanian, Jodi Carey, Grace Liu, S. Martin Shreeve, Steven Sun, Sen Hong Zhuang, Jessica Vermeulen, Louis M. Staudt, and Wyndham Wilson. 2019. 'Randomized Phase III Trial of Ibrutinib and Rituximab Plus Cyclophosphamide, Doxorubicin, Vincristine, and Prednisone in Non–Germinal Center B-Cell Diffuse Large B-Cell Lymphoma', *Journal of Clinical Oncology*, 37: 1285-95.

Young, C., and R. Brink. 2021. 'The unique biology of germinal center B cells', *Immunity*, 54: 1652-64.

Young, Ryan M., James D. Phelan, Wyndham H. Wilson, and Louis M. Staudt. 2019. 'Pathogenic B-cell receptor signaling in lymphoid malignancies: New insights to improve treatment', *Immunological Reviews*, 291: 190-213.

Young, Ryan M., Tianyi Wu, Roland Schmitz, Moez Dawood, Wenming Xiao, James D. Phelan, Weihong Xu, Laurence Menard, Eric Meffre, Wing-Chung C. Chan, Elaine S. Jaffe, Randy D. Gascoyne, Elías Campo, Andreas Rosenwald, German Ott, Jan Delabie, Lisa M. Rimsza, and Louis M. Staudt. 2015. 'Survival of human lymphoma cells requires B-cell receptor engagement by self-antigens', *Proceedings of the National Academy of Sciences*, 112: 13447-54.

Zhang, Huihui, Fang He, Pan Li, Philip R. Hardwidge, Nengzhang Li, and Yuanyi Peng. 2021. 'The Role of Innate Immunity in Pulmonary Infections', *BioMed Research International*, 2021: 1-14.

Zhang, J., D. Dominguez-Sola, S. Hussein, J. E. Lee, A. B. Holmes, M. Bansal, S. Vlasevska, T. Mo, H. Tang, K. Basso, K. Ge, R. Dalla-Favera, and L. Pasqualucci. 2015. 'Disruption of KMT2D perturbs germinal center B cell development and promotes lymphomagenesis', *Nat Med*, 21: 1190-8.

Zhang, J., S. Vlasevska, V. A. Wells, S. Nataraj, A. B. Holmes, R. Duval, S. N. Meyer, T. Mo, K. Basso, P. K. Brindle, S. Hussein, R. Dalla-Favera, and L. Pasqualucci. 2017. 'The CREBBP Acetyltransferase Is a Haploinsufficient Tumor Suppressor in B-cell Lymphoma', *Cancer Discov*, 7: 322-37.

Zhang, Liang, Yixin Yao, Shaojun Zhang, Yang Liu, Hui Guo, Makhdum Ahmed, Taylor Bell, Hui Zhang, Guangchun Han, Elizabeth Lorence, Maria Badillo, Shouhao Zhou, Yuting Sun, M. Emilia Di Francesco, Ningping Feng, Randy Haun, Renny Lan, Samuel G. Mackintosh, Xizeng Mao, Xingzhi Song, Jianhua Zhang, Lan V. Pham, Philip L. Lorenzi, Joseph Marszalek, Tim Heffernan, Giulio Draetta, Philip Jones, Andrew Futreal, Krystle Nomie, Linghua Wang, and Michael Wang. 2019. 'Metabolic reprogramming toward oxidative phosphorylation identifies a therapeutic target for mantle cell lymphoma', *Science Translational Medicine*, 11: eaau1167.

Zhang, M. C., S. Tian, D. Fu, L. Wang, S. Cheng, H. M. Yi, X. F. Jiang, Q. Song, Y. Zhao, Y. He, J. F. Li, R. J. Mu, H. Fang, H. Yu, H. Xiong, B. Li, S. J. Chen, P. P. Xu, and W. L. Zhao. 2023. 'Genetic subtype-guided immunochemotherapy in diffuse large B cell lymphoma: The randomized GUIDANCE-01 trial', *Cancer Cell*, 41: 1705-16 e5.

Zhang, N., J. N. Fu, and T. C. Chou. 2016. 'Synergistic combination of microtubule targeting anticancer fludelone with cytoprotective panaxytriol derived from panax ginseng against MX-1 cells in vitro: experimental design and data analysis using the combination index method', *Am J Cancer Res*, 6: 97-104.

Zhang, Xiao-Tuan, Xiao-Bei Hu, Han-Lin Wang, Wei-Juan Kan, Lei Xu, Zhi-Jia Wang, Yu-Qi Xiang, Wen-Biao Wu, Bo Feng, Jia-Nan Li, An-Hui Gao, Tian-Cheng Dong, Chun-Mei Xia, Yu-Bo Zhou, and Jia Li. 2020. 'Activation of unfolded protein response overcomes Ibrutinib resistance in diffuse large B-cell lymphoma', *Acta Pharmacologica Sinica*.

Zhou, Zhiyuan, Lei Zhang, Xinhua Wang, Xin Li, Ling Li, Xiaorui Fu, Xudong Zhang, Zhaoming Li, Zhenchang Sun, and Mingzhi Zhang. 2021. 'Ibrutinib combined with venetoclax for the treatment of relapsed/refractory diffuse large B cell lymphoma', *Annals of Hematology*, 100: 1509-16.

Zitvogel, Laurence, Jonathan M. Pitt, Romain Daillère, Mark J. Smyth, and Guido Kroemer. 2016. 'Mouse models in oncoimmunology', *Nature Reviews Cancer*, 16: 759-73.

11 Appendix

11.1 Supplementary Figures

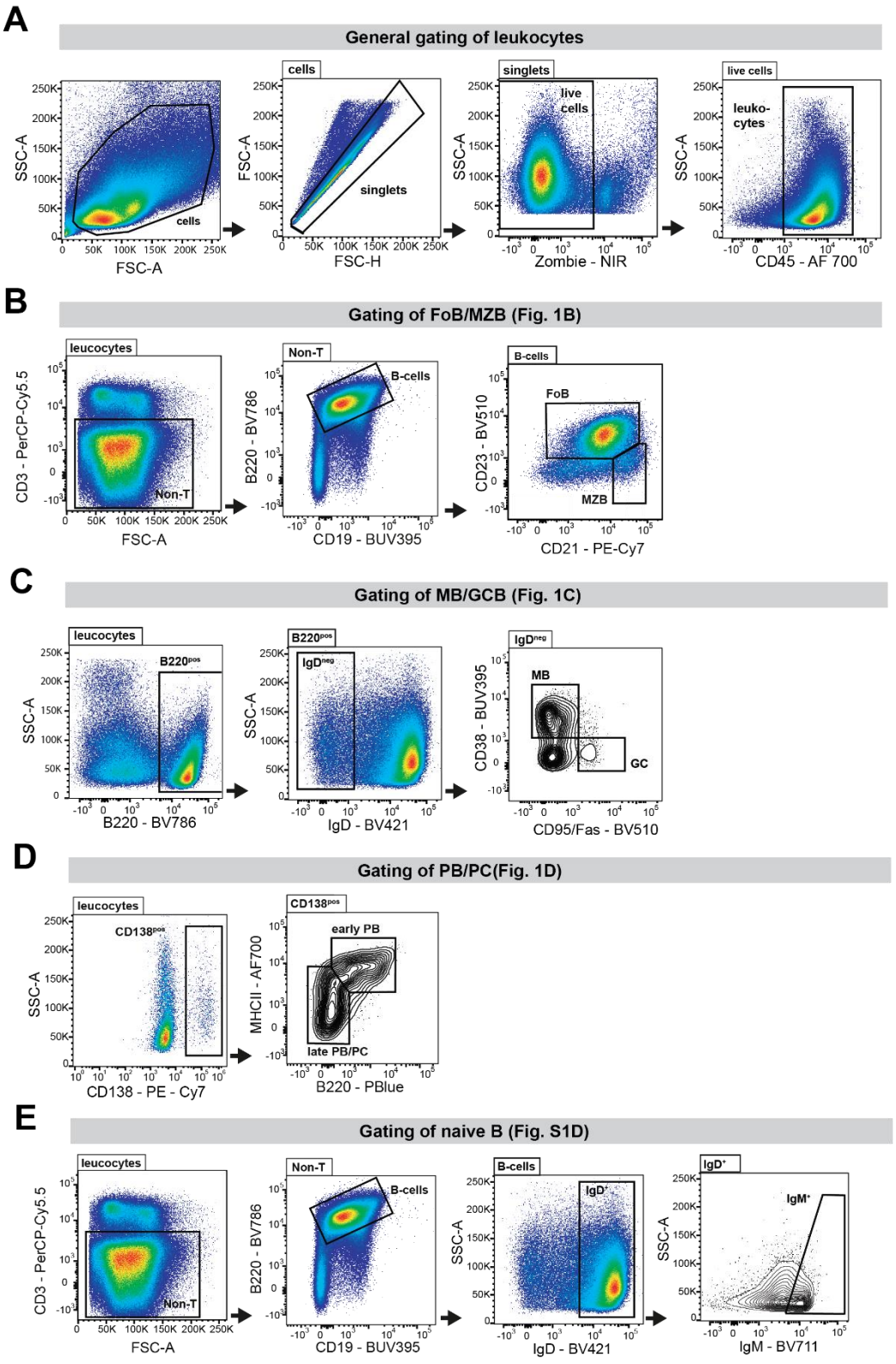

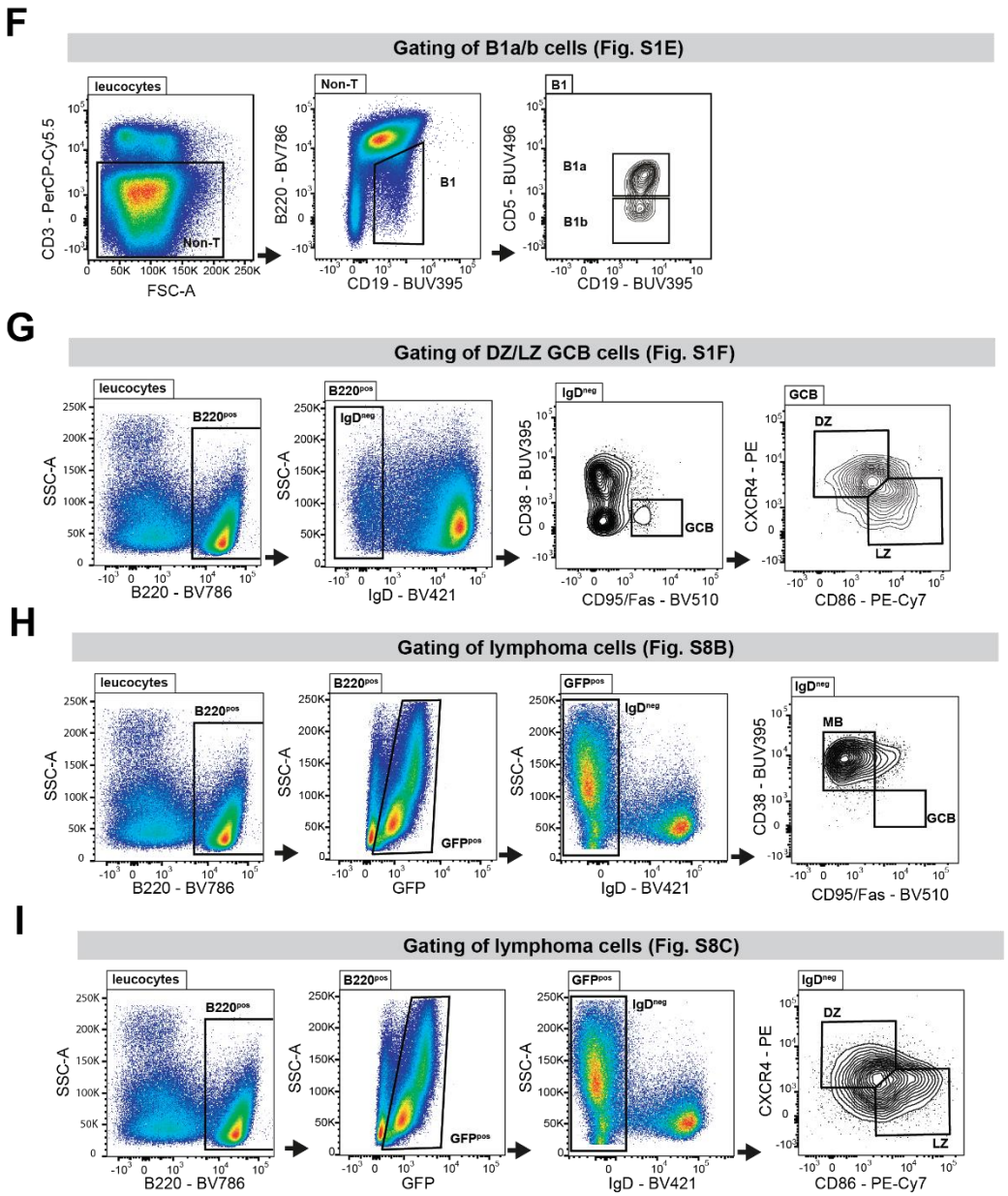

Figure SR1 Gating strategies for flow cytometry analyses of lymphocytes. The following subsets were analyzed: (A) leukocytes, (B) Follicular B (FoB) and Marginal zone B cells (MZB), (C) Memory B (MB) and GC B cells (GCB), (D) plasmablasts (PB) and plasma cells (PC), (E) naïve B cells, (F) B1a and B1b cells, (G) DZ and LZ GCBs, (H) MB and GCBs from GFP⁺ lymphoma cells analogously to (C), (I) DZ and LZ GCBs from GFP⁺ lymphoma cells analogously to (G). For details see section 4.6.

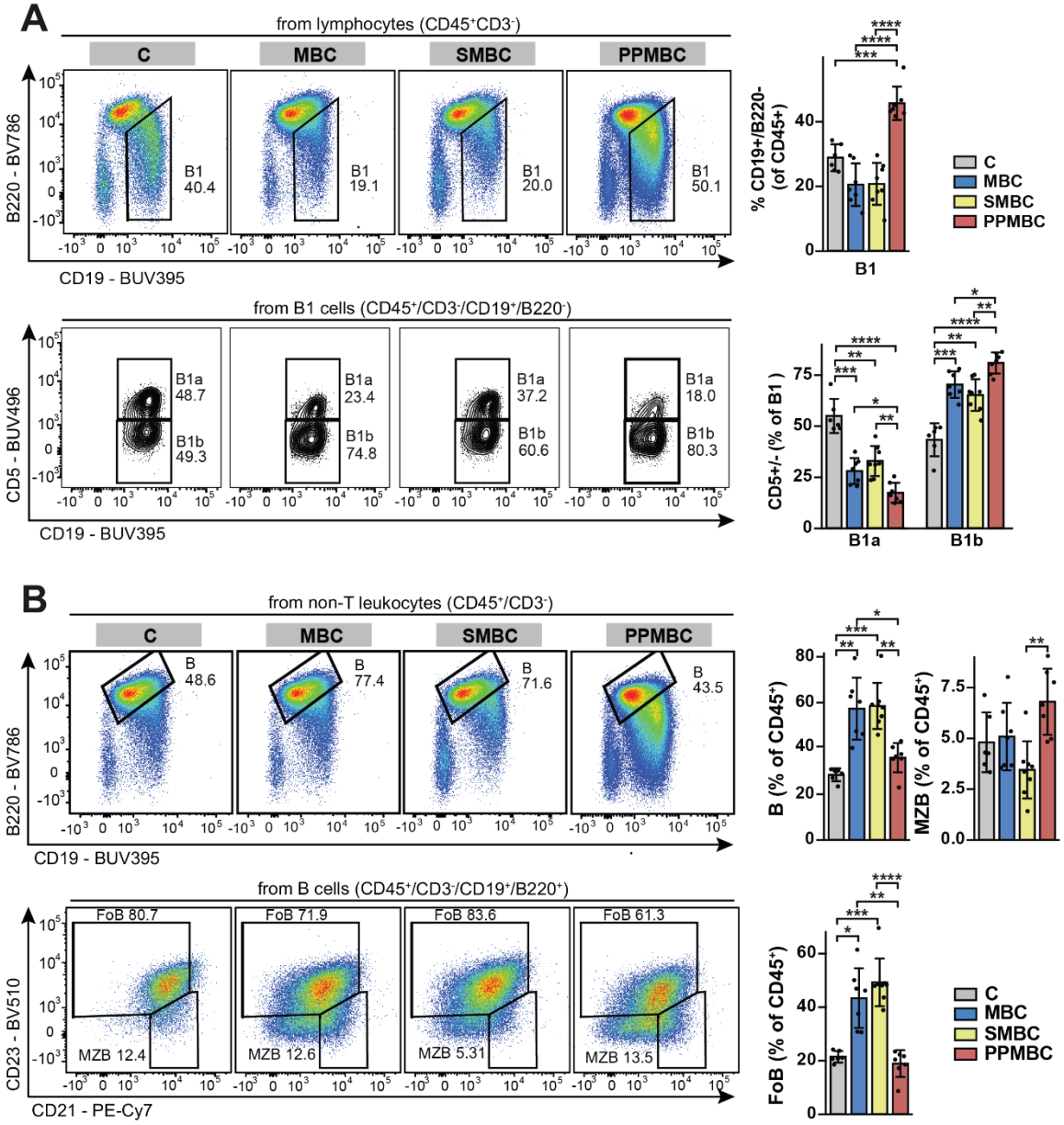

*Figure SR2 Flow cytometry analysis of premalignant PPMBC and SMBC mice show altered B-cell subsets in the peritoneal cavity. (A) CD19+B220- B1 cells, including B1a and B1b subsets. (B) CD19+B220+ B cells including follicular B (FoB) and marginal zone B cells (MZB). (C) CD138+ Plasmablasts (PB) and plasma cells (PC). *p≤0.05, **p≤0.01, ***p≤0.001, ****p≤0.0001. Welch unpaired two-tailed t test, error bars SD.*

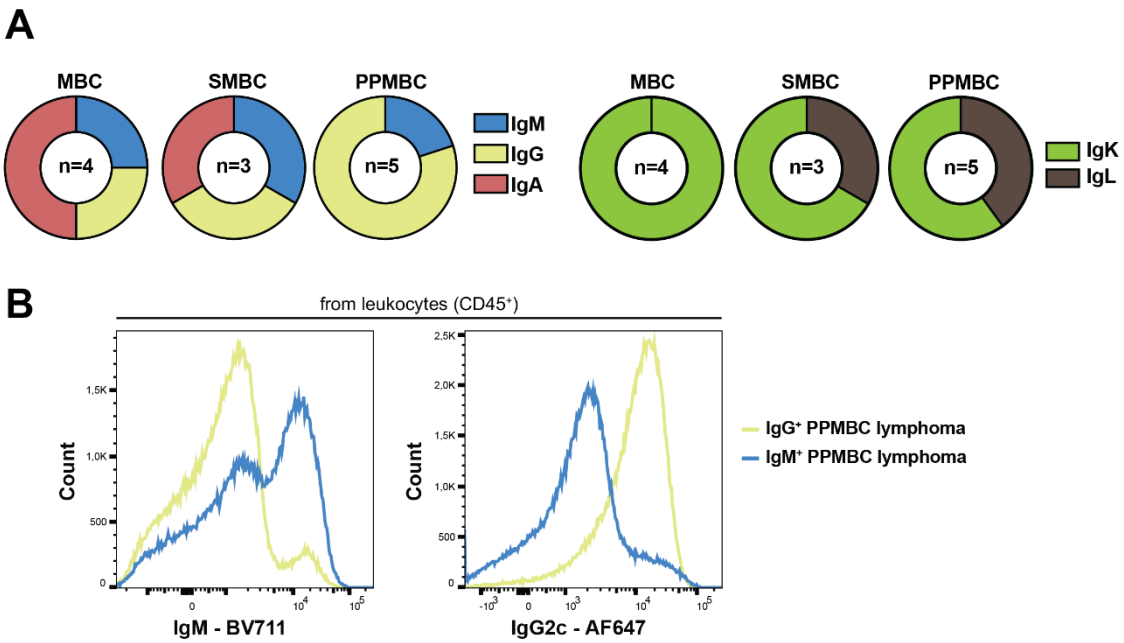

Figure SR3 Immunoglobulin usage in MBC, SMBC and PPMBC tumors. (A) Quantification of isotype of the dominant tumor clone in MBC, SMBC and PPMBC tumors. (B) Representative flow cytometry analysis of surface expression of IgM and IgG2c in an IgG+ and IgM+ PPMBC lymphoma sample.

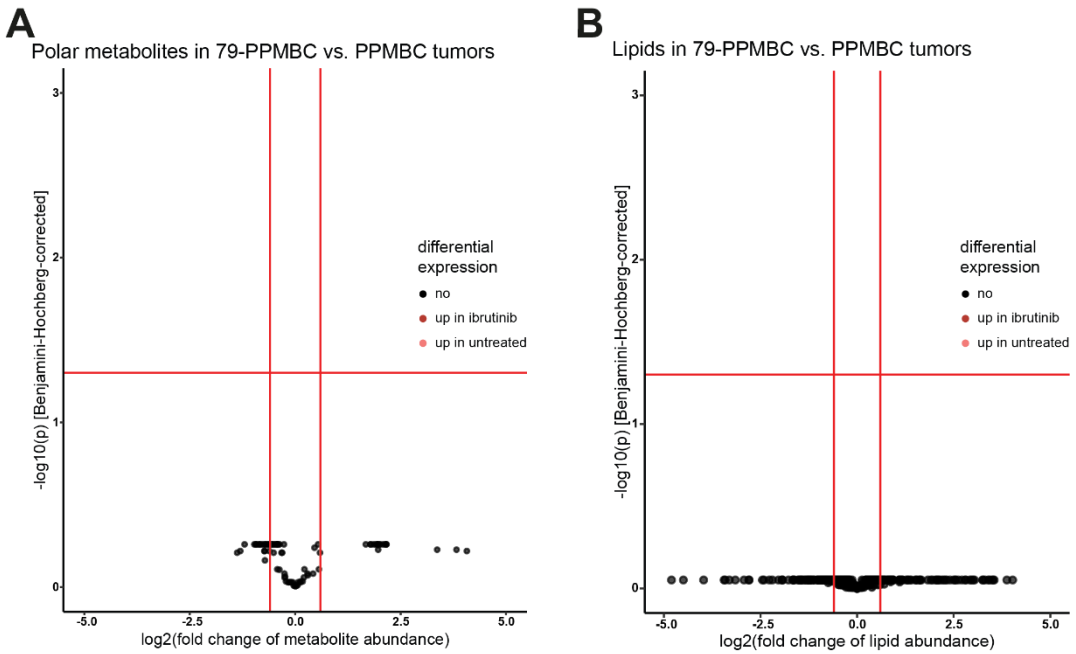

Figure SR4 Comparison of polar metabolites (A) and lipids (B) between 79-PPMBC (n = 6) and PPMBC (n = 6) tumor tissue. Unpaired two-samples t-test, Benjamini-Hochberg-corrected for multi hypothesis testing. Note that due to the high variance between samples and high number of tests, Benjamini Hochberg correction leads to p value saturation.

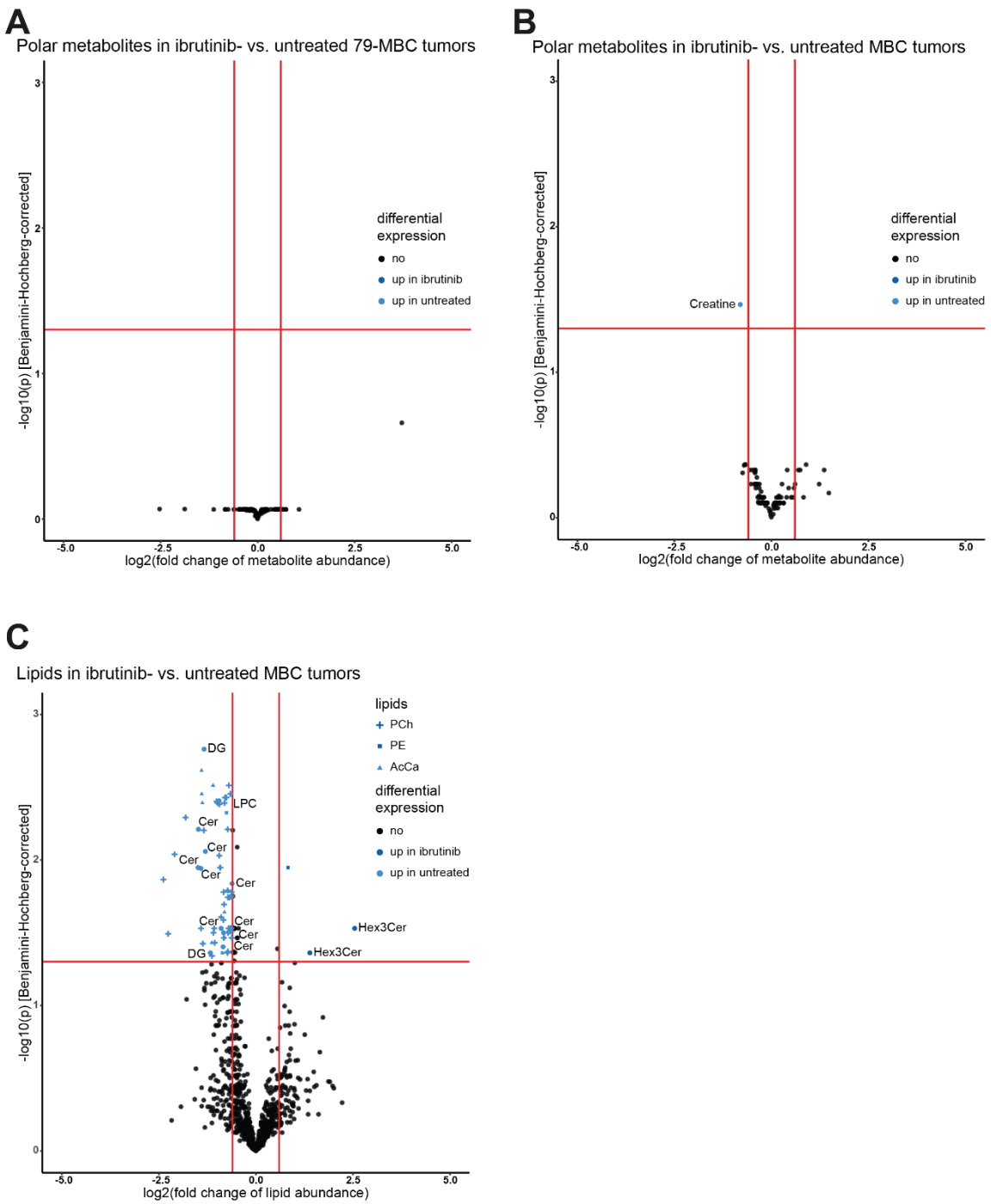

Figure SR5 (A) Comparison of polar metabolites between ibrutinib-treated (n = 5) and untreated 79-MBC (n = 3) tumor samples (B) Comparison of polar metabolites between ibrutinib-treated (n = 6) and untreated MBC (n = 6) tumor samples. (C) Comparison of lipids between ibrutinib-treated (n = 6) and untreated MBC (n = 6) tumor samples. Unpaired two-samples t-test, Benjamini-Hochberg-corrected for multi hypothesis testing.

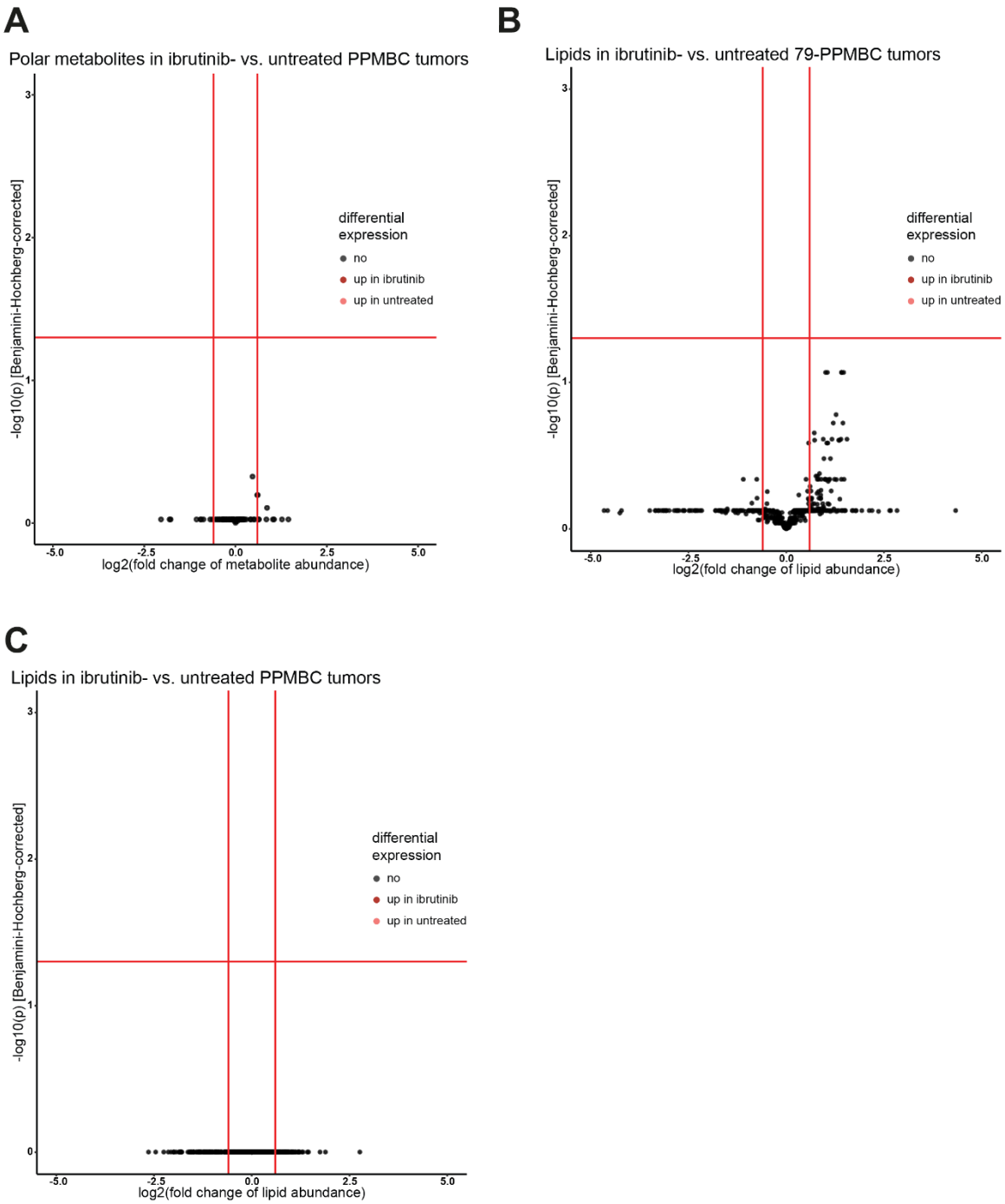

Figure SR6 Comparison of polar metabolites (A) and lipids (B, C) between ibrutinib-treated and untreated PPMBC (A,C) and 79-PPMBC (B) tumor tissue (n = 6 for each condition). Unpaired two-samples t-test, Benjamini-Hochberg-corrected for multi hypothesis testing. Note that due to the high variance between samples and high number of tests, Benjamini Hochberg correction leads to p value saturation.

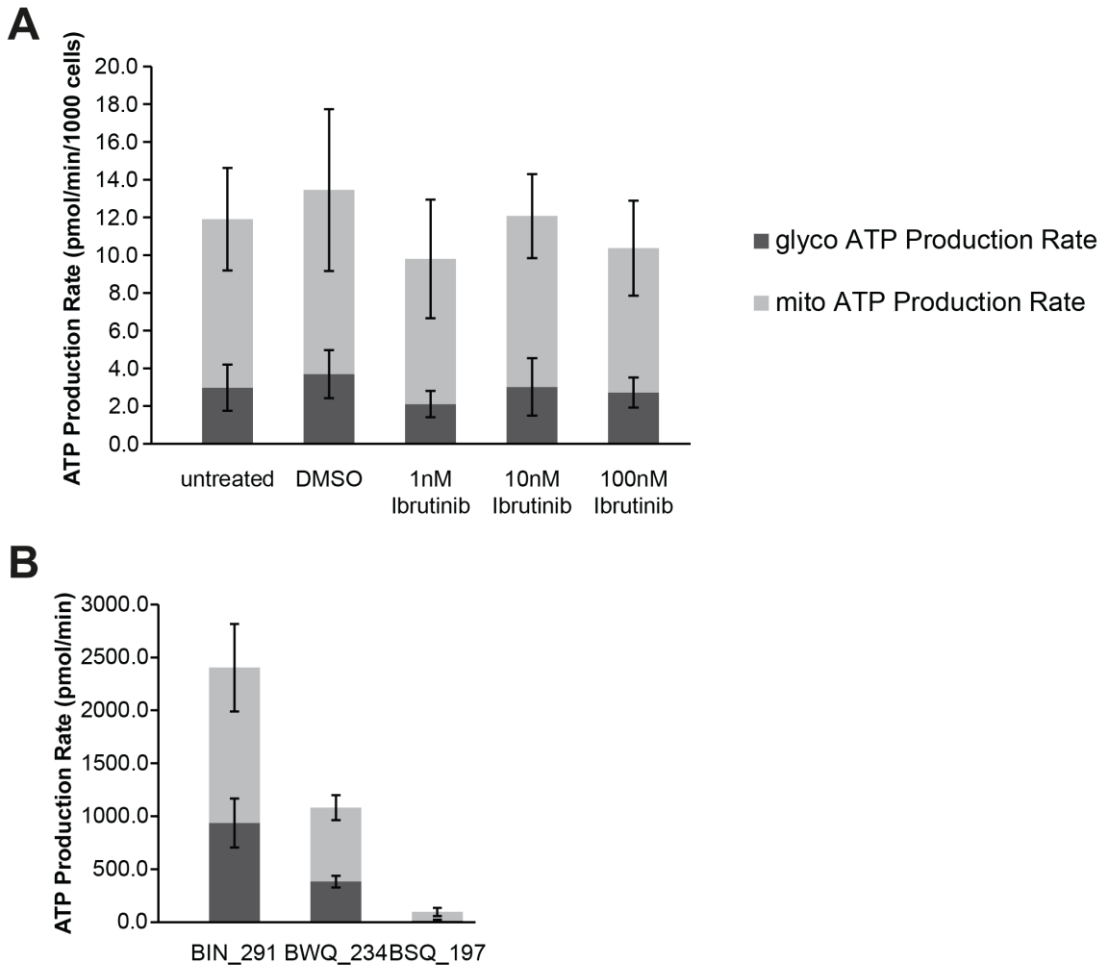

Figure SR7 SeaHorse Analysis of DMSO- and ibrutinib-treated murine cell lines does not reveal significant differences. (A) 79-MBC cell line BSQ_12 was treated for 1 day with DMSO or ibrutinib [repetition of R33A]. (B) MBC cell line BIN_291 and PPMBC cell line BWQ_234 were compared with primary 79-MBC tumor cells, BSQ_197. Note that data is not normalized to protein amount for better visibility.

11.2 Supplementary Tables

Supplementary Table 1 Differentially abundant lipids comparing untreated 79-MBC vs. MBC tumor samples. Column "Lipid" annotates the lipid in detail, combining the lipid class (e.g. "Cer"), the adduct used in MS (e.g. "H", "CH3COO"), the number of C atoms per bound fatty acid separated by a colon from the number of double bonds in that fatty acid (e.g. "d18:2" constitutes a fatty acid with 18 C atoms and 2 double bonds; d stands for delta or double bond). The weight and sum formula of the lipid are annotated at the end as well. "nlog10p" is the negative base 10 logarithm of the p value, "log2fc" the base 2 logarithm of the fold change, "diffexpressed" annotates differential expression: UP meaning upregulated in 79-MBC samples, DOWN meaning downregulated in 79-MBC samples.

Lipid	Class	nlog10p	log2fc	diffexpressed
AcCa(18:1)_H_AcCa_(18:1)_NA_NA_426.35778547_C25 H48 O4 N1	AcCa(18:1)	1.984596	-0.78044	DOWN
AcCa(18:2)_H_AcCa_(18:2)_NA_NA_424.34213547_C25 H46 O4 N1	AcCa(18:2)	1.398325	-1.01924	DOWN
AcCa(20:1)_H_AcCa_(20:1)_NA_NA_454.38908547_C27 H52 O4 N1	AcCa(20:1)	1.419312	-0.81347	DOWN
AcCa(20:2)_H_AcCa_(20:2)_NA_NA_452.37343547_C27 H50 O4 N1	AcCa(20:2)	1.593266	-1.04053	DOWN
LPC(20:2)_CH3COO_LPC_(20:2)_(20:2)_NA_606.377645529999_C30 H57 O9 N1 P1	LPC(20:2)	1.358451	-0.75254	DOWN
LPC(20:2)_H_LPC_(20:2)_NA_NA_548.37106847_C28 H55 O7 N1 P1	LPC(20:2)	1.419312	-0.79437	DOWN
PC(16:1_22:6)_CH3COO_PC_(16:1_22:6)_(16:1)_(22:6)_862.560360529999_C48 H81 O10 N1 P1	PC(16:1	1.477083	-0.77496	DOWN
PC(17:1_18:2)_CH3COO_PC_(17:1_18:2)_(17:1)_(18:2)_828.57601053_C45 H83 O10 N1 P1	PC(17:1	2.067048	-1.21239	DOWN
PC(18:2_18:2)_CH3COO_PC_(18:2_18:2)_(18:2)_(18:2)_840.57601053_C46 H83 O10 N1 P1	PC(18:2	1.984596	-1.01827	DOWN

PC(19:1_18:2)_CH3COO_PC_(19:1_18:2)_(19:1)_(18:2)_856.60731053_C47 H87 O10 N1 P1	PC(19:1	1.477083	-0.74593	DOWN
PC(33:0e)_H_PC_(33:0e)_NA_NA_734.60581847_C41 H85 O7 N1 P1	PC(33:0e)	1.385144	-1.02273	DOWN
PC(36:4)_H_PC_(18:2)_(18:2)_NA_782.56943347_C44 H81 O8 N1 P1	PC(36:4)	1.984596	-1.07844	DOWN
PC(36:4)_Na_PC_(18:2)_(18:2)_NA_804.55137847_C44 H80 O8 N1 P1 Na1	PC(36:4)	1.984596	-0.84653	DOWN
PC(36:5)_H_PC_(36:5)_NA_NA_780.55378347_C44 H79 O8 N1 P1	PC(36:5)	2.067048	-1.17601	DOWN
TG(52:5)_Na_TG_(16:1)_(18:2)_(18:2)_875.70991147_C55 H96 O6 Na1	TG(52:5)	1.593266	-2.15154	DOWN
TG(57:2)_NH4_TG_(16:0)_(18:1)_(23:1)_946.87971547_C60 H116 O6 N1	TG(57:2)	1.556364	-1.77159	DOWN
PC(22:2_20:4)_CH3COO_PC_(22:2_20:4)_(22:2)_(20:4)_920.638610529999_C52 H91 O10 N1 P1	PC(22:2	1.358451	0.614593	UP
PC(40:8e)_H_PC_(40:8e)_NA_NA_816.59016847_C48 H83 O7 N1 P1	PC(40:8e)	1.419312	1.195254	UP
PE(18:1_22:4)_H_PE_(18:1_22:4)_(18:1)_(22:4)_792.554880529999_C45 H79 O8 N1 P1	PE(18:1	1.356742	0.981179	UP
PE(20:2_20:4)_H_PE_(20:2_20:4)_(20:2)_(20:4)_790.539230529999_C45 H77 O8 N1 P1	PE(20:2	4.725929	0.843893	UP
PE(40:2)_Na_PE_(18:1)_(22:1)_NA_822.59832847_C45 H86 O8 N1 P1 Na1	PE(40:2)	1.984596	1.437509	UP
PE(40:5e)_H_PE_(18:0e)_(22:5)_NA_780.59016847_C45 H83 O7 N1 P1	PE(40:5e)	1.984596	0.707344	UP

PE(40:5e)_Na_PE_(18:0e)_(22:5)_NA_802.57211347_C45 H82 O7 N1 P1 Na1	PE(40:5e)	1.593266	0.767879	UP
PE(40:6e)_H_PE_(18:2e)_(22:4)_NA_778.57451847_C45 H81 O7 N1 P1	PE(40:6e)	1.685722	1.390949	UP

Supplementary Table 2 Differentially abundant lipids comparing treated vs. untreated MBC tumor samples. Column "Lipid" annotates the lipid in detail, combining the lipid class (e.g. "Cer"), the adduct used in MS (e.g. "H", "CH3COO"), the number of C atoms per bound fatty acid separated by a colon from the number of double bonds in that fatty acid (e.g. "d18:2" constitutes a fatty acid with 18 C atoms and 2 double bonds; d stands for delta or double bond). The weight and sum formula of the lipid are annotated at the end as well. "nlog10p" is the negative base 10 logarithm of the p value, "log2fc" the base 2 logarithm of the fold change, "diffexpressed" annotates differential expression: UP meaning upregulated in ibrutinib-treated samples, DOWN meaning downregulated in ibrutinib-treated samples.

Lipid	**Class**	**nlog10p**	**log2fc**	**diffexpressed**
AcCa(16:0)_H_AcCa_(16:0)_NA_NA_400.34213547_C23 H46 O4 N1	AcCa(16:0)	1.64	-0.81	DOWN
AcCa(16:1)_H_AcCa_(16:1)_NA_NA_398.32648547_C23 H44 O4 N1	AcCa(16:1)	2.51	-1.10	DOWN
AcCa(18:1)_H_AcCa_(18:1)_NA_NA_426.35778547_C25 H48 O4 N1	AcCa(18:1)	3.82	-1.32	DOWN
AcCa(18:2)_H_AcCa_(18:2)_NA_NA_424.34213547_C25 H46 O4 N1	AcCa(18:2)	2.39	-1.38	DOWN
AcCa(20:1)_H_AcCa_(20:1)_NA_NA_454.38908547_C27 H52 O4 N1	AcCa(20:1)	2.61	-1.40	DOWN
AcCa(20:2)_H_AcCa_(20:2)_NA_NA_452.37343547_C27 H50 O4 N1	AcCa(20:2)	2.45	-1.40	DOWN
AcCa(20:4)_H_AcCa_(20:4)_NA_NA_448.34213547_C27 H46 O4 N1	AcCa(20:4)	1.43	-1.14	DOWN
Cer(d18:1_24:1)_CH3COO_Cer_(d18:1_24:1)_(d18:1)_(24:1)_706.63549753_C44 H84 O5 N1	Cer(d18:1	1.84	-0.61	DOWN
Cer(d18:1_24:1)_H_Cer_(d18:1_24:1)_(d18:1)_(24:1)_646.614367529999_C42 H80 O3 N1	Cer(d18:1	1.54	-0.60	DOWN
Cer(d18:2_24:1)_CH3COO_Cer_(d18:2_24:1)_(d18:2)_(24:1)_704.619847529999_C44 H82 O5 N1	Cer(d18:2	1.53	-0.90	DOWN
Cer(d41:2)_CH3COO_Cer_(d41:2)_(d41:2)_NA_692.619847529999_C43 H82 O5 N1	Cer(d41:2)	1.94	-1.42	DOWN
Cer(d41:2)_H_Cer_(d18:2)_(23:0)_NA_634.61327047_C41 H80 O3 N1	Cer(d41:2)	2.21	-1.48	DOWN
Cer(d42:3)_H-H2O_Cer_(d18:2)_(24:1)_NA_628.60270547_C42 H78 O2 N1	Cer(d42:3)	1.50	-0.83	DOWN
Cer(d42:3)_H_Cer_(d18:2)_(24:1)_NA_646.61327047_C42 H80 O3 N1	Cer(d42:3)	1.40	-0.85	DOWN
Cer(t41:1)_H-2H2O_Cer_(t41:1)_NA_NA_616.602705469999_C41 H78 O2 N1	Cer(t41:1)	1.95	-1.49	DOWN

Cer(t42:1)_H-2H2O_Cer_(t42:1)_NA_NA_630.61835547_C42 H80 O2 N1	Cer(t42:1)	2.06	-1.30	DOWN
DG(36:3)_NH4_DG_(18:1)_(18:2)_NA_636.55615047_C39 H74 O5 N1	DG(36:3)	1.36	-1.17	DOWN
DG(38:5)_NH4_DG_(18:1)_(20:4)_NA_660.55615047_C41 H74 O5 N1	DG(38:5)	2.76	-1.33	DOWN
LPC(34:0)_Na_LPC_(34:0)_NA_NA_770.60341347_C42 H86 O7 N1 P1 Na1	LPC(34:0)	2.41	-0.95	DOWN
PC(16:0_22:4)_CH3COO_PC_(16:0_22:4)_(16:0)_(22:4)_868.60731053_C48 H87 O10 N1 P1	PC(16:0	1.46	-0.83	DOWN
PC(16:1e_18:1)_CH3COO_PC_(16:1e_18:1)_(16:1e)_(18:1)_802.59674553_C44 H85 O9 N1 P1	PC(16:1e	1.53	-1.08	DOWN
PC(16:1e_18:2)_CH3COO_PC_(16:1e_18:2)_(16:1e)_(18:2)_800.58109553_C44 H83 O9 N1 P1	PC(16:1e	1.95	-0.92	DOWN
PC(16:1e_20:4)_CH3COO_PC_(16:1e_20:4)_(16:1e)_(20:4)_824.58109553_C46 H83 O9 N1 P1	PC(16:1e	2.39	-0.81	DOWN
PC(17:0_20:4)_CH3COO_PC_(17:0_20:4)_(17:0)_(20:4)_854.59166053_C47 H85 O10 N1 P1	PC(17:0	1.51	-0.63	DOWN
PC(17:1_18:2)_CH3COO_PC_(17:1_18:2)_(17:1)_(18:2)_828.57601053_C45 H83 O10 N1 P1	PC(17:1	1.53	-0.71	DOWN
PC(18:0_20:2)_CH3COO_PC_(18:0_20:2)_(18:0)_(20:2)_872.638610529999_C48 H91 O10 N1 P1	PC(18:0	1.53	-0.63	DOWN
PC(18:0_22:5)_CH3COO_PC_(18:0_22:5)_(18:0)_(22:5)_894.622960529999_C50 H89 O10 N1 P1	PC(18:0	1.75	-0.63	DOWN
PC(18:0e_16:0)_CH3COO_PC_(18:0e_16:0)_(18:0e)_(16:0)_806.62804553_C44 H89 O9 N1 P1	PC(18:0e	2.38	-0.94	DOWN
PC(18:1_18:2)_CH3COO_PC_(18:1_18:2)_(18:1)_(18:2)_842.59166053_C46 H85 O10 N1 P1	PC(18:1	2.45	-0.66	DOWN
PC(18:1_24:1)_CH3COO_PC_(18:1_24:1)_(18:1)_(24:1)_928.701210529999_C52 H99 O10 N1 P1	PC(18:1	1.53	-1.41	DOWN
PC(19:1_18:1)_CH3COO_PC_(19:1_18:1)_(19:1)_(18:1)_858.622960529999_C47 H89 O10 N1 P1	PC(19:1	1.59	-0.84	DOWN
PC(19:1_18:2)_CH3COO_PC_(19:1_18:2)_(19:1)_(18:2)_856.60731053_C47 H87 O10 N1 P1	PC(19:1	2.39	-0.98	DOWN
PC(19:1_20:4)_CH3COO_PC_(19:1_20:4)_(19:1)_(20:4)_880.60731053_C49 H87 O10 N1 P1	PC(19:1	2.21	-0.72	DOWN
PC(33:0e)_H_PC_(33:0e)_NA_NA_734.60581847_C41 H85 O7 N1 P1	PC(33:0e)	1.61	-0.90	DOWN

PC(34:0)_H_PC_(18:0)_(16:0)_NA_762.60073347_C42 H85 O8 N1 P1	PC(34:0)	2.43	-0.80	DOWN
PC(34:0e)_H_PC_(34:0e)_NA_NA_748.62146847_C42 H87 O7 N1 P1	PC(34:0e)	2.40	-1.01	DOWN
PC(34:1)_H_PC_(16:0)_(18:1)_NA_760.58508347_C42 H83 O8 N1 P1	PC(34:1)	1.43	-1.06	DOWN
PC(34:1e)_H_PC_(18:1e)_(16:0)_NA_746.60581847_C42 H85 O7 N1 P1	PC(34:1e)	1.74	-0.67	DOWN
PC(34:1e)_H_PC_(34:1e)_NA_NA_746.60581847_C42 H85 O7 N1 P1	PC(34:1e)	2.43	-0.76	DOWN
PC(34:1e)_Na_PC_(18:1e)_(16:0)_NA_768.58776347_C42 H84 O7 N1 P1 Na1	PC(34:1e)	1.78	-0.62	DOWN
PC(34:2e)_H_PC_(16:1e)_(18:1)_NA_744.59016847_C42 H83 O7 N1 P1	PC(34:2e)	1.34	-1.13	DOWN
PC(34:2e)_Na_PC_(16:0e)_(18:2)_NA_766.57211347_C42 H82 O7 N1 P1 Na1	PC(34:2e)	2.03	-0.94	DOWN
PC(34:2e)_Na_PC_(16:1e)_(18:1)_NA_766.57211347_C42 H82 O7 N1 P1 Na1	PC(34:2e)	1.50	-1.09	DOWN
PC(34:3e)_H_PC_(16:1e)_(18:2)_NA_742.57451847_C42 H81 O7 N1 P1	PC(34:3e)	2.20	-1.34	DOWN
PC(35:0)_H_PC_(35:0)_NA_NA_776.61638347_C43 H87 O8 N1 P1	PC(35:0)	2.51	-0.69	DOWN
PC(35:2)_H_PC_(15:0)_(20:2)_NA_772.58508347_C43 H83 O8 N1 P1	PC(35:2)	1.46	-0.62	DOWN
PC(35:2e)_H_PC_(35:2e)_NA_NA_758.60581847_C43 H85 O7 N1 P1	PC(35:2e)	1.49	-2.26	DOWN
PC(36:3)_H_PC_(18:1)_(18:2)_NA_784.58508347_C44 H83 O8 N1 P1	PC(36:3)	1.79	-0.73	DOWN
PC(36:3e)_H_PC_(18:3e)_(18:0)_NA_770.60581847_C44 H85 O7 N1 P1	PC(36:3e)	1.87	-2.38	DOWN
PC(36:4)_Na_PC_(18:2)_(18:2)_NA_804.55137847_C44 H80 O8 N1 P1 Na1	PC(36:4)	1.74	-0.72	DOWN
PC(36:5e)_H_PC_(16:1e)_(20:4)_NA_766.57451847_C44 H81 O7 N1 P1	PC(36:5e)	1.95	-0.91	DOWN
PC(36:5e)_Na_PC_(16:1e)_(20:4)_NA_788.55646347_C44 H80 O7 N1 P1 Na1	PC(36:5e)	1.78	-0.83	DOWN
PC(37:1)_H_PC_(37:1)_NA_NA_802.63203347_C45 H89 O8 N1 P1	PC(37:1)	1.53	-0.66	DOWN

PC(37:2)_H_PC_(19:1)_(18:1)_NA_800.61638347_C45 H87 O8 N1 P1	PC(37:2)	1.43	-1.37	DOWN
PC(37:3)_H_PC_(37:3)_NA_NA_798.60073347_C45 H85 O8 N1 P1	PC(37:3)	1.69	-0.82	DOWN
PC(38:2)_Na_PC_(16:0)_(22:2)_NA_836.61397847_C46 H88 O8 N1 P1 Na1	PC(38:2)	1.37	-0.72	DOWN
PC(38:4e)_H_PC_(20:4e)_(18:0)_NA_796.62146847_C46 H87 O7 N1 P1	PC(38:4e)	1.51	-0.68	DOWN
PC(38:5)_H_PC_(16:0)_(22:5)_NA_808.58508347_C46 H83 O8 N1 P1	PC(38:5)	2.04	-2.09	DOWN
PC(38:5)_Na_PC_(16:0)_(22:5)_NA_830.56702847_C46 H82 O8 N1 P1 Na1	PC(38:5)	2.29	-1.81	DOWN
PC(44:4)_H_PC_(44:4)_NA_NA_894.69463347_C52 H97 O8 N1 P1	PC(44:4)	1.36	-0.73	DOWN
PC(44:5)_Na_PC_(44:5)_NA_NA_914.66092847_C52 H94 O8 N1 P1 Na1	PC(44:5)	1.50	-0.72	DOWN
PE(18:0e_22:4)_H_PE_(18:0e_22:4)_(18:0e)_(22:4)_780.59126553_C45 H83 O7 N1 P1	PE(18:0e	1.36	-0.86	DOWN
PE(38:3)_H_PE_(18:1)_(20:2)_NA_770.56943347_C43 H81 O8 N1 P1	PE(38:3)	1.46	-0.82	DOWN
PE(40:4e)_H_PE_(40:4e)_NA_NA_782.60581847_C45 H85 O7 N1 P1	PE(40:4e)	1.53	-0.88	DOWN
PE(40:6e)_Na_PE_(40:6e)_NA_NA_800.55646347_C45 H80 O7 N1 P1 Na1	PE(40:6e)	2.32	-0.76	DOWN
Hex3Cer(d34:1)_H_Hex3Cer_(d18:1)_(16:0)_NA_1024.67784547_C52 H98 O18 N1	Hex3Cer(d34:1)	1.53	2.55	UP
Hex3Cer(d42:2)_H_Hex3Cer_(d18:1)_(24:1)_NA_1134.78739546999_C60 H112 O18 N1	Hex3Cer(d42:2)	1.36	1.39	UP
PE(34:4p)_H_PE_(14:0p)_(20:4)_NA_696.49626847_C39 H71 O7 N1 P1	PE(34:4p)	1.95	0.83	UP

Supplementary Table 3 Differentially abundant lipids comparing treated vs. untreated 79-MBC tumor samples. Column "Lipid" annotates the lipid in detail, combining the lipid class (e.g. "Cer"), the adduct used in MS (e.g. "H", "CH3COO"), the number of C atoms per bound fatty acid separated by a colon from the number of double bonds in that fatty acid (e.g. "d18:2" constitutes a fatty acid with 18 C atoms and 2 double bonds; d stands for delta or double bond). The weight and sum formula of the lipid are annotated at the end as well. "nlog10p" is the negative base 10 logarithm of the p value, "log2fc" the base 2 logarithm of the fold change, "diffexpressed" annotates differential expression: UP meaning upregulated in ibrutinib-treated samples, DOWN meaning downregulated in ibrutinib-treated samples.

Lipid	**nlog10p**	**log2fc**	**diffexpressed**
Cer(d42:2)_H_Cer_(d42:2)_NA_NA_648.62892047_C42 H82 O3 N1	1.432083	-1.05797	DOWN
PC(38:1)_Na_PC_(38:1)_NA_NA_838.62962847_C46 H90 O8 N1 P1 Na1	1.665205	-0.80513	DOWN
PC(40:1)_H_PC_(40:1)_NA_NA_844.67898347_C48 H95 O8 N1 P1	2.614448	-0.71492	DOWN
PE(36:5)_Na_PE_(16:1)_(20:4)_NA_760.48877847_C41 H72 O8 N1 P1 Na1	1.320912	1.719209	UP

Supplementary Table 4 Ibrutinib concentrations used for Fig. R33.

cell line	IC10 [nM]	IC10_used [nM]	IC25 [nM]	IC25_used [nM]	IC50 [nM]	IC50_used [nM]
BIN_291	6.1	22.6	59.8	45.2	582.2	582
BWQ_234	2.2	4	18.8	22.6	159	159